SINGLE MOLECULE STUDIES OF THE LATERAL ORGANIZATION OF THE PLASMA MEMBRANE

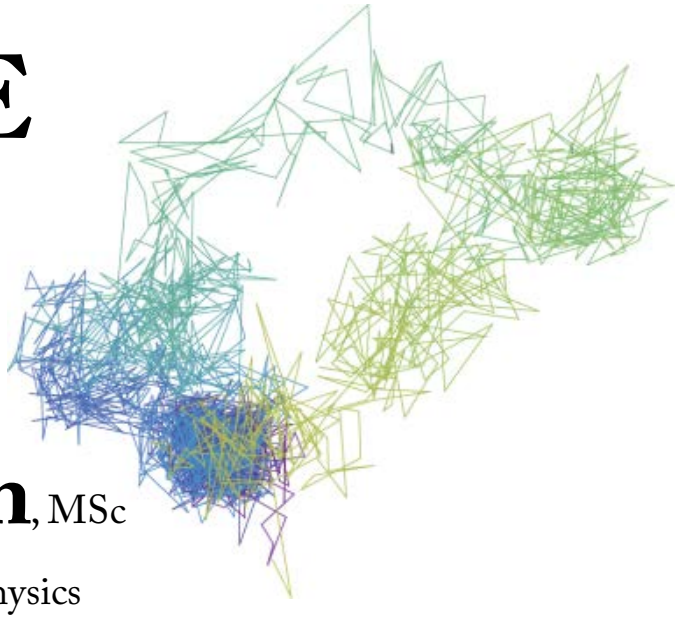

PhD dissertation by

Mathias P. Clausen, MSc

MEMPHYS – Center for Biomembrane Physics
University of Southern Denmark

Supervisors
Dr. B. Christoffer Lagerholm & Prof. Dr. Ole G. Mouritsen
October 2012

Preface

This thesis has been submitted as part of the requirements for obtaining a PhD degree at the University of Southern Denmark. The work has been conducted at the center of excellence MEMPHYS – Center for Biomembrane Physics, University of Southern Denmark, Odense, Denmark, in a period from November 2009 to October 2012, under supervision by Dr. B. Christoffer Lagerholm and Prof. Dr. Ole G. Mouritsen. Part of the work was conducted at the Department of NanoBiophotonics, Max Planck Institute, Göttingen, Germany, lead by Prof. Dr. Dr. Stefan W. Hell in collaboration with Dr. Christian Eggeling.

The general scientific field of the thesis is membrane biophysics, and the specific topic is the nanoscopic organization and lateral dynamics of the plasma membrane.

The thesis contains four studies; three experimental, and a literature review. The review was published as Clausen *et al.*, Curr Protein Pept Sci, 2011, while the experimental studies at present stage are unpublished; two of the studies are in the peer-reviewing process, while the last study is still ongoing.

The thesis includes a motivation for the project (chapter 1), the scientific aim of the project (chapter 2), an introduction (chapter 3-6), a summary of the results (chapter 7), concluding remarks (chapter 8), references (chapter 9), and the paper and manuscripts of the scientific studies (chapter 10). The introduction should give the reader an overview of the scientific topics of the thesis, including its biological background, and the methods and technologies used in the scientific work. The specific materials and methods, and data analyses are given together with the full length paper and manuscripts.

Mathias P. Clausen, October 2012

List of publications

The paper and manuscripts included for evaluation in this PhD thesis are:

- *Mathias P. Clausen* & B. Christoffer Lagerholm, "The Probe Rules in Single Particle Tracking". Current Protein and Peptide Science, 12 (8), 699-713, 2011 (Cover)
- *Mathias P. Clausen*, Eva C. Arnspang, Byron Ballou, James E. Bear & B. Christoffer Lagerholm, "Single Molecule Multi-species Tracking in Live Cells", *submitted*
- *Mathias P. Clausen* & B. Christoffer Lagerholm, "High-speed Single Particle Tracking in Plasma Membranes Using Quantum Dots", *submitted*
- Debora M. Andrade*, *Mathias P. Clausen**, Alf Honigman, Veronika Müller, Marc Bates, Stefan W. Hell, Christian Eggeling & B. Christoffer Lagerholm, "Compartmentalized Diffusion Revealed by STED-FCS", *in preparation*

The following manuscripts were based on work carried out during this PhD, but are not included for evaluation:

- Eva C. Arnspang, Jeremy Schwartzentruber, *Mathias P. Clausen*, Paul W. Wiseman, & B. Christoffer Lagerholm, "Bridging the Gap between Single Molecule and Ensemble Methods for Measuring Lateral Dynamics in the Plasma Membrane", *submitted*
- Thomas E. Rasmussen, *Mathias P. Clausen*, Eva C. Arnspang, Liselotte Jauffred, Lene Oddershede & B. Christoffer Lagerholm, "Single Molecule Applications of Quantum Dots", *in preparation*

Three poster abstracts of work from the thesis have been published:

- *Clausen, M.P.* & Lagerholm, C., "High-Speed Quantum Dot Tracking in Plasma Membranes Reveals Short-Lived Small-Size Corralled Diffusion". Biophysical Journal 102, 298a-298a (2012).
- Lagerholm, C. & *Clausen, M.P.*, "High-Speed Single Quantum Dot Imaging in Live Cells Reveals Hop Diffusion". Biophysical Journal 100, 252a-252a (2011).
- *Clausen, M.P.* & Lagerholm, C., "Influence of Quantum Dot Labels on Single Molecule Movement in the Plasma Membrane". Biophysical Journal 100, 479a-479a (2011).

Acknowledgements

Numerous people have had a hand in the course of the completion of my PhD thesis. I have been associated with MEMPHYS since February 2005, and have very warm feelings to this unique scientific and social environment. It has been a privilege to work at MEMPHYS, and I want to thank all present and previous members for having contributed to the MEMPHYS atmosphere. It is with a combination of sadness and great memories that I will soon leave the group. A number of people need a special mentioning:

B. Christoffer Lagerholm, for being my supervisor the last four years. Chris has a boundless drive and endless new ideas. He is always helpful, and I have learned a lot from him. I am pleased to have worked with Chris, and will remember the many great conference trips we have shared in Europe, and the US, the beer and the fun, and I appreciate all the people I have met through Chris's network.

Ole G. Mouritsen, for being my supervisor and mentor since I first came to MEMPHYS. Ole always has a good answer for any problem. He is an inspiration for any scientist, or scientist in spe. Ole has always given me unlimited trust, and opportunities, for which I am very grateful.

Christian Eggeling, for hosting me as part of his sub-group in the group of Stefan W. Hell at the Department of NanoBiophotonics at the Max Planck Institute in Göttingen during the winter and spring 2012 as part of our collaboration on using STED-FCS to investigate hop-diffusion. I have enjoyed the collaboration a lot, and the whole group is an amazing stimulating environment. I look forward joining Christian's new group at Oxford University in February 2013. Débora Machado Andrade is thanked for the outstanding enjoyable collaboration, and for the friendship evolving as its extension. Alf Honigman, Veronika Müller, Marc Bates, Sebastian Schubert, Franziska Brunner, Fransisco Balzarotti, Tanja Gilat, and many others are thanked for good scientific discussions, and social interactions.

Keith A. Lidke, for having me as a visitor in his group at the University of New Mexico in the summer of 2011 to learn about their latest QD tracking developments, and analysis tools. Peter Relich, Samantha L. Schwartz, and Patrick J. Cutler are thanked for great discussion, and being extremely helpful.

Matthias P. Wymann, for having me as visitor in his Cancer- and Immuno-biology group at the University of Basel in the winter of 2010 as part of a TraPPs collaboration. Even though my project did not evolve in that direction, I learned a lot from being in a biological laboratory. Thomas Bohnacker and Dominik Erhart are thanked for being helpful during my stay.

Eva Arnspang Christensen, for collaboration on the multi-color QD tracking project, and for starting several professional and social initiatives during her PhD, which I could continue organizing with great joy.

Martin V. Bennetzen, for our close educational and scientific partnerships during our studies. Since then, for valuable friendship, feedback, and discussion about whatever – whenever needed. My approach to science and engagement would not have been the same without Martin.

Jes Dreier, Morten Christensen, and Jakub Kubiak and many other MEMPHYS students, for PhD partnership during the last three years. The "Quantitative and analytical light microscopy" course in Woods Hole, the office chats, and the "Biophysics summer school" in Croatia are highlights.

Jonathan Brewer, Morten Christensen, and Jes Dreier, for valuable feedback on different parts of the thesis, and Thomas E. Rasmussen for help on Adobe Illustrator related issues.

Kadla R. Rosholm, Nikolai Lorenzen, Nicolaj Cruys-Bagger, Bitten Plesner, Jon G. Hansted, Morten Dueholm, Leigh Murphy, and Thomas Hecksher, for great collaboration on planning of the Annual Biophysics PhD Meetings over the last four years.

The Ministry of Science, Technology, and Innovation, for awarding me an EliteForsk PhD stipend 2011, which allowed me essentially unlimited traveling during my PhD. Lots of scientific input, and many connections, and acquaintances has been the outcome. Additional foundations are acknowledged for support prior to, during, and after my PhD: Alfred Benzon Foundation, SDUs Forsknings Fond, Fuhrmann Fonden, Mogens Rendals Fond, Novo Scholarship, Carlsberg Memorial Scholarship, Graduate School of Molecular Biophysics Scholarship, Oticon Scholarship, Læge Frk. Else Mogensens Fond, and A/S Tørrings Fond.

My family and friends, for being encouraging and supportive. In particular Signe Porsmose Clausen for being who she is, and for being my wife. The support and caring from her means the world of a difference, and nothing would have been the same without her.

Contents

Abstract

Methods with a combination of high spatial and high temporal resolutions are needed in order to study the lateral dynamics and structural organization of the plasma membrane. In this PhD project, we explore existing methods for plasma membrane lateral investigations, and push the limits of their use. In particular, we explore the use of fluorescent quantum dots (QDs) for single particle tracking (SPT). QDs have recently been introduced as a new category of biological probes, and have promising optical properties, which favor applications at the single molecule level.

The extreme photo-stability of QDs allows for tracking single bio-molecules over long periods of time. This is advantageous as recorded trajectories are long enough to allow for their individual analysis. Normally, a population of molecules is treated as one unity, and sub-population heterogeneities are hidden, but by detecting and analyzing single molecules separately, these heterogeneities can be accessed. We utilize this quality, and the multi-color abilities of QDs, to enable simultaneous tracking of three orthogonally targeted membrane species. Our analysis reveals differences in the single molecule populations of diffusion constants between plasma membrane molecules, which have all been associated with lipid rafts.

The superior brightness of QDs further allows us to track plasma membrane proteins and lipids at unprecedented fast acquisition rates. This has previously been inaccessible for fluorescence-based tracking experiments because of the limiting optical properties of organic dyes. We observe that proteins and lipids in a mouse embryo fibroblast cell line diffuse in a compartmentalized pattern when investigated at a fast time scale. The diffusion resembles that of the previously reported hop-diffusion, which has been observed using larger, and more invasive gold nano-particle tracking. We cross-validate our results of compartmentalized diffusion using the spatially and temporally complementary technique stimulation emission depletion fluorescence correlation spectroscopy (STED-FCS). We used molecules labeled with minimally invasive fluorescent dyes in the STED-FCS recordings, in order to rule out that our QD probes affected or induced the observed diffusion. The studies confirm that lipids experience restrictions due to a meshwork of confining barriers, and we determine those restrictions to be strongly dependent on the cellular actin cytoskeleton.

Dansk sammenfatning

Metoder med en kombination af høj rumlig og tidsmæssig opløsning er nødvendige for at kunne undersøge den laterale dynamik og strukturelle organisering af plasmamembranen. I dette ph.d.-projekt udforsker vi eksisterende metoder, der benyttes til undersøgelser af plasmamembranen, og flytter grænserne for deres anvendelse. Særligt udforsker vi brugen af fluorescerende "quantum dots" (QDs) i metoden "single particle tracking". QDs er for relativt nyligt blevet introduceret som en ny kategori af biologiske prober med lovende optiske egenskaber, som favoriserer deres anvendelse på enkeltmolekyleniveau.

QDs høje foto-stabilitet muliggør, at man kan spore enkelte biomolekyler over lang tid, hvorved det bliver muligt at analysere biomolekylernes bevægelsesbaner individuelt. Ofte behandles en population af molekyler samlet, og diversitet indenfor populationen er skjult, men ved at detektere og analysere enkelte molekyler individuelt, kan denne diversitet afsløres. Dette, samt QDs egenskaber i multi-farve eksperimenter, udnytter vi til simultant at følge tre ortogonalt mærkede membranspecier. Vores analyse viser, at der er forskelle mellem populationerne af diffusionskonstanter for de undersøgte plasmamembranmolekyler, som alle er blevet associeret med "lipid rafts".

QDs imponerende lysstyrke giver os endvidere mulighed for at følge plasmamembranproteiner og -lipider med hidtil uset hurtige optagelsesfrekvenser, hvilket tidligere har været umuligt i fluorescens-baserede video-mikroskopi på grund af de begrænsende optiske egenskaber af organiske fluoroforer. Vi observerer at proteiner og lipider diffunderer i et "ruminddelt" mønster, når de undersøges på en hurtig tidsskala i en muse-embryon fibroblast cellelinie. Diffusionen minder om den tidligere rapporterede type af diffusion kaldet "hop-diffusion", som er blevet observeret under anvendelse af guld nanopartikler, der er større og mere invasive end QDs. Vi validerer vores resultater ved hjælp af den rumligt og tidsligt komplementære teknik "stimulated emission depletion - fluorescence correlation spectroscopy" (STED-FCS). I disse STED-FCS målinger bruger vi membranlipider mærket med fluorescerende farvestoffer, der er minimalt invasive, for at kunne udelukke at vores QDs påvirker eller fremkalder det observerede diffusionsmønster. Undersøgelserne bekræfter, at lipider oplever restriktioner på grund af et netværk af indesluttende barrierer, og vi fastlægger at disse restriktioner er stærkt afhængige af det cellulære aktin-cytoskelet.

Abbreviations

ACP = Acyl Carrier Protein

CdSe = Cadmium Selenide

CdTe = Cadmium Telluride

CoA = Co enzyme A

CTB = Cholera Toxin subunit B

DOPE =1,2-DiOleoyl-*sn*-glycero-3-PhosphoEthanolamine

DPPE = 1,2-DiPalmitoyl-*sn*-glycero-3-PhosphoEthanolamine

DRM = Detergent Resistent Membranes

EDC = 1-Ethyl-3-(3-Dimethylaminopropyl)Carbodiimide

EGFR = Epidermal Growth Factor Receptor

EMCCD = Electron Multiplied Charge Coupled Device

FCS = Fluorescence Correlation Spectroscopy

FRAP = Fluorescence Recovery After Photo-bleaching

FRET = Förster Resonance Energy Transfer

FWHM = Full-Width-at-Half-Maximum

GPI = GlycosylPhosphatidylInositol

GPL = GlyceroPhosphaLipid

GSL = GlycoSphingoLipid

MSD = Mean Squared Displacement

PALM = Photo-Activated Light Microscopy

PEG = PolyEthylenGlycol

QD = Quantum Dot

SAv = StreptAvidin

SIM = Sturctured Illuminatoin Microscopy

SL = SphingoLipid

SM = SphingoMyelin

SMCC = Succinimidyl-4-(*N*-Maleinidomethyl) Cyclohexane-1-Carboxylate

SMFT = Single Molecule Fluorescent Tracking

SNR = Singal-toNoise-Ratio

SQT = Single Quantum dot Tracking

STED = Stimulated Emission Depletion

STORM = STocastic Optical Reconstruction Microscopy

svFCS = spot variation FCS

TIRF = Total Internal Reflection Fluorescence

TOPO = TriOctylPhosphine Oxide

ZnS = Zink Sulfide

1 Motivation for the project

The plasma membrane defines the boundary of a cell. It controls exchange of material between the cell and its surroundings, and it mediates all inter- and extracellular communication needed for the cell to respond to changes or stimuli in its environment. Many cell signaling processes initiate at the plasma membrane, and other key cellular functions such as endocytosis and exocytosis also involve the plasma membrane. In order to understand how such functions are conducted, and regulated, it is necessary to know how the plasma membrane laterally organizes the lipids and proteins that constitute it.

Biophysical studies of lipids and proteins in model systems have been instrumental for the understanding of the dominant forces and interactions between lipids and proteins [1]. Those studies have been carried out under well-controlled equilibrium conditions, but in order to probe the complexity of the plasma membrane, it is important to investigate lipids and proteins in their natural environment of a living cell.

Studies of lipids and proteins in cells have revealed that the lateral organization of the plasma membrane is very heterogeneous and highly dynamic. It has been suggested that the plasma membrane is compartmentalized, and spatially segregates its constituents into domains of different composition and functionalities [2, 3]. Lateral heterogeneity on many different length and time scales have been reported, but the consensus is that the most relevant scales for studying the organization are a spatial scale of 10 to few 100s of nanometers and a millisecond time scale [4]. An issue in many studies of the plasma membrane is therefore that the results are indirectly inferred because direct observations of small transient structures are unattainable using standard optical microscopy methods, which according to the Abbe resolution limit are restricted to observation above 200 nm [5]. This has prevented a detailed investigation of the plasma membrane at the molecular level.

In recent years, development of better probes and more sensitive detectors has opened up for the investigation of single molecules [6, 7]. Further, by applying different computational and physical strategies to surpass the resolution limit, optical so-called super-resolution microscopy techniques have been developed, e.g. photo-activated light microscopy (PALM), stochastic reconstruction optical microscopy (STORM), structured illumination microscopy (SIM), and stimulated emission depletion (STED) microscopy [8, 9]. These methods

allow for a spatial resolution below 40 nm, but not all of them are equally suitable for studying dynamical processes. STED microscopy is well-suited for studying fast dynamical processes, especially when combined with fluorescence correlation spectroscopy (FCS). STED-FCS studies have been used to unravel important details of differences in the dynamic behavior of different lipids in live cells [10].

Single particle tracking (SPT) can also be considered a classical super-resolution technique. In SPT, single molecules of interest labeled with gold nano-particles [11], fluorescent dyes [12], or recently developed fluorescent quantum dots (QDs) [13] are tracked using video-microscopy. The positions of single non-overlapping molecules are located with a precision of down to 10 nm using computational fitting of the signal intensity profile. Subsequently, the positions are linked frame-by-frame to reconstruct single molecule trajectories with great detail [14]. In this way, heterogeneities behind population averages have become approachable [15]. It has e.g. been shown that lipids and proteins in the plasma membrane, when studied on a fast time scale, undergo a type of motion termed "hop-diffusion" [16]. Observation of hop-diffusion requires fast temporal acquisition, and possibly also a long observation period, which so far only has been possible with Ø40 nm gold particles. Hop-diffusion has therefore been questioned because the large gold nano-particles might perturb the behavior of the target molecules [17]. Small fluorescent dyes in contrast do not reach an equivalent temporal scale, so the discussion remains unsettled.

As methods for studying the plasma membrane at the right spatial and temporal scales have just recently been developed, the existing tool-set is far from being comprehensive. Further developments and enhancements of existing methods for general and specific uses are needed. For instance, fluorescent semiconductor nano-crystal QDs seem a promising new type of probe; they have a moderate Ø20 nm size, and in particular, they feature unique optical properties such as broad absorption, narrow emission, and extreme brightness and photo-stability, which make them in particular well-suited for single molecule applications in a range of different biological systems [18, 19]. Cross-validation between different newly developed methods is also essential in order to evaluate their potential of use.

2 Scientific aim of the project

The overall aim of this PhD project has been to develop a better understanding of the lateral dynamics of plasma membrane species, and to find out how the plasma membrane laterally organizes its constituents at the nanoscopic level. In order to do so, we needed methods that allowed for simultaneous high spatial as well as temporal resolution. Part of the aim of the project has therefore been to push the limits and use of existing methods. In particular, we have explored the use of single particle tracking (SPT) methods using fluorescent quantum dot (QD) targeting, as QD have unique optical properties, which has not yet been fully exploited for tracking membrane species in cells. The project is divided into three experimental studies, and a literature review:

Study 1) With this study, we wanted to take advantage of the optical properties of QDs, which make them especially well-suited for multi-color imaging. In particular, we had an interest in following the motion of several different plasma membrane species simultaneously in the same cell in order to probe dynamics beyond any cell-to-cell variability. (A manuscript of this study is included in chapter 10.1 page I.)

Study 2) In this review, we did a survey of the lipid membrane SPT literature in order to understand the influence, artifacts, and limitations of different probes used, e.g. gold nano-particles, fluorescent dyes, and QDs. Especially, we focused on how the size of the probe affects the diffusion of a target molecule, and how the brightness and stability of the probe dictates the accessible experimental and informational time-scale. (A paper of this study is included in chapter 10.2 page II.)

Study 3) Our aim of this study was to take advantage of the extreme brightness and photo-stability of QDs to explore SPT at fast acquisition rates. This was done in order to access dynamic information of plasma membrane species on a fast time-scale. In particular, our interest was to address the type of diffusion termed “hop-diffusion”, which has previously been reported in SPT experiments using gold nano-particle that are much more invasive than QDs. (A manuscript of this study is included in chapter 10.3 page III.)

Study 4) In this study, we wanted to validate our fast QD tracking data with the complimentary high spatial and high temporal resolution method stimulated emission depletion fluorescence correlation spectroscopy, STED-FCS. Especially, we were interested in investigating if our observed lipid dynamics could be confirmed when having the same biological system, but using minimally invasive fluorescent dyes as probes in a different type of experimental setup. (The results of this study are included in chapter 10.4 page IV.)

3 The plasma membrane

The cellular plasma membrane is an intriguing and fascinating entity of the cell. It constitutes the border of the cell and controls material exchange and communication between the cell and its surroundings. The plasma membrane contains a myriad of different lipid and protein species, and it has become increasingly more evident, that it has a very complex structure and is highly dynamic. Tools for investigating the plasma membrane structure and dynamics on relevant spatial and temporal scales are still emerging, and knowledge about the plasma membrane is still to be acquired.

3.1 Plasma membrane lipids and proteins

The main constituents of the plasma membrane are amphiphilic lipids. These lipids have a hydrophilic part "the head" (head groups) and a hydrophobic part "the tails" (acyl chains) (Figure 3-1A). In aqueous solution, lipids will spontaneously self assemble into different structures (Figure 3-1B) [1]. This process is driven by the hydrophobic effect, and causes the lipid acyl chains and head groups to arrange in such a way that the contact area between solvent water molecules and the acyl chains is minimized. The structures are held together predominantly by the cooperative action of week interactions. The geometry of a formed structure will depend on the geometry of the lipids that constitutes it [1, 20]. Lipids have different head groups with different sizes, and the acyl chains have different lengths (number of carbons) and can be saturated or mono-, di-, or polyunsaturated (number of double bonds). This affects the effective geometry of the lipid (Figure 3-1C). In a lipid membrane, the lipids are arranged in a tail-to-tail fashion forming a lipid bilayer, which has a hydrophobic core flanked by hydrophilic surfaces on either sides (Figure 3-1D). A lipid membrane is thus only two molecules thick corresponding to approximately 5 nm, and hence the membrane thickness is much smaller than the diameter of the cell it surrounds. Yet, it is an efficient barrier.

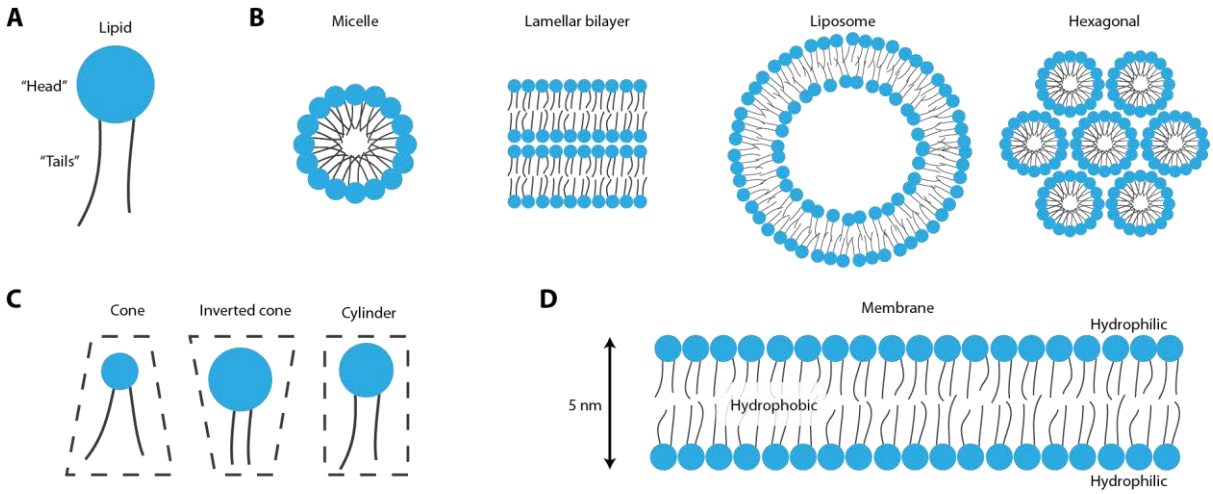

Figure 3-1: Lipids and lipid structures. A) Lipids are amphiphilic molecules with a "head" and "tails" (acyl chains). B) Lipids can self-assemble into different structures (many other lipid structures than shown here exist). C) Individual lipids have different effective shapes depending on the nature of the head group and the acyl chains. D) In a membrane in aqueous solution, lipids arrange themselves in a tail-to-tail fashion to create a membrane with a hydrophobic core, and a hydrophilic surface. A typical lipid membrane is only 5 nm thick. (Partly adapted from [1].)

Mammalian plasma membranes contain thousands of different lipid species with the main types being: i) glycerophospholipids (GPLs), ii) sphingolipids (SLs), and iii) cholesterol (Figure 3-2) [21, 22]. GPLs have a glycerol backbone to which two fatty acid hydrocarbon chains are bound the *sn*-1 and *sn*-2 positions. The *sn*-3 position of the glycerol is attached to a phosphate, which is further attached to an alcohol (e.g. choline, or ethanolamine). SLs are derivatives of sphingosine, which is an amino alcohol with a long hydrocarbon chain. A sphingosine with a fatty acid chain attached is called a ceramide, and a SL is a ceramide with either a phosphate alcohol head group, or one or more sugar moieties as head group (glycospingolipid, GSL). A sub-category of GSLs is gangliosides, which contain sialic acids, e.g. G_{M1}. Cholesterol is a sterol, which has a rigid four-ring hydrocarbon structure with a short hydrocarbon chain attached to it. Cholesterol further has a small head group constituted by just a hydroxyl group.

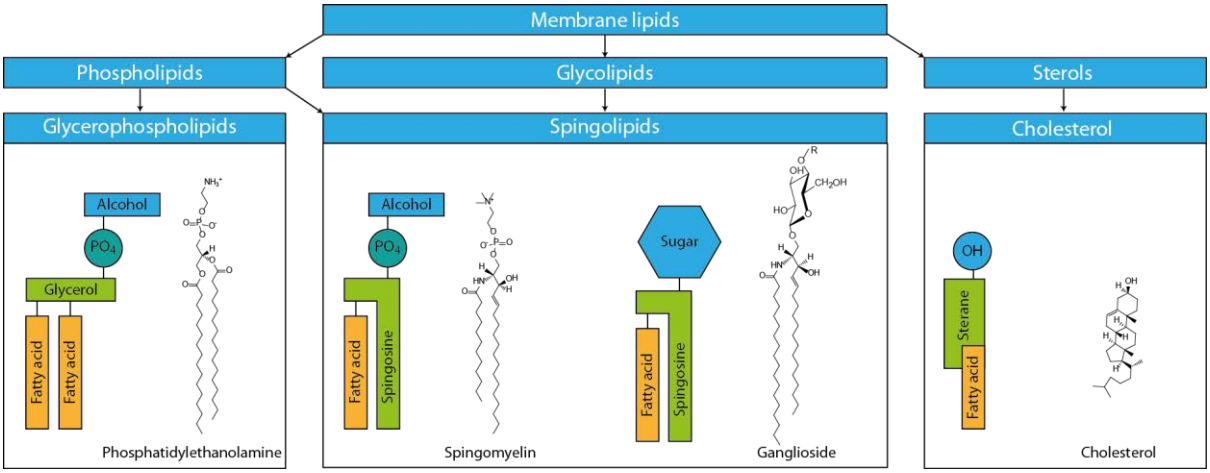

Figure 3-2: Lipid species. Glycerophospholipids have a glycerol backbone to which two variable fatty acid hydrocarbon chains are bound in the *sn*-1 and *sn*-2 positions. The *sn*-3 position of the glycerol is attached to a phosphate, which is further attached to an alcohol. Sphingolipids are derivatives of sphingosine, which is an amino alcohol with a long hydrocarbon chain. A variable fatty acid chain is coupled to the sphingosine, which is also coupled to either a phosphate-alcohol, or to one or more sugar moieties (glycospingolipid). Glycosphingolipids that contain sialic acids are called gangliosides. Cholesterol is a sterol, which has a rigid four-ring hydrocarbon with a short hydrocarbon chain attached in one end, and a hydroxyl group in the other. (Adapted from [23].)

GPLs and cholesterol are present in approximately equal amounts in the plasma membrane, and together they account for 85-90 % of the total lipids [21]. SLs account for a large majority of the remaining lipids. The distribution of lipids in the plasma membrane is asymmetric between the two lipid leaflets [1].

In model systems, the packing of lipids has been well characterized [1, 24]. In a single component lipid bilayer at low temperatures, some lipids species pack tightly in a so-called solid-ordered- (s_o-) or gel phase (Figure 3-3A). In the s_o-phase, the lipid heads are packed close together and the lipid chains are fully stretched out. At higher temperatures, above the phase transition temperature, T_m, the lipids pack in a liquid-disordered- (l_d) or fluid phase. In the l_d-phase, the lipids are able to diffuse laterally, and their acyl chains can take varying conformations (Figure 3-3A). The "solid/liquid" term refers to the packing of the head groups and the mobility of the lipids, while the "ordered/disordered" term refers to the ordering of the acyl chains. The transition between phases is a cooperative phenomenon, and the T_m is among other things influenced by the length and degree of unsaturation of the acyl chains, with higher T_m for bilayers of long and saturated lipids [25].

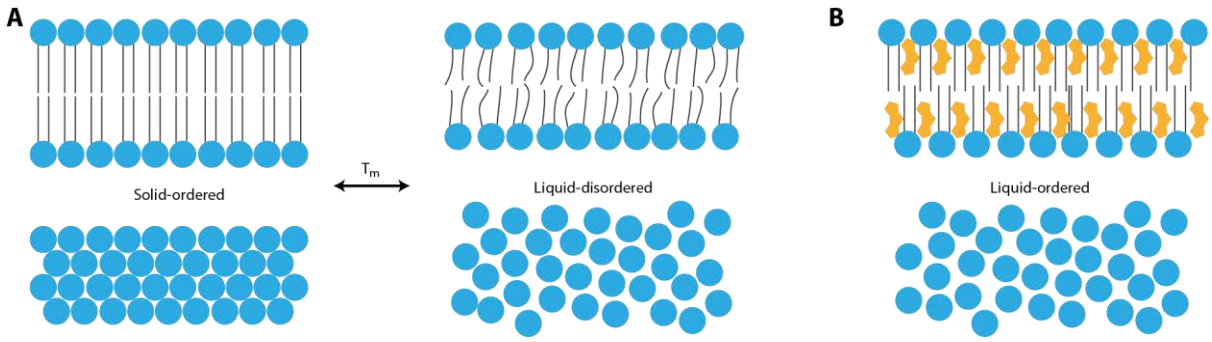

Figure 3-3: Lipid phases. A) In the s_o-phase, the head groups are tightly packed, and the acyl chains are stretched out and ordered. In the l_d-phase, the lipids are mobile, and the acyl chains take various conformations. The transition between the two phases is marked by a phase transition temperature, T_m. Note that the bilayer in the l_d-phase is thinner and laterally more expanded than in the s_o-phase. B) In the l_o-phase, cholesterol is present. The lipid chains are ordered, while the lipids are mobile. (Partly adapted from [25].)

In binary lipid mixtures, the bilayer can for certain temperatures and molar ratios of the lipids separate into co-existing phases of different compositions and physical state [20]. The lipids, which in a one-component system have the lowest T_m, will primarily be in the l_d-phase, whereas the lipids, which in a one-component system have the highest T_m, are enriched in the s_o-phase. [25]

The presence of cholesterol in a lipid bilayer has a significant impact on the packing. Because of its rigid hydrophobic sterol ring structure, cholesterol does not fit into the s_o-phase or the l_d-phase of most lipid bilayers. Instead, cholesterol can induce a so-called liquid-ordered- (l_o-) phase (Figure 3-3B) [26]. In the l_o-phase, the lipid chains are ordered around cholesterol, but the lipids are still free to diffuse laterally. Lipids with long saturated tails and SLs are often found to associate with cholesterol in the l_o-phase, as are lipids with big head groups such as glycolipids [21]. According to the "umbrella-model", the head groups of lipids in the l_o-phase screen the body of cholesterol at the water interface, which would otherwise be exposed because of the small head of cholesterol [21]. The observed preferential association of especially cholesterol and sphingolipids in model membranes is a central element in the "lipid-rafts-model" described further below [2, 27].

The plasma membrane also contains proteins. More than 30 % of the human genome consists of genes that code for membrane embedded proteins, and it is speculated that an equal or higher percentage codes for proteins that in one way or the other interacts with cellular membranes [20, 28]. The plasma membrane contains up to 50 % protein in terms of weight, and 20 % in terms of area covered, or corresponding to about one protein per 50 lipids [1]. Membrane proteins can be associated with the membrane in different ways and through many types of interactions (Figure 3-4A) [1, 29]. Integral membrane proteins (transmembrane proteins) are proteins that span the lipid bilayer completely. These proteins usually have hydrophilic domains on both sides of the bilayer, whereas the membrane spanning part is dominantly hydrophobic. The hydrophobic part of the protein has to match the thickness of the embedding lipid bilayer (or vice versa) in order not to expose hydrophobic patches of neither the protein nor the lipids to the surrounding aqueous milieu (Figure 3-4B) [30]. This "hydrophobic matching" can for proteins being taller than the bilayer, lead to stretching and

therefore ordering of the lipids closest to the protein and/or recruitment of lipids with longer acyl chains, or a compression of the protein [25, 30]. For proteins shorter than the embedding lipids the situation is the opposite. Hydrophobic matching can also cause local lipid annuli to arise around the proteins, and cause proteins of same hydrophobic lengths to cluster together, as a result of capillary forces acting in the membrane [31].

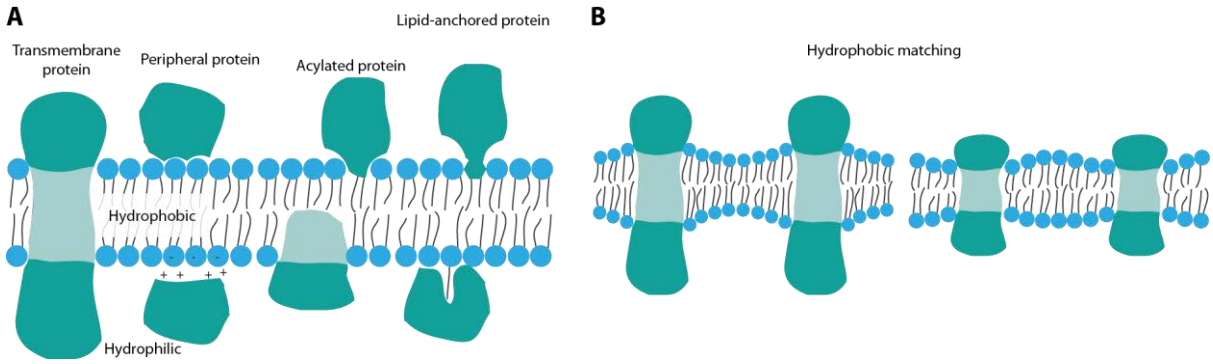

Figure 3-4: Membrane proteins. A) Transmembrane proteins have hydrophilic domains on both sides of the membrane, whereas the membrane embedded part is hydrophobic. Peripheral proteins are dominantly hydrophilic proteins that are attached to the membrane via specific or non-specific interactions. Lipid-anchored proteins are directly bound in the plasma membrane through covalent attachment to a lipid. Proteins can also be anchored directly to the membrane through attachment of one or more acyl chains. B) If there is a mismatch between the size of a membrane protein and the surrounding lipids, they will adjust to each other. This is called "hydrophobic matching". (Adapted from [1] and [30].)

Completely hydrophilic proteins can be peripherally attached to membranes via specific or non-specific interactions with the bilayer, or they can be anchored directly to the plasma membrane through covalent attachment to a lipid (e.g. glycosylphosphatidylinositol (GPI)-anchored proteins, which are attached to lipids with the monosaccharide inositol as head group and normally long saturated acyl chains), or the attachment of one or more acyl chains (e.g. palmitylation) [29].

Some membrane proteins are affected by membrane curvature stress, and e.g. preferentially bind areas of high membrane curvature [32]. Other membrane proteins are thought to be influenced by the lateral pressure profile in membranes [1, 33].

On the cytoplasmic side of a cell, the plasma membrane is supported by the cytoskeleton to which it also has direct membrane protein anchors [34]. The cytoskeleton is a fibrous network of actin filaments, microtubules, and intermediate filaments, which mechanically stabilize the shape of the cell, as well as it functions in many vital biological processes of the cell. Especially the cortical actin is closely associated to the plasma membrane, and plays an important role in the "membrane-skeleton-model" described further below [16, 35]. On the outside of the cell, the cell is surrounded by the extracellular matrix, which is a complex matrix meshwork composed of proteins and polysaccharides. A schematic of the cellular plasma membrane is given in Figure 3-5.

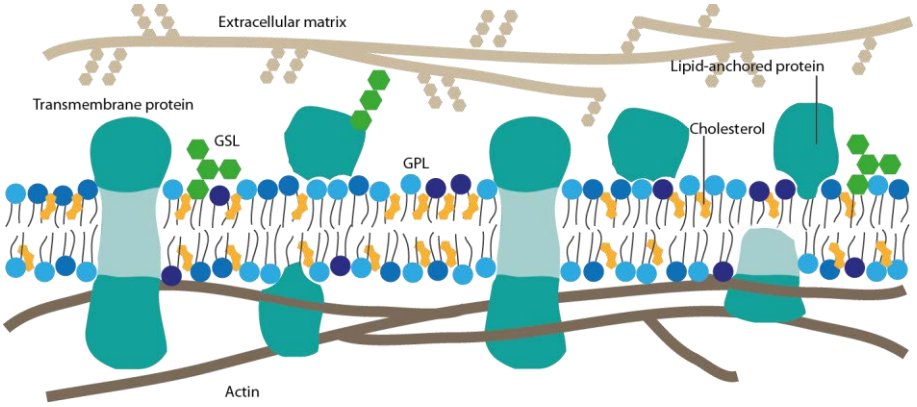

Figure 3-5: Schematic of the plasma membrane. The plasma membrane contains many different types of lipids (e.g. glycerophospholipids (GPL), glycosphingolipids (GSL), and cholesterol) and proteins (e.g. transmembrane proteins, and lipid-anchored proteins). The extracellular matrix on the outside and the actin cytoskeleton on the inside surround the plasma membrane.

The plasma membrane is involved in many essential processes of the cell, e.g. in order for any communication to take place between a cell and its surroundings, the plasma membrane has to be involved. This process can include binding of a ligand to a membrane receptor, which in response to this stimulus dimerizes with another receptor and leads to an intracellular conformational change that starts a signaling cascade, which involves the recruitment of other (membrane) proteins. This is for example the case for signaling through tyrosine kinases such as the Epidermal Growth Factor Receptor (EGFR). Other membrane processes such as endocytosis, where a region of the plasma membrane forms an intracellular vesicle, or exocytosis, where an intracellular vesicle fuses with the plasma membrane, also causes arrangements of both lipids and proteins in the plasma membrane that are necessary for the correct functioning of the cell. Such segregation of membrane constituents, which regulate cellular function, must be controlled in time and space, but it is unknown exactly how.

3.2 Lateral organization in the plasma membrane

The classical model explaining the plasma membrane organization is the “fluid-mosaic-model” proposed by Singer and Nicolson in 1972 [36]. In this model, the plasma membrane is considered to be free-floating, and lipids are considered relatively “dull”, acting as a solvent for the membrane proteins. The lipids and proteins are considered to diffuse freely in the lateral dimension.

Given the compositional diversity of plasma membrane lipids as well as proteins, and the range of different lipid-lipid, lipid-protein, and protein-protein interactions already mentioned, it has become increasingly clear that the plasma membrane is much more laterally structured than originally proposed, and the fluid-mosaic-model does not match the current understanding of the plasma membrane [29, 37]. A new model for the lateral organization of the plasma membrane is needed, and this model must take into account the numerous functions that are carried out in and around the plasma membrane, and that are under regulation and control.

A traditional method, which has been applied to study live cells, and that has shown lateral heterogeneity in the plasma membrane is fluorescence recovery after photo-bleaching (FRAP) [34, 38]. In this method, an immobile

fraction of labeled membrane molecules is often observed, and the fluorescence recovery dynamics is typically not explainable assuming free single-component diffusion, which would be sufficient to explain data in model membranes. Translational diffusion of membrane species in native biological membranes of live cells has been measured by a range of different methods, and this typically results in an apparent diffusion constant that is at least an order of magnitude smaller than what is found in reconstituted model membranes [16, 39]. This result is an indication that the plasma membrane contains obstacles that hinder or restrict free lateral motion. Ample evidence now exists, which suggests that the observed slower diffusion in native membranes is caused by a combination of different reasons including molecular crowding, specific molecular interactions, membrane topography, interactions with the actin cytoskeleton, and interactions with nanostructures within the membrane, [35, 37, 40-42].

Different models explaining plasma membrane organizing principles exist. The two that has caught the most attention are the "lipid-raft-model" and the "skeleton-fence-model" [2, 35].

3.3 Lipid raft domains

The lipid-raft-model has been proposed by Kai Simons and is a still evolving model [2, 27, 42-44]. It suggests that the plasma membrane laterally segregates its constituents into functional platforms that are enriched in cholesterol, SLs and specific proteins (e.g. GPI-anchored proteins). The model describes lipid rafts as dynamic, meta-stable, nano-scale, sterol-SL enriched ordered assemblies of proteins and lipids that can be stimulated to coalesce into larger more stable platforms by specific lipid-lipid, protein-lipid, and protein-protein interactions (Figure 3-6) [45, 46].

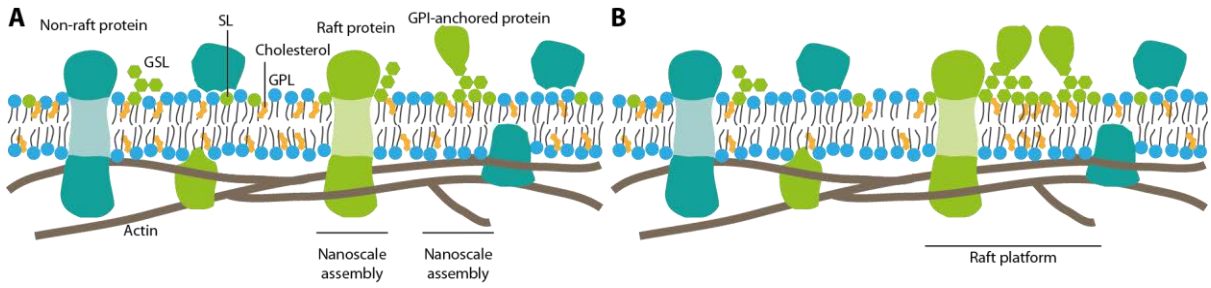

Figure 3-6: Lipid rafts. A) In the un-stimulated situation, raft molecules (light green) form small meta-stable nano-scale assemblies that are mixed with non-raft molecules (turquoise). B) Upon stimulation, raft nano-assemblies coalesce and form larger and more stable platforms. (Adapted from [42].)

The concept of lipid rafts has met some resistance and has been criticized [47, 48]. Part of the reasons for this is that, the concept of lipid rafts previously has been closely associated with detergent resistant membrane (DRM) fractions. These are fractions, which isolate independent from the plasma membrane upon non-ionic detergent disruption of cells at 4 °C, followed by sucrose gradient centrifugation [20, 49]. The DRM fraction is enriched in what have been coined raft molecules. An issue is that the plasma membrane clearly reorganizes during disruption and extraction, and that detergents directly can induce clustering of specific lipids, and further that

lipid-miscibility is different at 4 °C than at more physiological temperatures [25, 50, 51]. Lipid rafts were previously suggested to form a l_o-phase as observed for e.g. cholesterol and sphingomyelin (SM) in model membranes, but evidence that this phase exists in live cells is lagging. In model membranes, phase separation often result in formation of large micrometer-sized domains, but these has also not been observed in live cells [52, 53]. Results from FRAP and Förster resonance energy transfer (FRET) methods have given inconclusive results about the existence of rafts in cell plasma membranes [7].

Since lipid rafts are not visible by conventional optical microscopy, this has let to the agreements that rafts are small (below 200 nm). At the same time rafts are thought to be highly dynamic and short-lived (in the order of 10s to 100s of milliseconds). These two facts complicate the characterization of lipid rafts considerably, since quite advanced methods are needed to study rafts. Suitable methods that can reach the demand for simultaneous high spatial and temporal resolutions have only just become available in recent years, and they are still being developed and refined.

The development of super-resolution microscopy [54], and single-molecule microscopy and spectroscopy has provided more insight to the revised raft concept [55]. It has for instance been shown by homo-FRET, single particle tracking (SPT), and fluorescence correlation spectroscopy (FCS) that GPI-anchored proteins and other proteins dynamically partition within nano-scale clusters in a cholesterol-, SL- and GSL-dependent manner [56-58]. Using stimulated emission depletion (STED) super-resolution microscopy (or nanoscopy) combined with FCS, Christian Eggeling et al. showed that a SL (SM) and a GPI-anchored protein, in contrast to a GPL (1,2-dipalmitoyl-*sn*-glycero-3-phosphoethanolamine (DPPE)), are transiently trapped for 10 ms in cholesterol-dependent complexes of 20 nm in live PtK2 cells [10]. The study was followed up and supported using a SPT technique [59], and details of the molecular reasons for the association has further been unraveled [60].

In some case, the formation of lipid rafts has been reported to be dependent on actin [61]. Rafts have been reported to have a range of different sizes, and the model suggest that meta-stable small platforms exist in un-stimulated cells, and that the rafts upon stimulation of the cell coalesce and form larger signaling platforms. These platforms are functional and are created by specific lipid-lipid, protein-lipid, and protein-protein interactions, and physical and chemical specificity. Large raft platforms can also be induced artificially in cells by anti-body cross-linking [62]. Most functional studies of rafts come from studying T-cell signaling, cellular trafficking, and viral infection [42]. The studies are supported by lipodomic analyses, which find raft clusters to contain cholesterol and SLs [63, 64].

It has been questioned whether the compositional complexity of native plasma membranes would hinder the formation of phase separated domains in cells. It seems not to be the case, as phase separation has been observed in membrane spheres and giant plasma membrane vesicles prepared from intact plasma membranes of live cells [65, 66]. These preparations yield vesicles that in composition resemble that of the plasma membrane, but the

total protein content is lower. If cooled to below 12 °C, or if G_{M1} is externally cross-linked, a complete phase separation occurs, and those molecules that have been suggested to be associated with rafts partition in one phase. This phase in not identical to the l_o-phase, but has been termed the "raft-phase" in model systems. It is important to note that model membrane studies are very different in nature from studies in live cells. Studies in reconstituted membranes are usually carried out under well-controlled conditions at thermodynamic equilibrium and with no material exchange with the surroundings [20]. This is not the case for cells, where the cell constantly has to adapt to local environmental changes, and the membrane is in continuous flux, e.g. it is estimated that the equivalent of the entire cell surface is internalized one to five times per hour [67, 68].

It is evident that the plasma membrane has the potential to form lipid-based domains, but cells under normal conditions are not forming microscopically visible large domains. In cells, as opposed to the model membrane studies mentioned, the membrane is not freestanding, but supported by the actin cytoskeleton. It is hypothesized that the actin meshwork in close proximity to the plasma membrane regulates the formation of large lipid-raft domains.

3.4 Cytoskeleton compartments

The hypothesis that the actin cytoskeleton is the key player dominating the lateral organization of the plasma membrane has been stressed by Akihiro Kusumi in a series of papers and reviews (e.g. [3, 16, 35, 69-73]).

Using an ultra-fast single particle tracking method that allow for 50,000 Hz tracking of lipids and proteins labeled with gold nano-particles, membrane proteins are observed to be spatially confined within 30-300 nm compartments on a very short time-scale, whereas the molecules jump between these compartments on a longer time-scale (note that no long jumps are needed). The observed motion has been termed "hop-diffusion", and has let to proposal of the skeleton-fence-model. In this model, free motion of transmembrane proteins is restricted by collisions between their intracellular domains and the actin cytoskeleton. This results in corralling of the molecules within the cytoskeleton barriers. The barriers are eventually crossed by chance.

A surprising observation was that hop-diffusion also was observed for a lipid (1,2-dioleoyl-*sn*-glycero-3-phosphoethanolamine (DOPE)) in the outer leaflet of the plasma membrane as the lipid does not span the membrane and is therefore not able to interact directly with the cytoskeleton. As a consequence the model was extended to the "anchored-picket-fence-model". In this model, the motion of all membrane molecules is corralled because transmembrane proteins are anchored along the actin cytoskeleton thereby restricting free diffusion (Figure 3-7). The anchored immobile proteins do not only act as a steric hindrance for moving molecules, but they also cause a hydrodynamic friction-like effect, which causes diffusion to slow down near the immobile proteins [73]. When many transmembrane proteins are anchored along the actin cytoskeleton it becomes increasingly more difficult for other membrane species to cross the barrier, and only after a certain time the molecule will escape into a new compartment.

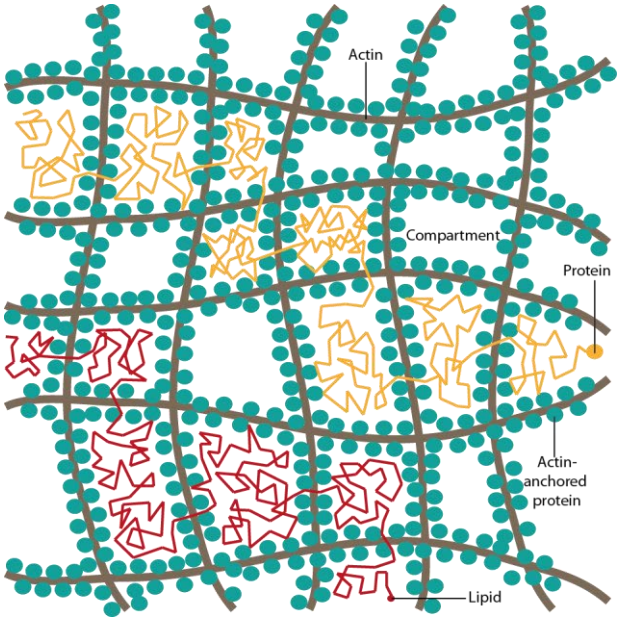

Figure 3-7: The anchored-transmembrane-picket-model. Membrane protein and lipid diffusion is restricted owing to steric hindrance and hydrodynamic-like friction effects of immobile actin anchored membrane proteins. Therefore, lipids and proteins alike exhibit hop-diffusive behavior. (Adapted from [16].)

The concept of the actin cytoskeleton as a defining barrier in plasma membranes has been supported by electron topography studies showing that the actin meshwork is within a distance of 0.8 nm from the plasma membrane, and that the compartment sizes are similar to those observed in hop-diffusion [74]. The hop-diffusion experiments can be used to explain the apparent slow diffusion in plasma membranes of live cells as compared to that in model membranes. Within compartments, it is reported that the diffusion constant is 5-8 $\mu m^2/s$, which is in agreement with the diffusion constants in model membranes. On a longer time-scale corresponding to the movement between compartments, the diffusion constant is reduced by a factor of 10-20. As the molecules only rest for 3-30 ms within the compartment, a method with extremely high temporal resolution is needed, and as this is not the case for most methods, the fast diffusion component is often averaged out, or overlooked.

The functional role of dividing the membrane in compartments is suggested to be to facilitate the formation of molecular signaling complexes. Once inside the same compartment, molecular interaction partners will meet more frequently than in a free-floating membrane, and the chance of meeting in the right orientation to form a complex is increased. As the formed complexes increase in size, they will have less chance of escaping the confinement, which will increase the chance of other partners to associate with the complex. If dissociation occurs, the chance of recombining is also increased by the presence of barriers [16].

The present actin cytoskeleton based model suggests that there is a hierarchical organization in the plasma membrane [3, 35, 69]. Proteins are allowed to dimerize and form small molecular complexes. Coalescence of these complexes is controlled by the lipid rafts, and the raft growth is controlled by the actin cytoskeleton and associated immobilized transmembrane proteins.

A caveat in the models based on hop-diffusion is that only limited experimental evidence from other research groups and complementary techniques is available [17, 75]. For instance, it would be expected that STED-FCS studies would have the spatial and temporal capability to show hop-diffusion in some cases [10, 59]. This has not been the case so far, and the fast diffusion component of 5-8 $\mu m^2/s$ has also not been confirmed. It has therefore been suggested that hop-diffusion is an induced artifact of the method used.

3.5 Small and transient structures

The perhaps biggest challenge in studies of the molecular organization of the plasma membrane has been, and still is, the lack of suitable methods that are capable of resolving possible small transient structures in the plane of the plasma membrane. In many cases domains and barriers are not directly visible, but have to be inferred from diffraction-limited methods [37]. During recent years, the development of advanced methods with high spatial as well as temporal resolution has added important layers of insight to the understanding of plasma membrane lateral organization, and it seems to be those methods that will be pivotal in revealing more details of the lateral structure of the plasma membranes in live cells.

4 Single particle tracking

In single particle tracking (SPT), single copies of molecules are labeled with e.g. gold particles, organic dyes, or quantum dots (QDs), and their motion is monitored over time with sub-diffraction limited spatial resolution. In this way, molecular trajectories of plasma membrane molecules can be reconstructed with nanometer precision and millisecond time resolution. From the motion of the single molecules, detailed information about the plasma membrane environment can be inferred.

4.1 General aspects of SPT

The advantage of SPT is that single copies of molecules can be specifically targeted and tracked with a combination of high spatial and high temporal resolution. More classical methods such as fluorescence recovery after photo-bleaching (FRAP) and fluorescence correlation spectroscopy (FCS) give diffraction-limited information on the average diffusive behavior of an ensemble of molecules [39, 76-78]. In these methods, the whole population of labeled molecules is treated as a unity, and it is difficult to discriminate sub-population heterogeneity. With the development of bright labels [9] and sensitive detection devices such as electron-multiplied charge coupled device (EMCCD) cameras (and to some extent optical sectioning tools such as confocal and total internal reflection fluorescence (TIRF) microscopy), imaging of single molecules has become possible, and the heterogeneities behind reported averages are approachable [15]. This opens up for gaining a comprehensive understanding of the spatial dynamics of molecular interactions in cellular plasma membranes at a spatial scale that is equivalent to the size of the molecules themselves.

SPT combines single molecule detection and resulting high spatial resolution with the ability to follow the movement of membrane molecules at high temporal resolution over extended time periods [11, 13, 14, 79]. The typical spatial resolution in an SPT experiment is 10-40 nm, and the temporal resolution ranges from video rate (25-30 Hz) to extremes of 50 kHz depending on the choice of label [70]. Single molecules can be tracked and analyzed individually to give a detailed description of their routes within the plasma membrane, and often a wide range of types of motions including free diffusion, anomalous diffusion, confined diffusion, and transiently confined diffusion (hop-diffusion) are observed in a way that would not be distinguishable in ensemble measurement (Figure 4-1) [57, 70, 80-82].

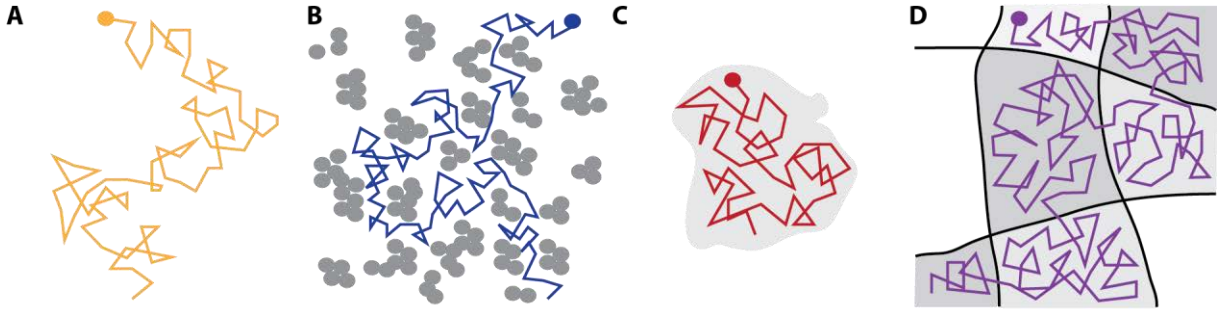

Figure 4-1: Different types of diffusion. A) Free Brownian diffusion. B) Anomalous sub-diffusion in a system with obstacles. C) Confined diffusion within a domain. D) Confined diffusion with permeable barriers (hop-diffusion). (Adapted from [83].)

In this way, SPT has been used to e.g. reveal structural aspects of the plasma membrane environment [70, 84-87], and to discern details of the local spatial regulation of signaling events in the plasma membrane [82, 88, 89]. SPT has the advantage that typically a large field of view is covered, providing an overview of a big part of the cell as opposed to a single spot. This has enabled observation of regional differences in motion [90]. One drawback of SPT is that only a subset of molecules is labeled, and that these molecules might not be representative for the whole population.

4.2 Labels for SPT

In order for single molecules to be visible in light microscopy, they need to be labeled. This is most typically done with latex beads, gold particles, fluorescent proteins, fluorescent dyes, or QDs. Historically, SPT experiments were done by measuring the scatter from e.g. anti-body coated micrometer-sized latex beads, or >40 nm gold nano-particles using interference contrast video microscopy [11]. These labels give high signal-to-noise-ratio (SNR), and can be imaged at ultra-high imaging rates [70]. The labels are relatively large, and they therefore have limited accessibility in the plasma membrane (e.g. they cannot access neural synapses, areas with a dense extracellular matrix, or pronounced topology), and may exert a hydrodynamic drag on the molecules to which they are attached [83, 91]. Further, the valence of the probes is difficult to control and this can lead to cross-binding of target molecules, and result in induced artifacts such as unintentional triggering of biological signaling, and reduced mobility [11].

More recently, SPT has been extended to track single fluorescent dyes and proteins (sometimes called single molecule fluorescent tracking, SMFT) [6, 12]. These labels are much smaller and less invasive than the gold nano-particles, and therefore favorable in this respect. Their optical properties, however, limit their use as they suffer from low luminescence brightness and fast photo-bleaching, which restricts the imaging rate and length of observation. A consequence of this is that single molecule trajectories cannot be analyzed individually, but have to be pooled to give an ensemble average of all molecules [14].

Relatively recently, QDs were introduced as a probe in biological applications [18, 92]. They can be viewed of as a compromise between the two other categories of labels. QDs have a moderate size (~20 nm in diameter), an

extreme brightness, an excellent resistance to photo-bleaching, and further they are easily surface functionalized towards binding of almost any molecular target of interest. This has made QDs a preferred choice of label in many SPT (or single QD tracking, SQT) studies [13, 19]. QDs do, however, blink and suffer from the same valence issue as the beads and gold nano-particles.

4.3 Sub-diffraction-limited spatial resolution

SPT is a light microscopy technique and the recorded images are therefore spatially limited in resolution by the diffraction of light. This has the consequence according to the Abbe resolution limit that structures being separated by a distance smaller than $d = \frac{\lambda}{NA_{condenser} + NA_{objective}}$ cannot be imaged using conventional light microscopy. In this equation λ is the wavelength of light, $NA_{condenser}$ is the numerical aperture of the condenser, and $NA_{objective}$ is the numerical aperture of the microscope objective [93]. In fluorescence light microscopy the objective function as condenser, and the equation is reduced to:

$$d = \frac{\lambda}{2\ NA_{objective}} \qquad \text{Eq. 4-1}$$

(is the wavelength of the emitted light (wide-field), or the excitation light (confocal)). The resolution limit is on the order of 200-250 nm.

The intensity profile of the diffraction-limited spot (the point spread function) in 2D forms a so-called Airy pattern of which the center is the Airy disc that contains ~84 % of the total luminous intensity (Figure 4-2A). Hence, the image of a single molecule is well approximated as an Airy disc (especially considering that additional contribution from the Airy rings is often lost in background noise).

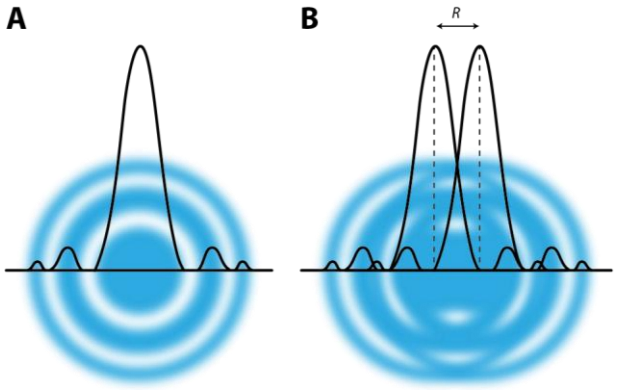

Figure 4-2: Airy disc pattern. A) The intensity profile of a diffraction limited spot forms an Airy pattern with the center spot containing 84 % of the total intensity. B) According to the Rayleigh criterion, two particles have to be separated by a distance larger than *R* in order to be resolved individually.

The profile of an Airy disc is well approximated by a 2D spatial Gaussian distribution [94, 95], $I \approx I_0 \exp\left(\frac{-r^2}{2w^2}\right)$, where I_0 is the intensity at the center of the disc, r is the distance from the center, and w is the standard deviation of the distribution which relates to radius of the Airy disc R given by:

$$R = \frac{0.61\,\lambda}{\mathrm{NA}_{\mathrm{objective}}} \qquad \text{Eq. 4-2}$$

According to the Rayleigh criterion, two single molecules can be resolved only if their Airy discs are separated by a distance larger than R (Figure 4-2B). Thus, in the case where the spatial separation of imaged single molecules exceeds the Rayleigh criterion it is possible to determine the center positions of the molecules very precisely by computational image analysis, and in this way obtain sub-diffraction-limited spatial information [17, 96].

4.4 Tracking procedures

In a SPT experiment, specific labeling is done at low labeling density for the particles' Airy discs not to overlap [14, 79, 97, 98]. Next, a time-lapse image series of the movement of the individual particles is recorded using video microscopy. The task is then to detect and localize particles in all frames, and to link the center positions of the localized particles between successive frames in order to be able to analyze the constructed molecular trajectories. In order for the detection, localization, and linking to be successful, relatively advances mathematical computer algorithms are required [12, 99-101].

The precision in the localization of a particle is strongly dependent on the signal-to-noise-ratio (SNR). Microscopy recordings have background signal from e.g. light scattering and cell auto-fluorescence, and a Poisson distributed noise component. These are added to the signal intensity profiles of the particles, and results in a non-ideal intensity profile making correct detection and localization more challenging (Figure 4-3A). Tracking algorithms therefore often include a global and frame-by-frame image restoration step that involves intensity normalization, local background subtraction, and camera noise correction [99, 100].

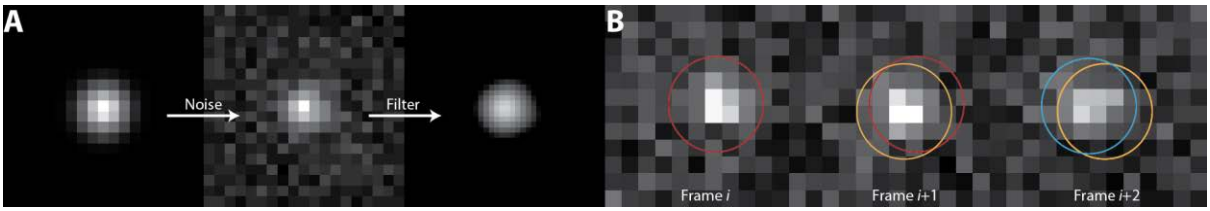

Figure 4-3: Localization and tracking. A) The intensity profile of a particle is distorted with background and noise in the sample, which can be filtered out by computational post-processing. The starting intensity profile is a Gaussian blob (left). This is superimposed with Poisson distributed noise (center). A wide Gaussian filter is used for background subtraction, while a narrow Gaussian filter is used for signal filtering (right). B) A particle is located in frame *i* (red circle, left). The tracking algorithm searches in frame *i*+1 (center) for a particle located within the specified distance of the particle located in frame *i*, and localizes it if found (orange circle). The procedure continues for successive frames (blue circle, right). (Partly adapted from [14].)

Particles are detected by doing a local maximum intensity search, which has as criterion that the detected spots constitute a certain fraction or percentile of the total image intensity [100], or have an intensity above a certain background threshold [99]. Identified spot regions are next used for an optimized sub-pixel localization of the peak center fitting the signal distribution to a Gaussian profile using e.g. a maximum likelihood approach [14].

Particles that correspond to each other in consecutive frames need to be recognized, and their positions connected. This can be done for each particle by searching in frame i+1 for a particle that is located within a specified radius of a particle localized in frame i (Figure 4-3B) [14]. The search radius will depend on the expected diffusion rate of the molecule, and the labeling density. If more than one particle or no particles are identified in frame i+1, the trajectory will be terminated. Alternative, the optimal way of connecting particles can be calculated using a statistical cost matrix that evaluates the cost associated with connecting any two particles between frames, and then minimizes the total cost of all possible connections [99, 100].

For high particle densities and for long recordings, the risk of trajectory crossover increases, and trajectory segments becomes shorter. Particles can disappear for a few frames, e.g. if they move out of focus, if the particles have the tendency to blink "on" and "off " (which particularly is an issue for QDs), or if particles merge or split. As longer trajectories are preferred over shorter trajectories, these phenomena can to some extent be accounted for in advanced tracking algorithms [99-101]. The search for a given particle can be continued for a specified number of frames if it disappears, and intensity information can be used to discriminate different particles [100]. Jaqaman et al. have made a tracking algorithm that minimizes a cost matrix that evaluates the global cost of merging, splitting and disappearing events [99]. The final result after having applied a tracking algorithm will be a file that contains particle positions for all particles connected between frames.

4.5 Membrane diffusion models

Plasma membrane molecules are mobile in the lateral dimension, and they constantly make random collisions. As a first approximation, one can assume the dominant type of motion to be free Brownian diffusion. In this case, Fick's law relates the time evolution of the probability density of a molecule's/particle's position $p(r, t)$ to its spatial profile [98]:

$$\frac{d}{dt}p(r,t) = D\nabla^2 p(r,t) \qquad \text{Eq. 4-3}$$

In this equation, D is the diffusion constant which is dependent on the thermal energy of the particle, the particle size, and the viscosity of the surrounding media. For a particle with radius of hydration, R_H, the diffusion constant in solution is given by the Stokes-Einstein equation, $D_{solution} = \frac{k_B T}{6\pi\ _{solution} R_H}$. Here, k_B is Boltzmann's constant, T is the absolute temperature, and $\mu_{solution}$ is the viscosity of the solution. Theoretical solutions for the translational diffusion constant for a particle embedded within a

two-dimensional membrane are more complex and different expressions exist [102-106]. For a homogeneous and continuous lipid bilayer an expression has been derived by Saffman and Delbrück [36]:

$$D_{membrane} = \frac{k_B T}{4\pi\ _{membrane}h}\left(\ln\left(\frac{_{membrane}h}{_{solution}R}\right) - \right) \quad \text{Eq. 4-4}$$

In this model the particle is approximated as being a hard cylinder with radius, R, and height, h, embedded within a membrane with the viscosity $_{membrane}$, and surrounded by aqueous phases with the viscosity $_{solution}$ on both sides, is Euler's constant (= 0.5772). The ratio $\frac{_{solution}}{_{membrane}}$ should be << 1, which is usually also the case because of the large viscosity difference between the membrane and the surrounding media.

The solution to Fick's Law for a particle diffusing freely in n dimensions and starting at origin at $t = 0$ is given by a Gaussian profile [98]:

$$p(r, t)dr = \frac{1}{(4\pi Dt)^{\frac{n}{2}}} \exp\left(\frac{-r^2}{4Dt}\right)dr \quad \text{Eq. 4-5}$$

The average position is the maximum of the Gaussian profile which is time independent and remains at the origin, $\langle r \rangle = 0$. The particle does, however, explore an increasingly larger area with time and the mean of the squared displacements (or mean squared displacement (MSD)) increases linearly with time according to $\langle r^2 \rangle = \text{MSD} = 2nDt$. For two-dimensional free diffusion in a membrane this equation is:

$$\text{MSD}_{\text{free}} = 4Dt \quad \text{Eq. 4-6}$$

As the diffusion of plasma membrane molecules in cells often experience restrictions to free diffusion due to molecular crowding, molecular clusters and domains, and other barriers, or obstacles, the apparent diffusion constant is often found to be time-dependent. In a general case where nothing is assumed about the nature of the obstacles, the diffusion is said to be anomalous, and the MSD is described by [11]:

$$\text{MSD}_{\text{anomalous}} = 4\ D\ t^{\alpha},\ 0<\alpha < 1 \quad \text{Eq. 4-7}$$

As the reasons for the anomaly can be many, the exponent α has no clear physical meaning [25], but it is loosely said to reflect the deviation from free Brownian diffusion ($\alpha = 1$ for Brownian diffusion). At short times, anomalous diffusion resembles free diffusion, but at larger times the diffusion appears slower and the apparent diffusion constant goes as $D_{apparent} \propto t^{\alpha-1}$.

The probability density functions have been derived or approximated for specific two-dimensional diffusion cases such as confined diffusion with both impermeable and permeable barriers, and they are much more complicated than the one for free diffusion [98]. The MSD for confined diffusion with impermeable barriers never exceeds the dimension of the confinement, and the can be given by [97]:

$$\mathrm{MSD}_{\mathrm{confined}} \approx \frac{L^2}{3}\left(1 - \exp\left[-\frac{12Dt}{L^2}\right]\right) \qquad \text{Eq. 4-8}$$

Here L^2 is the size of the confined area. If the confinement has permeable barriers the MSD has been approximated to [98, 107]:

$$\mathrm{MSD}_{\mathrm{confined,\,permeable}} = \alpha\left\{\frac{\alpha L^2}{3} - \frac{32\alpha L^2}{\pi^4}\sum_{n=1\,(\mathrm{odd})}^{\infty}\frac{1}{n^4}\exp\left[-\frac{(n\pi)^2}{\alpha L^2}Dt\right]\right\} + 4(1-\alpha)Dt \qquad \text{Eq. 4-9}$$

On a short time scale the diffusion is free with diffusion constant $D_{micro} = D$, whereas on a longer time scale the diffusion is again free, but with reduced diffusion coefficient $D_{macro} = (1-\alpha)\,D$.

4.6 Trajectory analysis

The most common way to analyze SPT data is by calculating MSD-values [11, 14, 97]. This can be done either independently for each detected single molecule trajectory, or in the case where the single molecules trajectories are very short, as an average for all trajectories. The MSD, for a single trajectory that has a total of N image frames each separated by a time-lag t_{lag}, is calculated at different time points $t = nt_{lag}$, where n is image frame number, using [97]:

$$\mathrm{MSD}(nt_{lag}) = \frac{1}{N-n}\sum_{i=1}^{N-n}\left(r\left((i+n)t_{lag}\right) - r(it_{lag})\right)^2 \qquad \text{Eq. 4-10}$$

To analyze the MSD, it is useful to plot the MSD as a function of time and evaluate the shape of the curve. Free diffusion will give a straight line, anomalous diffusion will result in a slope with negative curve, and confined diffusion will give a graph that levels of at an area proportional to the confinement (Figure 4-4).

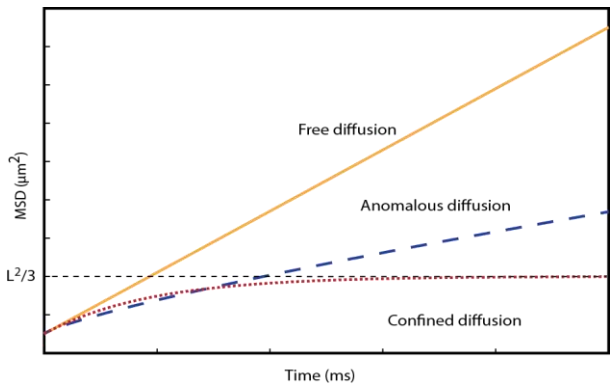

Figure 4-4: Plot of MSD vs. time. In a plot of the MSD vs. time, free diffusion will results in a straight line (full orange line), anomalous diffusion will result in a line with a negative curve (hatched blue line), while confined diffusion will result in a curve, which levels of a MSD proportional to the confinement size (dotted red line).

The calculated MSD can be fitted to any of Eq. 4-6 – Eq. 4-9 given above in order to classify the mode of motion. The fit should include a constant offset value that has to do with the positional localization error, e.g. $\mathrm{MSD} = 4Dt + c$. The localization error in x and y (σ_{xy}) results in trajectories that are distorted from the real

trajectories. The average virtual distance to each real position is $\sigma = \frac{\sigma_{xy}}{\sqrt{2}}$, and if the errors are normal distributed, the new MSD is increased by MSD = 4 D_{fit} nt_{lag} + 4σ_{xy}^2. If the localization error is not accounted for in the analysis, this might lead to a misinterpretation of the data concluding that free diffusion is anomalous diffusion [98].

Another effect that needs to be accounted for is movement during illumination [14, 108]. The illumination time t_{ill} is finite and as the particles move during illumination and emit photons along the way, this has the consequence that an average position during the illumination is recorded. The movement might alter the profile of the point-spread function if the molecules move further than the Airy disc radius. For instance, if a molecule has D = 1 μm²/s, and t_{ill} = 30 ms, the average distances moved is $\sqrt{\text{MSD}} \approx$ 350 nm, which is close to the diffraction-limited spot size. Effectively the movement during illumination reduces the MSD, as the particle already has moved closer to the next position recorded. The reduction in MSD for free diffusion is given by $\text{MSD}_{\text{effective}} = 4\,D\,t - \frac{4}{3}\,D\,t_{ill}$. The effect is even bigger if the diffusion is confined [14, 17], as the recorded position will always be shifted towards the center of the confinement. This can lead to a dramatic underestimation of the confinement area and the diffusion constant. Schultz et al. calculated the reduction for a molecule moving within a 100 nm domain with D = 1 μm²/s, and t_{ill} = 30 ms, to be a factor of 3.5 [14].

Because diffusion is a stochastic process no matter the nature of any possible restrictions to free diffusion, it is non-trivial to choose the diffusion model that describes the data best. Pure Brownian motion will often be better described by e.g. anomalous diffusion, or directed diffusion [11, 99, 109-111].

A method often used to fit SPT data is to assume that the particles are free to move at short time-scales, and then only fit the first few time points in the MSD [81]. In this way a diffusion constant is obtained, which is independent of the influence of barriers or other obstacles in the plasma membrane.

An alternative way to analyze SPT data is to analyze the step-size distribution of the particles [14, 112]. For free diffusion the step-size distribution is a Rayleigh distribution, and the cumulative probability of finding a squared displacement smaller than r^2 is given by $P = 1 - \exp\left(-\frac{r^2}{4Dt}\right)$. If a population contains two subpopulations with diffusion coefficients D_1 and D_2, respectively, with relative proportions β and (1- β), these can be found by:

$$\text{P} = 1-\beta\,\exp\left(-\frac{r^2}{4D_1 t}\right) - (1-\beta)\exp\left(-\frac{r^2}{4D_2 t}\right) \qquad \text{Eq. 4-11}$$

The squared displacements can also be analyzed without construction of trajectories. Schmidt et al. showed that single molecule positions can be correlated directly between frames [113]. Recently, Schutz and co-workers developed an analytical method, which has the advantage that it statistically compares a computer-simulated outcome of diffusion according to a specific diffusion model with experimental, data where the diffusion type in unknown [114].

5 Quantum dots

Quantum dots (QDs) are fluorescent nano-particles demonstrating unique optical properties that make them ideal for single particle tracking (SPT) applications. In particular, QDs have spectral properties that favor multi-color applications, and they are extremely bright, which enables imaging on fast time-scales, and for long periods of time.

5.1 Basic composition and origin of fluorescence

QDs are inorganic nanometer-sized crystals composed of semiconductor material and displaying fluorescent properties [19, 115, 116]. They are characterized by having physical dimensions smaller than the so-called Bohr exciton radius. In a semiconductor, an electron in the valence band can absorb a photon and become excited to a higher energy state in the conduction band leaving behind a positive hole in the valence band. The electron-hole pair is called an exciton. The Coulomb attraction between the electron and the hole keeps them together, and the electron orbits the hole with a characteristic exciton Bohr radius. When the exciton recombines a photon with an energy corresponding to the band gap energy (the minimum difference in energy between the valence- and conduction bands) is emitted. For a semiconductor crystal with a size smaller than the exciton Bohr radius, the exciton experiences quantum confinement effects, there is confinement energy and the energy states shift to higher levels [19, 117-120]. As a result, the band gap energy increases and the energy of an emitted photon increase. The practical and useful consequence of this is that by controlling QD sizes, the color of the emission light is controlled; smaller QDs are blue-shifted (for a given semiconductor material) (Figure 5-1).

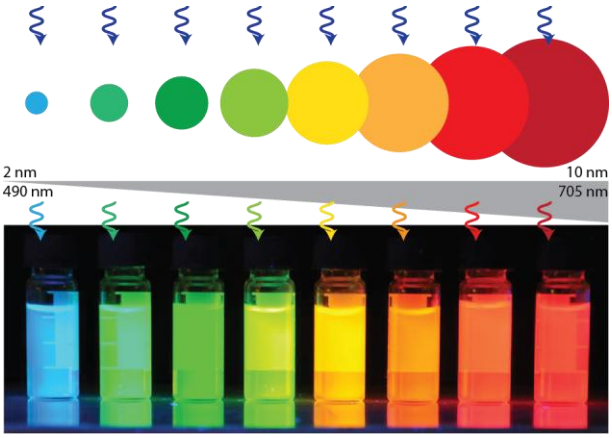

Figure 5-1: QD size dependent emission. QDs of different sizes emit light of different wavelengths spanning the whole visible range (same excitation wavelength). (Photo provided by Thomas E. Rasmussen.)

For biological applications, the most commonly used QDs are composed of cadmium selenide (CdSe), which have sizes of 2-10 nm corresponding to crystals containing ~200-25,000 atoms [19, 120-122] (Figure 5-2). These CdSe QDs emit light in the visible range (~450-660 nm), whereas cadmium telluride (CdTe), which are also used for biological applications, can be synthesized to emit in the far red (<805 nm). These "core-only" QDs are not very effective fluorescent emitters, since they have unbound bonds on the surfaces that can trap an electron or a hole, preventing their recombination and the emission of light. Therefore, a thin shell of a few nanometers of another semiconductor material with higher band gap energy is grown on top of the core to cap those free bonds [123-125]. The exciton is not allowed energetically to enter the shell material, and it has to recombine in the core and emit light. However, the most commonly used shell material for CdSe QDs, zinc sulfide (ZnS), has a crystal lattice mismatch of 12 % (the distance between the crystal structure bonds has an offset of 12 %) compared to CdSe. This results in imperfect shell growth during synthesis, the ZnS will cover only a fraction of the core surface area, and further shell growth will continue from the initial patches of ZnS [126, 127]. By mixing in Cd atoms during shell growth this problem is solved yielding nearly 100 % efficient fluorescent emitters [128, 129]. The QDs developed by Quantum Dot Corporation, sold by Invitrogen, and used in this study, are prepared in this way [19].

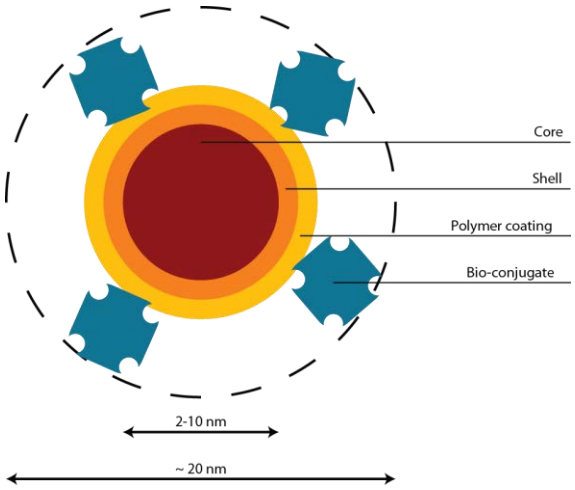

Figure 5-2: QD composition. QDs are composed of a semiconductor core of size 2-10 nm (typically CdSe). The core is surrounded by a thin shell of another semiconductor material (typically ZnS). The QD is further coated by an amphiphilic polymer (e.g. octylamine-modified polyacrylic acids), which can be functionalized with different bio-conjugates (e.g. StreptAvidin (SAv)) to give a total size of ~20 nm.

"Core-shell" QDs are synthesized in organic solvent and end up having organic capping ligands bound to their surfaces e.g. trioctylphosphine oxide (TOPO) [115, 116]. Several strategies exist in order to make QDs water soluble for biological relevant applications [18, 115, 116, 130, 131]. Keeping the original capping ligands in place gives the brightest QDs, and one way to do this is to use an amphiphilic co-block polymer, e.g. an octylamine-modified polyacrylic acid to coat the QDs [131]. The hydrophobic side chains of these polymers interdigitate with the organic ligands on the core-shell QDs, and the hydrophilic part constitutes the new surface of the now water soluble QDs, adding another 1-2 nm to their diameters [19, 132]. AMP Qdots® sold by Invitrogen are synthesized using amphiphilic co-block polymers. The hydrophilic ends of these QDs have reactive groups that are available for further bio-conjugation needed in order to direct the QD binding towards a specific target. Bio-conjugation of the QD will add to its final size, and typical bio-functional QDs have a size of ~20 nm.

5.2 Optical properties

The photo-physical properties of QDs are what make them unique. In particular, they are distinguished by; i) having broad absorption spectra, yet narrow and tunable emission spectra, ii) being photo-chemically stable and resistant to photo-bleaching, and iii) having very large absorption extinction coefficients and high fluorescence quantum yields making them exceptionally bright [133]. Since the valence band of semiconductors spans a broad range of energies, QDs can absorb light in a broad range of excitation wavelengths shorter than the emission wavelength. The absorption spectra of QDs of different colors are overlapping. The emission spectra are narrow and symmetric and they have no "red tail" as many organic dyes do (Figure 5-3). The full width at half maximum of QDs emitting at 655 nm (655QDs) is 29 nm, and 63 nm at 10 % of maximum, compared to 38 nm and 92 nm for the typically used dye Alexa 488. The width of the QD emission spectrum is partly due to

the spectral width of single QDs, and partly to a slight size variation (<10 %) of the QDs during synthesis [121, 134].

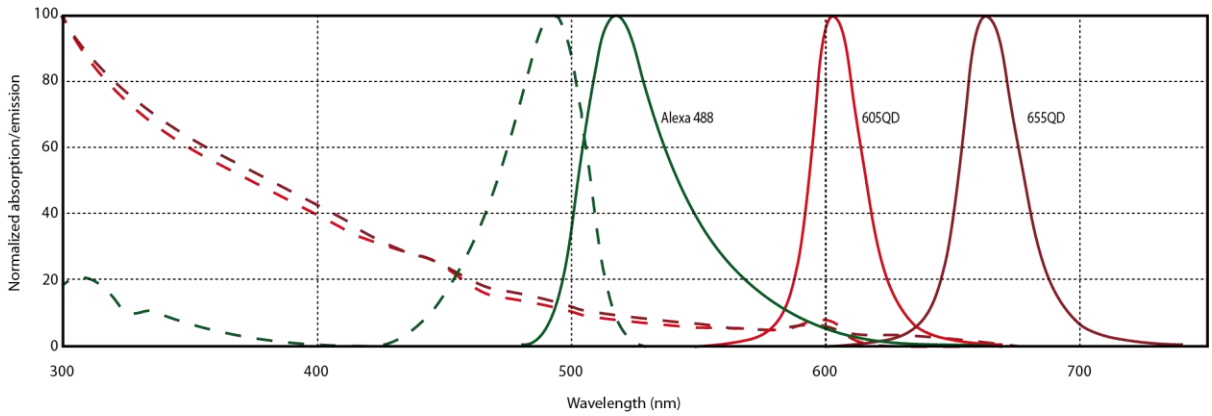

Figure 5-3: Fluorescence absorption and emission spectra. 605QDs and 655QDs have broad overlapping absorption (hatched red and dark red lines) and narrow emission (red and dark red lines). Dyes (here represented by Alexa 488) have narrow absorption spectra (green hatched line) with peak absorption close to the peak emission (green line). The dye emission spectrum has a "red tail". (Remade from SpectraViewer.)

Combined, the broad (and overlapping) absorption of different QDs that allows for excitation of multiple colors with the same excitation color, and the narrow emission spectra that facilitate detector channel separation, makes QDs ideal for multi-color applications [18, 135]. For dye excitation, multiple excitation channels are needed, and the emission colors need to be well separated to reduce color channel cross-talk. The spectra of QDs further allows for excitation far from the emission (large Stokes shift, typically > 100 nm), which makes it easier to filter out emission light, and minimizes auto-fluorescence signal. The Stokes shift of common organic dyes are 10-30 nm [118].

The inorganic nature of QDs makes them very stable as fluorescent emitters. They are resistant to photo-bleaching and can in bulk be imaged continuously for a long time without loss of intensity [131]. Studies have, however, shown that QDs start to blue-shift within minutes of continuous illumination [136, 137]. This change of color is undesirable especially for multi-color applications, but can be delayed by using small amounts of reducing agents during imaging. Compared to organic dyes, QDs are considered very robust and single QD imaging over at least several minutes is possible.

The QD extinction coefficients (ε) are at least an order of magnitude larger than even bright dyes. 655QDs have ε = 2,900,000 $M^{-1}cm^{-1}$ at 488 nm compared to e.g. ε = 80,000 $M^{-1}cm^{-1}$ for Alexa 488, $\varepsilon \approx$ 120,000 $M^{-1}cm^{-1}$ for most ATTO-dyes, and ε = 250,000 $M^{-1}cm^{-1}$ for Cy5, and much higher at shorter wavelengths. Combined with a quantum yield of close to 100 % this constitutes very bright fluorescent emitters that further can be modified without loss of intensity [133]. The brightness of QDs and the low auto-fluorescence background favors the detection of single QDs because of the high signal-to-noise-ratio (SNR). This practically means that the illumination light intensity can be lowered to minimize photo-damage, which is important for living specimens.

It also allows for very short image integration times such that biological processes happening on a short time-scale can be accessed. Not all QDs are equally bright, the intensity is color-dependent in the following manner for the Invitrogen Qdots®; 625QD ≈ 655QD > 605QD ≈ 705QD > 565QD ≈ 585QD ≈ 800QD > 525QD [138].

A challenge in using QDs for certain applications including SPT is the photo-luminescence intermittency exhibited by single crystals known as blinking [136, 139, 140]. QDs alternate between a bright "on"- and a dark "off"-state on all time scales [141]. The reason for this blinking is not fully understood, but is believed to be caused by trapping of a charge on the QD core surface resulting in enhancement of non-radiative recombination of the exciton [142]. The "on-off-ratio" is ~80 % for the CdSe QDs, and ~20 % for the CdSe/CdTe QDs, and is improved by adding a reducing agent during imaging [138]. QDs with reduced blinking have been synthesized by increasing the thickness of the shell and by using surface ligands [143-145]. Smaller non-blinking continuous emitting CdZnSe-ZnSe core-shell QDs have also been synthesized, but these QDs have three distinctive emission peaks making them unsuitable for multi-color applications [146]. The blinking of QDs can be used to ensure observation of individual crystals [147], but for SPT applications, the linking between consecutive frames becomes more demanding [97, 99, 101]. The fluorescence lifetime of QDs is ~20-40 ns, which is much longer than common organic dyes [148].

5.3 Bio-conjugation

As mentioned above, QDs have reactive chemical groups on their surfaces that are available for bio-functionalization necessary in order to direct the QDs towards a specific target in biological applications [18]. Often, the starting chemical groups on the surface are carboxylic groups, but these can be reacted with e.g. diamine polyethylene glycols (PEG) resulting in amino functionalized QDs, e.g. the Qdot® amino (PEG) sold by Invitrogen. Covalent bio-functionalization of carboxylic or amine QDs is easily achieved by cross-linkers, and various strategies exist depending on the conjugation partners (Figure 5-4A) [19, 149]. For example, 1-ethyl-3-(3-dimethylaminopropyl)carbodiimide (EDC) can be used to conjugate carboxylic groups on QDs to amine groups in e.g. proteins or peptides [150, 151]. The bi-functional cross-linker succinimidyl-4-(*N*-maleinidomethyl)cyclohexane-1-carboxylate (SMCC), which has a maleimide reactive group and an NHS ester, can be used to couple thiols on e.g. mildly and selectively reduced antibodies or antibody fragments, or small bio-molecules to amines on QDs [152, 153]. QD conjugation of two amine groups has been done using Traut's reagent and SIA [19]. Often a linker such as PEG is introduced between the QD and the bio-molecule to increase steric freedom, and to minimize unspecific binding of the QDs [154].

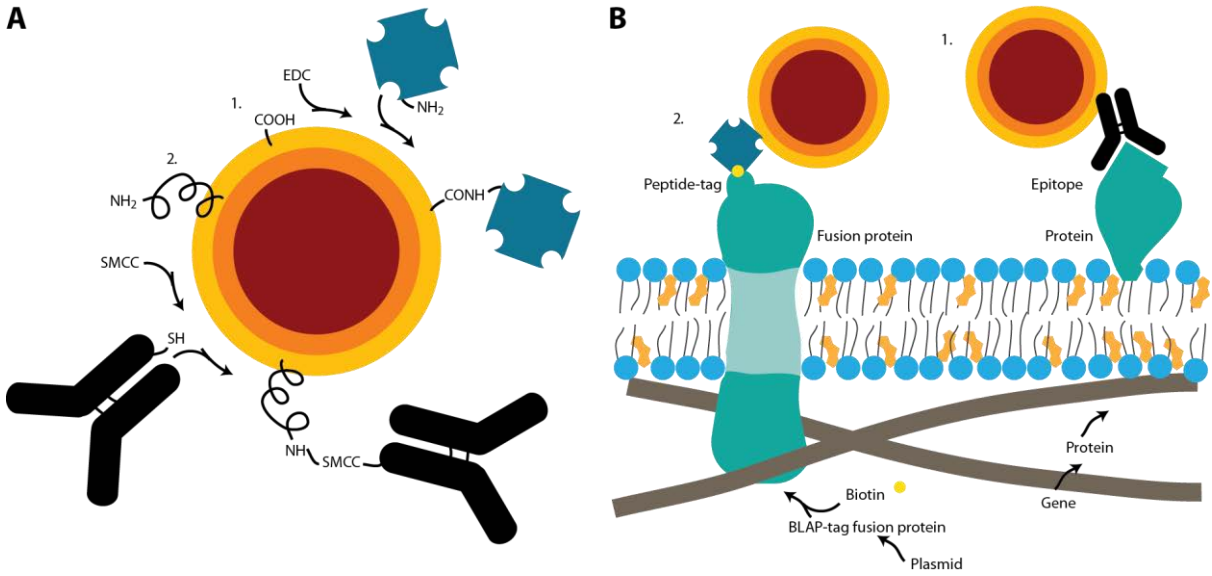

Figure 5-4: QD conjugation and targeting. A) Examples of QD conjugation. 1. A carboxylic acid on the QD surface is coupled to an anime on a protein using EDC. 2. A PEG-amino group on the QD surface is coupled to an antibody sulfhydryl group using the cross-linker SMCC. B) Examples of targeting strategies. 1. A QD bio-molecule conjugate targets a natural occurring epitope on a protein (or lipid, not shown), e.g. antibody-QD-epitope, or CTB-QD-G_{M1}. 2. A QD bio-molecule conjugate targets an artificially peptide-tagged fusion protein, e.g. SAv-QD-biotin-BLAP, or CoAQD-ACP.

5.4 Bio-molecular targeting systems

Bio-molecules with specific binding partners in cells can be classified into two categories; those that have affinities for naturally occurring targets (e.g. antibodies, antibody fragments, ligands, peptides, and certain toxins (e.g. Cholera Toxin subunit B (CTB))), and those that need insertion of a high-affinity peptide or protein epitope tag, or a chemical modification in the target molecule in order to introduce specific binding (e.g. StreptAvidin (SAv) and Co enzyme A (CoA)) (Figure 5-4B) [7, 155]. In the first category, antibodies are an obvious choice, and binding is achieved either by direct conjugation to the QD, or via antibody biotinylation and binding to SAv-QDs [92, 152]. Ligands and peptides can be used to study e.g. receptor movement during signaling events or endocytosis [88]. CTB-QDs have been prepared [151], CTB, which is the 58 kDa pentavalent non-toxic subunit B of cholera toxin, targets the naturally occurring ganglioside G_{M1} present in plasma membranes of many cells. Availability and purity of a given bio-conjugate with natural targets can be a problem. The binding is always non-covalent, and the binding affinity between the bio-conjugate and its target might not be sufficient or strong. A weak binding is generally undesirable, not least in SPT measurements. This therefore favors use of artificial high-affinity tags.

The epitope tags are often introduced via genetic insertion of a specific DNA sequence e.g. biotin ligase acceptor peptide (BLAP) for SAv [156], Acyl Carrier Protein (ACP) for CoA derivatives [157], SNAP-tag for benzylguanine derivatives [158], CLIP-tag for benzylcytosine derivatives [159], tetra-cysteine peptide motifs for the biarsenical derivatives FlAsH and ReAsH [160], and HaloTag for chloroalkane ligands [161], and can be either covalent or non-covalent [162, 163]. The BLAP tag is a 15 amino acid tag (GLNDIFEAQKIEWHE)

that can be fused to the N- or C-terminal of a protein [156, 164]. The peptide can then be biotinylated at the indicated lysine by bacterial biotin ligase (BirA) followed by incubation with SAv-QDs. BirA can be co-expressed in cells and directed to the endoplasmic reticulum, so plasma membrane target molecules are biotinylated during their secretory pathway if grown in presence of biotin [164]. SAv-QDs are commercially available. SAv is a tetravalent 56 kDa protein, which non-covalently binds the 244 Da vitamin B_7 biotin with very high affinity. CoA derivatives can be covalently attached to the ACP-tag under the action of a phosphopantetheine transferase, e.g. ACP Synthase. ACP is a 77 amino acid (8 kDa) polypeptide tag, which can be expressed with any protein. The ACP tag contains a conserved serine residue, to which the substituted phosphopantetheine group of the 811 Da CoA and CoA derivatives can be covalently linked [153]. CoA derivatives have also been shown to bind peptide tags only 12 amino acids long [165, 166]. Addition of genetic modifications may alter protein function, and requires transfection of cells, which typically leads to protein expression at non-physiological levels [167].

5.5 Limitations

There are certain limitations for the use of QDs. One of them already mentioned is blinking, and two others are multi-valence and their size. Multivalent QDs can cause cross-linking of target molecules, and activate signaling pathways and induce endocytosis [11]. When functionalizing QDs, multiple binding sites are available per QD, which is the cause of multivalent probes. Hence, even reaction conditions that strongly favor no conjugation of a given bio-molecule to the QDs will result in a population of multivalent QDs, e.g. a 2:1 molar ratio of bio-conjugate to QD would result in 60 % QDs with no conjugation, 30 % with one bio-molecule attached, 8 % with two, and 2 % with three or more attached bio-molecules. Preparation of monovalent QDs thus requires a purification step capable of separating those QDs that have only one bio-molecule from the rest. This has been accomplished by gel separation of QDs, which have been reacted with SAv [168-170], CTB [151], antibodies [171], or PEG polymers [172]. However, the attached bio-molecules in some cases, e.g. for antibodies, SAv, and CTB have multiple target molecule binding sites, and can by themselves induce unintended cross-linking. Using antibody Fab fragments, or engineered monovalent SAv with three genetically altered “dead” nonbinding subunits, and a single “alive” binding subunit [169] is a way to circumvent this issue. Commercial SAv-QDs have according to the specifications 5-10 SAv per QD, but the they have been reported to have between 2-80 biotin binding sites per QD depending on the color, and coating of the SAv-QD [173].

The final size of bio-functionalized QDs is ~20 nm in diameter [83]. Whereas this theoretically is not a big issue when it comes to frictional drag of a membrane target molecule, or in a flat planar membrane [91], it can be an issue for SPT in cells. A big probe will experience steric hindrance, and this can result in that only a subset of the target molecules is accessible for labeling because of e.g. a dense extracellular matrix, molecular crowding or membrane topology [41]. Access to synaptic gaps has been shown to be limited [174]. Smaller QDs are being prepared, but challenging to make them as stable and bright [19].

6 Stimulated emission depletion – fluorescence correlation spectroscopy

In fluorescence correlation spectroscopy (FCS), intensity bursts from fluorescently labeled molecules moving in and out of a stationary focal spot are measured, and the fluctuations are auto-correlated in time. Information on molecular diffusion dynamics on a microsecond time-scale can be accessed with FCS, and when combined with stimulated emission depletion (STED) illumination, a high spatial resolution is achievable as well. In this way, STED-FCS can be used to decipher different types of motion in the plasma membrane, and reveal the effects of the membrane structure on the dynamics in the membrane.

6.1 Fluorescence correlation spectroscopy

In an FCS experiment, an excitation laser is focused on a sample labeled with a dilute concentration of fluorescent molecules [175-177]. As the fluorescent molecules move though the focal spot, they will be excited and emit photons (Figure 6-1A). This gives rise to signal intensity bursts that are detected, and recorded as a function of time (Figure 6-1B). The amplitudes of the intensity bursts are proportional to the brightness of the molecules, and the number of fluorescent molecules in the focal spot. The widths of the bursts directly reflect the time it takes the molecules to transit through the focal spot, which depends on e.g. the area of the focal spot and the diffusion of the molecules. In a recorded intensity burst time trace, the signal intensity will fluctuate around an average intensity value. The deviations from this average value can be correlated to find the average number of fluorescent molecules in the focal spot, and their average transit time, τ_D.

Mathematically, the fluorescence intensity from a spot of a sample can be described as [178]:

$$F(t) = \langle F(t) \rangle + \delta F(t) \qquad \text{Eq. 6-1}$$

Here $\langle F(t) \rangle$ denotes the mean fluorescence intensity, and $\delta F(t)$ describes the fluctuations of the intensity around this mean value. The mean value of the fluctuations vanishes over time:

$$\langle \delta F(t) \rangle = 0 \qquad \text{Eq. 6-2}$$

The fluorescence intensity depends on a number of factors, and can be written as:

$$F(t) = Q \int \mathrm{d}r W(r) C(r, t) \qquad \text{Eq. 6-3}$$

is the detector sensitivity, Q the fluorophore quantum yield, $W(r)$ describes the illumination profile, and $C(r,t)$ is a function of the fluorophore concentration over time.

One can write the fluorescence auto-correlation as a function of a time-lag as:

$$g(t) = \langle F(t+)F(t)\rangle \qquad \text{Eq. 6-4}$$

Using Eq. 6-1 and Eq. 6-2, one gets:

$$g(t) = \langle F(t)\rangle^2 + \langle F(t+)F(t)\rangle \qquad \text{Eq. 6-5}$$

Eq. 6-5 can be re-written as:

$$G( ) = \frac{g( )}{\langle F(t)\rangle^2} - 1 = \frac{\langle F(t)\ F(t+)\rangle}{\langle F(t)\rangle^2} \qquad \text{Eq. 6-6}$$

Writing the auto-correlation in this way, ensures that the correlation function decays to zero for large . can vary from microseconds to seconds, and as a result, information over a wide range of temporal scales is accessible. The auto-correlation function compares the fluorescence intensity of a time point t with a later time point $t +$. For short time lags ($< \tau_D$), a molecule found in the focal spot at time t is also likely to reside within the spot at a later time $t +$, and the correlation is strong. For longer time lags ($> \tau_D$), the intensity at time $t +$, is on average not correlated to the intensity at time t because the molecules diffuse independent of each other.

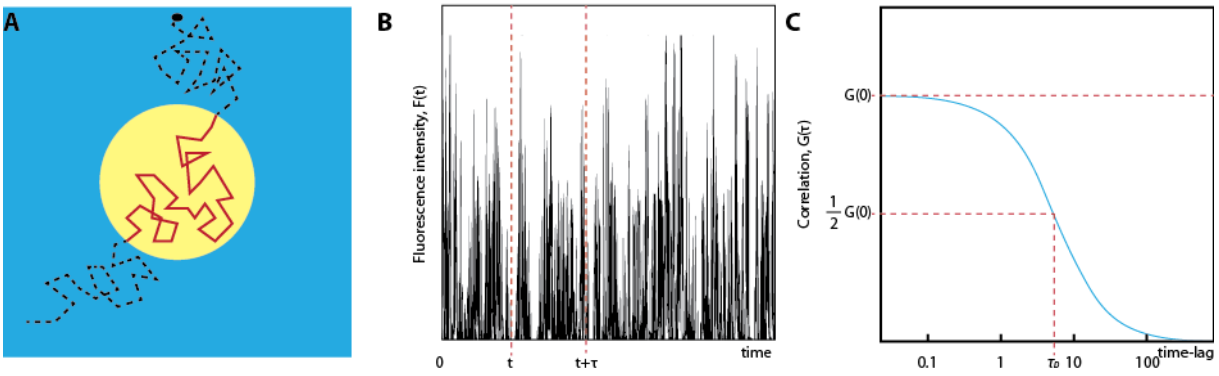

Figure 6-1: Fluorescence correlation spectroscopy. A) Schematic of a molecule moving through the FCS focal spot. Only while in the focal spot, the molecule will emit light (red line). B) The fluorescence intensity bursts are recorded as a function of time. C) The intensity fluctuations are auto-correlated. From the auto-correlation curve, the τ_D and $\langle N\rangle$ can be found.

A typical correlation curve is shown in Figure 6-1C. From this curve, as the fluctuations follow Poisson statistics, the average number of molecules in the focal spot, $\langle N\rangle$, can be estimated from the correlation

amplitude, $= 0, G(0) \propto \frac{1}{\langle N \rangle}$. The average transit time, τ_D, can be approximated by the point where the correlation amplitude has dropped to half its initial value, $\frac{1}{2}G(0) = {}_D$. More accurate determination of $\langle N \rangle$ and τ_D requires theoretical models, which describes the correlation function [179]. The illumination profile is often assumed Gaussian.

If assumed that the fluctuations in fluorescence intensity are caused by variations in the concentration of fluorescent molecules due to diffusion of the molecules, and chemical processes such as triplet state formation, the correlation curve can be written as [10]:

$$G(\ ) = \frac{1}{N} G_D(\ ) G_T(\ ) G_K(\ ) \qquad \text{Eq. 6-7}$$

$G_D(\ )$ and $G_T(\ )$ are the contributions to the correlation due to diffusion, and triplet state formation, respectively. $G_K(\ )$ includes other dye-related kinetic processes such as conformational changes, or chemical binding processes, which change the fluorescence brightness of the molecules [180].

For two-dimensional Brownian diffusion with translational diffusion constant D, the correlation term is given by [181]:

$$G_D(\ ) = \left(1 + \frac{\tau}{\tau_D}\right)^{-1} \qquad \text{Eq. 6-8}$$

The diffusion time $\tau_D = {}^{free}_{D} = \frac{w^2}{4D}$ is the average time it takes a freely moving molecules to traverse the Gaussian focal spot. w^2 is the focal beam waist.

For triplet state formation, the contribution to the correlation is given by [181, 182]:

$$G_T(\ ) = \frac{T}{1-T} \exp\left(-\frac{}{T}\right) \qquad \text{Eq. 6-9}$$

T is the fraction of molecules in the triplet state, and τ_T the triplet state life time. The triplet state contribution is fluorophore and excitation intensity dependent.

Additional fluorescence related kinetics processes contribute to the correlation according to:

$$G_T(\ ) = K \exp\left(-\frac{}{K}\right) \qquad \text{Eq. 6-10}$$

K is the amplitude of the kinetic processes, and τ_K is the characteristic life-time. Possible explanations for this kinetic term are either an additional dark state of the fluorophore or conformational fluctuations of the dye.

If molecules follow two-dimensional anomalous diffusion with anomaly factor α, the diffusion contribution to the correlation function is given by [183, 184]:

$$G_D(\ ) = \left(1 + \left(\frac{\tau}{\tau_D}\right)^{\alpha}\right)^{-1},\ 0 < \alpha \leq 1 \qquad \text{Eq. 6-11}$$

The average diffusion time of the constrained molecules following anomalous diffusion is $_D = {}^{anomalous}_{D} = \frac{w^2}{4D_{apparent}}$. This diffusion time equals the average diffusion time of a corresponding freely moving molecule having the apparent diffusion constant $D_{apparent}$ smaller than its real diffusion constant.

FCS using a single focal spot and following a single type of fluorescent molecule has been used to study membrane dynamics in both model membranes and live cells [24, 78, 183, 185]. FCS has further been extended in different directions [186] to e.g. cross-correlation FCS [187], two-focus FCS [188, 189], and scanning FCS [190, 191]. This enables determination of interactions between different membrane species, an improved accuracy in determining the diffusion constant, and the possibility to obtain information on diffusion in a large area, respectively.

6.2 Spot-variation FCS

In FCS, the only parameter that gives information of the diffusion dynamics of the observed molecules is the focal diffusion time. From this alone it is difficult to conclude anything about the type of diffusion. For instance, a long diffusion time could be caused by slow Brownian diffusion through the focal spot, or alternatively it could be a result of either the molecules being trapped in membrane domains, or the molecules being restricted by barriers they need to cross as they pass through the focal spot. To decipher between such different kinds of diffusion, Marguet and He introduced spot-variation (sv)FCS, where the diffusion times are recorded for different sizes of focal spots larger than the diffraction-limited focal spot (typically in the range of 200-400 nm) [75, 192]. The diffusion times for different types of diffusion will according to the so-called FCS diffusion law depend on the focal area in different ways. From a plot of τ_D vs. w^2 the underlying mode of diffusion can hence be inferred (Figure 6-2).

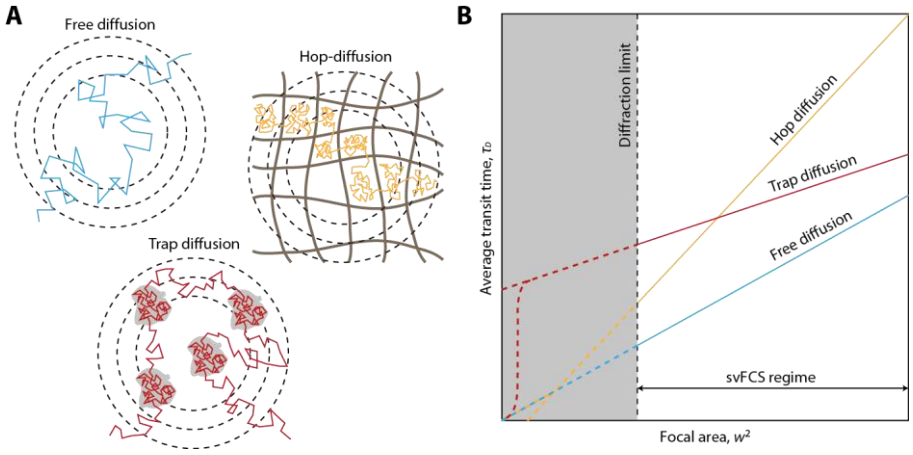

Figure 6-2: FCS diffusion law. A) Schematic of different diffusion types in varying FCS focal spot sizes: free diffusion (blue), trapped diffusion (red), and hop-diffusion (yellow). B) Average diffusion times, $_D$, as a function of focal areas, w^2, plotted for the three types of diffusion shown in A. All three types of diffusion will give a linear dependence between $_D$ and w^2, but the slopes and extrapolated intercepts with the axes are different: *i*) free diffusion will have a slope proportional to the inverse of the diffusion constant, and an intercept with the $_D$-axis in the origin, *ii*) trap diffusion will have a gentler slope compared to free diffusion, and a positive intercept with the $_D$-axis, while *iii*) hop-diffusion will give a steeper slope compared to free diffusion, and a negative intercepts with the $_D$-axis. Note that svFCS measures the transit time for focal spots larger than the diffraction barrier. Below the diffraction barrier, the diffusion times for trap- and hop-diffusion will when the focal spot becomes smaller than the trapping domain, and compartment, respectively, converge to that for free diffusion. (Adapted from [75, 192].)

The FCS diffusion law states that [192, 193]; if molecules diffuse freely, the transit time only depends on the time it takes the molecule to diffuse through the focal spot. This time is given in Eq. 6-8, and is directly proportional to the focal area. The slope is proportional to the inverse of the diffusion constant, and its extrapolation to focal spots below the resolution limit will go through the origin. If molecules are trapped in domains smaller that the focal spot, the total time it takes to traverse the focal spot is a combination of the diffusion time and the characteristic trapping time of the molecules in the domains [194]. The diffusion time will increase linearly with increased focal area, while the trapping time remains constant, and the slope in the τ_D vs. w^2 plot will therefore be less steep as compared to the slope for free diffusion. The extrapolation of the slope below the diffraction limit will have a positive intercept with the τ_D-axis. If molecules are restricted by barriers defining compartments smaller than the focal spot, and these barriers are crossed with a certain probability (as described for hop-diffusion), the slope in the τ_D vs. w^2 plot will be steeper than for free diffusion as the molecules have to cross more barriers when they passage through an increased focal spot. The extrapolation of the slope will have a negative intercept with the τ_D-axis. True for both the case of molecules being trapped in domains, and the case of the molecules being restricted to compartments, the diffusion times will converge to that of free diffusion when the focal spot is below the size of the domain or confinement.

svFCS has used to show cholesterol dependent transient trapping of GPI-anchored proteins in the plasma membrane, and cytoskeleton dependent hop-diffusion for transmembrane proteins [75, 193].

6.3 Combining FCS with stimulation emission depletion

Even though FCS has been usefully applied to study membrane organization and dynamics, the method is limited by the ability to focus light to a limited spot size; it is limited by the diffraction of light. Information below the diffraction of light can be indirectly inferred by extrapolation, yet it is preferable to directly access sub-diffraction limited resolution to gain a better understanding of the plasma membrane nano-scale heterogeneities. By combining FCS with the super-resolution method stimulated emission depletion (STED), Eggeling et al. showed that this is possible [10].

In STED, sub-diffraction limited spatial resolution is achieved by controlling the physical properties of fluorescent dyes. When a dye absorbs a photon, an electron is excited from its ground state S_0 to the first excited state S_1 (Figure 6-3A). After a certain time, the fluorescence lifetime, the electron returns to the ground state via spontaneous emission of a red-shifted photon. Spontaneous emission of a photon can be outcompeted by inducing stimulation emission. In stimulated emission, an incoming photon de-excites the electron from S_1 to S_0, while a second photon with the same energy and wavelength of the incoming light is emitted. This means that the fluorescence effectively can be depleted by stimulated emission, as the light emitted can be filtered from the fluorescence light using optical filters. It also means that information below the diffraction limit can be accessed [195].

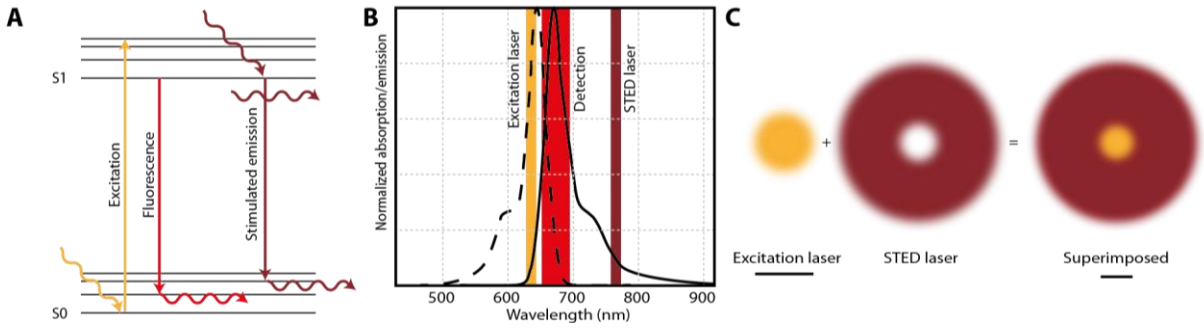

Figure 6-3: Fluorescence in STED microscopy. A) Jablonski diagram showing excitation, spontaneous fluorescence emission, and stimulated emission. B) Absorption and emission spectra for ATTO-647N including excitation-, detection-, and STED laser wavelengths. C) Excitation and STED lasers. When the two lasers are superimposed, the effective fluorescence focal spot is decreased.

In the most basic design of a STED microscope, an excitation laser beam is superimposed on a laser beam that induce stimulated emission; the STED laser. The STED laser is chosen such that it is spectrally well separated from the fluorescence signal, but still depletes the excited state efficiently (Figure 6-3B). By increasing the STED laser intensity, the fluorescence signal is gradually depleted. The fluorescence signal can selectively be depleted in the periphery of the excitation focus spot by patterning the STED laser to form the shape of a doughnut ring with zero intensity in the center. In this way, all molecules in the focal spot are excited, but only those in the center of the spot that are not affected by the STED laser will effectively contribute to the fluorescence signal (Figure 6-3C). The minimal size of the STED doughnut is determined by the diffraction

limit, and the resolution in STED microscopy is thus not improved by decreasing the doughnut size, but rather by tuning the efficiency by which dyes are depleted close to the zero intensity point. This is controlled by the STED laser intensity, I_{STED},; above a certain saturation intensity, I_S, characteristic for the specific dye, the fluorescence is efficiently depleted, and by increasing I_{STED}, the area from which the fluorescence originates is decreased. The STED resolution is given by [196]:

$$d_{STED} = \frac{d_{diffraction}}{\sqrt{1 + \frac{I_{STED}}{I_S}}} \qquad \text{Eq. 6-12}$$

$d_{diffraction}$ is the diffraction limited resolution.

STED is a unique super-resolution technique that does not require any post-acquisition data processing. It provides the opportunity to tune focal spot sizes, and in combination with FCS, the FCS diffusion law can be investigated below the diffraction limit, while keeping a microsecond time resolution [197]. STED-FCS has successfully been applied to determine the dynamics of lipids and proteins in living cells [10, 60]. The results show that sphingomyelin and GPI-anchored proteins as opposed to a glycerophospholipid are transiently trapped in cholesterol dependent domains with a size <20 nm.

7 Summary of results

7.1 Orthogonal multi-color QD tracking

Membrane molecules experience differences in spatial segregation depending on their expression level, their molecular distribution, and their local environment at a given time [87, 198]. This makes it non-trivial to directly compare the lateral dynamics of different membrane species. A method that can probe multiple different species simultaneously in the same cell and at the same time would therefore be desirable. QDs have properties ideal for multi-color studies, but so far the potential of multi-color QD tracking has not been fully exploited since only the same molecular species has been tracked in different colors at the same time [84, 138, 199-201].

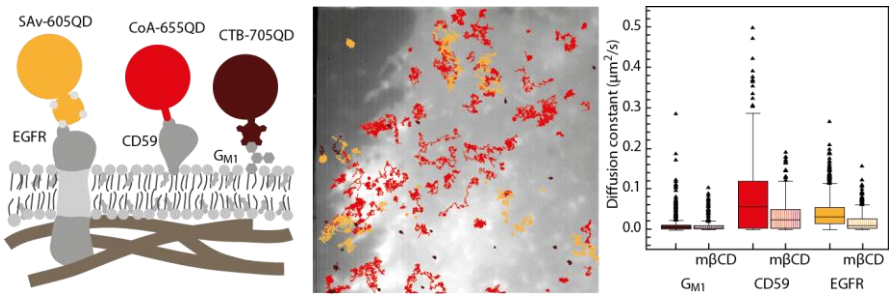

Figure 7-1: Highlight from " Single molecule multi-species tracking in live cells", page I. Illustration of labeling scheme (left), overlay of simultaneously acquired single molecules trajectories (center), and distribution of sinlge trajectory diffusion constants (right).

In this study, we demonstrate simultaneous tracking of three different plasma membrane species using QDs. The QDs emit light at three spectrally distinct and well-separated colors, and are bio-functionalized in different ways hence allowing for three orthogonal targeting strategies. We target and track three membrane species, which have all previously been classified as lipid raft markers:

i) The lipid ganglioside G_{M1} is targeted with Cholera Toxin subunit B (CTB) conjugated QDs having a peak emission at 705 nm (CTB-705QDs).

ii) The GPI-anchored CD59 fusion protein expressed with an Acyl Carrier Protein (ACP)-tag is targeted with Co enzyme A (CoA) conjugated QDs having a peak emission at 655 nm (CoA-655QDs).

iii) The single span transmembrane Epidermal Growth Factor Receptor (EGFR) expressed with a Biotin Ligase Acceptor Peptide (BLAP)-tag is targeted with StreptAvidin (SAv) conjugated QDs having a peak emission at 605 nm (SAv-605QDs).

We evaluate and optimize the QD conjugation, the targeting strategies, and the imaging conditions. We calculate diffusion constants for each individual trajectory and compare the populations of diffusion constants for the three different membrane species. The populations are heterogeneously distributed and statistical significantly different for all three membrane species. The lateral heterogeneity is decreased when depleting the plasma membrane cholesterol, but significant differences between the populations of diffusion constants remain.

The study supports the notion that cholesterol plays a role for the lateral dynamics of the three lipid raft markers investigated. It also suggests that not all lipid raft markers follow similar diffusion dynamics. The presented method enables parallel imaging of three different plasma membrane species at the single molecule level in the same area of the same cells, and in this sense, the method allows for detailed spatio-temporal investigations of the nanoscopic organization of the plasma membrane. The study, however, also stresses that further improvements in the probe design are still needed for a fully quantitative comparison of the molecules studied. In particular, a robust molecule-to-molecule comparison will require validated monovalent probes.

7.2 The influence of probes in SPT experiments

SPT studies reveal plasma membrane lateral structures and dynamics over a wide range of spatial and temporal scales [16, 39]. The studies are performed with a variety of different probes including gold nano-particles [11], QDs [13], or fluorescent dyes [14], but little attention is given to how the choice of probe influences the differences in obtained results. In this review, we point out that it is ultimately the probe used in a given SPT experiment that determines what information is accessible. We discuss advantages and disadvantages related to the use of different probes including available bio-functionalization strategies, and how the choice of probe affects the outcome of an experiment. Mainly, one has to make a compromise between large, bright, and photo-stable probes, which can give high spatial resolution, fast temporal acquisition, and long experimental duration, and small probes, which minimize the perturbation of the system under investigation.

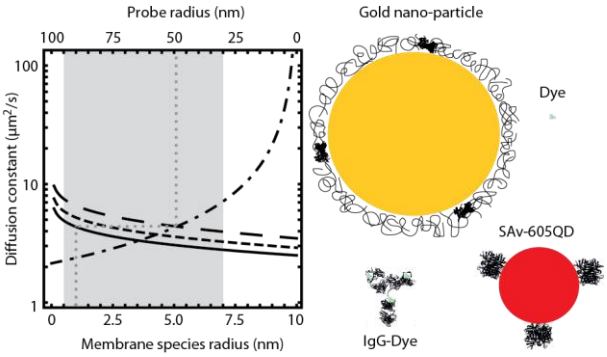

Figure 7-2: Highlights from " The probe rules in single particle tracking", page II. Realtionship between the size of a probe and its diffusion in solution, and between the size of a membrane molecule and its diffusion in the membrane, respectively (left), and an illustration of the relative sizes of different SPT probes (right).

In the review, we use the Stokes-Einstein and Saffmann-Delbrück [104] equations to argue under which conditions a large probe can be used to follow a small membrane target molecule, and rationalize that the conditions are no longer valid when the probe diffusion in solution approaches the diffusion of the target molecule in the membrane. We discuss the type of diffusion termed "hop-diffusion", which has only been observed with SPT using gold nano-particles [16]. We discuss if hop-diffusion is an artifact induced by the gold nano-particles, or if less invasive studies with fluorescent dyes, where the no hop-diffusion is observed [17], just not have sufficient temporal resolution to resolve it. We further discuss the fast 5-8 $\mu m^2/s$ diffusion constants, which have been reported within compartments for hop-diffusion. We argue that diffusion this fast cannot be distinguished from the diffusion of the gold nano-particles in solution, and further that protein crowding, and membrane topology in cells would prevent diffusion this fast.

We present preliminary fast QD tracking data, which try to bridge the observations using gold nano-particles and fluorescent dyes, respectively. We show that the observed lipid diffusion has a strong resemblance to hop-diffusion, except that the fast diffusion constant within compartments is not observed.

We emphasize that as the plasma membrane is heterogeneous at all possible temporal and spatial scales, it is important to choose the SPT probe in relation to the relevant temporal scales of the phenomena that is under investigation. Furthermore, it is of utmost importance that SPT results are carefully cross-validated either with SPT using different probes, or alternatively by alternative methods that allow for equivalent spatial and temporal resolutions.

7.3 Fast tracking with QDs reveal compartmentalized diffusion

The spatial nano-organization of the plasma membrane is tightly connected to lipid and protein dynamics on a millisecond and sub-millisecond time scale. Fast tracking studies with gold nano-particles show that lipids and proteins are subject to hop-diffusion in the plasma membrane [16]. These studies are questioned by less invasive tracking experiments using fluorescent dyes, which show free lipid and protein diffusion [17, 59]. A method

that can bridge these results is therefore of interest. QDs are smaller than gold nano-particles and have superior optical properties as compared to dyes, but so far QDs have not been exploited for fast tracking.

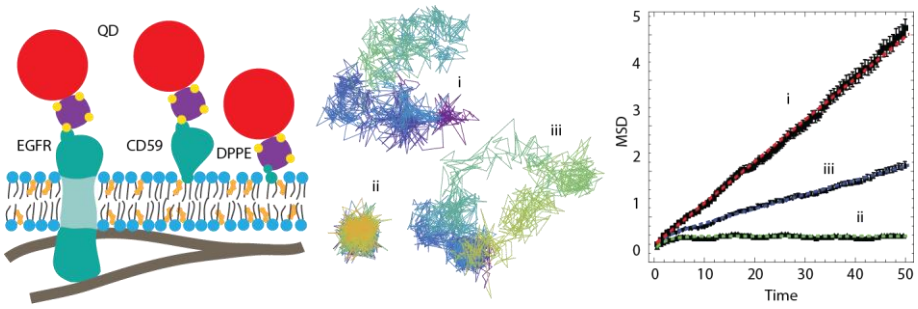

Figure 7-3: Highlights from "Transient confinement in plasma membranes explored by high-speed tracking using quantum dots" page III. Illustration of labeling scheme (left), examples of single molecule trajectories (center), and calculated MSDs, and best fits to different diffusion models (right).

In this study, we demonstrate fast tracking of plasma membrane species using QDs. We employ a standard wide-field fluorescence microscope equipped with an Hg arc lamp for low intensity excitation and an EMCCD camera with flexible and fast read-out. We target and track three different plasma membrane species at an acquisition rate of 1.8 kHz; i) the lipid DPPE, ii) the GPI-anchored protein CD59, and iii) the single span transmembrane protein EGFR. In the study, the acquisition rate is limited by the maximal camera read-out and not by the signal-to-noise-ratio.

We calculate mean squared displacements (MSD) of individual trajectories and statistically classify the motion based on the best MSD-fit to three different diffusion models; free diffusion, confined diffusion, and transiently confined diffusion. We see examples of free and confined diffusion, but the lateral dynamics is dominated by transiently confined or compartmentalized diffusion for all three membrane species investigated. The molecules experience transient (50-100 ms) confinement in nanoscopic (100-150 nm) compartments, but are free to move between compartments on a longer time-scale. The transient confinement is only observable at fast acquisition.

The results in this study have a strong resemblance to the previously reported hop-diffusion, though we think that the term "hop-diffusion" is a misnomer. This name lets one to think of long jumps between compartments, but this is not the case. Rather, the molecules move from one compartment to the adjacent by crossing a thin barrier. This movement is marked by a shift in the center of mass of the localized positions with no overlap in localized positions before and after the transition from one compartment to the next. In our results, we do not observe the reported fast diffusion constant for hop-diffusion, and discuss possible reasons for this. Following the argumentation from our review, we question whether the fast diffusion is a true representation of diffusion in the plasma membrane.

The presented method enables studies of the nano-organization of the plasma membrane on a sub-millisecond scale by demonstrating fast tracking using QDs with half the diameter (an eighth the volume) of gold nano-

particle, and using very low illumination intensity. Yet, QD multi-valence and resulting cross-binding of target molecules might induce or enhance the observation of hop-diffusion as clusters of molecules would experience different membrane dynamics than single molecules would. Further investigations are therefore needed to determine the influence of the probe on the observed compartmentalized diffusion.

7.4 Compartmentalized diffusion investigated by STED-FCS

Our fast tracking experiments using QDs show that plasma membrane lipids and proteins undergo compartmentalized diffusion in the mouse embryo fibroblasts IA32. Tracking experiments using fluorescent dyes in other cell lines do not show this, but these studies are limited in acquisition rate and trajectory length [17, 59], therefore making a direct comparison between the studies non-trivial. Unanswered questions remain about the influence the QDs in the fast tracking experiments. A method with a spatial and temporal resolution similar to the fast SPT studies, and having the ability to study fluorescently labeled molecules without being significantly limited by their optical properties is therefore of interest. This method is STED-FCS [10, 197].

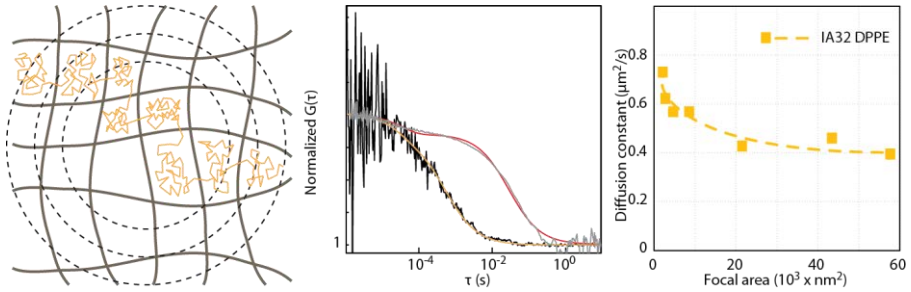

Figure 7-4: Highlights from " Compartmentalized diffusion revealed by STED-FCS", pageIV. Illustration of diffusion in a meshwork of confining barrier at different focal spot areas (left), normalized auto-correlation curves for lipid diffusion in confocal and STED focal spots (center), and apparent diffusion constant as a function of focal spot area (right).

In this study, we perform STED-FCS experiments of fluorescent lipid analogs in the plasma membrane. Fluorescent lipid analogs are minimally invasive, and have no inherent risk of introducing cross-linking between membrane molecules. We measure the lipid dynamics of ATTO-647N-labeled DPPE in different cells lines.

We record focal transit times for varying focal spots, and calculate the corresponding apparent diffusion constants. In the cell lines NRK and IA32, the apparent diffusion constants consistently increase for decreased focal spot sizes. This suggests that the lipid hop-diffuses in a meshwork of confining barriers. Previous studies in PtK2 cells did not show this [10, 60], but this might be due to the small compartment sizes in these cells.

We perturb the actin cytoskeleton in different ways, and find that the observation of compartmentalized diffusion is closely related to the presence of actin filaments. In contrast, cholesterol depletion leaves the observation of compartmentalized diffusion unaffected. We propose that when cortical actin is removed from the cell, the plasma membrane loses its mechanical support and therefore start to show more topology. This explains why we do not always observe an increase in diffusion constant when removing actin.

The STED-FCS study supports the idea that lipids experience compartmentalized hop-diffusion even when labeled with minimally invasive fluorescent dyes. The diffusion is found to be cell type dependent, and closely associated with the actin cytoskeleton.

8 Concluding remarks

In this PhD project, we have explored existing methods to study the lateral dynamics and nanoscopic organization of the plasma membrane, and pushed the limits of their use. In particular, we have explored the use of fluorescent QDs for SPT.

Using the optimal multi-color abilities of QDs, we gained insight to the heterogeneities of membrane dynamics. The heterogeneities become especially apparent when the studies are carried out at the single molecule level, and the diffusion of each followed molecule is displayed and analyzed individually without any population averaging. In this respect, QDs are therefore well-suited for SPT as the brightness and stability of the QDs yield molecular trajectories long enough to allow for single trajectory analysis. On the other hand, it also became clear that a direct comparison of molecules tracked with different types of QDs is not straight forward. The valence of QDs in some cases is difficult to control, and probe-induced differences in diffusion are difficult to distinguish from differences in diffusion caused by the molecules experiencing different molecular paths in the membrane. The multi-valence of QDs further contribute to the observed heterogeneity in diffusion by cross-linking molecules such that single molecules not always are followed, but instead small clusters with two or more bound molecules are followed. QDs with only one active binding site are therefore much preferable, especially in comparative studies.

The extreme brightness of QDs allowed us to address lipid and protein dynamics on an unprecedented fast time scale, which has previously been inaccessible for fluorescence based tracking studies, because of the limiting optical properties of organic fluorophores. Our interest was to find out if we would be able to observe hop-diffusion when tracking molecules with low excitation intensity and with probes smaller and less invasive than the gold nano-particles previously used to show hop-diffusion. In the investigated mouse embryo fibroblast cell line IA32, we surprisingly did see diffusion, which in many ways resembled that of hop-diffusion or compartmentalized diffusion (we think compartmentalized diffusion describes the motion better that the term hop-diffusion as this can lead to a misconception of the motion). We found molecules to explore compartments of the membrane one at the time with only rare transitions between compartments. We were, however, not able

to confirm the fast diffusion constant reported for hop-diffusion, and as argued, we believe that this fast diffusion constant must be an artifact of the gold nano-particle tracking method, or the analysis.

Knowing the limitations of QDs, we were skeptic about the observation of compartmentalized diffusion, and we therefore cross-validated the results in a STED-FCS setup using minimally invasive fluorescent dyes with no risk of inducing cross-linking. We were again surprised, as these studies were able to confirm compartmentalized diffusion in the IA32 cells, and also in NRK cells. We found the compartmentalized diffusion to be clearly actin dependent, which indeed confirms that actin plays a significant role for confining membrane molecules on a fast time scale – at least in some cell lines. Further studies are needed in order to determine the mechanism by which the actin restricts membrane molecules. Possible explanations are as previously proposed that transmembrane proteins acts as pickets, alternatively, it could also be that the actin acts more like tent poles, and that a strong inter-leaflet coupling between the intracellular and extracellular membrane sheets [24] mediates internal barriers to external restrictions.

9 References

1. Mouritsen, O.G., Life - as a matter of fat : the emerging science of lipidomics. The Frontiers collection. 2005, Berlin: Springer. xii, 276 p.

2. Lingwood, D. and K. Simons, Lipid rafts as a membrane-organizing principle. Science, 2010. 327(5961): p. 46-50.

3. Kusumi, A., T.K. Fujiwara, R. Chadda, M. Xie, T.A. Tsunoyama, Z. Kalay, . . . K.G. Suzuki, Dynamic Organizing Principles of the Plasma Membrane that Regulate Signal Transduction: Commemorating the Fortieth Anniversary of Singer and Nicolson's Fluid-Mosaic Model. Annu Rev Cell Dev Biol, 2012. 28: p. 215-50.

4. Pike, L.J., Rafts defined: a report on the Keystone Symposium on Lipid Rafts and Cell Function. J Lipid Res, 2006. 47(7): p. 1597-8.

5. Jacobson, K., O.G. Mouritsen, and R.G.W. Anderson, Lipid rafts: at a crossroad between cell biology and physics. Nature Cell Biology, 2007. 9(1): p. 7-14.

6. Joo, C., H. Balci, Y. Ishitsuka, C. Buranachai, and T. Ha, Advances in single-molecule fluorescence methods for molecular biology. Annu Rev Biochem, 2008. 77: p. 51-76.

7. Lagerholm, B.C., G.E. Weinreb, K. Jacobson, and N.L. Thompson, Detecting microdomains in intact cell membranes. Annu Rev Phys Chem, 2005. 56: p. 309-36.

8. Schermelleh, L., R. Heintzmann, and H. Leonhardt, A guide to super-resolution fluorescence microscopy. The Journal of Cell Biology, 2010. 190(2): p. 165-175.

9. Fernandez-Suarez, M. and A.Y. Ting, Fluorescent probes for super-resolution imaging in living cells. Nat Rev Mol Cell Biol, 2008. 9(12): p. 929-943.

10. Eggeling, C., C. Ringemann, R. Medda, G. Schwarzmann, K. Sandhoff, S. Polyakova, . . . S.W. Hell, Direct observation of the nanoscale dynamics of membrane lipids in a living cell. Nature, 2009. 457(7233): p. 1159-62.

11. Saxton, M.J. and K. Jacobson, Single-particle tracking: applications to membrane dynamics. Annu Rev Biophys Biomol Struct, 1997. 26: p. 373-99.

12. Schmidt, T., G.J. Schutz, W. Baumgartner, H.J. Gruber, and H. Schindler, Imaging of single molecule diffusion. Proc Natl Acad Sci U S A, 1996. 93(7): p. 2926-9.

13. Pinaud, F., S. Clarke, A. Sittner, and M. Dahan, Probing cellular events, one quantum dot at a time. Nat Methods, 2010. 7(4): p. 275-85.

14. Wieser, S. and G.J. Schutz, Tracking single molecules in the live cell plasma membrane-Do's and Don't's. Methods, 2008. 46(2): p. 131-40.

15. Brameshuber, M. and G.J. Schutz, How the sum of its parts gets greater than the whole. Nat Methods, 2008. 5(2): p. 133-4.

16. Kusumi, A., C. Nakada, K. Ritchie, K. Murase, K. Suzuki, H. Murakoshi, . . . T. Fujiwara, Paradigm shift of the plasma membrane concept from the two-dimensional continuum fluid to the partitioned fluid: high-speed single-molecule tracking of membrane molecules. Annu Rev Biophys Biomol Struct, 2005. 34: p. 351-78.

17. Wieser, S., M. Moertelmaier, E. Fuertbauer, H. Stockinger, and G.J. Schutz, (Un)confined diffusion of CD59 in the plasma membrane determined by high-resolution single molecule microscopy. Biophys J, 2007. 92(10): p. 3719-28.

18. Bruchez, M., Jr., M. Moronne, P. Gin, S. Weiss, and A.P. Alivisatos, Semiconductor nanocrystals as fluorescent biological labels. Science, 1998. 281(5385): p. 2013-6.

19. Rosenthal, S.J., J.C. Chang, O. Kovtun, J.R. McBride, and I.D. Tomlinson, Biocompatible quantum dots for biological applications. Chem Biol, 2011. 18(1): p. 10-24.

20. Mukherjee, S. and F.R. Maxfield, Membrane domains. Annu Rev Cell Dev Biol, 2004. 20: p. 839-66.

21. van Meer, G., D.R. Voelker, and G.W. Feigenson, Membrane lipids: where they are and how they behave. Nat Rev Mol Cell Biol, 2008. 9(2): p. 112-24.

22. Yetukuri, L., K. Ekroos, A. Vidal-Puig, and M. Oresic, Informatics and computational strategies for the study of lipids. Mol Biosyst, 2008. 4(2): p. 121-7.

23. Fantini, J., N. Garmy, R. Mahfoud, and N. Yahi, Lipid rafts: structure, function and role in HIV, Alzheimer's and prion diseases. Expert Rev Mol Med, 2002. 4(27): p. 1-22.

24. Machan, R. and M. Hof, Lipid diffusion in planar membranes investigated by fluorescence correlation spectroscopy. Biochim Biophys Acta, 2010. 1798(7): p. 1377-91.

25. Heimburg, T., Thermal biophysics of membranes. Tutorials in biophysics. 2007, Weinheim: Wiley-VCH Verlag. xv, 363 p.

26. Ipsen, J.H., G. Karlstrom, O.G. Mouritsen, H. Wennerstrom, and M.J. Zuckermann, Phase equilibria in the phosphatidylcholine-cholesterol system. Biochim Biophys Acta, 1987. 905(1): p. 162-72.

27. Simons, K. and E. Ikonen, Functional rafts in cell membranes. Nature, 1997. 387(6633): p. 569-72.

28. Wallin, E. and G. von Heijne, Genome-wide analysis of integral membrane proteins from eubacterial, archaean, and eukaryotic organisms. Protein Sci, 1998. 7(4): p. 1029-38.

29. Engelman, D.M., Membranes are more mosaic than fluid. Nature, 2005. 438(7068): p. 578-80.

30. Mouritsen, O.G. and M. Bloom, Mattress model of lipid-protein interactions in membranes. Biophys J, 1984. 46(2): p. 141-53.

31. Mouritsen, O.G. and K. Jorgensen, A new look at lipid-membrane structure in relation to drug research. Pharm Res, 1998. 15(10): p. 1507-19.

32. Kunding, Andreas H., Michael W. Mortensen, Sune M. Christensen, Vikram K. Bhatia, I. Makarov, R. Metzler, and D. Stamou, Intermembrane Docking Reactions Are Regulated by Membrane Curvature. Biophysical journal, 2011. 101(11): p. 2693-2703.

33. Cantor, R.S., Lateral Pressures in Cell Membranes: A Mechanism for Modulation of Protein Function. The Journal of Physical Chemistry B, 1997. 101(10): p. 1723-1725.

34. Jacobson, K., E.D. Sheets, and R. Simson, Revisiting the fluid mosaic model of membranes. Science, 1995. 268(5216): p. 1441-2.

35. Kusumi, A., Y.M. Shirai, I. Koyama-Honda, K.G. Suzuki, and T.K. Fujiwara, Hierarchical organization of the plasma membrane: investigations by single-molecule tracking vs. fluorescence correlation spectroscopy. FEBS Lett, 2010. 584(9): p. 1814-23.

36. Singer, S.J. and G.L. Nicolson, The fluid mosaic model of the structure of cell membranes. Science, 1972. 175(23): p. 720-31.

37. Jacobson, K., O.G. Mouritsen, and R.G. Anderson, Lipid rafts: at a crossroad between cell biology and physics. Nat Cell Biol, 2007. 9(1): p. 7-14.

38. Axelrod, D., D.E. Koppel, J. Schlessinger, E. Elson, and W.W. Webb, Mobility measurement by analysis of fluorescence photobleaching recovery kinetics. Biophys J, 1976. 16(9): p. 1055-69.

39. Owen, D.M., D. Williamson, C. Rentero, and K. Gaus, Quantitative microscopy: protein dynamics and membrane organisation. Traffic, 2009. 10(8): p. 962-71.

40. Niemela, P.S., M.S. Miettinen, L. Monticelli, H. Hammaren, P. Bjelkmar, T. Murtola, . . . I. Vattulainen, Membrane proteins diffuse as dynamic complexes with lipids. Journal of the American Chemical Society, 2010. 132(22): p. 7574-5.

41. Adler, J., A.I. Shevchuk, P. Novak, Y.E. Korchev, and I. Parmryd, Plasma membrane topography and interpretation of single-particle tracks. Nat Methods, 2010. 7(3): p. 170-1.

42. Simons, K. and M.J. Gerl, Revitalizing membrane rafts: new tools and insights. Nat Rev Mol Cell Biol, 2010. 11(10): p. 688-99.

43. Simons, K. and D. Toomre, Lipid rafts and signal transduction. Nat Rev Mol Cell Biol, 2000. 1(1): p. 31-9.

44. Simons, K. and W.L. Vaz, Model systems, lipid rafts, and cell membranes. Annu Rev Biophys Biomol Struct, 2004. 33: p. 269-95.

45. Pike, L.J., X. Han, and R.W. Gross, Epidermal growth factor receptors are localized to lipid rafts that contain a balance of inner and outer leaflet lipids: a shotgun lipidomics study. Journal of Biological Chemistry, 2005. 280(29): p. 26796-804.

46. Hancock, J.F., Lipid rafts: contentious only from simplistic standpoints. Nat Rev Mol Cell Biol, 2006. 7(6): p. 456-62.

47. Munro, S., Lipid rafts: elusive or illusive? Cell, 2003. 115(4): p. 377-88.

48. Shaw, A.S., Lipid rafts: now you see them, now you don't. Nat Immunol, 2006. 7(11): p. 1139-42.

49. Brown, D.A. and J.K. Rose, Sorting of GPI-anchored proteins to glycolipid-enriched membrane subdomains during transport to the apical cell surface. Cell, 1992. 68(3): p. 533-44.

50. Heerklotz, H., Triton promotes domain formation in lipid raft mixtures. Biophys J, 2002. 83(5): p. 2693-701.

51. Lingwood, D. and K. Simons, Detergent resistance as a tool in membrane research. Nat Protoc, 2007. 2(9): p. 2159-65.

52. Lommerse, P.H., H.P. Spaink, and T. Schmidt, In vivo plasma membrane organization: results of biophysical approaches. Biochim Biophys Acta, 2004. 1664(2): p. 119-31.

53. Semrau, S., T. Idema, T. Schmidt, and C. Storm, Membrane-mediated interactions measured using membrane domains. Biophys J, 2009. 96(12): p. 4906-15.

54. Schermelleh, L., R. Heintzmann, and H. Leonhardt, A guide to super-resolution fluorescence microscopy. J Cell Biol, 2010. 190(2): p. 165-75.

55. Owen, D.M., A. Magenau, D. Williamson, and K. Gaus, The lipid raft hypothesis revisited--new insights on raft composition and function from super-resolution fluorescence microscopy. Bioessays, 2012. 34(9): p. 739-47.

56. Kusumi, A., I. Koyama-Honda, and K. Suzuki, Molecular dynamics and interactions for creation of stimulation-induced stabilized rafts from small unstable steady-state rafts. Traffic, 2004. 5(4): p. 213-30.

57. Pinaud, F., X. Michalet, G. Iyer, E. Margeat, H.P. Moore, and S. Weiss, Dynamic partitioning of a glycosyl-phosphatidylinositol-anchored protein in glycosphingolipid-rich microdomains imaged by single-quantum dot tracking. Traffic, 2009. 10(6): p. 691-712.

58. Sharma, P., R. Varma, R.C. Sarasij, Ira, K. Gousset, G. Krishnamoorthy, . . . S. Mayor, Nanoscale organization of multiple GPI-anchored proteins in living cell membranes. Cell, 2004. 116(4): p. 577-89.

59. Sahl, S.J., M. Leutenegger, M. Hilbert, S.W. Hell, and C. Eggeling, Fast molecular tracking maps nanoscale dynamics of plasma membrane lipids. Proc Natl Acad Sci U S A, 2010. 107(15): p. 6829-34.

60. Mueller, V., C. Ringemann, A. Honigmann, G. Schwarzmann, R. Medda, M. Leutenegger, . . . C. Eggeling, STED nanoscopy reveals molecular details of cholesterol- and cytoskeleton-modulated lipid interactions in living cells. Biophys J, 2011. 101(7): p. 1651-60.

61. Viola, A. and N. Gupta, Tether and trap: regulation of membrane-raft dynamics by actin-binding proteins. Nat Rev Immunol, 2007. 7(11): p. 889-96.

62. Harder, T., P. Scheiffele, P. Verkade, and K. Simons, Lipid domain structure of the plasma membrane revealed by patching of membrane components. J Cell Biol, 1998. 141(4): p. 929-42.

63. Zech, T., C.S. Ejsing, K. Gaus, B. de Wet, A. Shevchenko, K. Simons, and T. Harder, Accumulation of raft lipids in T-cell plasma membrane domains engaged in TCR signalling. EMBO J, 2009. 28(5): p. 466-76.

64. Klemm, R.W., C.S. Ejsing, M.A. Surma, H.J. Kaiser, M.J. Gerl, J.L. Sampaio, . . . K. Simons, Segregation of sphingolipids and sterols during formation of secretory vesicles at the trans-Golgi network. J Cell Biol, 2009. 185(4): p. 601-12.

65. Levental, I., M. Grzybek, and K. Simons, Raft domains of variable properties and compositions in plasma membrane vesicles. Proc Natl Acad Sci U S A, 2011. 108(28): p. 11411-6.

66. Baumgart, T., A.T. Hammond, P. Sengupta, S.T. Hess, D.A. Holowka, B.A. Baird, and W.W. Webb, Large-scale fluid/fluid phase separation of proteins and lipids in giant plasma membrane vesicles. Proc Natl Acad Sci U S A, 2007. 104(9): p. 3165-70.

67. Grant, B.D. and J.G. Donaldson, Pathways and mechanisms of endocytic recycling. Nat Rev Mol Cell Biol, 2009. 10(9): p. 597-608.

68. Steinman, R.M., I.S. Mellman, W.A. Muller, and Z.A. Cohn, Endocytosis and the recycling of plasma membrane. J Cell Biol, 1983. 96(1): p. 1-27.

69. Kusumi, A., K.G. Suzuki, R.S. Kasai, K. Ritchie, and T.K. Fujiwara, Hierarchical mesoscale domain organization of the plasma membrane. Trends Biochem Sci, 2011. 36(11): p. 604-15.

70. Fujiwara, T., K. Ritchie, H. Murakoshi, K. Jacobson, and A. Kusumi, Phospholipids undergo hop diffusion in compartmentalized cell membrane. J Cell Biol, 2002. 157(6): p. 1071-81.

71. Murase, K., T. Fujiwara, Y. Umemura, K. Suzuki, R. Iino, H. Yamashita, . . . A. Kusumi, Ultrafine membrane compartments for molecular diffusion as revealed by single molecule techniques. Biophys J, 2004. 86(6): p. 4075-93.

72. Suzuki, K., K. Ritchie, E. Kajikawa, T. Fujiwara, and A. Kusumi, Rapid hop diffusion of a G-protein-coupled receptor in the plasma membrane as revealed by single-molecule techniques. Biophys J, 2005. 88(5): p. 3659-80.

73. Umemura, Y.M., M. Vrljic, S.Y. Nishimura, T.K. Fujiwara, K.G. Suzuki, and A. Kusumi, Both MHC class II and its GPI-anchored form undergo hop diffusion as observed by single-molecule tracking. Biophys J, 2008. 95(1): p. 435-50.

74. Morone, N., T. Fujiwara, K. Murase, R.S. Kasai, H. Ike, S. Yuasa, . . . A. Kusumi, Three-dimensional reconstruction of the membrane skeleton at the plasma membrane interface by electron tomography. J Cell Biol, 2006. 174(6): p. 851-62.

75. Lenne, P.F., L. Wawrezinieck, F. Conchonaud, O. Wurtz, A. Boned, X.J. Guo, . . . D. Marguet, Dynamic molecular confinement in the plasma membrane by microdomains and the cytoskeleton meshwork. EMBO J, 2006. 25(14): p. 3245-56.

76. Chen, Y., B.C. Lagerholm, B. Yang, and K. Jacobson, Methods to measure the lateral diffusion of membrane lipids and proteins. Methods, 2006. 39(2): p. 147-53.

77. Ries, J. and P. Schwille, New concepts for fluorescence correlation spectroscopy on membranes. Phys Chem Chem Phys, 2008. 10(24): p. 3487-97.

78. Chiantia, S., J. Ries, and P. Schwille, Fluorescence correlation spectroscopy in membrane structure elucidation. Biochim Biophys Acta, 2009. 1788(1): p. 225-33.

79. Alcor, D., G. Gouzer, and A. Triller, Single-particle tracking methods for the study of membrane receptors dynamics. Eur J Neurosci, 2009. 30(6): p. 987-97.

80. Chen, Y., W.R. Thelin, B. Yang, S.L. Milgram, and K. Jacobson, Transient anchorage of cross-linked glycosyl-phosphatidylinositol-anchored proteins depends on cholesterol, Src family kinases, caveolin, and phosphoinositides. J Cell Biol, 2006. 175(1): p. 169-78.

81. Kusumi, A., Y. Sako, and M. Yamamoto, Confined lateral diffusion of membrane receptors as studied by single particle tracking (nanovid microscopy). Effects of calcium-induced differentiation in cultured epithelial cells. Biophys J, 1993. 65(5): p. 2021-40.

82. Lidke, D.S., K.A. Lidke, B. Rieger, T.M. Jovin, and D.J. Arndt-Jovin, Reaching out for signals: filopodia sense EGF and respond by directed retrograde transport of activated receptors. J Cell Biol, 2005. 170(4): p. 619-26.

83. Clausen, M.P. and B.C. Lagerholm, The Probe Rules in Single Particle Tracking. Curr Protein Pept Sci, 2011.

84. Andrews, N.L., K.A. Lidke, J.R. Pfeiffer, A.R. Burns, B.S. Wilson, J.M. Oliver, and D.S. Lidke, Actin restricts FcepsilonRI diffusion and facilitates antigen-induced receptor immobilization. Nat Cell Biol, 2008. 10(8): p. 955-63.

85. Itano, M.S., A.K. Neumann, P. Liu, F. Zhang, E. Gratton, W.J. Parak, . . . K. Jacobson, DC-SIGN and influenza hemagglutinin dynamics in plasma membrane microdomains are markedly different. Biophys J, 2011. 100(11): p. 2662-70.

86. Jaqaman, K., H. Kuwata, N. Touret, R. Collins, W.S. Trimble, G. Danuser, and S. Grinstein, Cytoskeletal Control of CD36 Diffusion Promotes Its Receptor and Signaling Function. Cell, 2011. 146(4): p. 593-606.

87. Wieser, S., J. Weghuber, M. Sams, H. Stockinger, and G.J. Schutz, Cell-to-cell variability in the diffusion constants of the plasma membrane proteins CD59 and CD147. Soft Matter, 2009. 5(17): p. 3287-3294.

88. Lidke, D.S., P. Nagy, R. Heintzmann, D.J. Arndt-Jovin, J.N. Post, H.E. Grecco, . . . T.M. Jovin, Quantum dot ligands provide new insights into erbB/HER receptor-mediated signal transduction. Nat Biotechnol, 2004. 22(2): p. 198-203.

89. Heine, M., L. Groc, R. Frischknecht, J.-C. Béïque, B. Lounis, G. Rumbaugh, . . . D. Choquet, Surface Mobility of Postsynaptic AMPARs Tunes Synaptic Transmission. Science, 2008. 320(5873): p. 201-205.

90. Manley, S., J.M. Gillette, G.H. Patterson, H. Shroff, H.F. Hess, E. Betzig, and J. Lippincott-Schwartz, High-density mapping of single-molecule trajectories with photoactivated localization microscopy. Nat Methods, 2008. 5(2): p. 155-7.

91. Mascalchi, P., E. Haanappel, K. Carayon, S. Mazeres, and L. Salome, Probing the influence of the particle in Single Particle Tracking measurements of lipid diffusion. Soft Matter, 2012. 8(16): p. 4462-4470.

92. Dahan, M., S. Levi, C. Luccardini, P. Rostaing, B. Riveau, and A. Triller, Diffusion dynamics of glycine receptors revealed by single-quantum dot tracking. Science, 2003. 302(5644): p. 442-5.

93. Heintzmann, R. and G. Ficz, Breaking the resolution limit in light microscopy. Briefings in Functional Genomics & Proteomics, 2006. 5(4): p. 289-301.

94. Stallinga, S. and B. Rieger, Accuracy of the gaussian point spread function model in 2D localization microscopy. Opt Express, 2010. 18(24): p. 24461-76.

95. Mortensen, K.I., L.S. Churchman, J.A. Spudich, and H. Flyvbjerg, Optimized localization analysis for single-molecule tracking and super-resolution microscopy. Nat Methods, 2010. 7(5): p. 377-81.

96. Saxton, M.J., Single-particle tracking: connecting the dots. Nat Methods, 2008. 5(8): p. 671-2.

97. Bannai, H., S. Levi, C. Schweizer, M. Dahan, and A. Triller, Imaging the lateral diffusion of membrane molecules with quantum dots. Nat Protoc, 2006. 1(6): p. 2628-34.

98. Brameshuber, M. and G.J. Schutz, In vivo tracking of single biomolecules – what trajectories tell us about the acting forces.

99. Jaqaman, K., D. Loerke, M. Mettlen, H. Kuwata, S. Grinstein, S.L. Schmid, and G. Danuser, Robust single-particle tracking in live-cell time-lapse sequences. Nat Methods, 2008. 5(8): p. 695-702.

100. Sbalzarini, I.F. and P. Koumoutsakos, Feature point tracking and trajectory analysis for video imaging in cell biology. J Struct Biol, 2005. 151(2): p. 182-95.

101. Serge, A., N. Bertaux, H. Rigneault, and D. Marguet, Dynamic multiple-target tracing to probe spatiotemporal cartography of cell membranes. Nat Methods, 2008. 5(8): p. 687-94.

102. Guigas, G. and M. Weiss, Size-dependent diffusion of membrane inclusions. Biophys J, 2006. 91(7): p. 2393-8.

103. Hughes, B.D., B.A. Pailthorpe, L.R. White, and W.H. Sawyer, Extraction of membrane microviscosity from translational and rotational diffusion coefficients. Biophys J, 1982. 37(3): p. 673-6.

104. Saffman, P.G. and M. Delbruck, Brownian motion in biological membranes. Proc Natl Acad Sci U S A, 1975. 72(8): p. 3111-3.

105. Gambin, Y., R. Lopez-Esparza, M. Reffay, E. Sierecki, N.S. Gov, M. Genest, . . . W. Urbach, Lateral mobility of proteins in liquid membranes revisited. Proc Natl Acad Sci U S A, 2006. 103(7): p. 2098-102.

106. Hughes, B.D., B.A. Pailthorpe, and L.R. White, The Translational and Rotational Drag on a Cylinder Moving in a Membrane. Journal of Fluid Mechanics, 1981. 110(Sep): p. 349-372.

107. Powles, J.G., M.J.D. Mallett, G. Rickayzen, and W.A.B. Evans, Exact Analytic Solutions for Diffusion Impeded by an Infinite Array of Partially Permeable Barriers. Proceedings of the Royal Society of London Series a-Mathematical Physical and Engineering Sciences, 1992. 436(1897): p. 391-403.

108. Goulian, M. and S.M. Simon, Tracking single proteins within cells. Biophys J, 2000. 79(4): p. 2188-98.

109. Saxton, M.J., Lateral diffusion in an archipelago. Single-particle diffusion. Biophys J, 1993. 64(6): p. 1766-80.

110. Rudnick, J. and G. Gaspari, The shapes of random walks. Science, 1987. 237(4813): p. 384-9.

111. Qian, H., M.P. Sheetz, and E.L. Elson, Single particle tracking. Analysis of diffusion and flow in two-dimensional systems. Biophys J, 1991. 60(4): p. 910-21.

112. Kenworthy, A.K., B.J. Nichols, C.L. Remmert, G.M. Hendrix, M. Kumar, J. Zimmerberg, and J. Lippincott-Schwartz, Dynamics of putative raft-associated proteins at the cell surface. J Cell Biol, 2004. 165(5): p. 735-46.

113. Semrau, S. and T. Schmidt, Particle image correlation spectroscopy (PICS): retrieving nanometer-scale correlations from high-density single-molecule position data. Biophys J, 2007. 92(2): p. 613-21.

114. Wieser, S., M. Axmann, and G.J. Schutz, Versatile analysis of single-molecule tracking data by comprehensive testing against Monte Carlo simulations. Biophys J, 2008. 95(12): p. 5988-6001.

115. Pons, T. and H. Mattoussi, Investigating biological processes at the single molecule level using luminescent quantum dots. Ann Biomed Eng, 2009. 37(10): p. 1934-59.

116. Michalet, X., F.F. Pinaud, L.A. Bentolila, J.M. Tsay, S. Doose, J.J. Li, . . . S. Weiss, Quantum dots for live cells, in vivo imaging, and diagnostics. Science, 2005. 307(5709): p. 538-44.

117. Brus, L.E., Electron Electron and Electron-Hole Interactions in Small Semiconductor Crystallites - the Size Dependence of the Lowest Excited Electronic State. Journal of Chemical Physics, 1984. 80(9): p. 4403-4409.

118. Hotz, C.Z., Applications of Quantum Dots in Biology. 2005. p. 1-17.

119. Gaponenko, S.V., Optical properties of semiconductor nanocrystals. Cambridge studies in modern optics. 1998, Cambridge, UK ; New York, NY, USA: Cambridge Unviersity Press. xiv, 245 p.

120. Alivisatos, A.P., Semiconductor clusters, nanocrystals, and quantum dots. Science, 1996. 271(5251): p. 933-937.

121. Murray, C.B., D.J. Norris, and M.G. Bawendi, Synthesis and Characterization of Nearly Monodisperse Cde (E = S, Se, Te) Semiconductor Nanocrystallites. Journal of the American Chemical Society, 1993. 115(19): p. 8706-8715.

122. Peng, Z.A. and X. Peng, Formation of high-quality CdTe, CdSe, and CdS nanocrystals using CdO as precursor. Journal of the American Chemical Society, 2001. 123(1): p. 183-4.

123. Hines, M.A. and P. Guyot-Sionnest, Synthesis and characterization of strongly luminescing ZnS-Capped CdSe nanocrystals. Journal of Physical Chemistry, 1996. 100(2): p. 468-471.

124. Peng, X.G., M.C. Schlamp, A.V. Kadavanich, and A.P. Alivisatos, Epitaxial growth of highly luminescent CdSe/CdS core/shell nanocrystals with photostability and electronic accessibility. Journal of the American Chemical Society, 1997. 119(30): p. 7019-7029.

125. Dabbousi, B.O., J. RodriguezViejo, F.V. Mikulec, J.R. Heine, H. Mattoussi, R. Ober, . . . M.G. Bawendi, (CdSe)ZnS core-shell quantum dots: Synthesis and characterization of a size series of highly luminescent nanocrystallites. Journal of Physical Chemistry B, 1997. 101(46): p. 9463-9475.

126. McBride, J.R., T.C. Kippeny, S.J. Pennycook, and S.J. Rosenthal, Aberration-corrected Z-contrast scanning transmission electron microscopy of CdSe nanocrystals. Nano Letters, 2004. 4(7): p. 1279-1283.

127. Nirmal, M. and L. Brus, Luminescence Photophysics in Semiconductor Nanocrystals. Acc. Chem. Res., 1999. 32(5): p. 407-414.

128. McBride, J., J. Treadway, L.C. Feldman, S.J. Pennycook, and S.J. Rosenthal, Structural Basis for Near Unity Quantum Yield Core/Shell Nanostructures. Nano Letters, 2006. 6(7): p. 1496-1501.

129. Xie, R.G., U. Kolb, J.X. Li, T. Basche, and A. Mews, Synthesis and characterization of highly luminescent CdSe-Core CdS/Zn0.5Cd0.5S/ZnS multishell nanocrystals. Journal of the American Chemical Society, 2005. 127(20): p. 7480-7488.

130. Dubertret, B., P. Skourides, D.J. Norris, V. Noireaux, A.H. Brivanlou, and A. Libchaber, In vivo imaging of quantum dots encapsulated in phospholipid micelles. Science, 2002. 298(5599): p. 1759-62.

131. Wu, X., H. Liu, J. Liu, K.N. Haley, J.A. Treadway, J.P. Larson, . . . M.P. Bruchez, Immunofluorescent labeling of cancer marker Her2 and other cellular targets with semiconductor quantum dots. Nat Biotechnol, 2003. 21(1): p. 41-6.

132. Pellegrino, T., L. Manna, S. Kudera, T. Liedl, D. Koktysh, A.L. Rogach, . . . W.J. Parak, Hydrophobic nanocrystals coated with an amphiphilic polymer shell: A general route to water soluble nanocrystals. Nano Letters, 2004. 4(4): p. 703-707.

133. Watson, A., X. Wu, and M. Bruchez, Lighting up cells with quantum dots. Biotechniques, 2003. 34(2): p. 296-300, 302-3.

134. Bawendi, M. and S. Empedocles, Spectroscopy of Single CdSe Nanocrystallites. Acc. Chem. Res., 1999. 32(5): p. 389-396.

135. Jaiswal, J.K., H. Mattoussi, J.M. Mauro, and S.M. Simon, Long-term multiple color imaging of live cells using quantum dot bioconjugates. Nat Biotechnol, 2003. 21(1): p. 47-51.

136. Lee, S.F. and M.A. Osborne, Brightening, blinking, bluing and bleaching in the life of a quantum dot: friend or foe? Chemphyschem, 2009. 10(13): p. 2174-91.

137. Arnspang Christensen, E., P. Kulatunga, and B.C. Lagerholm, A Single Molecule Investigation of the Photostability of Quantum Dots. PLoS One, 2012. 7(8): p. e44355.

138. Arnspang Christensen, E., J.R. Brewer, and B.C. Lagerholm, Multi-color single particle tracking with quantum dots. 2012.

139. Nirmal, M., B.O. Dabbousi, M.G. Bawendi, J.J. Macklin, J.K. Trautman, T.D. Harris, and L.E. Brus, Fluorescence intermittency in single cadmium selenide nanocrystals. Nature, 1996. 383(6603): p. 802-804.

140. Kuno, M., D.P. Fromm, H.F. Hamann, A. Gallagher, and D.J. Nesbitt, "On"/"off" fluorescence intermittency of single semiconductor quantum dots. Journal of Chemical Physics, 2001. 115(2): p. 1028-1040.

141. Kuno, M., D.P. Fromm, S.T. Johnson, A. Gallagher, and D.J. Nesbitt, Modeling distributed kinetics in isolated semiconductor quantum dots. Physical Review B, 2003. 67(12).

142. Frantsuzov, P., M. Kuno, B. Janko, and R.A. Marcus, Universal emission intermittency in quantum dots, nanorods and nanowires. Nature Physics, 2008. 4(7): p. 519-522.

143. Hohng, S. and T. Ha, Near-complete suppression of quantum dot blinking in ambient conditions. J Am Chem Soc, 2004. 126(5): p. 1324-5.

144. Mahler, B., P. Spinicelli, S. Buil, X. Quelin, J.P. Hermier, and B. Dubertret, Towards non-blinking colloidal quantum dots. Nat Mater, 2008. 7(8): p. 659-64.

145. Chen, Y., J. Vela, H. Htoon, J.L. Casson, D.J. Werder, D.A. Bussian, . . . J.A. Hollingsworth, "Giant" Multishell CdSe Nanocrystal Quantum Dots with Suppressed Blinking. Journal of the American Chemical Society, 2008. 130(15): p. 5026-5027.

146. Wang, X., X. Ren, K. Kahen, M.A. Hahn, M. Rajeswaran, S. Maccagnano-Zacher, . . . T.D. Krauss, Non-blinking semiconductor nanocrystals. Nature, 2009. 459(7247): p. 686-9.

147. Lagerholm, B.C., L. Averett, G.E. Weinreb, K. Jacobson, and N.L. Thompson, Analysis method for measuring submicroscopic distances with blinking quantum dots. Biophys J, 2006. 91(8): p. 3050-60.

148. Dahan, M., T. Laurence, F. Pinaud, D.S. Chemla, A.P. Alivisatos, M. Sauer, and S. Weiss, Time-gated biological imaging by use of colloidal quantum dots. Opt Lett, 2001. 26(11): p. 825-7.

149. Hermanson, G.T., Bioconjugate techniques. 1996, San Diego: Academic Press. xxv, 785 p.

150. Medintz, I.L., H.T. Uyeda, E.R. Goldman, and H. Mattoussi, Quantum dot bioconjugates for imaging, labelling and sensing. Nat Mater, 2005. 4(6): p. 435-46.

151. Chakraborty, S.K., J.A. Fitzpatrick, J.A. Phillippi, S. Andreko, A.S. Waggoner, M.P. Bruchez, and B. Ballou, Cholera toxin B conjugated quantum dots for live cell labeling. Nano Lett, 2007. 7(9): p. 2618-26.

152. Pathak, S., M.C. Davidson, and G.A. Silva, Characterization of the functional binding properties of antibody conjugated quantum dots. Nano Letters, 2007. 7(7): p. 1839-45.

153. Sunbul, M., M. Yen, Y. Zou, and J. Yin, Enzyme catalyzed site-specific protein labeling and cell imaging with quantum dots. Chem Commun (Camb), 2008(45): p. 5927-9.

154. Jamieson, T., R. Bakhshi, D. Petrova, R. Pocock, M. Imani, and A.M. Seifalian, Biological applications of quantum dots. Biomaterials, 2007. 28(31): p. 4717-32.

155. Chen, I. and A.Y. Ting, Site-specific labeling of proteins with small molecules in live cells. Curr Opin Biotechnol, 2005. 16(1): p. 35-40.

156. Chen, I., M. Howarth, W. Lin, and A.Y. Ting, Site-specific labeling of cell surface proteins with biophysical probes using biotin ligase. Nat Methods, 2005. 2(2): p. 99-104.

157. Johnsson, N., N. George, and K. Johnsson, Protein chemistry on the surface of living cells. Chembiochem, 2005. 6(1): p. 47-52.

158. Keppler, A., S. Gendreizig, T. Gronemeyer, H. Pick, H. Vogel, and K. Johnsson, A general method for the covalent labeling of fusion proteins with small molecules in vivo. Nat Biotechnol, 2003. 21(1): p. 86-9.

159. Gautier, A., A. Juillerat, C. Heinis, I.R. Correa, Jr., M. Kindermann, F. Beaufils, and K. Johnsson, An engineered protein tag for multiprotein labeling in living cells. Chem Biol, 2008. 15(2): p. 128-36.

160. Ramadurai, S., A. Holt, V. Krasnikov, G. van den Bogaart, J.A. Killian, and B. Poolman, Lateral diffusion of membrane proteins. J Am Chem Soc, 2009. 131(35): p. 12650-6.

161. Los, G.V., L.P. Encell, M.G. McDougall, D.D. Hartzell, N. Karassina, C. Zimprich, . . . K.V. Wood, HaloTag: A Novel Protein Labeling Technology for Cell Imaging and Protein Analysis. ACS Chemical Biology, 2008. 3(6): p. 373-382.

162. Roullier, V., S. Clarke, C. You, F. Pinaud, G.G. Gouzer, D. Schaible, . . . M. Dahan, High-affinity labeling and tracking of individual histidine-tagged proteins in live cells using Ni2+ tris-nitrilotriacetic acid quantum dot conjugates. Nano Lett, 2009. 9(3): p. 1228-34.

163. So, M.K., H. Yao, and J. Rao, HaloTag protein-mediated specific labeling of living cells with quantum dots. Biochem Biophys Res Commun, 2008. 374(3): p. 419-23.

164. Howarth, M. and A.Y. Ting, Imaging proteins in live mammalian cells with biotin ligase and monovalent streptavidin. Nat Protoc, 2008. 3(3): p. 534-45.

165. Yin, J., P.D. Straight, S.M. McLoughlin, Z. Zhou, A.J. Lin, D.E. Golan, . . . C.T. Walsh, Genetically encoded short peptide tag for versatile protein labeling by Sfp phosphopantetheinyl transferase. Proc Natl Acad Sci U S A, 2005. 102(44): p. 15815-20.

166. Zhou, Z., P. Cironi, A.J. Lin, Y. Xu, S. Hrvatin, D.E. Golan, . . . J. Yin, Genetically encoded short peptide tags for orthogonal protein labeling by Sfp and AcpS phosphopantetheinyl transferases. ACS Chem Biol, 2007. 2(5): p. 337-46.

167. Yu, C., J. Hale, K. Ritchie, N.K. Prasad, and J. Irudayaraj, Receptor overexpression or inhibition alters cell surface dynamics of EGF-EGFR interaction: new insights from real-time single molecule analysis. Biochem Biophys Res Commun, 2009. 378(3): p. 376-82.

168. You, C., S. Wilmes, O. Beutel, S. Lochte, Y. Podoplelowa, F. Roder, . . . J. Piehler, Self-controlled monofunctionalization of quantum dots for multiplexed protein tracking in live cells. Angew Chem Int Ed Engl, 2010. 49(24): p. 4108-12.

169. Howarth, M., W. Liu, S. Puthenveetil, Y. Zheng, L.F. Marshall, M.M. Schmidt, . . . A.Y. Ting, Monovalent, reduced-size quantum dots for imaging receptors on living cells. Nat Methods, 2008. 5(5): p. 397-9.

170. Clarke, S., F. Pinaud, O. Beutel, C. You, J. Piehler, and M. Dahan, Covalent monofunctionalization of peptide-coated quantum dots for single-molecule assays. Nano Lett, 2010. 10(6): p. 2147-54.

171. Liu, H.Y. and X. Gao, Engineering monovalent quantum dot-antibody bioconjugates with a hybrid gel system. Bioconjug Chem, 2011. 22(3): p. 510-7.

172. Sperling, R.A., T. Pellegrino, J.K. Li, W.H. Chang, and W.J. Parak, Electrophoretic separation of nanoparticles with a discrete number of functional groups. Advanced Functional Materials, 2006. 16(7): p. 943-948.

173. Mittal, R. and M.P. Bruchez, Biotin-4-Fluorescein Based Fluorescence Quenching Assay for Determination of Biotin Binding Capacity of Streptavidin Conjugated Quantum Dots. Bioconjug Chem, 2011.

174. Groc, L., M. Heine, L. Cognet, K. Brickley, F.A. Stephenson, B. Lounis, and D. Choquet, Differential activity-dependent regulation of the lateral mobilities of AMPA and NMDA receptors. Nat Neurosci, 2004. 7(7): p. 695-6.

175. Elson, E.L. and D. Magde, Fluorescence correlation spectroscopy. I. Conceptual basis and theory. Biopolymers, 1974. 13(1): p. 1-27.

176. Magde, D., E.L. Elson, and W.W. Webb, Fluorescence correlation spectroscopy. II. An experimental realization. Biopolymers, 1974. 13(1): p. 29-61.

177. MAGDE, D., W.W. WEBB, and E. ELSON, Thermodynamic Fluctuations in a Reacting System - Measurement by Fluorescence Correlation Spectroscopy. Physical Review Letters, 1972. 29(11): p. 705-&.

178. Schwille, P. and E. Haustein, Fluorescence Correlation Spectroscopy: An Introduction to its Concepts and Applications.

179. Thompson, N.L., A.M. Lieto, and N.W. Allen, Recent advances in fluorescence correlation spectroscopy. Curr Opin Struct Biol, 2002. 12(5): p. 634-41.

180. Rigler, R. and E. Elson, Fluorescence Correlation Spectroscopy - Theory and Applications. 2001.

181. Haustein, E. and P. Schwille, Fluorescence correlation spectroscopy: novel variations of an established technique. Annu Rev Biophys Biomol Struct, 2007. 36: p. 151-69.

182. Widengren, J., U. Mets, and R. Rigler, Fluorescence correlation spectroscopy of triplet states in solution: a theoretical and experimental study. The Journal of Physical Chemistry, 1995. 99(36): p. 13368-13379.

183. Schwille, P., J. Korlach, and W.W. Webb, Fluorescence correlation spectroscopy with single-molecule sensitivity on cell and model membranes. Cytometry, 1999. 36(3): p. 176-82.

184. Wachsmuth, M., W. Waldeck, and J. Langowski, Anomalous diffusion of fluorescent probes inside living cell nuclei investigated by spatially-resolved fluorescence correlation spectroscopy. J Mol Biol, 2000. 298(4): p. 677-89.

185. Bacia, K., D. Scherfeld, N. Kahya, and P. Schwille, Fluorescence correlation spectroscopy relates rafts in model and native membranes. Biophys J, 2004. 87(2): p. 1034-43.

186. Haustein, E. and P. Schwille, Fluorescence correlation spectroscopy: novel variations of an established technique. Annual review of biophysics and biomolecular structure, 2007. 36: p. 151-169.

187. Schwille, P., F.J. Meyer-Almes, and R. Rigler, Dual-color fluorescence cross-correlation spectroscopy for multicomponent diffusional analysis in solution. Biophys J, 1997. 72(4): p. 1878-86.

188. Chiantia, S., J. Ries, N. Kahya, and P. Schwille, Combined AFM and two-focus SFCS study of raft-exhibiting model membranes. Chemphyschem, 2006. 7(11): p. 2409-18.

189. Dertinger, T., V. Pacheco, I. von der Hocht, R. Hartmann, I. Gregor, and J. Enderlein, Two-focus fluorescence correlation spectroscopy: a new tool for accurate and absolute diffusion measurements. Chemphyschem, 2007. 8(3): p. 433-43.

190. Ries, J., S. Chiantia, and P. Schwille, Accurate determination of membrane dynamics with line-scan FCS. Biophys J, 2009. 96(5): p. 1999-2008.

191. Gielen, E., N. Smisdom, M. vandeVen, B. De Clercq, E. Gratton, M. Digman, . . . M. Ameloot, Measuring diffusion of lipid-like probes in artificial and natural membranes by raster image correlation spectroscopy (RICS): use of a commercial laser-scanning microscope with analog detection. Langmuir, 2009. 25(9): p. 5209-18.

192. He, H.T. and D. Marguet, Detecting nanodomains in living cell membrane by fluorescence correlation spectroscopy. Annu Rev Phys Chem, 2011. 62: p. 417-36.

193. Wawrezinieck, L., H. Rigneault, D. Marguet, and P.F. Lenne, Fluorescence correlation spectroscopy diffusion laws to probe the submicron cell membrane organization. Biophys J, 2005. 89(6): p. 4029-42.

194. Ruprecht, V., S. Wieser, D. Marguet, and G.J. Schutz, Spot variation fluorescence correlation spectroscopy allows for superresolution chronoscopy of confinement times in membranes. Biophys J, 2011. 100(11): p. 2839-45.

195. Hell, S.W. and J. Wichmann, Breaking the diffraction resolution limit by stimulated emission: stimulated-emission-depletion fluorescence microscopy. Opt Lett, 1994. 19(11): p. 780-2.

196. Harke, B., J. Keller, C.K. Ullal, V. Westphal, A. Schonle, and S.W. Hell, Resolution scaling in STED microscopy. Opt Express, 2008. 16(6): p. 4154-62.

197. Kastrup, L., H. Blom, C. Eggeling, and S.W. Hell, Fluorescence fluctuation spectroscopy in subdiffraction focal volumes. Phys Rev Lett, 2005. 94(17): p. 178104.

198. Li, G.W. and X.S. Xie, Central dogma at the single-molecule level in living cells. Nature, 2011. 475(7356): p. 308-15.

199. Low-Nam, S.T., K.A. Lidke, P.J. Cutler, R.C. Roovers, P.M. van Bergen En Henegouwen, B.S. Wilson, and D.S. Lidke, ErbB1 dimerization is promoted by domain co-confinement and stabilized by ligand binding. Nature Structural and Molecular Biology, 2011. 18(11): p. 1244-9.

200. You, C.J., S. Wilmes, O. Beutel, S. Lochte, Y. Podoplelowa, F. Roder, . . . J. Piehler, Self-Controlled Monofunctionalization of Quantum Dots for Multiplexed Protein Tracking in Live Cells. Angewandte Chemie-International Edition, 2010. 49(24): p. 4108-4112.

201. Andrews, N.L., J.R. Pfeiffer, A.M. Martinez, D.M. Haaland, R.W. Davis, T. Kawakami, . . . D.S. Lidke, Small, mobile FcepsilonRI receptor aggregates are signaling competent. Immunity, 2009. 31(3): p. 469-79.

10 Papers and manuscripts

10.1 Single molecule multi-species tracking in live cells

SINGLE MOLECULE MULTI-SPECIES TRACKING IN LIVE CELLS

Mathias P. Clausen[†], Eva C. Arnspang[†], Byron Ballou[‡], James E. Bear[§], B. Christoffer Lagerholm[†,*]

[†]MEMPHYS – Center for Biomembrane Physics and Danish Molecular Biomedical Imaging Center (DaMBIC), University of Southern Denmark, Campusvej 55, DK-5230 Odense M, Denmark

[‡]Molecular Biosensor and Imaging Center (MBIC), Mellon Institute, Carnegie Mellon University, 4400 Fifth Ave, Pittsburgh, PA 15212

[§]Lineberger Comprehensive Cancer Center and Dept. of Cell & Developmental Biology, Howard Hughes Medical Institute, University of North Carolina, Chapel Hill NC 27599

[*]Corresponding Author: Campusvej 55, DK-5230 Odense M, Denmark

(Phone) +45 6550 3505

(Fax) +45 6550 4048

(E-mail) lagerholm@memphys.sdu.dk

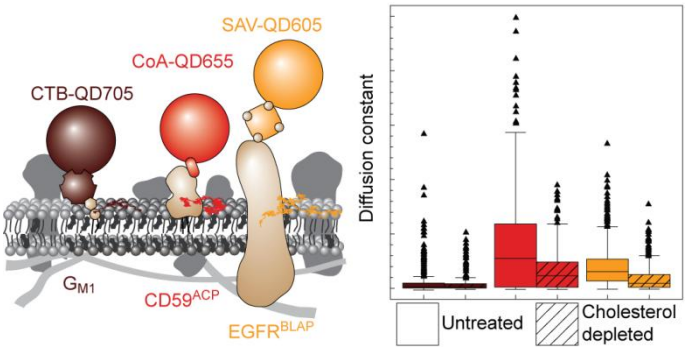

Key words: single particle tracking, lateral dynamics, lipid rafts, multi-color imaging, plasma membrane organization, EGFR, CD59, G_{M1}, quantum dots

In review PLOS ONE

ABSTRACT

Quantum dots are available in a range of spectrally separated emission colors and furthermore with water-stabilizing surface coatings that offers great flexibility for enabling bio-specificity. In this study, we have taken advantage of this to demonstrate that it is possible to perform a simultaneous investigation of the lateral dynamics in the plasma membrane of the purported lipid raft markers: i) the sphingolipid G_{M1}, ii) the glucosylphospatidylinositol-anchored protein CD59, and iii) the transmembrane receptor EGFR, in a single mouse embryo fibroblast cell. We show that the method results in tracks that are sufficiently long to allow for robust single trajectory analysis. This analysis shows that the populations of the diffusion coefficients are heterogeneously distributed for all species, but differ between the different species. We have further investigated the effect of plasma membrane cholesterol on the single molecule movement, and find that both the average diffusion coefficients and the population heterogeneities are decreased after cholesterol depletion, but to different extents depending on the molecule.

INTRODUCTION

Gene expression at the single molecule level is stochastic such that genomically identical cells vary widely in protein expression (*1*). In addition, many proteins are either known to, or thought to be spatially segregated within the cells thus also leading to intracellular heterogeneity in the localization distributions. For example, proteins and also lipids in the plasma membrane have further long been speculated to spatially segregate in nano-domains (*2, 3*) contributing to a significant degree of lateral heterogeneity. A comprehensive understanding of biological structure and function at the molecular level henceforth requires methods that are able to probe the interactions of biomolecules at levels beyond both possible inter- and intra-cellular variations.

Single particle tracking (SPT) is the classical example (*4*) of the presently fast growing set of optical super-resolution microscopy techniques (e.g. STED, PALM, STORM etc.) (*5, 6*), and still it offers the best combination of high spatial resolution (20 – 30 nm), fast temporal sampling (25 Hz – 50 kHz), and a large field of view (typically > 100 μm^2) (*7, 8*). The classical SPT probe is 40 nm diameter gold particles that are additionally stabilized and functionalized for specific molecular binding (*7, 9*) resulting in a hydrodynamic radii, R_H, of ≥ 25 nm. These probes can be imaged at very high sampling frequencies (≤ 50 kHz) for very long periods of time (~ minutes) (*9, 10*), but their non-invasiveness in cells due to their large size remains a contested topic (*7, 11, 12*). Furthermore, as a consequence of the detection by Rayleigh scattering, high light intensity is needed, and multi-species SPT with gold particles is impractical.

SPT is also possible with fluorescent dyes and proteins; however, the photostability of fluorescent dyes and proteins typically limits the trajectory length to a median of 5-15 displacements (*13, 14*). In this case, while SPT is a single molecule method at the detection level, the subsequent analysis is, due to the stochastic nature of Brownian motion, most typically performed to yield an ensemble average both in time and space. For example, SPT data is typically analyzed either by calculation of the mean square displacements (MSD) (*15*), or by analysis of the probability distribution of all squared displacements (*14*) as a function of a given time lag. The data is in most cases also spatially averaged for all trajectories, and for several cells. This averaging is a statistical necessity because of the limited trajectory lengths (*13, 14*). Spatial averaging is likely to obscure possible interactions between individual molecules and e.g. the postulated lipid–protein nano-domains within

biological membranes. Especially in the case where such interactions are weak and short lived such that the single molecules only spend a fraction of their time in these domains as proposed by e.g. Sharma *et al.* (*16*). A recent study has further shown that the intercellular variability in the mean diffusion constant of a glucosylphospatidylinositol-anchored protein (GPI-AP) and a transmembrane protein is five-fold greater than the corresponding intracellular variability (*17*). Thus, it would be much preferable that it would be possible to probe the lateral motion of several types of molecules simultaneously, in the same cell, and at the same time. This however requires a capability to image multiple molecular species at single molecule sensitivity for long periods of time and in the same cell.

More recently, we and others have shown that it is possible to perform multi-color single particle labeling of the *same* molecular species by use of quantum dots (QDs) (*18-22*). QDs, which are fluorescent nanometer-sized semiconductor crystals, have very unique optical properties (*23-25*), and are a very attractive compromise between gold particles and fluorescent dyes and proteins. In particular QDs are distinguished by: a) their very large absorption extinction coefficients and high fluorescence quantum yields making them exceptionally bright and well suited for single molecule detection, b) their photochemical stability which enables imaging over extended time periods, and c) their narrow, tunable emission spectra and overlapping excitation spectra. Further, biocompatible and biofunctional QDs are commercially available, or are easily prepared by chemical coupling employing standard chemistries (*23, 26-28*). Biofunctionalized QDs are also intermediate in size between gold particles and fluorescent dyes and proteins, e.g. commercial streptavidin-QDs have a $R_H \approx 10$ nm which corresponds to about twice the size of a mouse IgG1 (*7*). These features make QDs ideal for SPT experiments, principally though due to their still relatively large size, for tracking of membrane species in the *extracellular* leaflet of the plasma membrane. However, the potential of QDs has not yet been fully exploited for multi-color SPT as thus far no study of *simultaneous* tracking of *different* molecular species has been performed.

In this work, we have extended our previous work (*22*) to also show that it is possible to perform a study of multi-species SPT demonstrating that simultaneous imaging of several different molecules in the same live cell by *orthogonal* targeting of QDs to three distinct membrane species, a lipid (G_{M1}), a GPI-AP (CD59), and a transmembrane protein (EGFR) is possible. We further demonstrate the method by investigating the cholesterol sensitivity of the lateral dynamics of the three distinct membrane species at short time lags, $1 \leq n \leq 5$, here corresponding to $40 \leq n\ t_{lag} \leq 200$ ms, where $t_{lag} = 1 / f$ is the acquisition time interval and f is the image acquisition frequency (here $f = 25$ Hz).

EXPERIMENTAL PROCEDURES

QD conjugations

CTB-QD705

CTB-QD705 were custom made as previously described(*29*) from Qdot® 705 ITK™-carboxyl QDs (Invitrogen) and CTB (Sigma) via the cross-linker 1-ethyl-3(3-dimethylamino propyl) carbodiimideHCl (EDC) (Pierce). The CTB-QD705s used in this study were gel separated to ensure 1 CTB pr. QD.

CoA-QD655

CoA-QD655 were custom made from Qdot® 655 ITK™ amino (PEG) QDs (Invitrogen) and CoA-SH (Covalys) via the cross-linker succinimidyl-4-(*N*-maleinidomethyl)-cyclohexane-1-carboxylate (SMCC) (Sigma) with slight variation from a previously published protocol (*28*) (Figure S1a). The 655 QDs have a CdSe core and a ZnS shell, which is coated with an amino-pegylatedtriblock co-polymer(*30*). A solution of amino QD655 (50 µL, 4 µM) in 50 mM borate buffer were activated with SMCC (5.6 µL, 10 mM) in DMSO for 1 h at RT. Unreacted SMCC was removed by size exclusion chromatography on a 50 mM MES buffer (2 mM EDTA, pH 6.0) equilibrated NAP-5 column by collecting the first 0.5 mL of colored solution. CoA-SH in PBS (10 mM phosphate, 138 mMNaCl 2.7 mMKCl, pH 7.2) was mixed with the activated QDs in molar ratios of 10 CoA pr. QD (1 µL, 2 mM) and 20 CoA pr. QD (2 µL, 2 mM) as compared to the original QD concentration and allowed to react for 1 h at RT. The reaction was quenched by addition of β-ME (10 µL, 10 mM) in milliQ-water for ½ h at RT. The CoA-conjugates (CoA-QD655) were purified by centrifugation in 50 kDa ultra-filtration tubes, and the buffer was exchanged to PBS on a Sephacryl 200 column. To characterize the effectiveness of the conjugation reaction and monodispersity of both the original amino, SMCC and CoA-QD preparations, we used agarose gel electrophoresis (Figure S1b). Only the QDs made using 10 CoA per QD were used in this work.

Cell culture

Mouse embryonic fibroblasts from an Ink4a/Arf null mouse (IA32) were used for microscopy studies(*31*). These cells are very large and flat making them highly suitable for SPT measurements in 2D. Cells were grown in humidified atmosphere at 37 °C in 5 % CO_2. Cells were grown until 80-90 % of confluence and split every third day in 1:5-1:10 ratios using the endopeptidase Trypsin (Sigma). Cells were grown in Dulbecco's modified eagle's medium (DMEM) with high glucose (Dulbecco), with standard concentrations of glutamax (Gibco) and penicillin-streptomycin (Sigma), and 10 % fetal bovine serum (FBS) (Sigma). Cells were seeded in appropriate density and number (30,000) on coverslips in 6-well plates, and left for six-eight hours to attach to the glass. Cells were then transfected and left over night in media containing 10 µM biotin (Sigma), and labeled and imaged the following two days.

Plasmids and transfection

The plasmids used for transfection were; pAEMTX-ACPwt-GPI (Covalys) encoding the GPI-anchored membranes protein CD59 with an extracellular ACP-tag, pcDNA3-EGFR-BLAP, encoding the EGFR with a BLAP-tag in an extracellular domain (*32*), pDISPLAY-BirA-KDEL encoding bacterial biotin ligase with an ER anchor (*33*), and K-Ras2-YFP (ATCC plasmid 10089283) encoding the first 19 amino acids of the C-terminus of the plasma membrane protein K-Ras2 with a YFP-tag. Cells were transfected with a total of 3.1 µg of DNA per well in a 1:1:1:0.1 ratio of the plasmids and a 1:2 (w/v) ratio of the transfection agent JetPEI (Polyplus Transfection).

Multi-color labeling and cholesterol depletion

Cells were washed twice in complete media before successive labeling with the three kinds of QDs. Cells were labeled in CoA-QD655 labeling solution (300 µL complete medium, 10 mM $MgCl_2$, 1 nM CoA-QD655, 0.4 µM ACP Synthase) for no longer than 15 minutes at RT to minimize cross-linking of target molecules. The cells were washed three times in PBS (1 % BSA, 0.1 mg/mL $MgCl_2$, 0.1 mg/mL $CaCl_2$) and incubated with or

without 3 mM methyl-β-cyclo dextran (mβCD) for 10 minutes at 37 °C to deplete cholesterol from the cells (*34*). Cells were then labeled with a combination of 200 pM CTB-QD705 and 1 nM SAV-QD605 (300 µL, PBS, 1 % BSA, 0.1 mg/mL $MgCl_2$, 0.1 mg/mL $CaCl_2$) for two minutes with the addition of biotin (100 µL, 1 mM) after 30 s – 1 min to block further binding of SAV-QD605 (SI 2). Cells were washed three times in PBS (1 % BSA, 0.1 mg/mL $MgCl_2$, 0.1 mg/mL $CaCl_2$) and imaged within 1½ h in presence of 50 µM β-mercaptoethanol (β-ME) (Sigma) (SI 4).

Microscopy setup

Imaging was done using an Olympus IX-81 inverted microscope as has been described (*22*). Fluorescence images were acquired at 10 ms integration time using a 100 W Hg arc lamp, a 470/40 nm bandpass excitation filter at 150X magnification with a 1.45 NA objective (Olympus) focusing on apical membrane of the lamelopodia of the cells. Detection of all colors was done simultaneously through a QuadView emission splitter (dichroic mirrors at 585, 630, and 690 nm, and emission bandpass filters 535/30, 605/20, 655/20, and empty position) and an Andor EMCCD camera at 25 Hz. The spectral overlap of the QDs among the different image channels have previously been shown to be that >99% of QD605s, and >95% of QD655s and QD705s appear in the correct image channels (*22*). Image acquisition was controlled by Andor IQ software and movies of 1200 frames (~48 s) were recorded at RT. The signal-to-noise in the image channel of the YFP-KRas2 fusion protein under the chosen imaging conditions (10 ms camera integration, 25 Hz imaging rate) is very low on an image frame by frame basis. Hence we have so far only used these images to provide a very detailed image of the footprint of the plasma membrane of each cell for the duration of the time lapse sequence by generation of a Sum Intensity Projection image in ImageJ.

Image Analysis

Single acquired time-lapse sequences were analyzed by use of a Particle Tracker plug-in in ImageJ (*35*) as has been described previously (*22*). This analysis generates a text file containing the positions of the detected QD particle positions in each image frame as well as linked trajectories describing the motion of individual QDs in time. In this analysis, a major limitation to the use of QDs in SPT is apparent by the generation of a large number of short trajectories rather than a more desirable few very long continuous particle trajectories. In order to minimize the number of inaccurate particle linking events, this analysis was done with very conservative particle linking criteria, corresponding to a particle link range of 5 image frames and a maximum allowed particle displacement of one pixel per image frame. In order to further analyze the hence detected particle motion, the thus generated data was post-processed in custom written Mathematica routines. This post-processing included further linking of particle trajectories by a coincidence search routine in time and space of all trajectories, with a minimal length greater than a cut-off value (here 50 frames) with other trajectories that were separated in time by < 100 image frames and in space by < (0.1 x the actual number of image frames in between trajectories) pixels^2. We next calculated the mean squared displacements for each single trajectory, *m*, that contained $n > 50$ image frames, and for all possible time intervals, $n\ t_{lag}$,

$$\mathrm{MSD}\ (\quad) \frac{1}{\quad}\sum_{1}\left[\left(\quad\left(\left(\quad\right)\quad\right)\qquad\right)^2\ \left(\quad\left(\left(\quad\right)\quad\right)\quad\left(\quad\right)\right)^2\right]$$

where t_{lag} is the time interval between images, and N is the total number of frames in a trajectory(*15*).The MSD curves for each single trajectory, m, were curve fit at short time intervals, $1 \leq n \leq 5$ (corresponding to $40 \leq t \leq 200$ ms) to a model for free diffusion with fit weights equal to the inverse variance ($1/\sigma^2$)

$$\mathrm{MSD}\left(\quad\right) 4 \quad _5$$

whereD_5 is the diffusion coefficient and c is an off-set constant that has been proposed to be related to the spatial precision by which we can determine the position of a single molecule (*13*).

Monte Carlo Simulations

In order to evaluate the accuracy by which we can analyze single particle trajectories we ran a series of Monte Carlo simulations of free Brownian diffusion in 2D. In these simulations, we kept the total number of displacements of all trajectories constant at 10,000 while we varied the number of displacements per trajectory and in accordance the number of trajectories. Simulations were run for 10, 50, 100, 200, and 500 displacements per trajectory. The simulated diffusion coefficient, $D_{Simulation}$, was 0.5 $\mu m^2/s$ and the time lag, t_{lag}, was 40 ms in all simulations. The simulations were run in Mathematica by use of the RandomReal[] function for generation of two random numbers, a random direction of $0 \leq \theta \leq 2\pi$ and a random displacement, r, where the distribution of the random displacements followed a Raleigh distribution, $P(\quad,\quad) \frac{}{2} \exp -\frac{^2}{4}$. The simulated particle trajectories were subsequently analyzed in a similar manner to the experimental data by calculation of the MSD and by curve fitting. We next evaluated the accuracy of the single trajectory data analysis by calculating the percentage difference for each trajectory between the simulated diffusion coefficient, $D_{Simulation}$, and the fitted diffusion coefficient, D_{Fitted}, from

$$\mathrm{Difference}\ 100 \frac{\qquad\qquad}{}$$

and by determining the mean (± s.t.d.) percentage difference as a function of the number of displacements per trajectory. We also evaluated the accuracy by which we could recover the simulated diffusion coefficient, $D_{Simulation}$, from curve fitting to the mean MSD($n\ t_{lag}$) curve, <MSD($n\ t_{lag}$)> for all displacements for each condition. For further discussion of the simulations see SI 6.

Statistical tests

The non-parametric Kolmogorov-Smirnov test (K-S test) was used to evaluate the differences between the different populations of D_5. The K-S test quantifies the distance between the cumulative density function of the two test populations. The null hypothesis is that the two test populations are drawn from the same distribution. The distributions are considered continuous, but are otherwise not restricted.

RESULTS AND DISCUSSION

Multi-species QD targeting strategy

It has previously been shown that it is possible to perform parallel multi-color SPT in live cells of the *same* species labeled with two (*18-20*) and four colors (*22*). In this work, we show that it is possible to also extend

multi-color SPT to include parallel imaging of *different* molecular species by *orthogonally* targeting QDs of different colors to three distinct membrane species (Figure 1).

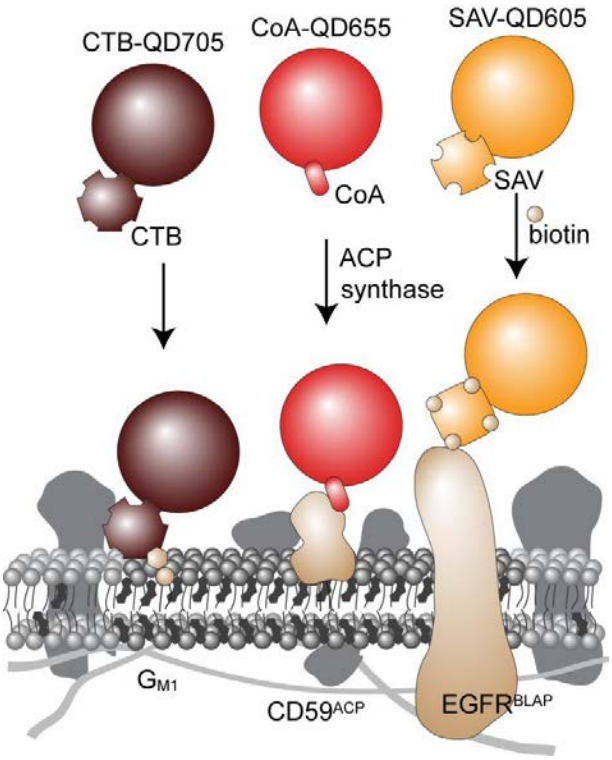

Figure 1. Multi-species SPT labeling strategy. CTB-QD705 labels specifically ganglioside G_{M1} through direct binding of CTB to G_{M1} (left). CoA-QD655 is covalently coupled to GPI-AP $CD59^{ACP}$ in presence of the enzyme ACP synthase (center). SAV-QD605 targets biotinylated $EGFR^{BLAP}$. The BLAP-tag is biotinylated during the secretory transport pathway when cells are grown in presence of biotin and are co-expressing bacterial biotin ligase (BirA-IgGκ-KDEL)(*36*).

The targeted membrane molecules were: i) the ganglioside G_{M1}, 2) an acyl carrier protein (ACP)-epitope tagged version of the GPI-AP $CD59^{(ACP)}$, and 3) a biotin ligase acceptor peptide (BLAP)-epitopetagged version of the epidermal growth factor receptor $EGFR^{(BLAP)}$(*32*). All three molecules have previously been classified as functional lipid raft markers by classic biochemical detergent extraction experiments(*37, 38*), although, the classification of EGFR as a raft marker is questioned(*39*). The targeted molecules were labeled specifically with respectively cholera toxin subunit B (CTB) conjugated QD705s (QDs with peak emission at 705 nm) for G_{M1}(*29*), Co enzyme A (CoA) conjugated QD655sfor $CD59^{ACP}$ (in presence of ACP synthase), and streptavidin (SAV) conjugated QD605s for $EGFR^{BLAP}$ (*32*) (Figure 1). In the study, we have further combined the three-color QD tracking with simultaneous imaging of a fusion protein consisting of the 19 C-terminal amino acids of K-Ras2 and yellow fluorescent protein (YFP). This fusion protein localizes to the plasma membrane with high specificity, and can therefore be used to obtain a high contrast image of the plasma membrane of each imaged cell.

QD conjugates and QD labeling procedure

A series of control experiments (SI 1-5) was performed in order to quantify the effect of the QD conjugates and the QD labeling procedure for each labeled molecule.

The CTB-QD705 conjugates used were gel separated to ensure only one CTB per QD (*29*), but as CTB is pentavalent it is nevertheless likely that small clusters of G_{M1} instead of single G_{M1}molecules were tracked with CTB-QD705s. The monodispersity of the CoA-QD655 conjugates were also checked by gel separation (Figure S1b), and the lowest reaction ratio of CoA to QD, where high specific binding was observed, were used (ratio 10:1).The binding of CoA-QD655s to the plasma membrane ACP-target was further controlled by limiting the enzymatic incubation time with CoA Synthase. The commercial SAV-QD605s used have been reported to have ~15 SAV per QD (*40*). Further, SAV is tetravalent and inherently there is therefore a high potential of probe induced cross-linking, when using these probes. The cross-linking was, however, strongly minimized by addition of a >1000 fold excess of biotin shortly following QD labeling (Figure S2), resulting in a 120 % increase of the mean diffusion coefficient, $<D_5>$, for short time lags $1 \leq n \leq 5$ as compared to when no biotin.

The specificity of the binding of the CoA and SAV QDs was validated by the labeling of non-expressing cells. In these samples most cells had no QDs on the surface; however, some cells had a few QDs bound unspecific on the surface. We also measured the size of the three QD conjugates by fluorescence correlation spectroscopy (FCS) and found that the hydrodynamic radii (R_H) of the different conjugates were approximately equal and were ~10 nm (SI 3, Table S3 and Figure S3).

A direct comparison of the CoA-QD655 and SAV-QD605 probes was further made by targeting $CD59^{ACP}$ and $CD59^{BLAP}$, respectively (Figure S4). This shows that there is only a slight absolute difference in $<D_5>$, (0.074 $\mu m^2/s$ vs. 0.072 $\mu m^2/s$). The distributions of the individual trajectory diffusion coefficients, D_5, however, are not from similar populations, and therefore a direct comparison of the lateral dynamics is non-trivial.

All imaging was done in 50 µM β-mercaptoethanol (β-ME) in order to minimize QD intermittency and bleaching. Control experiments of $EGFR^{BLAP}$ labeled with SAV-QD605s (Figure S5) showed that there was no difference in the diffusion between cells imaged with and without 50 µM β-ME, but that the mean trajectory length increased by ~50 . Experiments with 500 µM β-ME showed an increase in $<D_5>$by ~40% suggesting that steric hindrance due to e.g. disulfide bonds of the extracellular matrix could be an issue in the experiments. We believe that the use of trace amounts of β-ME in this case is further justified since e.g. stem cells are often grown in much higher concentrations to aid nutrient uptake (*41*).

Single trajectory analysis

Cell were labeled successively with the CTB-QD705s, CoA-QD655, and SAV-QD605s and pharmacologically treated (in case of cholesterol depletion). Multi-color time-lapse imaging at an image acquisition frequency of 25 Hz (time lag t_{lag}= 40 ms) was performed in a setup previously described with a spatial precision of $\delta = (\delta^2+\delta^2)^{1/2} < 30$ nm (*22*). Figure 2 shows a representative example of an overlay of the single molecule trajectories of the three QD tracked species on a K-Ras2-YFP membrane contrast image.

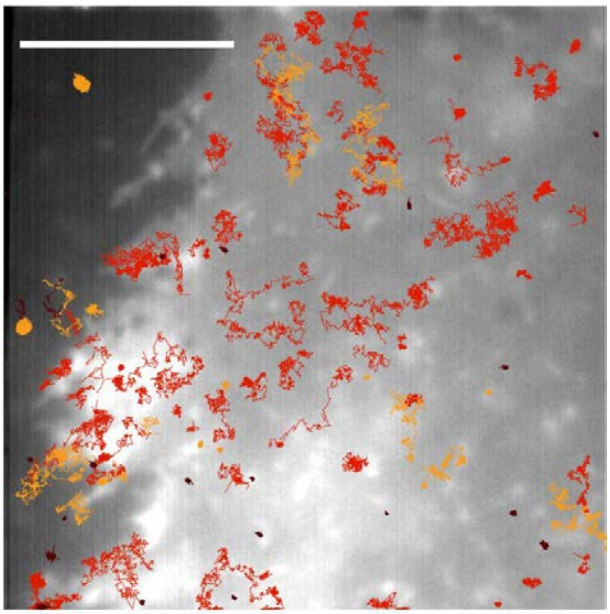

Figure 2. SPT trajectory example. Overlay of summed intensity image of K-Ras2-YFP and the calculated QD trajectories longer than 50 displacements. Dark red is G_{M1}, red $CD59^{ACP}$, and orange $EGFR^{BLAP}$. Scale bar is 10 µm.

The SPT analysis was based on the analysis of single trajectories, where only trajectories having $N > 50$ displacements were included and analyzed by calculation of the MSD($t = n\ t_{lag}$) for $1 \leq n \leq 5$, with n being the number of steps between the calculated displacements, and by fitting to a Brownian diffusion model: MSD = $4\ D_5\ t$ + c. This analysis gives a microscopic diffusion coefficient D_5 that describes the lateral dynamics at short time intervals (40 ms < t < 200 ms).

The trajectory length cut-off of N = 50 was based on Monte-Carlo simulations of Brownian diffusion in an infinite 2D plane by evaluation of the ability to recover the simulated diffusion coefficient from the analysis of single simulated trajectories as a function of the number of displacements, N (Figure 3)(SI 6, Figure S6, Table S6).

With a cut-off of N=50, the mean trajectory length of the experimental data was for all molecules >200 displacements (Table 1). The simulations showed a percentage error (±std.) of the fitted D_5 compared to the simulated diffusion coefficient $D_{Simulation}$ of 23 ± 18 % for N = 50 and 11 ± 8 % for N = 200. The percentage error for N = 10 was 57 ± 47 % explaining why single trajectory analysis is not possible for trajectories this short.

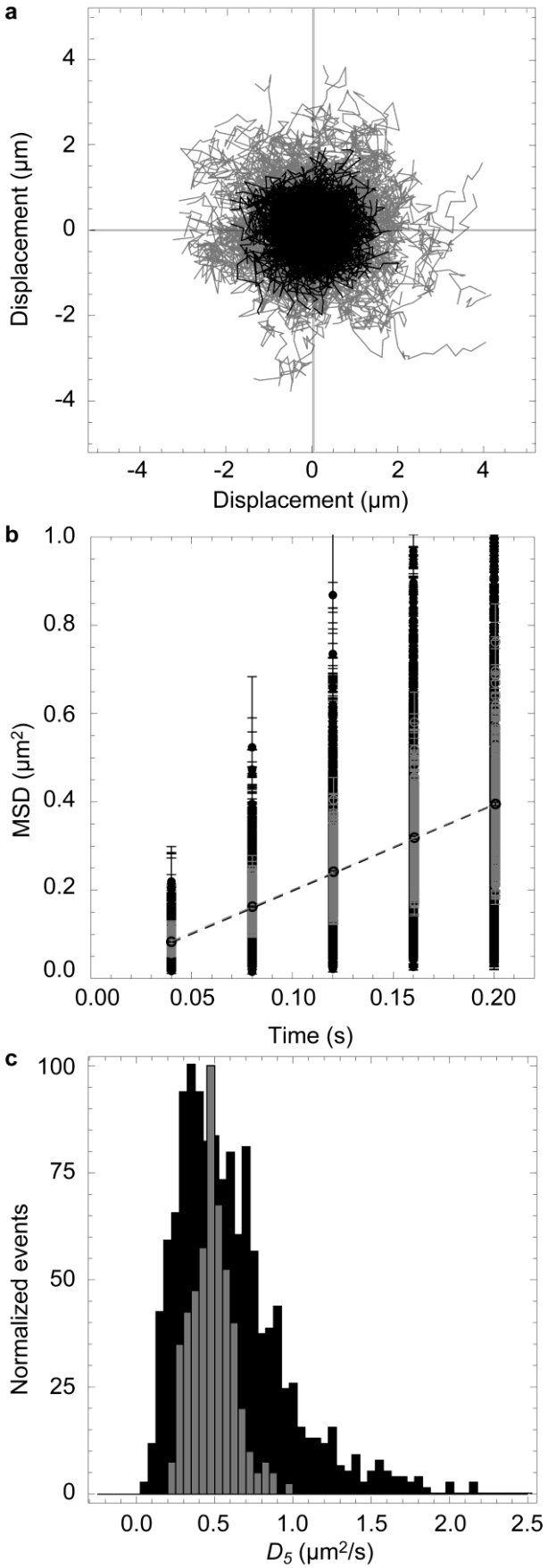

Figure 3. Monte Carlo simulation of 2D Brownian motion. Simulated data: 1000 particle trajectories of 10 displacements (black), 200 particle trajectories of 50 displacements (grey). a) All simulated particle trajectories. b) MSD plot for each particle trajectory and best fit to the mean MSD of all displacements (dashed lines). c) Histogram of single trajectory D_5. (Further discussion, see text and SI 6.)

Lateral diffusion of G_{M1}, CD59 and EGFR

The distributions of D_5 from the single trajectory analysis are shown in Figure 4, and Table 1 summarizes the trajectory data.

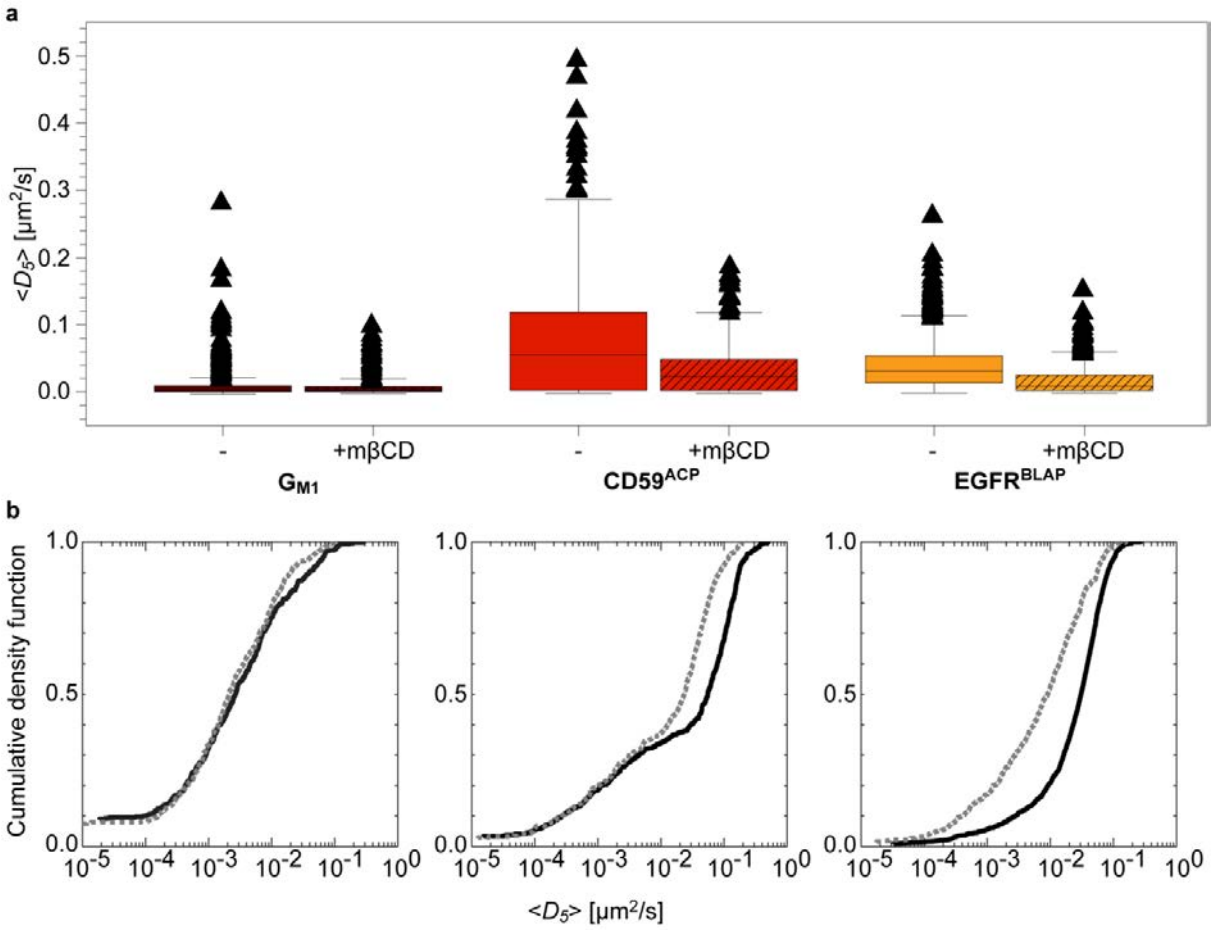

Figure 4. Single molecule diffusion of G_{M1}, $CD59^{ACP}$, and $EGFR^{BLAP}$. a) Box-and-whisker plots of the single molecule diffusion coefficients $D_5$for the three molecular species; G_{M1} (dark red), $CD59^{ACP}$ (red), and $EGFR^{BLAP}$ (orange), in non-treated (full color) and cholesterol depleted (hatched color) cells, respectively. b) Cumulative density functions of the D_5 for untreated (black) and cholesterol depleted (grey dashed) cells. A statistical significant difference between the populations of D_5 (K-S test) after cholesterol treatment was observed for $CD59^{ACP}$ and $EGFR^{BLAP}$. Statistical significant differences were also observed between the different molecular species both in non-treated and cholesterol depleted cells.

The distribution of D_5 ranges between 0.00 – 0.30 μm²/s for G_{M1} (unperturbed) and 0.00 – 0.10 μm²/s (cholesterol depleted), 0.00 – 0.50 μm²/s for $CD59^{ACP}$ (unperturbed) and 0.00 – 0.20 μm²/s (cholesterol depleted), and 0.00 – 0.30 μm²/s for $EGFR^{BLAP}$ (unperturbed) and 0.00 – 0.20 μm²/s (cholesterol depleted) in a heterogeneous significantly non-Gaussian way determined from a Kolmogorov-Smirnov statistical test (K-S test). The K-S test was also applied in a pairwise fashion to evaluate whether the data – given the heterogeneity – suggested that the populations of $D_5$for the different molecules (both before and after cholesterol depletion) were alike (p-values in Table S7). This showed a significant difference in lateral mobility in a cholesterol independent manner when comparing between different species. When comparing the same species before and after cholesterol depletion, a change between the populations of D_5 was observed in the cases of $CD59^{ACP}$ and $EGFR^{BLAP}$, but not for G_{M1} (p-value = 0.17).

	G_{M1}		$CD59^{ACP}$		$EGFR^{BLAP}$	
QD conjugate	CTB-QD705		CoA-QD655		SAV-QD605	
Cell treatment	-	mβCD	-	mβCD	-	mβCD
# of trajectories	411	365	511	341	1557	499
$<N>$ per trajectory	208	206	304	299	350	580
$<D_5>$ ± s.e.m. [$\mu m^2/s$]	0.013 ± $6.8 \cdot 10^{-5}$	0.008 ± $4.1 \cdot 10^{-5}$	0.074 ± $16 \cdot 10^{-5}$	0.034 ± $11 \cdot 10^{-5}$	0.038 ± $2.1 \cdot 10^{-5}$	0.018 ± $4.7 \cdot 10^{-5}$
MAD [$\mu m^2/s$]	0.0025	0.0019	0.054	0.022	0.020	0.0081

Table 1. Trajectory and diffusion data. Data from all single trajectories displayed in Figure 4. Data from non-treated cells was collected from a total of 18 cells, while data from cholesterol depleted (mβCD treatment) cells was collected from a total of 20 cells.

To further quantify the molecular lateral diffusive heterogeneity and the effect of cholesterol depletion, the relative change in the median absolute deviation (MAD) was calculated, and was observed to decrease after cholesterol depletion by 25 % for G_{M1}, 59 % for $CD59^{ACP}$, and 59 % for $EGFR^{BLAP}$. Also the population mean diffusion coefficient $<D_5>$ was lowered for all three species by38 % for G_{M1}, 55% for $CD59^{ACP}$, and 52 % for $EGFR^{BLAP}$. There was, however, still large differences between the D_5 for all species as an indicative of the complex stochastic single molecule behavior with apparent examples of Brownian, confined, and directed motion and combinations thereof (Figure S8).

The results support the notion that cholesterol plays a role in the lateral dynamics of all three species (although not statistically significant using a K-S test in the case of G_{M1}). However, the observed differences in the populations of D_5 between the different species suggest that not all molecules that have been classified as lipid raft markers by classical biochemistry are alike, and further that these specific molecules are differentially affected by cholesterol depletion. It is noticed that $CD59^{ACP}$ and $EGFR^{BLAP}$ was affected in very similar ways by cholesterol depletion, possibly indicating a relationship between the two species.

CONCLUSION

In conclusion, we have shown an example of an *orthogonal* multi-color QD labeling strategy that enables *parallel* imaging of three separate bio-molecules at the single molecule level in the same sub-area of living cells(a fourth color was also imaged simultaneously in the setup, but not at single molecule level). We further have shown that the resulting trajectory lengths are sufficient to enable robust single trajectory analysis such that it is possible to sample the heterogeneity of the lateral motion for each species. Finally, we have used the method to show that the lateral dynamics of the three purported lipid raft markers G_{M1}, $CD59^{ACP}$, and $EGFR^{BLAP}$ are statistically different, and we have quantified the effect of cholesterol on the lateral diffusion.

This multi-species SPT technique fills a gap in the lack of suitable methods for simultaneously studying membrane lateral dynamics of multiple species in the same area of the same cell, and opens up for very detailed spatio-temporal investigations of the plasma membrane nanoscopic organization.

While this manuscript firmly establishes that it is possible to investigate the lateral motion of several species simultaneously in the same sub-region of live cells further improvements in the probe design are still needed. In particular a robust molecule to molecule comparison will require conclusively validated monovalent probes.

ACKNOWLEDGEMENTS

We thank A. Y. Ting for the pcDNA3-EGFR-BLAP construct. This work was supported by the VillumKann Rasmussen Foundation (to BioNET), Leo PharmaForskningsfond, the Lundbeck Foundation, the Novo Nordisk Foundation, and the Danish Natural Research Foundation (to MEMPHYS – Center for Biomembrane Physics) and DaMBIC (Danish Molecular Biomedical Imaging Center).J. E. B. was supported by NIH grant GM083035.B. B. was supported by NIH grant R01 EB000364.

SUPPORTING INFORMATION

Supporting information available: S1: CoA-QD conjugation and validation, S2: Effect of blocking SAV-QD605s with biotin, S3: Hydrodynamic radius of QD conjugates, S4: Comparison of SAV-QD605 and CoA-QD655 conjugates, S5: Effect of β-mercapthoethanol on SAV-QD605 trajectories, S6: Monte Carlo simulation of 2D Brownian diffusion, S7: p-values for Kolmogorov-Smirnov test, S8: Single trajectory heterogeneity examples. This material is available free of charge via the Internet at http://pubs.scs.org.

AUTHOR CONTRIBUTIONS

BB provided the CTB-QD705 conjugates. JEB provided the Ink4a/Arf null mouse embryo fibroblasts. EAC and BCL designed the microscope. MPC, EAC, and BCL designed the experiments. MPC performed the experiments. BCL wrote the analysis program. MPC and BCL analyzed the experiments.

ABBREVIATIONS

ACP – Acyl Carrier Protein, β-ME – beta-mercaptoethanol, BLAP – Biotin Ligase Acceptor Peptide, CoA – Co Enzyme A, CTB – Cholera Toxin B, EGFR – Epidermal Growth Factor Receptor, MSD – Mean Squared Displacement, QD – Quantum Dot, SAV – Streptavidin, SPT – Single Particle Tracking.

REFERENCES

(1) Li, G. W., and Xie, X. S. (2011) Central dogma at the single-molecule level in living cells. *Nature 475*, 308-15.

(2) Jacobson, K., Mouritsen, O. G., and Anderson, R. G. (2007) Lipid rafts: at a crossroad between cell biology and physics. *Nat Cell Biol 9*, 7-14.

(3) Lingwood, D., and Simons, K. (2010) Lipid rafts as a membrane-organizing principle. *Science 327*, 46-50.

(4) Saxton, M. J., and Jacobson, K. (1997) Single-particle tracking: applications to membrane dynamics. *Annu Rev Biophys Biomol Struct 26*, 373-99.

(5) Eggeling, C., Ringemann, C., Medda, R., Schwarzmann, G., Sandhoff, K., Polyakova, S., Belov, V. N., Hein, B., von Middendorff, C., Schonle, A., and Hell, S. W. (2009) Direct observation of the nanoscale dynamics of membrane lipids in a living cell. *Nature 457*, 1159-62.

(6) Patterson, G., Davidson, M., Manley, S., and Lippincott-Schwartz, J. (2010) Superresolution imaging using single-molecule localization. *Annu Rev Phys Chem 61*, 345-67.

(7) Clausen, M. P., and Lagerholm, B. C. (2011) The Probe Rules in Single Particle Tracking. *Curr Protein Pept Sci 12*, 699-713.

(8) Suzuki, K., Ritchie, K., Kajikawa, E., Fujiwara, T., and Kusumi, A. (2005) Rapid hop diffusion of a G-protein-coupled receptor in the plasma membrane as revealed by single-molecule techniques. *Biophys J 88*, 3659-80.

(9) Fujiwara, T., Ritchie, K., Murakoshi, H., Jacobson, K., and Kusumi, A. (2002) Phospholipids undergo hop diffusion in compartmentalized cell membrane. *J Cell Biol 157*, 1071-81.

(10) Umemura, Y. M., Vrljic, M., Nishimura, S. Y., Fujiwara, T. K., Suzuki, K. G., and Kusumi, A. (2008) Both MHC class II and its GPI-anchored form undergo hop diffusion as observed by single-molecule tracking. *Biophys J 95*, 435-50.

(11) Mascalchi, P., Haanappel, E., Carayon, K., Mazeres, S., and Salome, L. (2012) Probing the influence of the particle in Single Particle Tracking measurements of lipid diffusion. *Soft Matter 8*, 4462-4470.

(12) Clausen, M. P., and Lagerholm, B. C. (2011) The Probe Rules in Single Particle Tracking. *Curr Protein Pept Sci*.

(13) Wieser, S., Moertelmaier, M., Fuertbauer, E., Stockinger, H., and Schutz, G. J. (2007) (Un)confined diffusion of CD59 in the plasma membrane determined by high-resolution single molecule microscopy. *Biophys J 92*, 3719-28.

(14) Wieser, S., and Schutz, G. J. (2008) Tracking single molecules in the live cell plasma membrane-Do's and Don't's. *Methods 46*, 131-40.

(15) Bannai, H., Levi, S., Schweizer, C., Dahan, M., and Triller, A. (2006) Imaging the lateral diffusion of membrane molecules with quantum dots. *Nat Protoc 1*, 2628-34.

(16) Sharma, P., Varma, R., Sarasij, R. C., Ira, Gousset, K., Krishnamoorthy, G., Rao, M., and Mayor, S. (2004) Nanoscale organization of multiple GPI-anchored proteins in living cell membranes. *Cell 116*, 577-89.

(17) Wieser, S., Weghuber, J., Sams, M., Stockinger, H., and Schutz, G. J. (2009) Cell-to-cell variability in the diffusion constants of the plasma membrane proteins CD59 and CD147. *Soft Matter 5*, 3287-3294.

(18) Andrews, N. L., Lidke, K. A., Pfeiffer, J. R., Burns, A. R., Wilson, B. S., Oliver, J. M., and Lidke, D. S. (2008) Actin restricts FcepsilonRI diffusion and facilitates antigen-induced receptor immobilization. *Nat Cell Biol 10*, 955-63.

(19) Low-Nam, S. T., Lidke, K. A., Cutler, P. J., Roovers, R. C., van Bergen En Henegouwen, P. M., Wilson, B. S., and Lidke, D. S. (2011) ErbB1 dimerization is promoted by domain co-confinement and stabilized by ligand binding. *Nature Structural and Molecular Biology 18*, 1244-9.

(20) You, C. J., Wilmes, S., Beutel, O., Lochte, S., Podoplelowa, Y., Roder, F., Richter, C., Seine, T., Schaible, D., Uze, G., Clarke, S., Pinaud, F., Dahan, M., and Piehler, J. (2010) Self-Controlled Monofunctionalization of Quantum Dots for Multiplexed Protein Tracking in Live Cells. *Angew Chem Int Edit 49*, 4108-4112.

(21) Andrews, N. L., Pfeiffer, J. R., Martinez, A. M., Haaland, D. M., Davis, R. W., Kawakami, T., Oliver, J. M., Wilson, B. S., and Lidke, D. S. (2009) Small, mobile FcepsilonRI receptor aggregates are signaling competent. *Immunity 31*, 469-79.

(22) Arnspang Christensen, E., Brewer, J. R., and Lagerholm, B. C. (2012) Multi-color single particle tracking with quantum dots.

(23) Rosenthal, S. J., Chang, J. C., Kovtun, O., McBride, J. R., and Tomlinson, I. D. (2011) Biocompatible quantum dots for biological applications. *Chem Biol 18*, 10-24.

(24) Michalet, X., Pinaud, F. F., Bentolila, L. A., Tsay, J. M., Doose, S., Li, J. J., Sundaresan, G., Wu, A. M., Gambhir, S. S., and Weiss, S. (2005) Quantum dots for live cells, in vivo imaging, and diagnostics. *Science 307*, 538-44.

(25) Bruchez, M., Jr., Moronne, M., Gin, P., Weiss, S., and Alivisatos, A. P. (1998) Semiconductor nanocrystals as fluorescent biological labels. *Science 281*, 2013-6.

(26) Howarth, M., Liu, W., Puthenveetil, S., Zheng, Y., Marshall, L. F., Schmidt, M. M., Wittrup, K. D., Bawendi, M. G., and Ting, A. Y. (2008) Monovalent, reduced-size quantum dots for imaging receptors on living cells. *Nat Methods 5*, 397-9.

(27) Medintz, I. L., Uyeda, H. T., Goldman, E. R., and Mattoussi, H. (2005) Quantum dot bioconjugates for imaging, labelling and sensing. *Nat Mater 4*, 435-46.

(28) Sunbul, M., Yen, M., Zou, Y., and Yin, J. (2008) Enzyme catalyzed site-specific protein labeling and cell imaging with quantum dots. *Chem Commun (Camb)*, 5927-9.

(29) Chakraborty, S. K., Fitzpatrick, J. A., Phillippi, J. A., Andreko, S., Waggoner, A. S., Bruchez, M. P., and Ballou, B. (2007) Cholera toxin B conjugated quantum dots for live cell labeling. *Nano Lett 7*, 2618-26.

(30) Gao, X., Cui, Y., Levenson, R. M., Chung, L. W., and Nie, S. (2004) In vivo cancer targeting and imaging with semiconductor quantum dots. *Nat Biotechnol 22*, 969-76.

(31) Cai, L., Makhov, A. M., Schafer, D. A., and Bear, J. E. (2008) Coronin 1B antagonizes cortactin and remodels Arp2/3-containing actin branches in lamellipodia. *Cell 134*, 828-42.

(32) Chen, I., Howarth, M., Lin, W., and Ting, A. Y. (2005) Site-specific labeling of cell surface proteins with biophysical probes using biotin ligase. *Nat Methods 2*, 99-104.

(33) Howarth, M., Takao, K., Hayashi, Y., and Ting, A. Y. (2005) Targeting quantum dots to surface proteins in living cells with biotin ligase. *Proc Natl Acad Sci U S A 102*, 7583-8.

(34) Mahammad, S., and Parmryd, I. (2008) Cholesterol homeostasis in T cells. Methyl-beta-cyclodextrin treatment results in equal loss of cholesterol from Triton X-100 soluble and insoluble fractions. *Biochim Biophys Acta 1778*, 1251-8.

(35) Sbalzarini, I. F., and Koumoutsakos, P. (2005) Feature point tracking and trajectory analysis for video imaging in cell biology. *J Struct Biol 151*, 182-95.

(36) Howarth, M., and Ting, A. Y. (2008) Imaging proteins in live mammalian cells with biotin ligase and monovalent streptavidin. *Nat Protoc 3*, 534-45.

(37) Brown, D. A., and Rose, J. K. (1992) Sorting of GPI-anchored proteins to glycolipid-enriched membrane subdomains during transport to the apical cell surface. *Cell 68*, 533-44.

(38) Lagerholm, B. C., Weinreb, G. E., Jacobson, K., and Thompson, N. L. (2005) Detecting microdomains in intact cell membranes. *Annu Rev Phys Chem 56*, 309-36.

(39) Pike, L. J. (2005) Growth factor receptors, lipid rafts and caveolae: An evolving story. *Biochimica et Biophysica Acta (BBA) - Molecular Cell Research 1746*, 260-273.

(40) Mittal, R., and Bruchez, M. P. (2011) Biotin-4-fluorescein based fluorescence quenching assay for determination of biotin binding capacity of streptavidin conjugated quantum dots. *Bioconjug Chem 22*, 362-8.

(41) Thomson, J. A., Itskovitz-Eldor, J., Shapiro, S. S., Waknitz, M. A., Swiergiel, J. J., Marshall, V. S., and Jones, J. M. (1998) Embryonic stem cell lines derived from human blastocysts. *Science 282*, 1145-7.

SINGLE MOLECULE MULTI-SPECIES TRACKING IN LIVE CELLS

SUPPLEMENTARY INFORMATION

Mathias P. Clausen, Eva C. Arnspang, Byron Ballou, James E. Bear, B. Christoffer Lagerholm

SI 1: COA-QD CONJUGATION AND VALIDATION

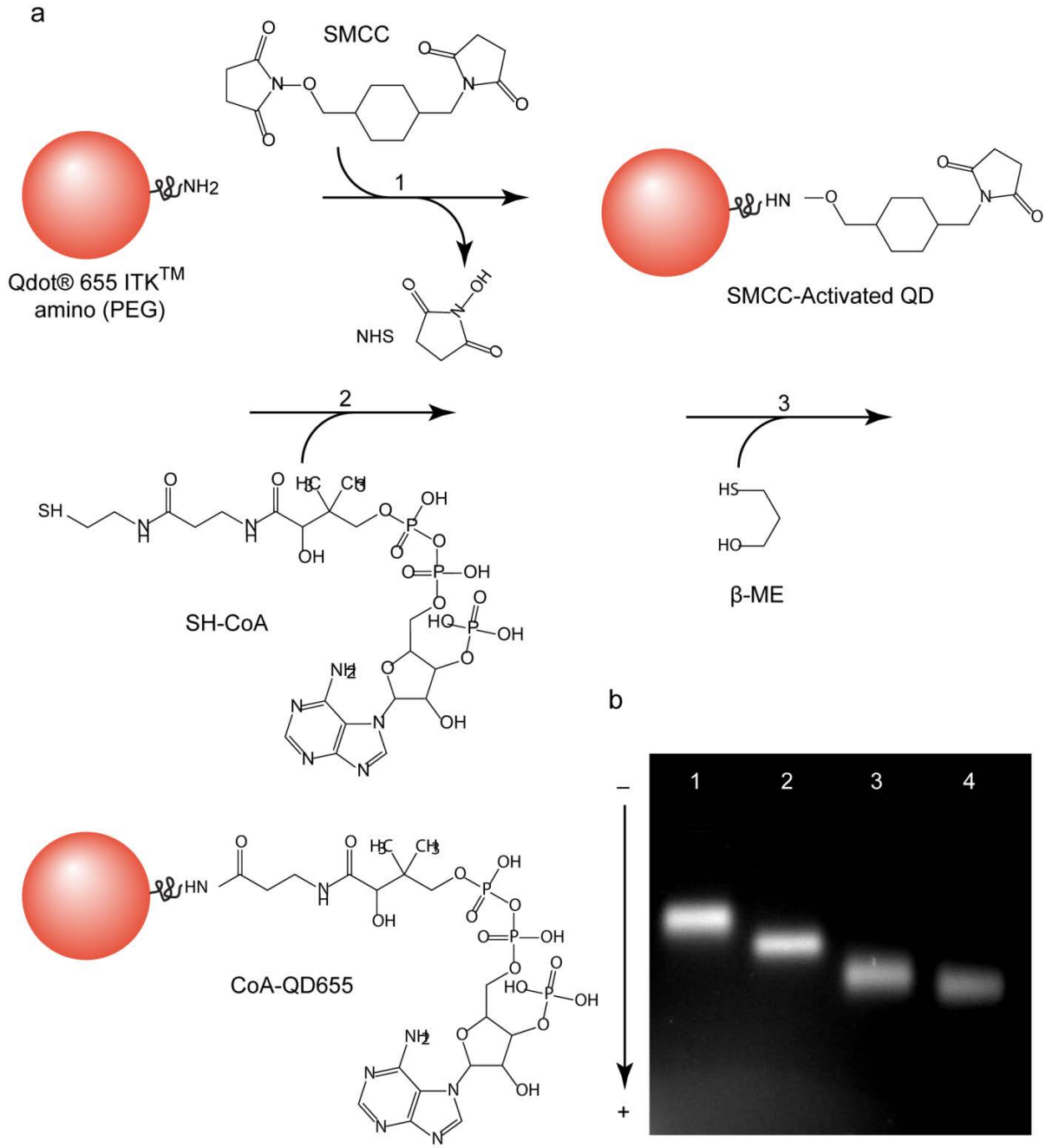

Figure S1. Synthesis of CoA-QD655 conjugates. a) In reaction 1 the NH_2-group on the PEG-QD655 reacts with the NHS-ester of the cross-linker Succinimidyl-4-(*N*-maleimidomethyl)cyclohexane-1-carboxylate (SMCC). In reaction 2 the second reactive group of SMCC, the maleimide, reacts with the SH-group of SH-CoA. Reaction 2 is quenched in reaction 3 by the addition of excess β-ME which reacts and blocks unreacted maleimide. The final product is CoA-QD655. b) 2 % agarose gel. Lane 1: NH_2-PEG-QDs. Lane 2: QDs activated with SMCC and quenched with β-ME. Lane 3: CoA-QD655 (molar ratio 10:1). Lane 4: CoA-QD655 (molar ratio 20:1). The QDs moved from negative to positive as indicated.

SI 2: EFFECT OF BLOCKING SAV-QD605S WITH BIOTIN

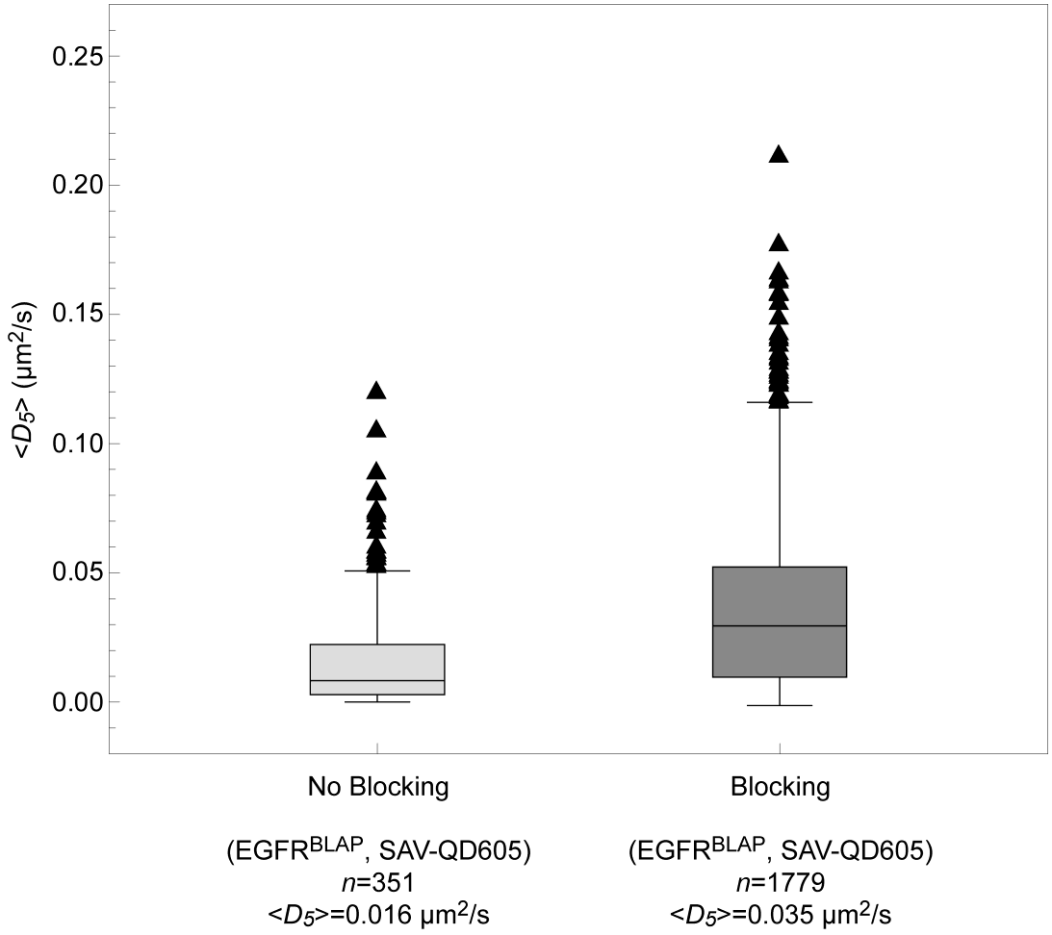

Figure S2. Effect of blocking SAV-QD605s with biotin. Box-and-whiskers plot of the diffusion coefficients for $EGFR^{BLAP}$ targeted with SAV-QD605, with (dark gray) and without blocking (light gray) with excess biotin ½-1 min post SAV-QD605 labeling, respectively. The mean diffusion coefficient increased as indicated on the figure by ~120 %. The reduced mean diffusion coefficient when not blocking with biotin indicates that SAV-QD605 induced cross-binding of $EGFR^{BLAP}$.

SI 3: HYDRODYNAMIC RADIUS OF QD CONJUGATES

Fluorescence correlation spectroscopy (FCS) measurements

The FCS measurements reported in this paper were made on a custom builtmultiphoton excitation microscope as has been described previously (*1*). The objective used in the experiments was a 60X, 1.2 NA water immersion objective. The excitation light source was a femtosecond Ti:Sa laser (Deep See, Spectra Physics, Mountain View, CA) and the excitation wavelength was 780 nm. The correlation data was collected at 50 kHz for ~1 min and where each reported measurement is the average measurement from at least five independent measurements. The correlation data was curve fit to

$$G(\ ) \quad (\ )\left(\frac{\ }{\ ^2}\right)\left(\frac{\ }{\sqrt{\ ^2}}\right) \quad \left(\frac{\ }{2}\right)^{3\ 2} \quad ^2 \qquad \text{Eq.}$$

Where D is the diffusion coefficient, is the correlation time, and where r_0 is beam waist in the radial direction and $z_0$is the beam waist in the axial direction, and V_{eff} is the excitation volume. In these experiments, we used Alexa488 labeled mouse IgG1 as a reference size standard with a known hydrodynamic radius of R_H(Ms IgG1) = 5.6 ± 0.2 nm (*2*) in order to calibrate the excitation volume, $V_{eff.}$. The diffusion coefficient, D, is inversely dependent on the molecular size, R_H, and is given by the Stokes-Einstein relation

$$\frac{\ }{6} \qquad \text{Eq.2}$$

wherek_B is the Boltzmann constant, T is the absolute temperature of the measurement, and is the absolute viscosity of the solution that the measurement was performed in. In this case, all FCS measurements were performed in 50 mM sodium borate pH 8.2 with 1% (w:v) BSA at RT (293K). The relative size of molecular species when compared to a size standard, are independent of the viscosity and are given by

$$\frac{\ }{\ } \quad \frac{\ }{\ } \qquad \text{Eq.3}$$

In order to also convert the relative hydrodynamic radius values to absolute values, we estimated of the solution by assuming that BSA is a hard sphere in the sodium borate solution and by using

$$(\ 2.5 \quad 6.2\ ^2) \qquad \text{Eq. 4}$$

where $_s$ is the viscosity of the solvent (here taken as that of pure water at 293K ($_s$ = 1.002 cP)) and is the volume fraction occupied by BSA in the buffer. At 1% BSA (w:v) and using a R_H of 3.42 nm for BSA (*3*), the volume fraction, , is 0.015 yielding a viscosity, , of 1.04 cP at 293K.

Probe	N	D_S μm^2/s)	g robe / robe R g	R_H
Alexa488-Mouse IgG1	6	37.8±3.3	1.00±0.12	5.6±0.7
CTB-QD705	6	21.9±1.7	1.73±0.20	9.7±1.2
CoA-QD655	6	20.2±0.6	1.87±0.17	10.5±1.0
SAV-QD605	6	21.7+1.1	1.75±0.18	9.8±1.0

Table S3: Hydrodynamic radius of QD conjugates.

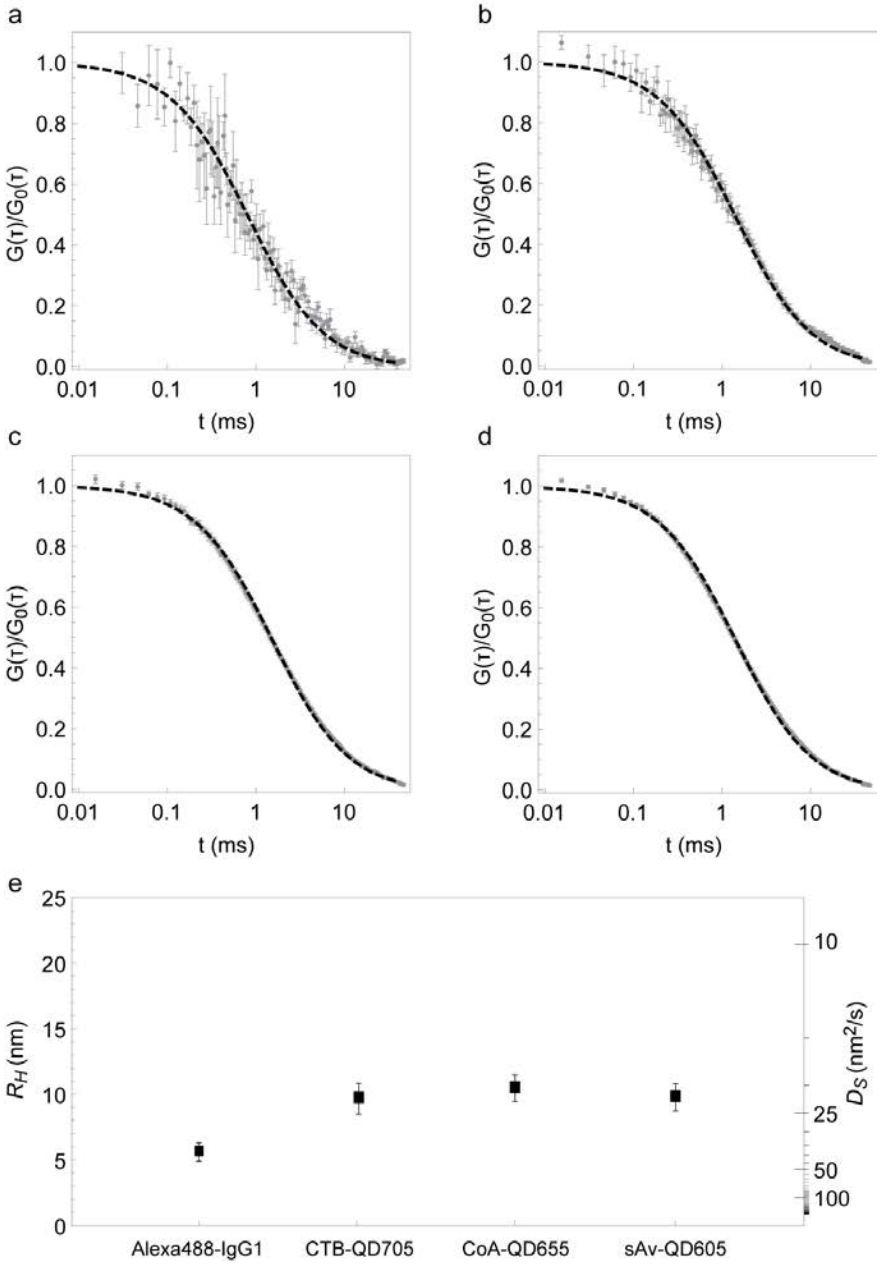

Figure S3. Hydrodynamic radius of QD conjugates. The hydrodynamic radii, R_H, of the QD conjugates were determined by FCS as has been described previously (*1*). Shown in a-d is the mean (± s.e.m.) of $N = 6$ independent correlation curves for a) Alexa488-labeled mouse IgG1, b)CTB-QD705, c) CoA-QD655, and d) SAV-QD605. Also shown in a-d is the best fit to the theoretical expression of the mean of the autocorrelation curves, $G(\ )$, for free diffusion in solution and using two-photon excitation. e) Plot of the fitted diffusion coefficients in solution, D_S, and the calculated hydrodynamic radius (R_H, mean ± s.e.m.) from the Stokes-Einstein relation of the samples in a-d. All measurements were performed in 50 mM sodium borate pH 8.2 with 10 mg/ml BSA at RT and by using a Alexa488 labeled mouse IgG1 as a reference standard of a known hydrodynamic radius of R_H(Ms IgG1) = 5.6 ± 0.2 nm(*2*).

SI 4: COMPARISON OF SAV-QD605 AND COA-QD655 CONJUGATES

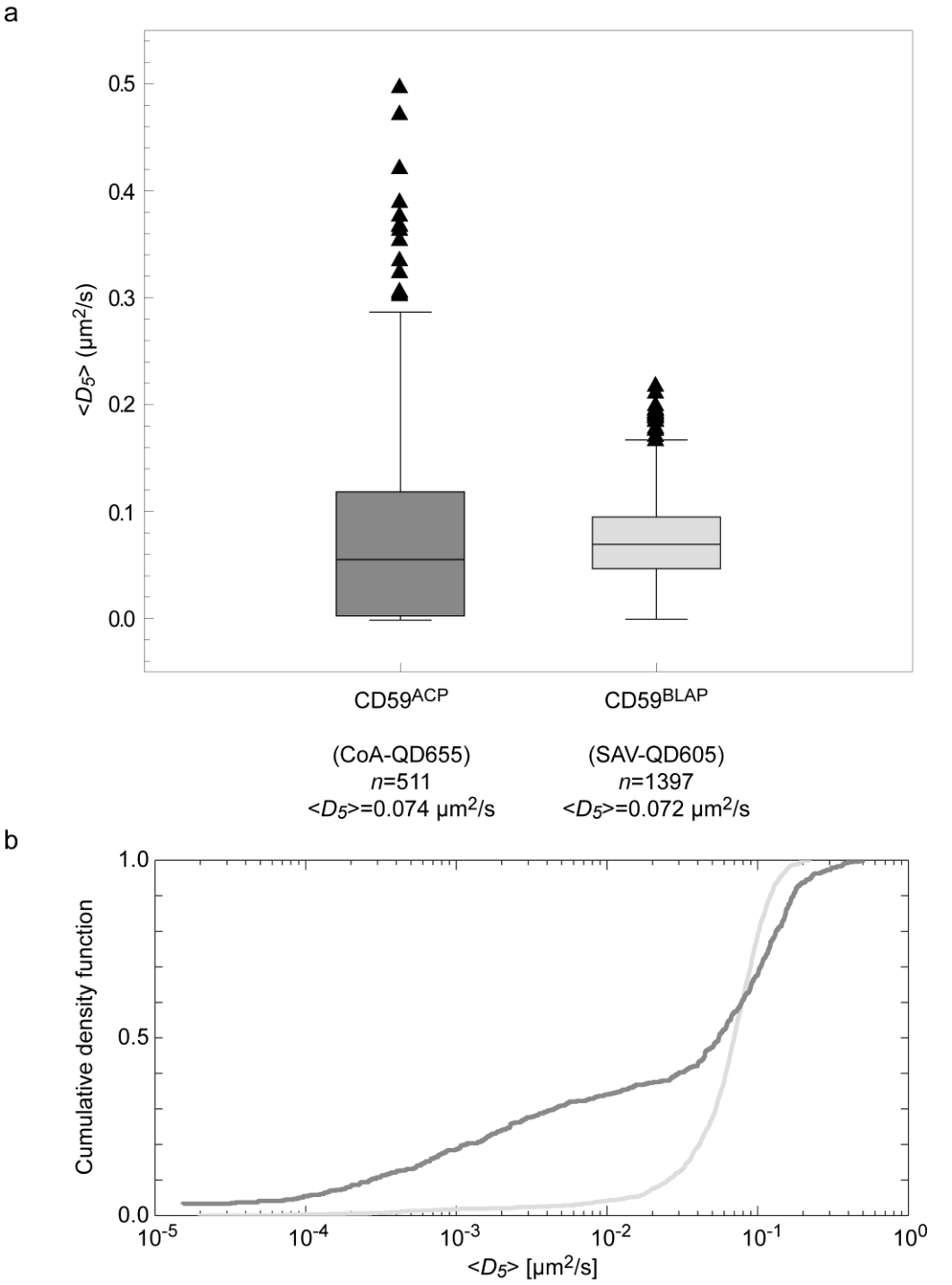

Figure S4. Comparison of SAV-QD605 and CoA-QD655 conjugates. a) Box-and-whiskers plot of the diffusion coefficients for $CD59^{ACP}$ and $CD59^{BLAP}$ targeted with CoA-QD655 (dark gray) and SAV-QD605 (light gray). The mean diffusion coefficients of the two populations are numerically very close.b) Cumulative density function plot of the diffusion coefficients of $CD59^{ACP}$ and $CD59^{BLAP}$showing that the distributions are non-identical.

SI 5: EFFECT OF B-MERCAPTHOETHANOL ON SAV-QD605 TRAJECTORIES

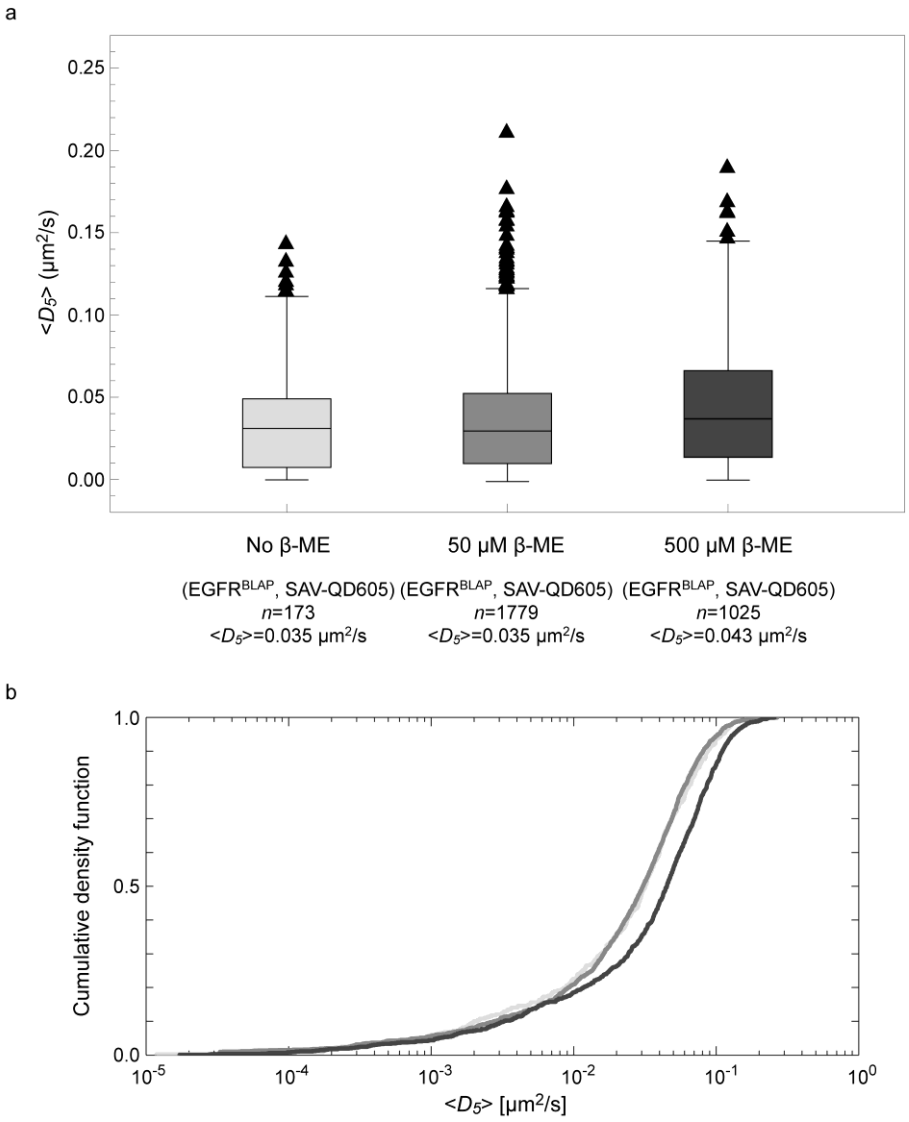

Figure S5. Effect of β-mercapthoethanol on SAV-QD605 trajectories. a) Box-and-whiskers plot of the diffusion coefficients for $EGFR^{BLAP}$ targeted with SAV-QD605, with no β-ME (light gray), 50 μM β-ME (medium gray), and 500 μM β-ME (dark gray) in the imaging buffer, respectively. The mean diffusion coefficients of the populations for no β-ME and 50 μM β-MEare identical, whereas there was an increase 23 % for 500 μM. b Cumulative density function of β-ME, 50 μM β-ME, and 500 μM β-ME, respectively. A K-S test showed no difference between the distributions when using no and 50 μM β-ME (p-value 0.70), whereas there was a significant difference when using 500 μM β-ME (p-value << 0.05).

n accordance with these results, all experiments were performed with 50 μM β-ME in order to reduce QD color shifting and blinking (*4*). Addition of 50 μM β-ME increased the mean number of displacements per trajectory from 235 to 350 for 50 μM β-ME as compared to no β-ME.

SI 6: MONTE CARLO SIMULATION OF 2D BROWNIAN DIFFUSION

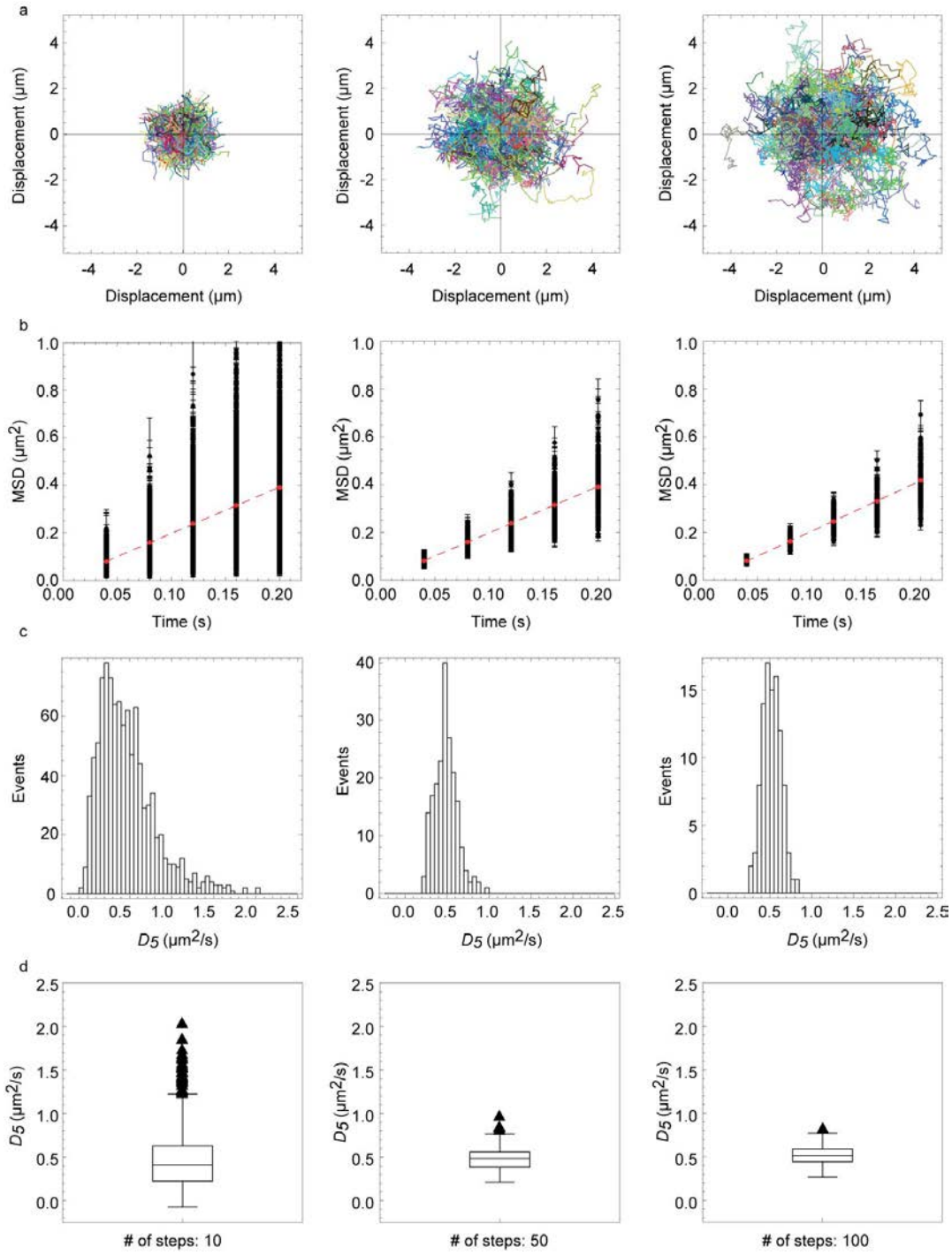

Figure S6. Monte Carlo simulations of 2D Brownian diffusion. The precisionby by which we could analyze single particle trajectories was estimated by a set of simulations (see Methods). Left column: 1000 particle trajectories of 10 displacements per trajectory, Center column: 200 particle trajectories of 50 displacements per trajectory, and Right column: 100 particle trajectories of 100 displacements per trajectory. a) All simulated particle trajectories (mixed colors) b) MSD plots for each particle trajectory and best fit to the mean MSD(<MSD>) of all displacements (dashed red line). c) Histograms of the fitted diffusion coefficients, D_{Fitted}, for each independent simulated particle trajectory.d) Box-and-whisker plots of D_{Fitted} for each independent simulated particle trajectory. Numbers for fitted diffusion and error are given in Table S6.

# of trajectories		1000	200	100	50	20
# of displacements per trajectory		10	50	100	200	500
Single Trajectory Analysis	D_{Fitted} (mean±s.t.d.; μm^2/s)	0.486±0.386	0.485±0.137	0.520±0.109	0.497±0.070	0.501±0.047
	%Difference $\frac{\lvert D_{Simulation} - D_{Fitted} \rvert}{D_{Simulation}}$	57±47	23±18	17±14	11±8.2	6.6±6.6
Average Trajectory Analysis	$\langle D_{Fitted} \rangle$±a.s.e. (μm^2/s)	0.504±0.001	0.502±0.001	0.489±0.001	0.497±0.001	0.502±0.001
	%Difference $\frac{\lvert D_{Simulation} - \langle D_{Fitted} \rangle \rvert}{D_{Simulation}}$	0.80±0.00	0.40±0.00	2.20±0.00	0.60±0.00	0.40±0.00

Table S6. Results from Monte Carlo simulations.All simulations were done with $D_{Simulation}$=0.5 μm^2/s and t_{lag}=40 ms.

Brief discussion of Monte Carlo simulation results

The results of the MSD analysis of the simulated data for Brownian diffusion in 2Dshows that that both the accuracy and the precision of the single trajectory analysis improves significantly as the length of the trajectories increases (Row 4 in Table S6). In this work, we have chosen to analyze only those trajectories that have >50 displacements. With this cut-off the mean trajectory lengths for all molecules and conditions were >200 displacements (Table 1 in main text). Hence both the accuracy and the precision, according to the simulations, of the presented single trajectory analysis ranges from ±~20% for the shortest trajectories to much less for the longer trajectories, while the mean accuracy and precision is approximately ±10%. The results of the simulations further indicates that it is possible to recover the magnitude of the simulated diffusion coefficient, $D_{Simulation}$, with high accuracy for all possible simulated combinations either by analyzing single trajectories separately to determine the populations of D_5 and by determining the mean of these populations (Row 3 in Table S6) or by curve fitting to the mean $\langle MSD(t_{lag}) \rangle$ (Row 5 in Table S6). This of course assumes that the observed noise from the SPT analysis is caused by the stochastic nature of Brownian diffusion and not by heterogeneity among different single particle trajectories. It is important to note, however, that this is not the case in these experiments as the observed heterogeneity of the experimental data vastly exceeds the observed stochastic noise in the results from the SPT analysis of the Monte Carlo simulations. This suggests that the observed experimental heterogeneity is not a result of the stochastic nature of Brownian lateral dynamics but rather is a reflection of the properties of the molecules as well as the organization of the plasma membrane. This is also clearly seen in Figure S8.

SI 7: P-VALUES FOR KOLMOGOROV-SMIRNOV TEST

Species 1	p-value	Species 2
Intramolecular (+/- βC)		
G_{M1} (-mβCD	0.17	G_{M1} m βCD
$CD59^{ACP}$ (-mβCD	9.35E-17	$CD59^{ACP}$ m βCD
$EGFR^{BLAP}$ (-mβCD	1.83E-42	$EGFR^{BLAP}$ mβCD
Intermolecular (- βC)		
G_{M1} (-mβCD	1.26E-48	$CD59^{ACP}$ (-mβCD
$CD59^{ACP}$ (-mβCD	7.90E-30	$EGFR^{BLAP}$ (-mβCD
$EGFR^{BLAP}$ (-mβCD	4.06E-87	G_{M1} (-mβCD
c (+ βC)		
G_{M1} m βCD	1.40E-32	$CD59^{ACP}$ m βCD
$CD59^{ACP}$ m βCD	7.04E-11	$EGFR^{BLAP}$ mβCD
$EGFR^{BLAP}$ mβCD	5.92E-15	G_{M1} m βCD

Table S7. p-values for Kolmogorov-Smirnov test. The table shows p-values for the significance of the difference in the populations of D_5 between two species. All species compared are significantly different at significance level □=0.05, except G_{M1}before and after cholesterol depletion (p-value 0.17).

SI 8: SINGLE TRAJECTORY HETEROGENEITY EXAMPLES

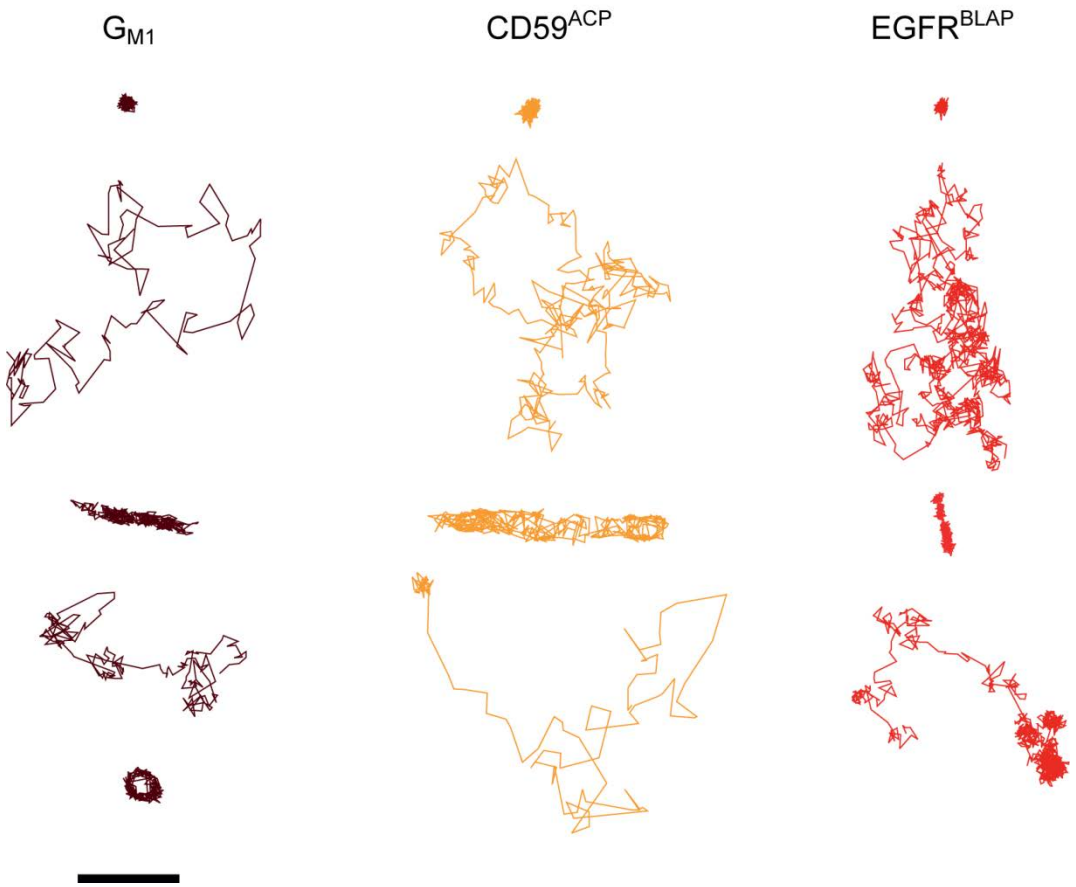

Figure S8. Single trajectory heterogeneity examples. Examples of single trajectories for the three different molecular species. In all cases are seemingly examples of confined, free Brownian, and directed motion as well as various combinations thereof. Scalebar 1 µm.

SUPPLEMENTARY REFERENCES

(1) Arnspang Christensen, E., Brewer, J. R., and Lagerholm, B. C. (2012) Multi-color single particle tracking with quantum dots.

(2) Bauer, R., Muller, A., Richter, M., Schneider, K., Frey, J., and Engelhardt, W. (1997) Influence of heavy metal ions on antibodies and immune complexes investigated by dynamic light scattering and enzyme-linked immunosorbent assay. *Biochim Biophys Acta 1334*, 98-108.

(3) Tu, R. S., and Breedveld, V. (2005) Microrheological detection of protein unfolding. *Phys Rev E Stat Nonlin Soft Matter Phys 72*, 041914.

(4) Arnspang Christensen, E., Kulatunga, P., and Lagerholm, B. C. (2012) A Single Molecule Investigation of the Photostability of Quantum Dots. *PLoS One 7*, e44355.

10.2 The probe rules in single particle tracking

Abstracted/Indexed In: Chemical Abstracts, MEDLINE/Index Medicus, BIOSIS, Science Citation Index Expanded™, Index to Scientific Reviews®, Biochemistry & Biophysics Citation index™, Journal Citation Reports®, BIOBASE, EMBASE/Excerpta Medica, ISI, Journal Citation Reports/Science Edition, BIOSIS Previews, BIOSIS Reviews Reports and Meetings, Scopus, EMBASE, EMBiology, Genamics JournalSeek

Impact Factor: 3.830 (2010 SCI Journal Citation Reports)

Eureka Xpress

CURRENT PROTEIN & PEPTIDE SCIENCE

DECEMBER 2011

VOL. 12, NO. 8, PP. 684-766

ISSN: 1389-2037

Current Protein & Peptide Science

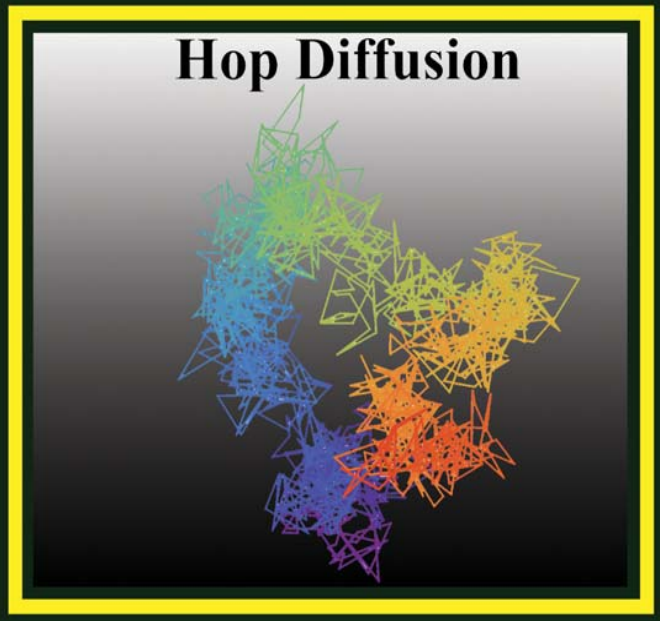

SCI JOURNAL CITATION REPORTS Impact Factor: 3.830

The international journal for timely in-depth reviews in Protein & Peptide Science

BENTHAM SCIENCE

The Probe Rules in Single Particle Tracking

Mathias P. Clausen and B. Christoffer Lagerholm*

Department of Physics and Chemistry, and MEMPHYS – Center for Biomembrane Physics, University of Southern Denmark, Campusvej 55, DK-5230 Odense M, Denmark

Abstract: Single particle tracking (SPT) enables light microscopy at a sub-diffraction limited spatial resolution by a combination of imaging at low molecular labeling densities and computational image processing. SPT and related single molecule imaging techniques have found a rapidly expanded use within the life sciences. This expanded use is due to an increased demand and requisite for developing a comprehensive understanding of the spatial dynamics of bio-molecular interactions at a spatial scale that is equivalent to the size of the molecules themselves, as well as by the emergence of new imaging techniques and probes that have made historically very demanding and specialized bio-imaging techniques more easily accessible and achievable. SPT has in particular found extensive use for analyzing the molecular organization of biological membranes. From these and other studies using complementary techniques it has been determined that the organization of native plasma membranes is heterogeneous over a very large range of spatial and temporal scales. The observed heterogeneities in the organization have the practical consequence that the SPT results in investigations of native plasma membranes are time dependent. Furthermore, because the accessible time dynamics, and also the spatial resolution, in an SPT experiment is mainly dependent on the luminous brightness and photostability of the particular SPT probe that is used, available SPT results are ultimately dependent on the SPT probes. The focus of this review is on the impact that the SPT probe has on the experimental results in SPT.

Keywords: Diffusion, domains, dyes, gold particles, lateral dynamics, plasma membrane organization, quantum dots, single molecule imaging.

1. INTRODUCTION

The molecular composition and organization of the mammalian plasma membrane is very complex [1-9]. Hundreds if not thousands of different lipid species are present in the plasma membrane with the main lipid types being phospholipids (with a variety of fatty acid chain lengths and degrees of unsaturation), cholesterol, and sphingolipids. Phospholipids and cholesterol are present in about equal amounts and together account for 85-90 % of the total lipids while sphingolipids account for a large majority of the remaining lipids [10]. It has further been estimated that ~30 % of the genome in eukaryotic organisms encodes for membrane inserted and membrane associated proteins giving rise to thousands of different membrane protein species, many of which are present in the plasma membrane [11]. The relative proportion of lipids and membrane proteins in the plasma membrane has been shown to be approximately equal by weight, corresponding to about one protein per 50 lipids [12]. However, while the general features of the composition are well characterized, the molecular organization of the plasma membrane of mammalian cells is not known [1-4]. Much controversy exists in particular about the existence of lipid rafts, lipid-stabilized nanodomains which are thought to be highly enriched in cholesterol, glycosphingolipids (GSLs), and a wide variety of membrane proteins (e.g. glucosyl-phosphatidyl-inositol (GPI) anchored proteins) that are important for a range of cell signaling pathways [3, 5]. There are also other complementary models for the nanoorganization of the plasma membrane of cells that still remain to be fully evaluated [2, 7]. These include for example the anchored-transmembrane-picket-model, where the long-range lateral diffusion of membrane proteins and lipids in native plasma membranes is hindered by integral membrane proteins that are immobilized by direct interaction with the actin cytoskeleton [8].

The biggest challenge in studies of the molecular organization of the plasma membrane has been, and still is, the lack of experimental techniques that are capable of directly resolving possible small transient structures in the plane of the plasma membrane. The methods of choice to date have been the closely related single particle tracking (SPT) and single molecule fluorescent tracking (SMFT) imaging techniques. In both of these techniques information about the molecular organization of the plasma membrane is inferred from careful analysis of the motion of single lipids and membrane proteins that are embedded in the plasma membrane. Because SPT and SMFT are closely related imaging techniques, differing primarily only in the identity of the probe that has been attached to the target molecules, where for SPT the probe is composed of a particle (e.g. a gold particle, a fluorescent bead, or a fluorescent quantum dot (QD)) and for SMFT the probe is composed of a fluorescent dye or a fluorescent protein (FP), we will henceforth use the acronym SPT to refer to both.

As mentioned above, the organization of the native plasma membrane deviates significantly from that of simple,

*Address correspondence to this author at the Department of Physics and Chemistry, and MEMPHYS – Center for Biomembrane Physics, University of Southern Denmark, Campusvej 55, DK-5230 Odense M, Denmark; Tel: +45 6550 3505; Fax: +45 6550 4048; E-mail: lagerholm@memphys.sdu.dk

1389-2037/11 $58.00+.00 © 2011 Bentham Science Publishers

homogenous artificial model membranes. In fact, SPT experiments suggest that the native plasma membrane contains a variety of barriers that limits the motion of lipids and membrane proteins over a wide range of sizes, from tens to hundreds of nanometers, and durations, from a few milliseconds to seconds [8]. Consequently, in SPT experiments in native plasma membranes, there is an intricate relationship between the optical characteristics of the SPT probe and the accessible temporal sampling, the duration of an experiment, the spatial resolution, the results, and the interpretation of the results. This is because the brighter the probe is, the faster is the accessible temporal sampling and the better is the spatial resolution. Furthermore, the more photostable the probe is, the longer is the total accessible duration of an experiment. However, because available bright and photostable probes, e.g. QDs and gold particles are relatively large, SPT experiments at very fast sampling intervals, or for very long durations, have so far mainly only been possible with large probes. But larger probes are typically also more susceptible to artifacts from e.g., steric hindrance as result of membrane topology and molecular crowding, and as a result of probe induced cross-linking due to difficulties in the preparation of large monovalent probes (e.g. gold particles and QDs). Consequently, there are unanswered questions about whether SPT results acquired at very fast sampling intervals are an artifact of the large probe size or are a reflection of the native organization of the plasma membrane.

The primary focus of this review is the relationship between the SPT probe and the SPT results, in particular with respect to the suggested organization of the native plasma membrane. In this review we give a brief introduction to the relevant theoretical expressions and a brief overview of experimental results of motion in a membrane. This is followed by a brief description of SPT and a more detailed description of relevant SPT probes. Finally, we give a summary of recent SPT results with an emphasis on investigations of the plasma membrane organization.

2. MOLECULAR MOTION IN SOLUTION AND IN BIOLOGICAL MEMBRANES

2.1. Theoretical Expressions for Diffusion

A free molecule in a dilute and uniform solution, or in a homogeneous biological membrane, will undergo random Brownian motion that is characterized by a diffusion coefficient D. The diffusion coefficient relates to the thermal energy of the system under study and the frictional drag experienced by the molecule. The distance a molecule diffuses, measured as the mean square displacement (MSD), in a time interval t is linearly dependent on the diffusion coefficient:

$$\mathrm{MSD} = (2\delta)Dt \qquad \text{(Eq. 1)}$$

where δ is the number of dimensions of the system under study. In solution, the molecule is free to diffuse in three dimensions (i.e. δ = 3) while in a membrane the diffusion is within a two dimensional plane (i.e. δ = 2).

The diffusion coefficient, D_S, of a molecule, with a radius of hydration R_H, in solution is given by the Stokes-Einstein equation:

$$D_S = \frac{k_B T}{6\pi\mu_S R_H} \qquad \text{(Eq. 2)}$$

where k_B is the Boltzman constant, T is the absolute temperature, and μ_S is the viscosity of the solution.

Theoretical expressions for the translational diffusion of a molecule embedded within a membrane are much more complex. In the limit where the molecular radii, R, of the membrane molecule is less than or equal to the radii of the lipids, the appropriate theoretical formulations for the translational diffusion, D_M, are given according to the free area theory [13-15]. For membrane molecules with a molecular radii, R, larger than the lipids but where the dimensionless parameter, $\varepsilon = 2\mu_S R / \mu_M h$, is << 1, the translational diffusion, D_M, can be approximated by the hydrodynamic continuum theory which was derived by Saffman and Delbrück [16]:

$$D_M = \frac{k_B T}{6\pi\mu_M h}\left(\ln\left(\frac{\mu_M h}{\mu_S R}\right) - \gamma\right) \qquad \text{(Eq. 3)}$$

In this model, the membrane molecule is approximated as a hard cylinder of radius R and height h, which is embedded within a membrane with viscosity μ_M and surrounded by aqueous phases of viscosity μ_S on both sides, and γ is Euler's constant (γ = 0.5772). This equation has been derived for the case of a homogeneous and continuous lipid bilayer membrane based on the Singer-Nicolson fluid mosaic model [17].

Importantly, the Saffman-Delbrück relation predicts that there is a much weaker dependence on the molecular radii, R, for diffusion in a membrane (∝ ln(1/R)) than in solution (∝ 1/R). Also worth noting is that the lateral diffusion coefficient of molecules that are embedded within a membrane as given by the Saffman-Delbrück equation is much slower than the corresponding diffusion of equally sized molecules in solution as given by the Stokes-Einstein equation. This is because the viscosity in the membrane, μ_M, is about 100 times larger than the viscosity in the surrounding aqueous space, μ_S [16, 18-19]. The large relative ratio of the viscosities further predicts that the diffusion of a molecule within a membrane is determined by the part of the molecule that is embedded within the membrane. This is also the rationale for why an exogenous probe that has been attached to a membrane molecule is expected to only minimally perturb the diffusion, even in cases where the probe is much bigger than the membrane molecule. This is of course only true to a limit as the diffusion coefficient of the probe molecule decreases as its size increases, eventually approaching that of the membrane target molecule. The diffusion coefficients of a membrane species and a probe in solution as given by the Saffman-Delbrück and Stokes-Einstein equations, respectively, are plotted in Fig. (**1**). The plot can be used to estimate the relative influence of an attached probe on the diffusion of a membrane molecule, for example the diffusion coefficient, D_M, for a membrane molecule with R = 1 nm, h = 4 nm, and μ_M/μ_S = 100 is ~4.3 μm^2/sec which corresponds to the diffusion coefficient, D_S, of a molecule in solution with $R_H \approx$ 49 nm. Hence, in this case the probe should be << 49 nm in radius. Worth noting, for the forthcoming discussion, is also that a probe of R_H = 20 nm has a $D_S \approx$ 11 μm^2/sec in water (μ_S = 1.002 cP) at 20 °C.

The Saffman-Delbrück relation (Eq.3) has also been further extended for all values of the dimensionless parameter ε by Hughes et al. [20-22]. In addition a phenomenological model with an inverse dependence of the molecular radii ($1/R$) for membrane molecules in the size range of $0.5 < R < 3$ nm has been recently introduced [23]. None of the alternative models have, however, been conclusively experimentally verified to be better than the Saffman-Delbrück relation in the case of describing the dependence of the molecular radii over a range of $0.5 < R < 7$ nm, and the diffusion coefficient, D_M, for monomers of membrane proteins and small oligomers of membrane spanning peptides and membrane proteins (see also the discussion below) [18-19, 24-25].

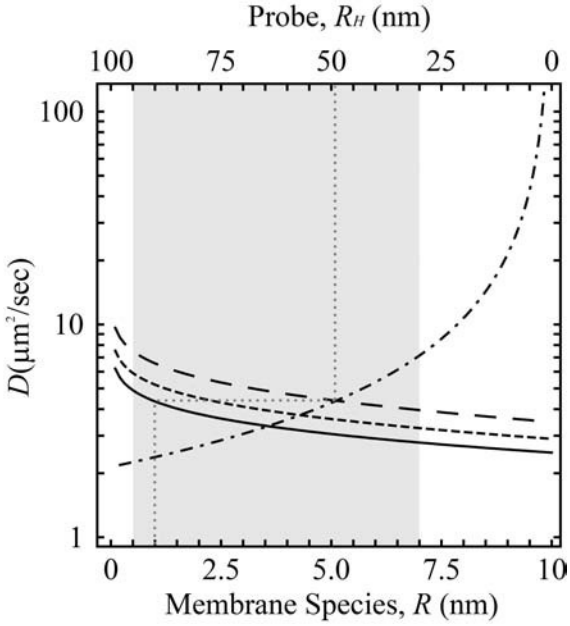

Fig. (1). Theoretical dependences of the diffusion coefficients, D, on the molecular radius, R, for a membrane species embedded within a membrane and on the radius of hydration, R_H, of a probe in solution (dot-dashed line). The dependence for the membrane species was calculated from the Saffman-Delbrück equation with μ_S = 1.002 cP, h = 4 nm, T = 293 K, and for μ_M/μ_S = 100 (solid line), μ_M/μ_S = 80 (short dashed line), μ_M/μ_S = 60 (long dashed line). The dependence for the probe in solution was calculated from the Stokes-Einstein relation with μ_S = 1.002 cP, and T = 293 K. Also shown is the equivalence relation of the diffusion coefficient ($D_M = D_S \approx 4.3$ μm^2/s) of a membrane molecule, with R_H = 1 nm, h = 4 nm, and μ_M/μ_S = 100, and a probe in water with $R_H \approx 49$ nm and μ_S = 1.002 cP at 293 K (grey dotted line). The relevant molecular size range, $0.5 < R < 7$ nm, where the Safmann-Delbrück equation has been validated is shown in gray shading [25].

2.2. Experimental Results for Diffusion in Membranes

In general, for reconstituted lipid membranes, e.g. supported lipid bilayers (SLBs) and giant unilamellar vesicles (GUVs), the translational diffusion rates are typically reported to be in a range of ~1-10 μm^2/sec with variations due to the specific molecules and a number of factors depending on the experimental setup [26]. That is, under otherwise identical conditions, diffusion in SLBs is generally twofold slower than in GUVs, and where measurements in SLBs indicate that there is strong inter-leaflet coupling with identical diffusion coefficients in both leaflets [27]. Furthermore for SLBs, the aqueous layer between the support and the bilayer is important for the motion of molecules [28]. Lipid diffusion has also been found to decrease with increased concentrations of NaCl [29] and hydrogen bonding of lipid head groups, containing mono- and disaccharides, also decreases the diffusion by a factor of as much as three [30]. The diffusion of lipids and proteins in reconstituted membranes are also correlated as an increase of the membrane protein concentration result in slower diffusion of both lipids and proteins [19, 31]. However, the most important factor for the translational diffusion rate in reconstituted model membranes seem to be the lipid composition as the acyl chain length and particularly the presence of sterols (e.g. cholesterol) have large impacts on the diffusion and importantly on the phase of the bilayer under study. In ternary phospholipid-cholesterol-sphingolipid mixtures which are thought to reflect the composition of lipid rafts, micrometer sized liquid-ordered domains rich in cholesterol and sphingolipids form where diffusion rates are 2-20 times slower than in the liquid-disordered phase of the same bilayer [32-33].

The dependency of the molecular radii, R, on the diffusion coefficient, D_M, has been investigated for a large number of systems (e.g. [14, 18-19, 24, 31, 34]). In these studies and others, the existence of two parameter regimes with a transition region for a molecular area of ~1 nm^2 (corresponding to $R \sim 0.6$ nm) has been validated by investigating the diffusion of a combination of lipid and membrane proteins [34-35], and more recently also by systematic investigations of the diffusion of lipid-like macrocyclic polyamides [36] and selectively aggregated membrane spanning peptides [24]. Furthermore, the weak dependency of the diffusion coefficient, D_M, on the molecular radii, R, for larger membrane molecules as predicted by the Saffman-Delbrück relation, has been experimentally validated for e. g. bacteriorhodopsin ($2R = 4.3 \pm 0.5$ nm) in large multilamellar vesicles composed of DMPC [18] and more recently for membrane proteins, ranging in size from $0.5 < R < 4$ nm, which had been incorporated at low protein concentrations (~10-100 proteins/μm^2) in GUVs composed of DOPC: DOPG (3:1, mol:mol) [19]. The relation has further been verified by mesoscopic simulation for $R <$ ~7 nm [25]. Combined, these results suggest that the Saffmann-Delbrück relation (Eq. 3) a reasonable model in the size range of $0.5 < R < 7$ nm (see Fig. (**1**)).

In both the experimental cases, it was also found that the diffusion coefficient of both lipids and proteins depends strongly on the membrane protein density. Peters and Cherry found that the diffusion coefficient of bacteriorhodopsin was reduced from ~3.4 μm^2/sec at a lipid to protein (L/P) ratio of 210:1 (corresponding to ~6,500 proteins/μm^2 with a lipid area of 0.65 nm^2) to ~0.15 μm^2/sec at a more physiologically relevant L/P ratio of 30:1 (corresponding to ~28,000 proteins/μm^2). Ramadurai *et al.* found that the diffusion coefficients of both lipids and proteins decreased linearly with increasing protein concentrations further indicating that molecular crowding plays a significant role in the motion of molecules in membranes. An extrapolation of the linear dependence of the diffusion coefficients to the approximated protein densities of ~25,000 proteins/μm^2 in biological

membranes in this case would result in an order of magnitude decrease in the diffusion coefficient from that observed at protein concentrations of ~3000 proteins/μm^2. This decrease in the diffusion coefficients at greater protein densities is not predicted by the Saffman-Delbrück equation but is consistent with a long known discrepancy between measurements of the thermal motion of lipids and membrane proteins in reconstituted lipid membranes as compared to in the native biological membranes of live cells [37-39].

In contrast to the above results which were obtained in free-standing vesicles, Gambin *et al.*, have investigated the dependence of the molecular radii, R, on the diffusion coefficient, D_M, of single-spanning peptides and multi-pass spanning membrane proteins with a size range of $0.5 < R < 3$ nm in model membranes that are in contact with a solid substrate [23]. Based on these results the authors have introduced a heuristic model with an inverse dependence of the molecular radii ($1/R$) on the diffusion coefficient, D_M, for the tested size range. The validity of these results is, however, likely very strongly influenced by non-specific interactions between the substrate surface and the membrane molecules as is e.g. illustrated by the very slow diffusion that these authors obtained for bacteriorhodopsin (0.08 μm^2/sec) as compared to that measured by Peters and Cherry (3.4 μm^2/sec) in free-standing membranes [18-19].

In contrast, the translational diffusion of lipids and proteins in native biological membranes of live cells is typically found to be at least an order of magnitude slower than in reconstituted membranes, or ~0.01-0.5 μm^2/sec, again with variations due to the specific molecule, cell type, and measurement technique [8, 40]. Ample evidence exist that suggests that the slower diffusion in native membranes is caused by a combination of reasons including molecular crowding, specific molecular interactions, membrane topology, interactions with the actin cytoskeleton, and interactions with nanostructures within the membrane (e.g. caveolae, clathrin coated pits, and hypothesized lipid rafts) [2, 7, 41]. This is perhaps also to be expected considering the complicated composition of the native plasma membrane that is also not an isolated entity but rather contains physical links to both the extracellular space and the cytoplasm that can act as barriers to the translational diffusion of molecules within the lipid bilayer of the membrane. In addition, native membranes are in continuous flux, for example the equivalent of the entire cell surface is estimated to be internalized one to five times per hour [42-43].

3. SINGLE PARTICLE TRACKING

Classical methods like fluorescence recovery after photobleaching (FRAP) and fluorescence correlation spectroscopy (FCS) has found frequent and often successful use in characterizing the lateral dynamics of lipids and proteins in a variety of reconstituted membrane model systems [44]. However, in the case of experiments in native biological membranes, the results from these techniques are more difficult to interpret. For example, FRAP experiments in native biological membranes often result in a fluorescence recovery rate that is not well described by a single diffusing component. In addition, these experiments often also result in only partial fluorescence intensity recovery indicative of the presence of an immobile fraction. Similarly, FCS experiments will often also result in autocorrelation data that is not well described by a single diffusing component [45-46]. While these results suggest that native biological membranes are more complex in organization than reconstituted membrane model systems the full extent of the complexity cannot generally be resolved. In the case of both FRAP and FCS, the resulting experimental data is further an ensemble time average for the fluorescently labeled molecules that diffuse through the observation volume for the duration of the measurement. The heterogeneity behind these averages can only be accessed by using single molecule techniques, with SPT being the technique that allows giving the most information on the individual single molecules [39, 47-49]. SPT is typically done as a 2D measurement although 3D measurements are also possible, however, at a much reduced sampling rate [50].

3.1. Technical Principles of SPT

SPT is a light microscopy technique in which the motion of single molecules, that have been specifically labeled with e.g. a gold particle, a fluorescent dye, protein, or nanoparticle (e.g. QD) are imaged at an acquisition rate of ~10-50,000 Hz [8, 39, 47, 49, 51]. Importantly, using SPT it is possible to greatly surpass the spatial resolution limit of light microscopy, d, which due to the diffraction of light is limited according to the Abbe resolution limit to $d = \lambda/(2NA_{obj})$, where λ is the wavelength of the emitted light, and NA_{obj} is the numerical aperture of the microscope objective. For λ = 500 nm and NA_{obj} = 1.3 the Abbe resolution limit is ~190 nm.

The optical principle behind SPT is that an image of a single point object, acquired from a diffraction limited light microscope, is an Airy pattern, the center of which is the Airy disc and which contains the bulk of the luminous intensity (~84 %). The image of a single molecule can hence for all practical purposes, considering in particular typical signal-to-noise ratios (SNR) of relevant single molecule probes and at appropriate image acquisition settings, be approximated as an Airy disc. The intensity profile of the Airy disc, and hence of a single molecule, is well approximated by a 2D spatial Gaussian, $I \approx I_0 \exp[-r^2/(2w^2)]$, where I_0 is the intensity at the center of the disc, and w is the full width at half maximum (FWHM) intensity and which for fluorescence microscopy is equal to $w \approx 0.61\lambda/NA_{obj}$. The case where the maximum of one Airy disc falls on top of the minimum of another Airy disc is also known as the Rayleigh criterion, and this is the minimum distance by which two single molecules have to be separated in order to still be resolvable as two separate single molecules. In the limit, where the spatial separation of the imaged single molecules are separated by a distance that exceeds the Rayleigh criterion it is possible to determine the centroid position of single molecules very precisely by computational image analysis [47, 49, 52-53]. Using this approach, the localization of single molecules can typically be done with a spatial precision of ~10-40 nm dependent on the SNR, the image acquisition time, and the diffusion rate of the observed molecule.

The thus obtained centroid positions for each single molecule are subsequently linked between image frames in order to be able to obtain trajectories that describe the

motion of each detected single molecule as a function of time. Using these trajectories it is then possible to characterize the motion of the single molecules. This is most typically done by calculating the mean square displacement (MSD), either independently for each detected single molecule trajectory, or in the case where the single molecules trajectories are very short as an average for all detected single molecule trajectories [47, 49, 54]. Using this approach, it is possible to classify the modes of motion by analysis of the shape of the MSD versus time plots. This is most often done as a comparative classification relative to the motion expected for a single molecule that undergoes free Brownian diffusion in a 2D membrane [39, 47, 49]. Alternatively, it is also possible to obtain information about the motion by analysis of the probability distribution of the squared displacements at different time points [47, 55]

A typical result from SPT experiments in plasma membranes is that the MSD plots are timedependent and often show negative curvature, meaning that the diffusion coefficients are greater at shorter distances and time intervals than at longer distances and time intervals [56]. This is indicative of spatial and temporal confinement where the diffusion is free on a spatial and temporal scale much smaller than the characteristic distance between the confining barriers in the membrane. This has resulted in that SPT results are often characterized by a short range diffusion coefficient, D_{micro}, which is determined by the slope from a linear fit of only the first few points (e.g. points 2-4) of the MSD plot, and sometimes also by a long range diffusion coefficient, D_{macro}, which is determined by the slope from a linear fit of a greater number of points on the MSD plot. In the case of a homogenous and continuous membrane such as the case of the fluid lipid mosaic model of Singer and Nicholson [17] the expectation would be that $D_{micro} = D_{macro}$, while in the case of a heterogeneous, compartmentalized membrane the expectation would be that $D_{micro} > D_{macro}$.

3.2. SPT Probes

In SPT there is a very intricate relationship between the optical characteristics of the probe and the accessible sample integration times, the sampling interval, the total duration of an experiment, the spatial resolution, the experimental results, and the interpretation of the results. This is because the brighter the probe is, the faster is the accessible sampling intervals and the better is the spatial resolution, and the more photostable a probe is, the longer is the experimental durations of an experiment.

3.2.1. General Aspects

SPT probes consist of two components, a "specificity module" which renders specificity to a membrane target molecule and a "label module" which renders indirect visibility of the membrane target molecule where relevant membrane target molecules are any molecule that directly interacts with the biological membrane of interest and can e.g. be a lipid, an integral membrane protein, or a lipid-anchored protein. The choice of the combination of the two modules can have a large impact on the execution of an experiment and on the experimental results. The ideal SPT probe would consist of a specificity module with a high specificity towards its membrane target molecule, and a label module which was infinitely bright, to enable experiments at infinite fast time intervals, and infinitely stable, to enable experiments for an infinite time period. The probe, as well as the specificity module, should ideally be monovalent to prevent probe induced cross-linking, which could result in the activation of signaling pathways or reduced mobility [39]. The probe size, which as discussed could be much larger than the target membrane molecule without perturbing the observed diffusion coefficient, should yet preferably be minimal in size in order to maximize access to the membrane target molecule and to minimize possible steric hindrance. Steric hindrance could for example result in that only a subset of target molecules is accessible for labeling e.g. due to molecular crowding or membrane topology [41].

Commonly used SPT probes consist of a combination of labels like; fluorescent dyes, FPs, and QDs, and gold particles, and specificity modules like; antibodies (Abs), Fab fragments, and sAv *etc*. The probes and the individual parts are shown according to their relative sizes in Fig. (**2A**). In Fig. (**2B**), experimental FCS autocorrelation curves of probe molecule diffusing in solution are shown together with that for the diffusion of DPPE-Rhodamine in a GUV. The corresponding diffusion coefficients and hydrodynamic radii are given in Table **1**. The last column in this table gives the ratio between the probe diffusion in solution and the diffusion of a labeled membrane target molecule (DPPE-Rhodamine) in a GUV, as an indicator for the frictional drag effect of the probe size on diffusion of a membrane target molecule, see also to the discussion in relation to Fig. (**1**). This ratio should preferable be >>1 for the probe to have minimal influence on the motion of the membrane target molecule. Properties of specificity modules and labels are further discussed below.

3.2.2. Specificity Modules

The specificity modules used in SPT can generally be classified into two categories; those that have affinities for naturally occurring membrane targets e.g. Abs, DNA and RNA aptamers, lectins, and various toxins such as cholera toxin subunit B (CTB), and those that first need the insertion of an artificial peptide or protein epitope tag in the target molecule in order to introduce labeling specificity [58-59]. Epitope tags are often introduced via genetic insertions of sequences e.g. the biotin ligase acceptor peptide (BLAP) for streptavidin, [60], the acyl carrier protein (ACP) for Coenzyme A (CoA) derivatives [61], the SNAP tag for benzylguanine derivatives [62], and tetra-cysteine peptide motifs for the biarsenical derivatives FlAsH and ReAsH [63]. A special case is the FPs since the tag and the specificity is combined in one unit together with the visible label module genetically expressed in immediate continuation of the target protein giving a pseudo-intrinsic probe with absolute specificity. In addition to the artifacts that a modification can induce, the main disadvantage of genetically introduced tags is that the modified proteins are typically expressed at non-physiological levels [64].

The size of the specificity module can change the total size of the entire probe considerably. This is especially the case when labeling is done by immunolabeling using both a primary and secondary Ab, sometimes even in combination

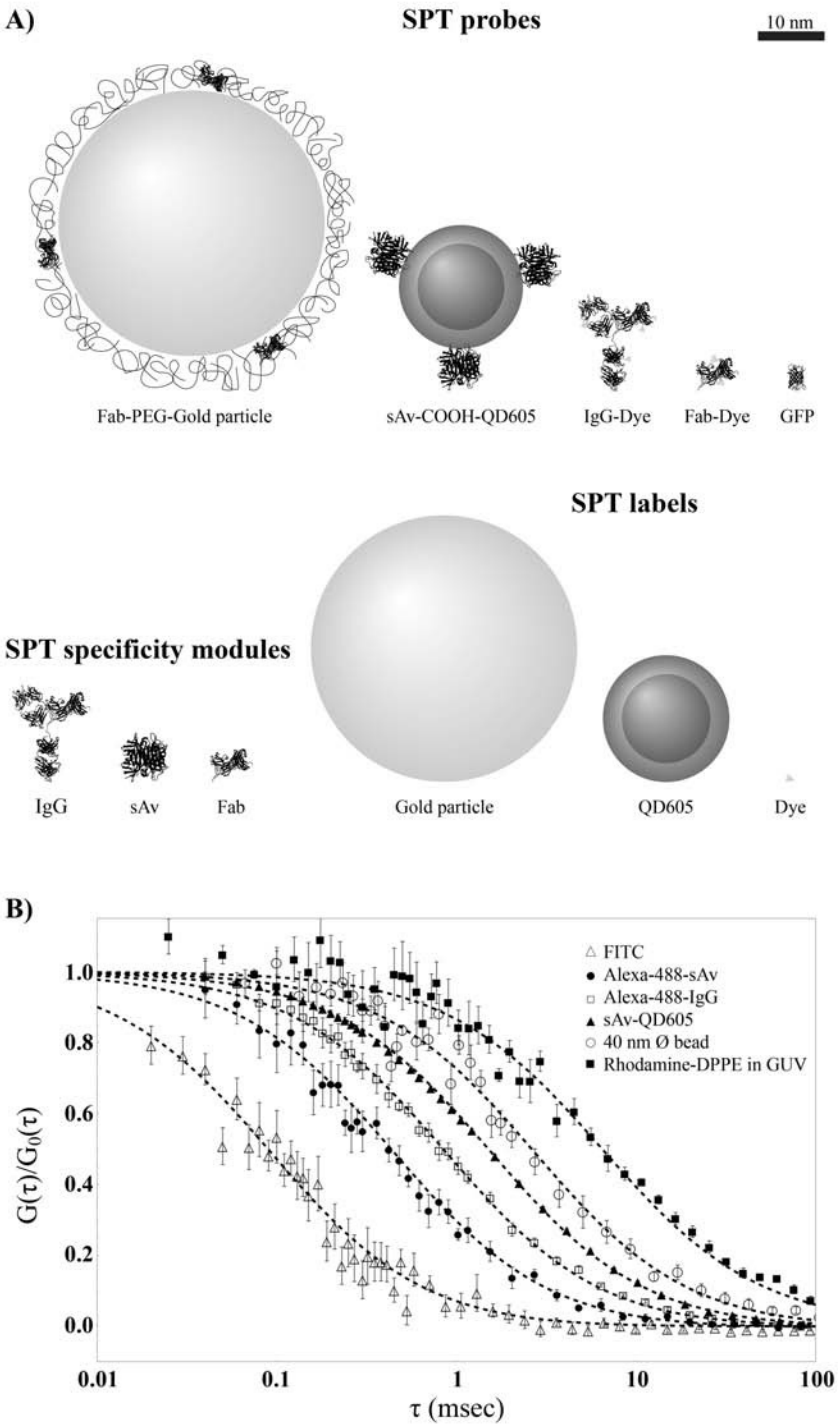

Fig. (2). A) Common probes used in SPT and their individual modules represented illustrating their relative sizes as measured by FCS. The probes are: Ø 40 nm (Fab-PEG-) gold particle coated with a PEG polymer and functionalized with Fab fragments ($R_H \gtrsim 25$ nm), sAv-functionalized COOH-QDs emitting at 605 nm (sAv-COOH-QD605, $R_H \approx 9.7$ nm), dye labeled immunoglobulin G (IgG-dye, $R_H \approx 5.8$ nm), dye labeled Fab fragment (Fab-dye, $R_H \approx 2.9$ nm [123]), and the green fluorescent protein (GFP, $R_H \approx 2.3$ nm [57]). The shown specificity modules are: IgG, Fab and streptavidin (sAv, $R_H \approx 3.4$ nm), whereas the un-functionalized labels are: Ø 40 nm gold particle, COOH-QD605 ($R_H \approx 6.0$ nm), and a FITC dye ($R_H \approx 0.7$ nm). **B**) FCS correlation curves for typical SPT probes in solution compared to that of Rhodamine-DPPE in a lipid GUV. The raw data shown is for the mean±s.e.m normalized correlation function from n = 5 or 6 independent correlation curves. The FCS data for the probes in solution was curve fit to $G(\tau) = G_0(\tau)\ (1+8D_S\tau/r^2)^{-1}(1+8D_S\tau/z^2)^{-1/2}$ (solid lines) while the FCS data for lipid diffusion in a GUV was fit to $G(\tau) = G_0(\tau)\ (1+8D_M\tau/r^2)^{-1}$ (dashed line). The values for the diffusion coefficient obtained from the curve fit are given in Table **1**.

Table 1. Diffusion coefficients, D_S, and hydrodynamic radii, R_h, of SPT probe molecules in solution obtained by FCS. The diffusion coefficient of rhodamine-DPPE in a GUV was D_M = 4.5±0.3 μm²/sec. This value is used in the ratio D_S/D_M to estimate the diffusion effect of the probe size relative to the membrane target. A value >>1 means that the probe has minimal effect.

Probe	R_h (nm) mean±s.e.m.	D_S (μm²/sec) mean±s.e.m.	D_S/D_M mean±s.e.m.
Ø 40 nm bead	20.3±3.0	10.7±1.6	2.4±0.4
sAv-QD605	9.7±0.5	21.3±1.2	4.7±0.4
Alexa488- IgG	5.8±0.2	36.5±1.6	8.1±0.6
Alexa488-sAv	3.4±0.2	64.0±3.9	14±1.3
GFP [57]	2.3±0.05	93.2±2.2	21±1.5
FITC	0.7±0.2	316±72	70±17

with labeled sAv. In addition, some specificity modules are multivalent, e.g. Abs which are bivalent, native sAv which is tetravalent, and CTB which is pentavalent, and are hence capable of inducing cross-linking of the membrane target molecules. The problem of cross-linking can be circumvented by use of monovalent Fab Ab fragments or genetically engineered monovalent streptavidin [65]. Probe multivalency is also a problem in the case where the labels are gold particles or QDs. This is because these labels contain multiple surface binding sites for the specificity modules and because as a result any reaction between the two is limited by Poisson statistics. Hence even reaction conditions that strongly favor no binding of the specificity module to the label will result in a population of multivalent labels, e.g. a 2:1 (mol:mol) ratio of label to specificity module which, assuming a 100 % reaction yield, would result in ~60 % of labels with no specificity module, ~30 % of labels with one specificity module, ~8 % of labels with two specificity modules, and ~2 % of labels with more than 2 specificity modules. The preparation of monovalent probes, in the case where the label is a particle, thus requires a purification step capable of separating those particles that have only one specificity module from the rest. This has been accomplished by agarose gel electrophoresis of QDs that had been reacted with sAv [66-68] or poly-ethylene glycol (PEG) polymers [69], and for gold particles that had been reacted with DNA [70].

3.2.3. Labels

3.2.3.1. Fluorescent Dyes and Fluorescent Proteins

The smallest possible SPT labels are small organic fluorescent dyes. These can e.g. be directly attached to lipids creating fluorescent lipid analogs (e.g. Rhodamine-DPPE, NBD-DPPC, Bodipy-Cholesterol *etc.*). However, fluorescent lipid analogs, which may either have been modified in the hydrophobic acyl chain tails or the hydrophilic head groups, have significantly different chemical structure than the corresponding unmodified lipids and as a consequence the behavior of fluorescent lipids will often be altered. This is especially true for cholesterol, since attached dyes are almost equal in size to cholesterol, are often polar or even charged. Consequently no existing fluorescent cholesterol analog mimics the properties of native cholesterol [71]. Specific protein labeling with small dyes is also possible with for example systems like FlAsH, ReAsH, BLAP, ACP, SNAP and CLIP systems [59, 72], were the dyes can bind directly to peptide tags in the target protein and render a probe that is smaller or comparable in size to FPs. However, in most cases fluorescent dyes are used in combination with e.g. intact Abs, Ab Fab fragments, or sAv in order to confer specificity towards the molecular target, hence increasing the size of the label and with the potential risk of causing cross-linking artifacts as discussed above.

The main disadvantages of fluorescent dyes are low brightness and poor photo-stability, thereby preventing single molecule imaging at very fast time intervals (not bright enough) and for long time durations (not stable enough). However, recently developed dyes like e.g. Alexa-647, which has a high molar extinction coefficient (ε = 220,000 $M^{-1}cm^{-1}$ at 647 nm), moderate quantum yield (QY = 0.33), and a high saturation intensity, has enabled SPT imaging at image acquisition rates up to 2000 Hz, but only for less than ten images [73]. In contrast, SPT experiments with the dye Atto647N (ε = 150,000 $M^{-1}cm^{-1}$ at 644 nm, QY = 0.65) have been reported at 10 Hz, but with a mean time duration of single molecule trajectories of 15 seconds [74]. FPs, like fluorescent dyes, also exist in a wide range of different colors [75], and in a variety of modified forms such as e.g. photo-switchable FPs. The optical properties of FPs in terms of brightness and stability, however, are inferior to that of the better dyes, e.g. enhanced green fluorescent protein has a molar extinction coefficient, ε = 56,000 $M^{-1}cm^{-1}$ at 484 nm, and a QY of 0.6. As a result, SPT with FPs is typically performed at 10-30 Hz, but has in the case of enhanced yellow FP (EYFP) been accomplished even at 200 Hz [76]. In both cases, the duration is typically limited to less than twenty image frames before the FPs irreversibly photobleach.

3.2.3.2. Quantum Dots

QDs are semi-conductor nanoparticles that are composed of inorganic cores of ~Ø 2-10 nm and which are the origin for their fluorescence properties with the size relating to the emission color. However, stabilization and functionalization of QDs in aqueous media requires that additional layers are added resulting in a final total size of ~Ø 15-30 nm. Functionalization of QDs with e.g. sAv [60], CoA [77], CTB

[78], Fab fragments [79], or any other preferred bio-molecule is relatively standardized and easy, but the number of attached bio-molecules, and hence the valence of the entire QD is difficult to control, with potential risk of cross-linking target molecules when used in SPT. The size of some QDs was also shown to limit their access to synapses [80], but monovalent and size-reduced QDs have been made with markedly improved accessibility [67-68]. More improvements along this direction are also expected.

The fluorescent properties of QDs are far superior to those of dyes and FPs. They have very high extinction coefficients (ε = 1,100,000 $M^{-1}cm^{-1}$ for sAv-QD605 at 488 nm) and yet moderate quantum yields (QY ≈ 0.5) which account for their extreme brightness. In our laboratory we have successfully imaged single moving QDs on the cell surface at rates up to 1760 Hz and ~0.5 msec integration time with the limiting factor being the readout speed of the camera. In terms of stability, the QDs do not photobleach easily on a time scale relevant for most SPT studies, thus they can be readily imaged for periods of several tens of seconds to minutes. A limitation to this being the observed blinking (alternation between a fluorescent on- and an off-state) [81] when imaged at the single molecule level, making SPT linking algorithms more demanding [52-53]. QDs of different colors show similar and broad excitation, and have narrow symmetric emission spectra, making them ideal for multi-color imaging. This advantage has also been used in demonstrating that multispecies SPT with QDs is possible [66, 82]. More detailed information on QDs is available from other sources [83-86].

3.2.3.3. Gold Particles

Colloidal gold particles differ from the other labels in that the detected signal is based on light scattering rather than fluorescence, where the amount of scattered light is strongly dependent on the particle size. The scattering nature of the gold particles means that SPT with gold particles can only be performed for a single type of molecule at a time. In the case of SPT on native plasma membranes, the SNR typically dictates that Ø 40 nm non-functionalized gold particles are required. The large size of gold particles used in SPT is likely to restrict access to certain areas on the cell surface due to steric effects. Furthermore, as shown in Table **1**, the diffusion of a Ø 40 nm particle in solution is only twice that of a lipid molecule diffusing in a model membrane, thus gold particles are likely to have a notable influence on the diffusion of the membrane target molecules.

Specificity of gold particles is accomplished by charge mediated absorption of relevant specificity modules such as Abs or Fab fragments to the surface of the particles [87]. Similarly to QDs, however, colloidal gold particles also have to be stabilized for use in physiological conditions, in this case in order to prevent aggregation in presence of salts. Stabilization is typically accomplished by absorption of proteins to also include the mixed absorption of relevant specificity modules in combination with passive ligands that can be proteins e.g. Abs or Fab fragments that have no binding specificity at the investigated membrane, BSA (R_H ≈ 3 nm) or poly-ethylene glycol (PEG) polymers e.g. Carbowax 20M which has an average molecular weight of 17.5 kDa [88] and an estimated radius of gyration, $R_g \approx 9$ nm (using $R_g \approx N_0^{3/4}$, where N_0 is the number of PEG monomers). The functionalization and stabilization of gold particles will thus most likely add at least ~10 nm to the diameter. Functionalized gold particles are hence ~2 times larger in diameter than a QD, and correspondingly have an 8 times larger volume. However, in terms of signal, gold particles are beyond comparison to any of the other labels. Accordingly, Kusumi and co-workers have performed SPT with gold particles at a frame rate of 50,000 Hz over extended time periods [89].

3.3. SPT Results

SPT has been in particular instrumental in revealing the extent of the spatio-temporal heterogeneity in the organization of plasma membranes [52, 73, 87, 90-92]. This is because SPT is currently the experimental method that offers the best available combination in spatial and temporal resolution. This has enabled SPT to detect very small (~20-50 nm) and transient (~1-10 msec) organization as well as small (~100-300 nm) and longer lived (~1 sec) organization within the mammalian plasma membrane [87, 90, 93-94]. In general, the SPT results of the detected modes of motion of lipids and membrane proteins in the plasma membrane are, independent of the SPT probe (and associated sampling intervals and the time durations) very heterogeneous, typically always displaying a large range of modes of motion to include free diffusion, confined diffusion, and combinations thereof [54, 74, 87, 92, 95]. A schematic of some typical modes of motion is found in Fig. (**3**).

A frequent use of SPT is investigations of the plasma membrane nanostructure to include interactions with e.g. caveolae, clathrin coated pits, and hypothesized lipid rafts [54, 73-74, 82, 87, 89-93, 96-101]. In these studies, SPT sampling intervals have ranged from an extreme speed at 50,000 Hz with Ø 40 nm gold particles [89, 93], 1000-1760 Hz with QDs [95], 1000-2000 Hz with Alexa-647 [73], 200 Hz with EYFP [99], to a more typical sampling of ~30 Hz or slower for all the different labels. SPT data has furthermore been collected for a variety of time durations ranging from many tens of thousands of images for Ø 40 nm gold particles, thousands to a few tens of thousands of images for QDs, to less than ten to a few hundreds of images for fluorescent dyes and FPs. In a comparison of this SPT data it is apparent that the results of plasma membrane nanostructure are dependent on the acquisition parameters and consequently possibly also on the SPT probes.

Experiments at very fast temporal sampling rates of 40-50 kHz have so far only been possible in the Kusumi lab and by using Ø 40 nm gold particles as the label [2, 87, 89, 93, 101]. A unifying result from these studies is that all possible types of membrane target molecules, e.g. lipids, lipid anchored membrane proteins, and single and multi-pass integral membrane proteins, are confined in compartment sizes of ~30-250 nm for average residency times of ~1-20 msec, where the characteristic sizes and times were found to vary in a cell dependent fashion [2, 100]. This confinement, which has been coined hop-diffusion, is dependent on the actin cytoskeleton, but neither on the presence of cholesterol nor on the removal of the major fraction of the extracellular domains of membrane protein or the extracellular matrix [2, 87, 100].

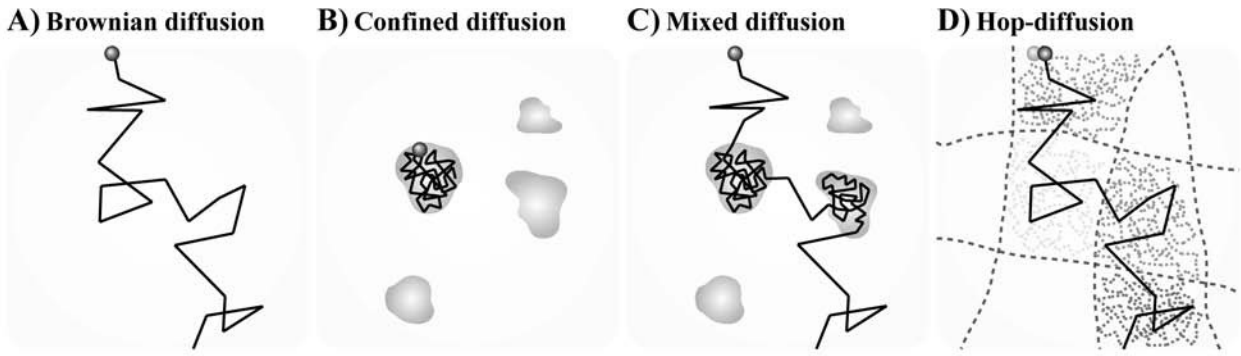

Fig. (3). Sketch of various diffusive behaviors in a membrane dependent on the dominating underlying structure. **A**) Brownian diffusion; the molecule is not influenced by any membrane structures. **B**) Confined diffusion where the motion is limited to a restricted area (dark grey) of the membrane. **C**) Mixed diffusion with areas of free diffusion and areas of confined diffusion (anomalous sub-diffusion). **D**) Hop-diffusion where the molecule is temporarily confined (dotted grey trajectory) by the underlying cytoskeleton (dashed lines). This phenomenon is only observed for SPT with large probes when imaging at very fast imaging rate, whereas at slow imaging rates the diffusion will appear free (black trajectory).

In the case of one cell line, NRK fibroblasts, the mean short range diffusion coefficient, D_{micro}, over a 100 μs time window, of the lipid DOPE within these compartments (~230 nm) has been reported to be 5.4 μm^2/sec [87], with similar numbers also being reported in the same cell type for an integral membrane protein, the transferrin receptor (D_{micro} = 5.2 μm^2/sec) [87], and a 7-transmembrane protein, the G-coupled protein receptor (GPCR) μ-opiod receptor (D_{micro} = 4.2 μm^2/sec) [93]. The mean long range diffusion coefficient, D_{macro}, over a 100 ms time window in these studies and for these molecules were typically independent of the label type (gold particles or Cy3) in the range of ~0.1-0.5 μm^2/sec [87, 93, 100].

These results are particular surprising because even the phospholipids DOPE, and GPI-anchored proteins, neither of which have direct contact with the cytoplasmic space, are confined in compartments equal in size to those found for integral membrane proteins such as the transferrin receptor and the GPCR receptor [87, 89, 93, 100-101]. In response to these results, the anchored protein picket model has been proposed. In this model, membrane proteins that are anchored to and aligned with the actin cytoskeleton act as pickets in a fence to restrict the free lateral diffusion of molecules in the membrane by a combination of steric hindrance and hydrodynamic friction [2, 8]. Because many of the membrane proteins extend into the extracellular space this model could then explain why membrane target molecules such as lipids and lipid anchored proteins also undergo hop-diffusion. This model is further supported by electron microscopy data that shows that actin filaments are in close proximity of the plasma membrane and forms compartments that are similar in size to those conferred by the SPT data [102].

Another surprising aspect of this work is the proposed magnitudes of the diffusion coefficients of lipids and proteins alike within the confinement zones of ~5-8 μm^2/sec [87, 89, 93, 100]. This is equal in magnitude to that found in reconstituted model membranes, but only at much lower proteins densities than are considered to be physiologically relevant [18-19]. The authors further justifies the proposed magnitude of the diffusion coefficient by reporting that similar magnitudes are also measured in cell blebs that are absent of actin cytoskeleton. However, the protocol used for preparing the blebs (incubation with 1 mM menadione for 1 h at 37 ^oC) has also been shown to reduce the cell surface density of transferrin and LDL receptor by ~70 % by inhibition of receptor recycling after incubation with only one fifth the dose of menadione (200 μM) under similar conditions [103]. Similarly, reduction of the total protein content has further been demonstrated for other bleb forming protocols [104]. The reported short range diffusion coefficients in NRK cells for DOPE (D_{micro} = 5.4 μm^2/sec), transferrin (D_{micro} = 5.2 μm^2/sec), and μ-opiod receptor (D_{micro} = 4.2 μm^2/sec) also suggests that the dependence on the diffusion coefficient on the molecular radii within the confinement zones is weaker even than that suggested by the Saffman-Delbrück equation. We also note that the reported magnitude of the diffusion coefficients of the lipids and protein within the confinement zones are equal to, or at best only one half the expected magnitude of, the diffusion coefficient of the free gold particles in solution hence suggesting that there should also be a significant frictional drag effect of the probe on the measured diffusion coefficient of the membrane target molecules (see also Fig. (**1**)).

A caveat in these studies is of course that these results are so far obtained with one technique, SPT with Ø 40 nm gold particles. In response to this, Wieser *et al.* used SPT with significantly smaller probes consisting of either a Fab fragment ($R_H \approx$ 2.9 nm) or an intact Ab labeled with the fluorescent dye Alexa-647 ($R_H \approx$ 5.8 nm) in order to investigate the high-speed motion of the GPI-anchored protein CD59 in T24 (ECV) cells [73]. In this cell line, Murase *et al.* had previously reported that the lipid DOPE undergoes hop diffusion between compartments with a mean (±s.d.) size of 120±53 nm for an average residency time of 16 msec and with a *D* of 0.20±0.08 μm^2/sec (for gold-labeled DOPE with a 100 msec time window) [100]. In these experiments, SPT data was collected with acquisition times ranging from 50 μsec to 1 msec and with sampling intervals ranging from ~10-2000 Hz. The representative duration in the case of using Fab fragments at 1000 Hz was only six image frames hence prohibiting individual trajectory analysis. Consequently all data

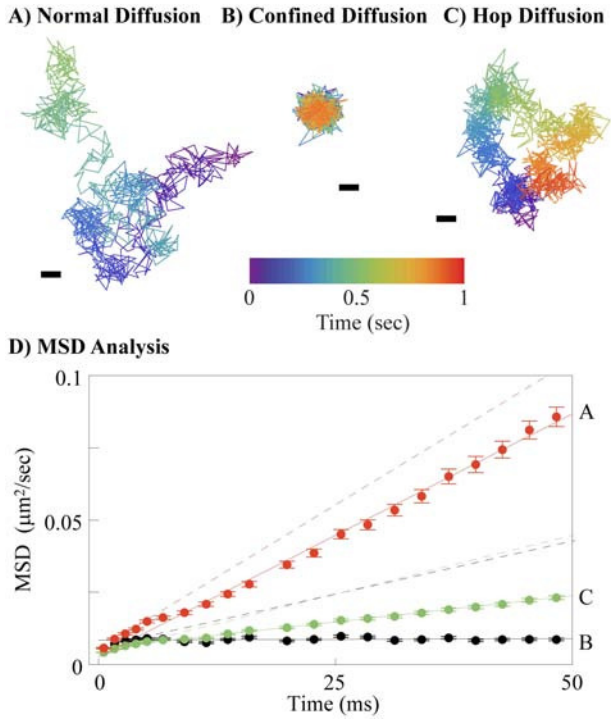

Fig. (4). Single QD trajectories showing the diffusion of a lipid, biotin-cap-DPPE, which had been artificially bulk loaded into a mouse embryo fibroblast and labeled with sAv-QD655. Images were acquired with 0.52 msec integration at 1760 Hz and analyzed by standard particle tracking methods. The points in each trajectory are linearly color coded as a function of the time after the start of the first point in the respective trajectory. In these experiments, we always see three types of motion indicative of the heterogeneous nature of the plasma membrane, **A**) approximately normal diffusion (total trajectory time ~930 pts corresponding to ~0.53 sec), **B**) very confined diffusion (total trajectory time ~1550 pts corresponding to ~0.88 sec), **C**) and hop diffusion (total trajectory time ~1670 pts, 0.95 sec). The mode of motion of each trajectory was further analyzed by calculating the mean squared displacement (MSD) of each trajectory separately as a function of time, t and by subsequent curve fitting to MSD = $4D_{micro/macro}t$ for two separate time windows, 1) short term diffusion, D_{micro}, corresponding to analysis of image frame 2-4 (δt ~1.5 msec), and 2) long term diffusion, D_{macro}, corresponding to analysis of image frames 2-88 (δt ~50 msec). The results of this analysis was for A) normal diffusion (red points) D_{micro} ≈ 0.50 μm^2/sec (best fit, red dashed line), D_{macro} ≈ 0.42 μm^2/sec (best fit, red line), B) very confined (immobile) diffusion (black points) D_{micro} ≈ 0.20 μm^2/sec (best fit, black dashed line), D_{macro} ≈ 0.00 μm^2/sec (best fit, black line), and C) hop diffusion (green points) D_{micro} ≈ 0.20 μm^2/sec (best fit, green dashed line) D_{macro} ≈ 0.09 μm^2/sec (best fit, green line). Scale bar 100 nm.

analysis was done by time averaging over multiple trajectories from several cells but by using both MSD analysis and by analysis of the probability distributions of the squared displacements. The conclusions from this analysis was that the lipid anchored protein CD59, on average, undergoes normal Brownian diffusion ($D_{micro} = D_{macro}$) for all conditions that were tested. The diffusion coefficients at 37 °C were found to range from 0.46±0.05 μm^2/sec for Fab fragments acquired at ~1000 Hz to 0.17±0.01 μm^2/sec with intact Abs acquired at ~600 Hz, thus indicating that in this case there is a very strong dependence on the probe, from a combination of probe induced cross-linking and possibly also probe size. This data hence indicates that the hop-diffusion that is observed by use of gold particles may very well be an artifact of the probe. However, this data while acquired with a much less invasive probe is yet limited by that the representative trajectory duration (~6 msec) is much less than the reported lifetime (~16 msec) of the proposed domains. Hence, we believe that further work is required to validate or disprove the concept of hop diffusion as it is currently presented.

Along this line, we have also initiated work in order to be able to validate the presented concept of hop-diffusion. In our preliminary results, we have imaged the molecular motion of an artificial lipid, biotin-cap-DPPE, in mouse embryo fibroblasts (MEFs) by using commercially available sAv-QDs emitting at 655 nm (R_H ≈ 11.4 nm; data not shown) in combination with an EMCCD camera (DU-860; Andor). In these experiments we have used an illumination time of ~0.52 msec and a sampling rate of ~1760 Hz Fig. (**4**). A preliminary analysis of this data indicates that the motion of a majority of lipids is restricted at short time intervals (~50-200 msec) to domains with a size range of ~100-200 nm in diameter and with a D_{micro} (time window of ~1.5 msec, points 2-4) of 0.20 μm^2/sec and a D_{macro} (time window of ~50 msec, points 2-88) of 0.09 μm^2/sec. This data suggests that lipids that have been labeled with sAv-QDs in MEFs behave in a similar fashion to lipids that have been labeled with larger gold particles [87, 100]. However, much further statistical analysis of this data is needed to fully characterize the observed confinement in this case. This data is however of course also subject to all the limitations associated with the use of larger probes.

SPT acquired at ~10-30 Hz reveals an entirely different picture for the plasma membrane organization. At this slower sampling rate hop diffusion is not observed. Instead observed confinement regions are either larger, longer lived or both. For example, SPT data acquired at ~30 Hz has identified membrane areas of ~100-300 nm diameter in which certain membrane targeting molecules (e.g. GPI-anchored proteins, GSLs, and phospholipids) are temporally confined to, but free to move within, for several seconds [54, 90, 94, 96, 105]. These areas, which are sometimes referred to as transient confinement zones (TCZs), are identified by probabilistic means by comparison of the instantaneous displacements in comparison to the expected displacements for a molecule that undergoes random diffusion [94, 105]. TCZs have been shown to be cholesterol dependent and to be dependent on GSL synthesis. This has led to the suggestion that TCZs are a kind of lipid raft [96, 105]. However, the size and lifetimes of identified TCZs are dependent on the time resolution of SPT [105]. Furthermore, it has been reported that TCZs are not observed even in data acquired at 30 Hz in the absence of probe-induced cross-linking [106]. This suggests that TCZs are an experimental artifact that is induced by probe induced cross-linking. SPT has also been used in this context to investigate sparse signaling of membrane proteins by use of intentionally multivalent gold particles. Using this method Chen *et al.* have found that GPI-anchored proteins undergo transient anchorage for periods ranging from 300 msec to 10

sec [92]. This transient anchorage was found to be dependent on cholesterol and Src family kinases [92]. Using a similar method, Suzuki *et al.* have also shown that small clusters of CD59 will transiently recruit several intracellular signaling molecules resulting in what the authors have termed stimulation-induced temporary arrest of lateral diffusion (STALL) with an average duration of 0.57 sec occurring every 2 sec [91, 101].

In addition to the proposed nanostructures observed by SPT, SPT has also been used to identify specific interactions between plasma membrane molecules and molecular protein targets and the actin cytoskeleton inside the cell [52, 82, 107-113].

4. COMPLEMENTARY TECHNIQUES

Many other forms of traditional light microscopy techniques, for example FRAP and FCS have the sufficient temporal resolution to be able to resolve transient structures, down to within a lifetime range of milliseconds to seconds, but the spatial resolution of information from the bleach spot and focal spot, respectively, are limited by diffraction to >200 nm (for reviews of traditional light microscopy techniques used to study membrane lateral organization see [40, 44]). In contrast, electron microscopy, which has sufficient spatial resolution but of course no temporal resolution and which has been used to visualize relatively static nanostructures such as caveolae and clathrin-coated pits, has so far not been able to conclusively resolve additional nanostructure in the plasma membrane. More recently, new light microscopy techniques have also been introduced which offer sub-diffraction limited spatial resolution, for example the related techniques photoactivated localization microscopy (PALM) and stochastic reconstruction microscopy (STORM). These methods can reach a spatial resolution of 20-40 nm by computational fitting of single molecule point spread functions in an image series where only a subset of labels are emitting in each frame [114-115], but the best temporal resolution reached by these techniques is 50 msec in the so-called sptPALM [116]. Perhaps the most significant developments, however, has been the introduction of stimulated emission depletion FCS (STED-FCS) by Eggeling *et al.* where the focal spot of FCS is significantly decreased to ~30 nm [117], and an orthogonal confocal microscope based tracking technique developed by the same group reaching the same spatial and temporal resolution by determining the positions of dye labeled molecules using three point detectors placed in close proximity [118]. By these techniques it has been shown that sphingolipids in contrast to phospholipids are temporarily trapped for ~10 msec in ~10-20 nm sized domains in a cholesterol dependent manner [117-118].

5. OUTLOOK AND CONCLUSION

Gaining a better understanding of the molecular organization of the mammalian plasma membrane is expected to have far reaching consequences and may offer many rewards in biomedicine. For example, possible spatial regulation of cell signaling as a result of plasma membrane organization could help explain how specificity in externally mediated cell signaling cascades is maintained in the cytoplasm [119]. This is especially relevant considering that intracellular cell signaling cascades are extremely complex and involve multiple overlapping signaling second messengers, e.g. phosphoinositides (PtdIns) such as PtdIns(3,4,5)P_3 and PtdIns(4,5)P_2 which are downstream mediators in a variety of cell signaling pathways that are activated by an equally diverse number of extracellular stimuli including growth factor receptors, GPCRs, and immunoglobulin super family receptors [120]. Spatial regulation in cell signaling also offers the potential for drug targeting to receptor complexes rather than single receptors, a mechanism that could increase drug specificity and avidity.

A general consensus in the field is that the organization of the native plasma membrane is very heterogeneous and complex. This consensus view is strongly supported by SPT results which show a range of molecular motions (e.g. Brownian, confined and combinations thereof) and nanostructures from very transient (<100 msec) and small (<100 nm) to more stable (>1 sec) and large (>100 nm). A consequence of the observed heterogeneity is also that the lateral motion in the plasma membrane is time dependent such that the detection of structures requires that the accessible temporal sampling is faster, the duration is longer, and the spatial resolution is less than the lifetime and size of the structures. A second consequence is that the SPT results are strongly influenced by the probes that are used since it is the optical properties of the probe that dictates the accessible experimental spatial and temporal resolution. This is especially apparent in the case of hop diffusion which has repeatedly been shown by use of SPT with large functionalized gold particles (of ~Ø50 nm), since the required very fast sampling intervals, and for long durations, have thus far only been possible with these large probes. However, there are still many open questions about whether the results with larger probes in this case are a reflection of the membrane organization or is an artifact stemming from the probe size (e.g. frictional drag, steric interactions, and artificially induced cross-linking), in particular with respect to the reported magnitude of the diffusion coefficient. In contrast, even though SPT experiments with fluorescent dyes and proteins are less invasive, the temporal sampling is either too slow or the duration is too short to directly and conclusively observe or rule out transient and small structures such as those suggested for hop diffusion. The appropriate choice of probe in an SPT experiment should then always be made in relation to the relevant temporal scales, both in terms of the frequency and the duration, of the phenomena that are under investigation. Furthermore, considering the intricate link that exists in SPT between the probe and the results as well as the potential risks of probe induced artifacts, it is of utmost importance that all SPT results are carefully cross-validated, either with SPT using different probes, or alternative by the emerging techniques that are in some cases enabling investigations at equivalent spatial and temporal resolutions.

In relation to one of the other suggested nanostructures in the plasma membrane, the lipid rafts, there are also many remaining questions. In model membranes, lipid mixtures that are thought to be representative of lipid rafts form micrometer sized domains [33]. These domains are not observed in live cells, even though their formation can be artificially induced in cell blebs and plasma membrane spheres (PMS) [121-122]. Membrane blebs and PMS have in com-

mon that they exclude links to the actin cytoskeleton. A plausible explanation is then that actin filaments, in addition to restricting the free motion of membrane species as suggested by SPT results with gold particles, also are a limiting factor in the formation of large lipid domains, and which as a consequence only exist as small domains [117-118]. This possibility has previously been suggested by Kusumi *et al.* [2]. Membrane topology, which is caused by e.g. actin cytoskeleton extensions and membrane ruffling could also have a significant influence on the observed molecular motion in the plasma membrane and should not be forgotten in the discussion of plasma membrane lateral organization [41].

ACKNOWLEDGEMENTS

We thank Jakub Kubiak for the FCS data of rhodamine-DPPE in GUVs and Thomas E. Rasmussen for the FCS data of FITC, sAv, IgG, and Ø 40 nm beads. This work was supported by grants from the Danish National Research Foundation (to MEMPHYS), the Villum Kann Rasmussen Foundation (to BioNET), the Lundbeck Foundation (to B. C. L), the Novo Nordisk Foundation (to B. C. L.), the Leo Pharma Research Foundation (to B. C. L.). This work furthermore benefitted from the establishment of the Danish Biomedical Imaging Center (DaMBIC) at the University of Southern Denmark by Danish Ministry of Science.

ABBREVIATIONS

Ab	=	Antibody
ACP	=	Acyl carrier protein
BLAP	=	Biotin ligase acceptor peptide
CoA	=	Coenzyme A
CTB	=	Cholera toxin subunit B
D	=	Diffusion coefficient
D_M	=	Diffusion coefficient in membrane
D_{macro}	=	Long range diffusion coefficient
D_{micro}	=	Short range diffusion coefficient
D_S	=	Diffusion coefficient in solution
ε	=	Molar extinction coefficient
FCS	=	Fluorescence correlation spectroscopy
FP	=	Fluorescent protein
FRAP	=	Fluorescence recovery after photobleaching
FWHM	=	Full width at half maximum
GSL	=	Glycosphingolipid
GUV	=	Giant unilamellar vesicle
IgG	=	Immunoglobulin G
μ_M	=	Membrane viscosity
μ_S	=	Solution viscosity
MSD	=	Mean square displacement
PALM	=	Photoactivated localization microscopy
QD	=	Quantum dot
QY	=	Quantum yield
R	=	Molecular radii
R_H	=	Radius of hydration
sAv	=	Streptavidin
SLB	=	Supported lipid bilayer
SMFT	=	Single molecule fluorescence tracking
SNR	=	Signal to noise ratio
SPT	=	Single particle tracking
STED	=	Stimulated emission depletion
STORM	=	Stochastic reconstruction microscopy
Ø	=	Diameter

REFERENCES

[1] Shaikh, S. R.; Edidin, M. A. Membranes are not just rafts. *Chem. Phys. Lipids*, **2006**, *144* (1), 1-3.

[2] Kusumi, A.; Shirai, Y. M.; Koyama-Honda, I.; Suzuki, K. G.; Fujiwara, T. K. Hierarchical organization of the plasma membrane: investigations by single-molecule tracking vs. fluorescence correlation spectroscopy. *FEBS Lett.*, **2010**, *584* (9), 1814-23.

[3] Lingwood, D.; Simons, K. Lipid rafts as a membrane-organizing principle. *Science*, **2010**, *327* (5961), 46-50.

[4] Lommerse, P. H.; Spaink, H. P.; Schmidt, T. In vivo plasma membrane organization: results of biophysical approaches. *Biochim. Biophys. Acta.*, **2004**, *1664* (2), 119-31.

[5] Edidin, M. The state of lipid rafts: from model membranes to cells. *Annu. Rev. Biophys. Biomol. Struct.*, **2003**, *32*, 257-83.

[6] Anderson, R. G.; Jacobson, K. A role for lipid shells in targeting proteins to caveolae, rafts, and other lipid domains. *Science*, **2002**, *296* (5574), 1821-5.

[7] Jacobson, K.; Mouritsen, O. G.; Anderson, R. G. Lipid rafts: at a crossroad between cell biology and physics. *Nat. Cell Biol.*, **2007**, *9* (1), 7-14.

[8] Kusumi, A.; Nakada, C.; Ritchie, K.; Murase, K.; Suzuki, K.; Murakoshi, H.; Kasai, R. S.; Kondo, J.; Fujiwara, T. Paradigm shift of the plasma membrane concept from the two-dimensional continuum fluid to the partitioned fluid: high-speed single-molecule tracking of membrane molecules. *Annu. Rev. Biophys. Biomol. Struct.*, **2005**, *34*, 351-78.

[9] Engelman, D. M. Membranes are more mosaic than fluid. *Nature*, **2005**, *438* (7068), 578-80.

[10] van Meer, G.; Voelker, D. R.; Feigenson, G. W. Membrane lipids: where they are and how they behave. *Nat. Rev. Mol. Cell Biol.*, **2008**, *9* (2), 112-24.

[11] Wallin, E.; von Heijne, G. Genome-wide analysis of integral membrane proteins from eubacterial, archaean, and eukaryotic organisms. *Protein Sci.*, **1998**, *7* (4), 1029-38.

[12] Mouritsen, O. G. Life - as a matter of fat : the emerging science of lipidomics. Springer: Berlin, 2005; p xii, 276 p.

[13] Galla, H. J.; Hartmann, W.; Theilen, U.; Sackmann, E. On two-dimensional passive random walk in lipid bilayers and fluid pathways in biomembranes. *J. Membr. Biol.*, **1979**, *48* (3), 215-36.

[14] Gudmand, M.; Fidorra, M.; Bjornholm, T.; Heimburg, T. Diffusion and partitioning of fluorescent lipid probes in phospholipid monolayers. *Biophys. J.*, **2009**, *96* (11), 4598-609.

[15] Javanainen, M.; Monticelli, L.; Bernardino de la Serna, J.; Vattulainen, I. Free volume theory applied to lateral diffusion in Langmuir monolayers: atomistic simulations for a protein-free model of lung surfactant. *Langmuir*, **2010**, *26* (19), 15436-44.

[16] Saffman, P. G.; Delbruck, M. Brownian motion in biological membranes. *Proc. Natl. Acad. Sci. USA.*, **1975,** *72* (8), 3111-3.

[17] Singer, S. J.; Nicolson, G. L. The fluid mosaic model of the structure of cell membranes. *Science*, **1972**, *175* (23), 720-31.

[18] Peters, R.; Cherry, R. J. Lateral and rotational diffusion of bacteriorhodopsin in lipid bilayers: experimental test of the Saffman-Delbruck equations. *Proc. Natl. Acad. Sci. USA.,* **1982**, *79* (14), 4317-21.

[19] Ramadurai, S.; Holt, A.; Krasnikov, V.; van den Bogaart, G.; Killian, J. A.; Poolman, B. Lateral diffusion of membrane proteins. *J. Am. Chem. Soc.*, **2009**, *131* (35), 12650-6.

[20] Hughes, B. D.; Pailthorpe, B. A.; White, L. R. The Translational and Rotational Drag on a Cylinder Moving in a Membrane. *J. Fluid. Mech.*, **1981**, *110* (Sep), 349-372.

[21] Hughes, B. D.; Pailthorpe, B. A.; White, L. R.; Sawyer, W. H. Extraction of membrane microviscosity from translational and rotational diffusion coefficients. *Biophys. J.*, **1982**, *37* (3), 673-6.

[22] Petrov, E. P.; Schwille, P. Translational diffusion in lipid membranes beyond the Saffman-Delbruck approximation. *Biophys. J.*, **2008**, *94* (5), L41-3.

[23] Gambin, Y.; Lopez-Esparza, R.; Reffay, M.; Sierecki, E.; Gov, N. S.; Genest, M.; Hodges, R. S.; Urbach, W. Lateral mobility of proteins in liquid membranes revisited. *Proc. Natl. Acad. Sci. USA* **2006**, *103* (7), 2098-102.

[24] Lee, C. C.; Revington, M.; Dunn, S. D.; Petersen, N. O. The lateral diffusion of selectively aggregated peptides in giant unilamellar vesicles. *Biophys. J.*, **2003**, *84* (3), 1756-64.

[25] Guigas, G.; Weiss, M., Size-dependent diffusion of membrane inclusions. *Biophys. J.*, **2006**, *91* (7), 2393-8.

[26] Machan, R.; Hof, M. Lipid diffusion in planar membranes investigated by fluorescence correlation spectroscopy. *Biochim. Biophys. Acta.*, **2010**, *1798* (7), 1377-91.

[27] Przybylo, M.; Sykora, J.; Humpolickova, J.; Benda, A.; Zan, A.; Hof, M. Lipid diffusion in giant unilamellar vesicles is more than 2 times faster than in supported phospholipid bilayers under identical conditions. *Langmuir*, **2006**, *22* (22), 9096-9.

[28] Renner, L.; Osaki, T.; Chiantia, S.; Schwille, P.; Pompe, T.; Werner, C. Supported lipid bilayers on spacious and pH-responsive polymer cushions with varied hydrophilicity. *J. Phys. Chem. B.*, **2008**, *112* (20), 6373-8.

[29] Bockmann, R. A.; Hac, A.; Heimburg, T.; Grubmuller, H. Effect of sodium chloride on a lipid bilayer. *Biophys. J.*, **2003**, *85* (3), 1647-55.

[30] van den Bogaart, G.; Hermans, N.; Krasnikov, V.; de Vries, A. H.; Poolman, B. On the decrease in lateral mobility of phospholipids by sugars. *Biophys. J.*, **2007**, *92* (5), 1598-605.

[31] Vaz, W. L. C.; Goodsaid-Zalduondo, F.; Jacobson, K. Lateral diffusion of lipids and proteins in bilayer membranes. *FEBS Lett.*, **1984**, *174* (2), 199-207.

[32] Chiantia, S.; Ries, J.; Kahya, N.; Schwille, P. Combined AFM and two-focus SFCS study of raft-exhibiting model membranes. *Chemphyschem*, **2006**, *7* (11), 2409-18.

[33] Dietrich, C.; Bagatolli, L. A.; Volovyk, Z. N.; Thompson, N. L.; Levi, M.; Jacobson, K.; Gratton, E. Lipid rafts reconstituted in model membranes. *Biophys. J.*, **2001**, *80* (3), 1417-28.

[34] Vaz, W. L.; Criado, M.; Madeira, V. M.; Schoellmann, G.; Jovin, T. M. Size dependence of the translational diffusion of large integral membrane proteins in liquid-crystalline phase lipid bilayers. A study using fluorescence recovery after photobleaching. *Biochemistry*, **1982**, *21* (22), 5608-12.

[35] Vaz, W. L. C.; Derzko, Z. I.; Jacobson, K. A., Photobleaching Measurements of the Lateral Diffusion of Lipids and Proteins in Artificial Phospholipid-Bilayer Membranes. *Cell Surf. Rev.*, **1982**, *8*, 83-135.

[36] Liu, C.; Paprica, A.; Petersen, N. O. Effects of size of macrocyclic polyamides on their rate of diffusion in model membranes. *Biophys. J.*, **1997**, *73* (5), 2580-7.

[37] Webb, W. W.; Barak, L. S.; Tank, D. W.; Wu, E. S. Molecular mobility on the cell surface. *Biochem. Soc. Symp.*, **1981**, (46), 191-205.

[38] Bacia, K.; Scherfeld, D.; Kahya, N.; Schwille, P. Fluorescence correlation spectroscopy relates rafts in model and native membranes. *Biophys. J.*, **2004**, *87* (2), 1034-43.

[39] Saxton, M. J.; Jacobson, K. Single-particle tracking: applications to membrane dynamics. *Annu. Rev. Biophys. Biomol. Struct.*, **1997**, *26*, 373-99.

[40] Owen, D. M.; Williamson, D.; Rentero, C.; Gaus, K. Quantitative microscopy: protein dynamics and membrane organisation. *Traffic*, **2009**, *10* (8), 962-71.

[41] Adler, J.; Shevchuk, A. I.; Novak, P.; Korchev, Y. E.; Parmryd, I. Plasma membrane topography and interpretation of single-particle tracks. *Nat. Methods*, **2010**, *7* (3), 170-1.

[42] Grant, B. D.; Donaldson, J. G. Pathways and mechanisms of endocytic recycling. *Nat. Rev. Mol. Cell Biol.*, **2009,** *10* (9), 597-608.

[43] Steinman, R. M.; Mellman, I. S.; Muller, W. A.; Cohn, Z. A. Endocytosis and the recycling of plasma membrane. *J. Cell Biol.*, **1983**, *96* (1), 1-27.

[44] Chen, Y.; Lagerholm, B. C.; Yang, B.; Jacobson, K. Methods to measure the lateral diffusion of membrane lipids and proteins. *Methods*, **2006**, *39* (2), 147-53.

[45] Ries, J.; Schwille, P. New concepts for fluorescence correlation spectroscopy on membranes. *Phys. Chem. Chem. Phys.*, **2008**, *10* (24), 3487-97.

[46] Chiantia, S.; Ries, J.; Schwille, P. Fluorescence correlation spectroscopy in membrane structure elucidation. *Biochim. Biophys. Acta.*, **2009**, *1788* (1), 225-33.

[47] Wieser, S.; Schutz, G. J. Tracking single molecules in the live cell plasma membrane-Do's and Don't's. *Methods*, **2008**, *46* (2), 131-40.

[48] Brameshuber, M.; Schutz, G. J. How the sum of its parts gets greater than the whole. *Nat. Methods*, **2008**, *5* (2), 133-4.

[49] Bannai, H.; Levi, S.; Schweizer, C.; Dahan, M.; Triller, A. Imaging the lateral diffusion of membrane molecules with quantum dots. *Nat. Protoc.*, **2006**, *1* (6), 2628-34.

[50] Ram, S.; Prabhat, P.; Chao, J.; Ward, E. S.; Ober, R. J. High accuracy 3D quantum dot tracking with multifocal plane microscopy for the study of fast intracellular dynamics in live cells. *Biophys. J.*, **2008**, *95* (12), 6025-43.

[51] Alcor, D.; Gouzer, G.; Triller, A. Single-particle tracking methods for the study of membrane receptors dynamics. *Eur. J. Neurosci.*, **2009**, *30* (6), 987-97.

[52] Jaqaman, K.; Loerke, D.; Mettlen, M.; Kuwata, H.; Grinstein, S.; Schmid, S. L.; Danuser, G. Robust single-particle tracking in live-cell time-lapse sequences. *Nat. Methods*, **2008**, *5* (8), 695-702.

[53] Serge, A.; Bertaux, N.; Rigneault, H.; Marguet, D. Dynamic multiple-target tracing to probe spatiotemporal cartography of cell membranes. *Nat. Methods*, **2008**, *5* (8), 687-94.

[54] Pinaud, F.; Michalet, X.; Iyer, G.; Margeat, E.; Moore, H. P.; Weiss, S. Dynamic partitioning of a glycosyl-phosphatidylinositol-anchored protein in glycosphingolipid-rich microdomains imaged by single-quantum dot tracking. *Traffic*, **2009**, *10* (6), 691-712.

[55] Schutz, G. J.; Schindler, H.; Schmidt, T. Single-molecule microscopy on model membranes reveals anomalous diffusion. *Biophys. J.*, **1997**, *73* (2), 1073-80.

[56] Qian, H.; Sheetz, M. P.; Elson, E. L. Single particle tracking. Analysis of diffusion and flow in two-dimensional systems. *Biophys. J.*, **1991**, *60* (4), 910-21.

[57] Hink, M. A.; Griep, R. A.; Borst, J. W.; van Hoek, A.; Eppink, M. H.; Schots, A.; Visser, A. J. Structural dynamics of green fluorescent protein alone and fused with a single chain Fv protein. *J. Biol. Chem.*, **2000**, *275* (23), 17556-60.

[58] Lagerholm, B. C.; Weinreb, G. E.; Jacobson, K.; Thompson, N. L. Detecting microdomains in intact cell membranes. *Annu. Rev. Phys. Chem.*, **2005**, *56*, 309-36.

[59] Chen, I.; Ting, A. Y. Site-specific labeling of proteins with small molecules in live cells. *Curr. Opin. Biotechnol.*, **2005**, *16* (1), 35-40.

[60] Chen, I.; Howarth, M.; Lin, W.; Ting, A. Y. Site-specific labeling of cell surface proteins with biophysical probes using biotin ligase. *Nat. Methods*, **2005**, *2* (2), 99-104.

[61] Johnsson, N.; George, N.; Johnsson, K. Protein chemistry on the surface of living cells. *Chembiochem.*, **2005**, *6* (1), 47-52.

[62] Keppler, A.; Gendreizig, S.; Gronemeyer, T.; Pick, H.; Vogel, H.; Johnsson, K. A general method for the covalent labeling of fusion proteins with small molecules in vivo. *Nat. Biotechnol.*, **2003**, *21* (1), 86-9.

[63] Griffin, B. A.; Adams, S. R.; Tsien, R. Y. Specific covalent labeling of recombinant protein molecules inside live cells. *Science*, **1998**, *281* (5374), 269-72.

[64] Yu, C.; Hale, J.; Ritchie, K.; Prasad, N. K.; Irudayaraj, J. Receptor overexpression or inhibition alters cell surface dynamics of EGF-EGFR interaction: new insights from real-time single molecule analysis. *Biochem. Biophys. Res. Commun.*, **2009**, *378* (3), 376-82.

[65] Howarth, M.; Chinnapen, D. J.; Gerrow, K.; Dorrestein, P. C.; Grandy, M. R.; Kelleher, N. L.; El-Husseini, A.; Ting, A. Y. A monovalent streptavidin with a single femtomolar biotin binding site. *Nat. Methods*, **2006**, *3* (4), 267-73.

[66] You, C.; Wilmes, S.; Beutel, O.; Lochte, S.; Podoplelowa, Y.; Roder, F.; Richter, C.; Seine, T.; Schaible, D.; Uze, G.; Clarke, S.; Pinaud, F.; Dahan, M.; Piehler, J. Self-controlled monofunctionalization of quantum dots for multiplexed protein tracking in live cells. *Angew. Chem. Int. Ed. Engl.*, **2010**, *49* (24), 4108-12.

[67] Howarth, M.; Liu, W.; Puthenveetil, S.; Zheng, Y.; Marshall, L. F.; Schmidt, M. M.; Wittrup, K. D.; Bawendi, M. G.; Ting, A. Y., Monovalent, reduced-size quantum dots for imaging receptors on living cells. *Nat Methods* **2008,** *5* (5), 397-9.

[68] Clarke, S.; Pinaud, F.; Beutel, O.; You, C.; Piehler, J.; Dahan, M., Covalent monofunctionalization of peptide-coated quantum dots for single-molecule assays. *Nano Lett* **2010,** *10* (6), 2147-54.

[69] Sperling, R. A.; Pellegrino, T.; Li, J. K.; Chang, W. H.; Parak, W. J. Electrophoretic separation of nanoparticles with a discrete number of functional groups. *Adv. Func. Mat.*, **2006**, *16* (7), 943-948.

[70] Zanchet, D.; Micheel, C. M.; Parak, W. J.; Gerion, D.; Alivisatos, A. P. Electrophoretic Isolation of Discrete Au Nanocrystal/DNA Conjugates. *Nano. Letts.*, **2000**, *1* (1), 32-35.

[71] Wustner, D. Fluorescent sterols as tools in membrane biophysics and cell biology. *Chem. Phys. Lipids*, **2007**, *146* (1), 1-25.

[72] Sosinsky, G. E.; Gaietta, G. M.; Hand, G.; Deerinck, T. J.; Han, A.; Mackey, M.; Adams, S. R.; Bouwer, J.; Tsien, R. Y.; Ellisman, M. H. Tetracysteine genetic tags complexed with biarsenical ligands as a tool for investigating gap junction structure and dynamics. *Cell Commun. Adhes.*, **2003**, *10* (4-6), 181-6.

[73] Wieser, S.; Moertelmaier, M.; Fuertbauer, E.; Stockinger, H.; Schutz, G. J. (Un)confined diffusion of CD59 in the plasma membrane determined by high-resolution single molecule microscopy. *Biophys. J.*, **2007**, *92* (10), 3719-28.

[74] Espenel, C.; Margeat, E.; Dosset, P.; Arduise, C.; Le Grimellec, C.; Royer, C. A.; Boucheix, C.; Rubinstein, E.; Milhiet, P. E. Single-molecule analysis of CD9 dynamics and partitioning reveals multiple modes of interaction in the tetraspanin web. *J. Cell Biol.*, **2008**, *182* (4), 765-76.

[75] Giepmans, B. N.; Adams, S. R.; Ellisman, M. H.; Tsien, R. Y. The fluorescent toolbox for assessing protein location and function. *Science*, **2006**, *312* (5771), 217-24.

[76] Lommerse, P. H. M.; Vastenhoud, K.; Pirinen, N. J.; Magee, A. I.; Spaink, H. P.; Schmidt, T. Single-molecule diffusion reveals similar mobility for the Lck, H-Ras, and K-Ras membrane anchors. *Biophys. J.*, **2006**, *91* (3), 1090-1097.

[77] Sunbul, M.; Yen, M.; Zou, Y.; Yin, J. Enzyme catalyzed site-specific protein labeling and cell imaging with quantum dots. *Chem. Commun. (Camb.)*, **2008**, (45), 5927-9.

[78] Chakraborty, S. K.; Fitzpatrick, J. A.; Phillippi, J. A.; Andreko, S.; Waggoner, A. S.; Bruchez, M. P.; Ballou, B. Cholera toxin B conjugated quantum dots for live cell labeling. *Nano. Lett.*, **2007**, *7* (9), 2618-26.

[79] Durisic, N.; Bachir, A. I.; Kolin, D. L.; Hebert, B.; Lagerholm, B. C.; Grutter, P.; Wiseman, P. W. Detection and correction of blinking bias in image correlation transport measurements of quantum dot tagged macromolecules. *Biophys. J.*, **2007**, *93* (4), 1338-46.

[80] Groc, L.; Heine, M.; Cognet, L.; Brickley, K.; Stephenson, F. A.; Lounis, B.; Choquet, D. Differential activity-dependent regulation of the lateral mobilities of AMPA and NMDA receptors. *Nat. Neurosci.*, **2004**, *7* (7), 695-6.

[81] Hohng, S.; Ha, T. Near-complete suppression of quantum dot blinking in ambient conditions. *J. Am. Chem. Soc.*, **2004**, *126* (5), 1324-5.

[82] Andrews, N. L.; Lidke, K. A.; Pfeiffer, J. R.; Burns, A. R.; Wilson, B. S.; Oliver, J. M.; Lidke, D. S. Actin restricts FcepsilonRI diffusion and facilitates antigen-induced receptor immobilization. *Nat. Cell Biol.*, **2008**, *10* (8), 955-63.

[83] Pons, T.; Mattoussi, H. Investigating biological processes at the single molecule level using luminescent quantum dots. *Ann. Biomed. Eng.*, **2009**, *37* (10), 1934-59.

[84] Michalet, X.; Pinaud, F.; Lacoste, T. D.; Dahan, M.; Bruchez, M. P.; Alivisatos, A. P.; Weiss, S. Properties of fluorescent semiconductor nanocrystals and their application to biological labeling. *Single Mol.*, **2001**, *2* (4), 261-276.

[85] Bruchez, M., Jr.; Moronne, M.; Gin, P.; Weiss, S.; Alivisatos, A. P. Semiconductor nanocrystals as fluorescent biological labels. *Science*, **1998**, *281* (5385), 2013-6.

[86] Wu, X.; Liu, H.; Liu, J.; Haley, K. N.; Treadway, J. A.; Larson, J. P.; Ge, N.; Peale, F.; Bruchez, M. P. Immunofluorescent labeling of cancer marker Her2 and other cellular targets with semiconductor quantum dots. *Nat. Biotechnol.*, **2003**, *21* (1), 41-6.

[87] Fujiwara, T.; Ritchie, K.; Murakoshi, H.; Jacobson, K.; Kusumi, A. Phospholipids undergo hop diffusion in compartmentalized cell membrane. *J. Cell Biol.*, **2002**, *157* (6), 1071-81.

[88] Wong, S. F.; Meng, C. K.; Fenn, J. B. Multiple Charging in Electrospray Ionization of Poly(Ethylene Glycols). *J. Phys. Chem-Us.*, **1988**, *92* (2), 546-550.

[89] Umemura, Y. M.; Vrljic, M.; Nishimura, S. Y.; Fujiwara, T. K.; Suzuki, K. G.; Kusumi, A. Both MHC class II and its GPI-anchored form undergo hop diffusion as observed by single-molecule tracking. *Biophys. J.*, **2008**, *95* (1), 435-50.

[90] Sheets, E. D.; Lee, G. M.; Simson, R.; Jacobson, K. Transient confinement of a glycosylphosphatidylinositol-anchored protein in the plasma membrane. *Biochemistry*, **1997**, *36* (41), 12449-58.

[91] Suzuki, K. G.; Fujiwara, T. K.; Edidin, M.; Kusumi, A. Dynamic recruitment of phospholipase C gamma at transiently immobilized GPI-anchored receptor clusters induces IP3-Ca2+ signaling: single-molecule tracking study 2. *J. Cell Biol.*, **2007**, *177* (4), 731-42.

[92] Chen, Y.; Thelin, W. R.; Yang, B.; Milgram, S. L.; Jacobson, K. Transient anchorage of cross-linked glycosyl-phosphatidylinositol-anchored proteins depends on cholesterol, Src family kinases, caveolin, and phosphoinositides. *J. Cell Biol.*, **2006**, *175* (1), 169-78.

[93] Suzuki, K.; Ritchie, K.; Kajikawa, E.; Fujiwara, T.; Kusumi, A. Rapid hop diffusion of a G-protein-coupled receptor in the plasma membrane as revealed by single-molecule techniques. *Biophys. J.*, **2005**, *88* (5), 3659-80.

[94] Simson, R.; Sheets, E. D.; Jacobson, K. Detection of temporary lateral confinement of membrane proteins using single-particle tracking analysis. *Biophys. J.*, **1995**, *69* (3), 989-93.

[95] Murcia, M. J.; Minner, D. E.; Mustata, G. M.; Ritchie, K.; Naumann, C. A. Design of quantum dot-conjugated lipids for long-term, high-speed tracking experiments on cell surfaces. *J. Am. Chem. Soc.*, **2008**, *130* (45), 15054-62.

[96] Dietrich, C.; Yang, B.; Fujiwara, T.; Kusumi, A.; Jacobson, K. Relationship of lipid rafts to transient confinement zones detected by single particle tracking. *Biophys. J.*, **2002**, *82* (1 Pt 1), 274-84.

[97] Kenworthy, A. K.; Nichols, B. J.; Remmert, C. L.; Hendrix, G. M.; Kumar, M.; Zimmerberg, J.; Lippincott-Schwartz, J. Dynamics of putative raft-associated proteins at the cell surface. *J. Cell Biol.*, **2004**, *165* (5), 735-46.

[98] Rhode, S.; Grurl, R.; Brameshuber, M.; Hermetter, A.; Schutz, G. J. Plasma membrane fluidity affects transient immobilization of oxidized phospholipids in endocytotic sites for subsequent uptake. *J. Biol. Chem.*, **2009**, *284* (4), 2258-65.

[99] Lommerse, P. H.; Vastenhoud, K.; Pirinen, N. J.; Magee, A. I.; Spaink, H. P.; Schmidt, T. Single-molecule diffusion reveals similar mobility for the Lck, H-ras, and K-ras membrane anchors. *Biophys. J.*, **2006**, *91* (3), 1090-7.

[100] Murase, K.; Fujiwara, T.; Umemura, Y.; Suzuki, K.; Iino, R.; Yamashita, H.; Saito, M.; Murakoshi, H.; Ritchie, K.; Kusumi, A. Ultrafine membrane compartments for molecular diffusion as revealed by single molecule techniques. *Biophys. J.*, **2004**, *86* (6), 4075-93.

[101] Suzuki, K. G.; Fujiwara, T. K.; Sanematsu, F.; Iino, R.; Edidin, M.; Kusumi, A. GPI-anchored receptor clusters transiently recruit Lyn and G alpha for temporary cluster immobilization and Lyn activation: single-molecule tracking study 1. *J. Cell Biol.*, **2007**, *177* (4), 717-30.

[102] Morone, N.; Fujiwara, T.; Murase, K.; Kasai, R. S.; Ike, H.; Yuasa, S.; Usukura, J.; Kusumi, A. Three-dimensional reconstruction of the membrane skeleton at the plasma membrane interface by electron tomography. *J. Cell Biol.*, **2006**, *174* (6), 851-62.

[103] Malorni, W.; Testa, U.; Rainaldi, G.; Tritarelli, E.; Peschle, C. Oxidative stress leads to a rapid alteration of transferrin receptor intravesicular trafficking. *Exp. Cell Res.*, **1998**, *241* (1), 102-16.

[104] Frick, M.; Schmidt, K.; Nichols, B. J. Modulation of lateral diffusion in the plasma membrane by protein density. *Curr. Biol.*, **2007**, *17* (5), 462-7.

[105] Chen, Y.; Yang, B.; Jacobson, K. Transient confinement zones: a type of lipid raft? *Lipids,* **2004**, *39* (11), 1115-9.

[106] Kusumi, A.; Koyama-Honda, I.; Suzuki, K. Molecular dynamics and interactions for creation of stimulation-induced stabilized rafts from small unstable steady-state rafts. *Traffic*, **2004**, *5* (4), 213-30.

[107] Chen, H.; Titushkin, I.; Stroscio, M.; Cho, M. Altered membrane dynamics of quantum dot-conjugated integrins during osteogenic differentiation of human bone marrow derived progenitor cells. *Biophys. J.*, **2007**, *92* (4), 1399-408.

[108] Bates, I. R.; Hebert, B.; Luo, Y.; Liao, J.; Bachir, A. I.; Kolin, D. L.; Wiseman, P. W.; Hanrahan, J. W. Membrane lateral diffusion and capture of CFTR within transient confinement zones. *Biophys. J.*, **2006**, *91* (3), 1046-58.

[109] Haggie, P. M.; Kim, J. K.; Lukacs, G. L.; Verkman, A. S. Tracking of quantum dot-labeled CFTR shows near immobilization by C-terminal PDZ interactions. *Mol. Biol. Cell.*, **2006**, *17* (12), 4937-45.

[110] Thelin, W. R.; Chen, Y.; Gentzsch, M.; Kreda, S. M.; Sallee, J. L.; Scarlett, C. O.; Borchers, C. H.; Jacobson, K.; Stutts, M. J.; Milgram, S. L. Direct interaction with filamins modulates the stability and plasma membrane expression of CFTR. *J. Clin. Invest.*, **2007**, *117* (2), 364-74.

[111] Lidke, D. S.; Lidke, K. A.; Rieger, B.; Jovin, T. M.; Arndt-Jovin, D. J. Reaching out for signals: filopodia sense EGF and respond by directed retrograde transport of activated receptors. *J. Cell Biol.*, **2005**, *170* (4), 619-26.

[112] Lidke, D. S.; Nagy, P.; Heintzmann, R.; Arndt-Jovin, D. J.; Post, J. N.; Grecco, H. E.; Jares-Erijman, E. A.; Jovin, T. M. Quantum dot ligands provide new insights into erbB/HER receptor-mediated signal transduction. *Nat. Biotechnol.*, **2004**, *22* (2), 198-203.

[113] Kodippili, G. C.; Spector, J.; Sullivan, C.; Kuypers, F. A.; Labotka, R.; Gallagher, P. G.; Ritchie, K.; Low, P. S. Imaging of the diffusion of single band 3 molecules on normal and mutant erythrocytes. *Blood*, **2009**, *113* (24), 6237-45.

[114] Rust, M. J.; Bates, M.; Zhuang, X. Sub-diffraction-limit imaging by stochastic optical reconstruction microscopy (STORM). *Nat. Methods*, **2006**, *3* (10), 793-5.

[115] Betzig, E.; Patterson, G. H.; Sougrat, R.; Lindwasser, O. W.; Olenych, S.; Bonifacino, J. S.; Davidson, M. W.; Lippincott-Schwartz, J.; Hess, H. F. Imaging intracellular fluorescent proteins at nanometer resolution. *Science*, **2006**, *313* (5793), 1642-5.

[116] Manley, S.; Gillette, J. M.; Patterson, G. H.; Shroff, H.; Hess, H. F.; Betzig, E.; Lippincott-Schwartz, J. High-density mapping of single-molecule trajectories with photoactivated localization microscopy. *Nat. Methods*, **2008**, *5* (2), 155-7.

[117] Eggeling, C.; Ringemann, C.; Medda, R.; Schwarzmann, G.; Sandhoff, K.; Polyakova, S.; Belov, V. N.; Hein, B.; von Middendorff, C.; Schonle, A.; Hell, S. W. Direct observation of the nanoscale dynamics of membrane lipids in a living cell. *Nature*, **2009**, *457* (7233), 1159-62.

[118] Sahl, S. J.; Leutenegger, M.; Hilbert, M.; Hell, S. W.; Eggeling, C., Fast molecular tracking maps nanoscale dynamics of plasma membrane lipids. *Proc. Natl. Acad. Sci. USA*, **2010**, *107* (15), 6829-34.

[119] Lajoie, P.; Partridge, E. A.; Guay, G.; Goetz, J. G.; Pawling, J.; Lagana, A.; Joshi, B.; Dennis, J. W.; Nabi, I. R. Plasma membrane domain organization regulates EGFR signaling in tumor cells. *J. Cell Biol.*, **2007**, *179* (2), 341-56.

[120] Wymann, M. P.; Schneiter, R. Lipid signalling in disease. *Nat. Rev. Mol. Cell Biol.*, **2008**, *9* (2), 162-76.

[121] Baumgart, T.; Hammond, A. T.; Sengupta, P.; Hess, S. T.; Holowka, D. A.; Baird, B. A.; Webb, W. W. Large-scale fluid/fluid phase separation of proteins and lipids in giant plasma membrane vesicles. *Proc. Natl. Acad. Sci. USA*, **2007**, *104* (9), 3165-70.

[122] Lingwood, D.; Ries, J.; Schwille, P.; Simons, K. Plasma membranes are poised for activation of raft phase coalescence at physiological temperature. *Proc. Natl. Acad. Sci. USA*, **2008**, *105* (29), 10005-10.

[123] Armstrong, J. K.; Wenby, R. B.; Meiselman, H. J.; Fisher, T. C. The hydrodynamic radii of macromolecules and their effect on red blood cell aggregation. *Biophys. J.*, **2004**, *87* (6), 4259-70.

Received: September 29, 2010 Revised: January 25, 2011 Accepted: January 27, 2011

10.3 Transient confinement in plasma membranes explored by high-speed tracking using quantum dots

PLASMA MEMBRANE COMPARTMENTALIZATION EXPLOITED BY HIGH-SPEED QUANTUM DOT TRACKING

Mathias P. Clausen and B. Christoffer Lagerholm*

MEMPHYS – Center for Biomembrane Physics and DaMBIC – Danish Molecular Biomedical Imaging Center, University of Southern Denmark

*Corresponding author.

Address: Campusvej 55, DK-5230 Odense M, Denmark

Phone: +45 6550 3505

E-mail: lagerholm@memphys.sdu.dk

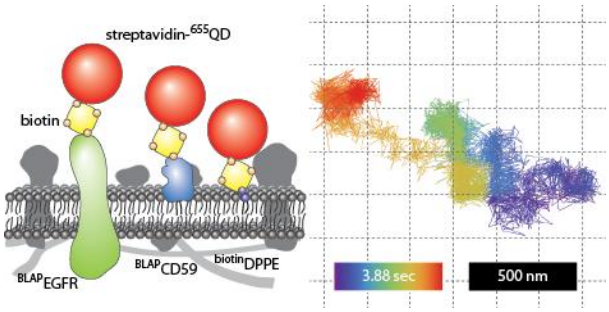

Keywords: Fluorescence, Hop-diffusion, Micro-domains, Plasma membrane, Quantum dot, Single particle tracking

In review NanoLetters

ABSTRACT

In this study, we track quantum dot targeted plasma membrane species in live cells for several seconds at sampling frequencies of 1.75 kHz. The tracking is done with high spatial precision using a conventional wide-field microscope. We obtain long trajectories that are analyzed individually and show that a majority of the investigated molecules move between nanoscopic compartments with a size of 100-150 nm, where they are transiently confined for 50-100 ms.

TEXT

Single particle tracking (SPT) with gold nano-particles[1], quantum dots (QDs)[2], or fluorescent dyes or fluorescent proteins[3] allows for reconstruction of molecular trajectories of single molecules with nanometer precision. Accordingly, SPT offers the possibility to gain detailed information on the dynamics of molecules and from the course of the motion of molecules, important aspects of their environment can further be inferred. [4] SPT has therefore become a valuable experimental tool within the life sciences and has found a rapidly expanded use over the last few decades.[3, 5, 6] The method has in particular been instrumental in revealing the extent of the spatio-temporal heterogeneity of the lateral dynamics and organization in plasma membranes.[7-11]

The plasma membrane is nowadays known to be highly complex and heterogeneous in both composition and organization.[12] This is a necessity, in order for the plasma membrane to control and regulate material exchange and communication between the cell and its surroundings. The plasma membrane has been proposed to spatially segregate its constituents into functional platforms in a molecule specific way upon e.g. cellular signaling events.[13] These platforms are known as lipid rafts, and the concept has been backed up by SPT findings.[14] A further indication of the lateral heterogeneity in the plasma membrane, SPT experiments typically results in the detection of a large range of types of motions, which include examples of free diffusion, confined diffusion, directed diffusion, and various combinations thereof.[8, 14-16]

Concerns in SPT experiments include limited temporal resolution, different analysis approaches, the need for high illumination intensities, and the influence of the probe used. Different results are reached depending on the sampling frequency, and it is primarily the probe that dictates the accessible time regime of the observation.[17] A typical experiment involves slow sampling, which here is considered as video-rate or slower (<30 Hz) is possible with gold particles, QDs, and dyes, and those studies have shown that certain molecules are transiently confined for several seconds in nano-domains with a size of 100-300 nm in diameter.[14, 18-21] Some of these domains have been related to lipid rafts. Not all phenomena and processes are, however, accessible at slow sampling frequencies, so a faster temporal sampling is needed. At extremely fast sampling frequencies of 50 kHz, which is possible only with minimum Ø 40 nm gold particles, Kusumi and co-workers have proposed that the motion of both plasma membrane lipids and proteins is dominated by transient confinement in nanoscopic compartments with a size range of 30-230 nm for a duration of 1-20 ms dependent on the cell type.[8, 22-24] Within these compartments, the molecules have been proposed to diffuse freely and very fast with a diffusion constant of 5-8 $\mu m^2/s$, while on a longer time scale the molecules move between adjacent compartments resulting in much slower long-term diffusion of 0.04-0.3 $\mu m^2/s$.[24]

Consequently, this behavior, which has been termed hop diffusion, can only be observed at sampling frequencies that are significantly faster than the corresponding duration of time that the molecules spend within these nanoscopic compartments.[25] Hop diffusion has also been suggested as an explanation for some spot variation FCS data, but in general it has been questioned due to the need of high illumination intensity, and the use of large probes, which might perturb the natural motion of the molecules.[14, 25, 27, 28] In dye tracking studies trying to access a fast temporal resolution[26, 27], a sampling frequency of approximately 1 kHz has been reached, but no hop diffusion was observed.[17, 26, 28, 29] Those observations are, however, strongly limited by the photo-physical properties of the organic dyes used, which besides having a limited brightness, is limited in the length of the trajectories to just few displacements before irreversible photo-bleaching. A direct consequence of this is that single molecule trajectories cannot be analyzed individually, but have to be pooled to give an ensemble average of all molecules in time and space.[3, 17] Consequently, while the technique is a single molecule method in terms of detection, it becomes an ensemble average method in terms of analysis. It therefore still remains unsettled if hop diffusion is an illusion, or a consequence of biological barriers in the cell membranes.More recently fluorescent semiconductor nanocrystals known as QDs have also been used in SPT.[7, 14, 30] QDs are an attractive compromise between the fluorescent dyes and the gold particles.[2, 31] QDs have very high signal intensity and signal stability as compared to conventional fluorescent dyes and fluorescent proteins, and are about half the diameter of gold particles. However, thus far QDs have not been exploited for fast tracking.

In this study we have taken advantage of the large brightness and photo-stability of QDs to show that it is possible to image QDs for extended time periods (seconds) and fast sampling frequencies (1.75 kHz). This is done with a simple experimental setup using a standard wide-field microscope equipped with a 100 W mercury arc lamp, for low illumination intensity, and an EMCCD camera with fast and flexible readout over a large field of view (~66 μm^2). We have tracked streptavidin (SAv) conjugated QDs with a peak emission at 655 nm (SAv-^{655}QD). These QDs have been found to be the brightest of the available QDs from Life Technologies[32], and to have a hydrodynamic radius of 10±1 nm or ~1.7X the radius of a mouse IgG1.[17] The spatial precision by which we can localize the centroids of single SAv-^{655}QDs non-specifically immobilized on glass coverslides, at sampling frequencies of f=1.75 kHz and image integration times of t_{int}=0.52 ms was found to be δ_x=30 nm and δ_y=26 nm (Supplementary Figure 1). This corresponds to a spatial precision of λ/(15 NA) or ~1/5 of the projected pixel size. This precision is similar to what is found in other fluorescence-based tracking experiments, but the fact that we can track QDs over extended time periods, and at high frequencies and low illumination intensity is new. Further, we found that in these studies, the sampling frequency was limited by the readout rate of the camera and not the probe signal, and therefore even faster sampling is expected with the development of faster but equally sensitive cameras.

To demonstrate the use of high-speed QD tracking, we investigated the lateral dynamics of three categories of membrane species, which are all present in the mammalian plasma membrane; i) a glycerophospholipid (1,2-dipalmitoyl-*sn*-glycero-3-phosphoethanolamine (DPPE)-cap-biotin), ii) a glucosylphosphatidylinositol (GPI)-anchored protein (CD59), and iii) a transmembrane protein (the Epidermal Growth Factor Receptor, EGFR). The tracking studies were performed at room temperature (RT) in the lamellipods of the apical plasma membrane in a

mouse embryo fibroblast cell line (IA32) from an Ink4a/Arf null mouse [33]. These cells are characterized by having unusually large and flat lamellipods. We introduced the molecules of interest exogenously by either bulk loading the lipid to the cells using 1 μg/ml biotin-CAP-DPPE in 0.1 % fatty-acid free BSA (Sigma, A-8806) for 5 minutes at RT[34], or by transfecting the cells with plasmids encoding recombinant biotin ligase acceptor peptide (BLAP) fusion proteins of CD59 or EGFR[35]. The cells were co-transfected with a plasmid encoding bacterial biotin ligase with an ER anchor[36], and grown overnight in the presence of 10 μM biotin such that the fusion proteins were biotinylated during the secretory pathway (see details in SI2). In this approach, all three molecules of interest are hence designed to contain a single biotin residue to which we could subsequently label specifically with the same batch of SAv-^{655}QD. The labeling was done by first blocking for non-specific binding with 1% BSA for 1-2 minutes, and then labeling cells with a 1 nM filtered solution (0.22 μm syringe filter) of SAv-^{655}QD in PBS with 1% BSA for 2 minutes at RT after which further binding was blocked by addition of 100 μl of 1 mM biotin, and a further incubation at RT for 2 minutes. Labeled cells were finally washed and imaged in PBS with 1% BSA. Cells were imaged on an Olympus IX-81 inverted microscope with a 150X 1.45 NA UApo TIRFM oil immersion objective (Olympus) equipped with a 100W Hg arc lamp for fluorescence excitation. The excitation power at the objective back aperture plane and with a filter cube consisting of a HQ470/40 nm fluorescence excitation filter, a Q495LP dichroic mirror (Chroma Technology) and a 510LP emission filter was measured to be 35 mW/cm^2. Data was acquired on an EMCCD camera (Andor DU860D-CS0-BW). We acquired time-lapse image sequences consisted of 9000 image frames of a field of view of 20x128 pixel^2 (or 3.2x20.5 μm^2), where the camera chip was aligned to match the camera readout direction, and operated in frame transfer mode. The resulting image series were analyzed by a combination of the use of an ImageJ plugin[37] and custom written routines in Mathematica designed to minimize the effect of QD intermittency as has been described before.[38]

In the data analysis, we time-averaged the trajectories by calculating the mean squared displacements (MSD) individually for each single trajectory, *m*. Only trajectories with a total number of image frames *N* above 200 were analyzed. The trajectories were analyzed for time intervals, $nt_{lag} \leq 50$ ms, with *n* being the image frame number, and t_{lag} being the time between successive image frames. The MSD was calculated by[39]:

$$\left(\quad \right) \; \frac{}{} \; \Sigma \; \left[\left(\quad \left(\quad \right) - \quad \left(\quad \right) \right) \quad \left(\quad \left(\quad \right) - \quad \left(\quad \right) \right) \right] \qquad \text{Eq. 1}$$

Subsequently, we used non-linear curve fitting to fit the MSD curves to three simple nested diffusion models given further below. In this analysis approach, we could then use conventional F-statistics in order to statistically determine the simplest diffusion model (i.e. the model with least number of free parameters) that could describe the data. The F-statistics was calculated by:

$$\left(\frac{}{} \right) \quad \left(\frac{}{} \right) \qquad \text{Eq. 2}$$

where RSS_1 and RSS_2 is the residual sum of squares of the models compared, and p_1 and p_2 are the number of free fitting parameters of the models, and where $p_2 > p_1$. The calculated F-statistics for the individual trajectories were

next compared to the critical F-distribution with (p_2-p_1, n-p_2) degrees of freedom and a significance level of α = 0.05.

The diffusion models were:

1) Brownian diffusion with diffusion constant D_{free} (free diffusion):

( ) Eq. 3

2) Diffusion within a limited area L^2 with diffusion constant D_{conf} (confined diffusion)[39]:

( ) –(- [———]) Eq. 4

With L^2 given by:

Eq. 5

Where $_{barrier}$ is the time it takes for the molecule to experience the effect of the barrier of the confinement.

3) Diffusion having both a long-term free diffusion component and a short-term confined component (compartmentalized diffusion):

$_m$ ( ) –(- [———]) Eq. 6

The time that a molecule is confined to a nanoscopic compartment of size L^2 is given by:

—— Eq. 7

There are also many alternative diffusion models in the literature for fitting MSD curves. These include anomalous diffusion, MSD(nt_{lag}) = 4 D n t_{lag}^{α}, where 0<α≤ (α=1 corresponds to free diffusion) [3, 40], but this type of diffusion is difficult to interpret. In addition, a model for hop diffusion, which contains an infinite sum of components, has been derived by Powles *et al.*[41]. In this work, we have, however, opted for the much simpler models given above. We think this approach with using nested diffusion models has the great advantage of that the classification of the motion type of each trajectory can be determined by a standard statistical F-test. Our diffusion analysis was carried out on 272, 444, and 124 molecular trajectories of EGFR, CD59, and DPPE, respectively, and the median number of displacements per trajectory was 646, 661, and 475, respectively (Table 1). The results of the analysis showed that there were numerous examples of each type of motion for all types of molecules that we investigated, but the motion of the majority of molecules was statistically best described by compartmentalized diffusion (Table 1). Independent of the type of molecule, the motion was statistically best described by free diffusion (Eq. 3) for 5-10 % of all molecules, by entirely confined diffusion (Eq. 4) in nanoscopic compartments of L=100-150 nm for about 30 % of all molecules, and by compartmentalized diffusion (Eq. 6) between nanoscopic compartments of L=100-150 nm for

a duration of τ_{comp}=50-100 ms for about 60-70 % of all molecules. Representative examples of trajectories under each classification and respective diffusion model fits are shown in Figure 1. The full distributions of the fitted diffusion values for all single trajectories are shown as box-and-whisker plots in Figure 2.[1]

Molecule	**EGFR**			**CD59**			**DPPE**		
# of traj.		272			444			124	
# of disp. per traj.		1112±1387 (646)			1019±1014 (661)			656±537 (475)	
Model	Free	Confined	Compartmentalized	Free	Confined	Compartmentalized	Free	Confined	Compartmentalized
Fraction of total	8 %	28 %	64 %	5 %	27 %	68 %	10 %	31 %	59 %
D_{free} **(μm²/s)**	0.083±0.062 (0.091)	-	0.041±0.032 (0.034)	0.17±0.14 (0.14)	-	0.061±0.049 (0.050)	0.27±0.18 (0.23)	-	0.081±0.084 (0.047)
D_{conf} **(μm²/s)**	-	0.20±0.24 (0.14)	0.29±0.24 (0.21)	-	0.31±0.29 (0.21)	0.45±0.40 (0.33)	-	0.24±0.17 (0.20)	0.57±0.52 (0.38)
$\tau_{barrier}$ **(ms)**	-	8.8±7.0 (6.9)	6.6±13.4 (2.25)	-	8.4±7.5 (4.8)	5.4±9.0 (2.3)	-	9.4±6.2 (6.7)	8.0±14 (2.5)
L **(nm)**	-	109±37 (99)	98±55 (84)	-	129±55 (109)	119±60 (102)	-	143±49 (129)	151±92 (131)
τ_{comp} **(ms)**	-	∞	133±426 (53)	-	∞	103±121 (55.3)	-	∞	137±139 (88.4)

Table 1: Summary of diffusion values obtained from analyzing trajectories individually. The diffusion values are given as mean±std.dev. (median).

[1] In box-and-whisker plots, the box ranges from the first to the third quartiles, and the median is the center line in the box. The whiskers extend to the farthest point that is within ±1.5x the interquartile range, while remaining points are plotted individually as outliers (triangles).

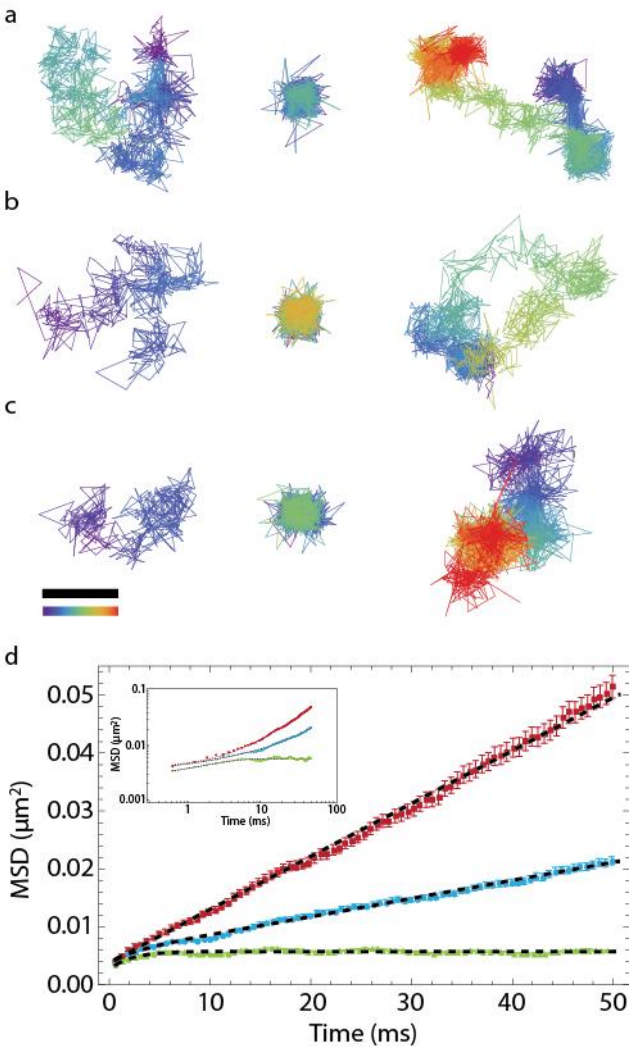

Figure 1. Trajectories and mean squared displacements (MSD) plot. a-c) Representative examples of trajectories representing free diffusion (left), confined diffusion (center), and compartmentalized diffusion (right) for EGFR (a), CD59 (b), and DPPE (c). The color scale represents time from 0 s (purple) to 2 s (red). Scale bar 400 nm. d) MSD-vs.-time plot for the three example trajectories for EGFR in (a) fitted to free (red), confined (green), and compartmentalized (blue) diffusion. The insert shows the data and fits on a logarithmic scale to highlight the early time points.

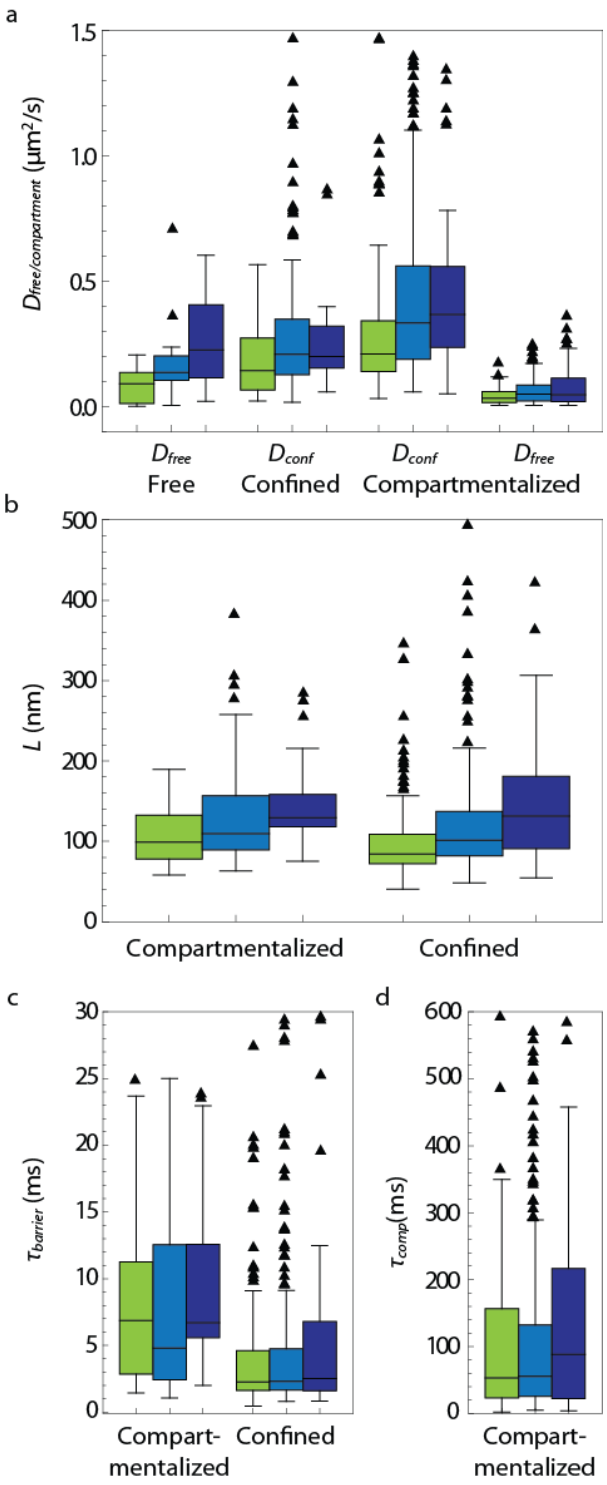

Figure 2. Box-and-whisker plots of the full distributions of diffusion values. a) Free (D_{free}) and confined (D_{conf}) diffusion constants for the three different diffusion models (free, confined, and compartmentalized). b) Nanoscopic compartment size (L) for confined and compartmentalized diffusion. c) The time it takes for the molecules showing confined and compartmentalized diffusion to be affected by the barrier of the nanoscopic compartment ($_{barrier}$). d) The time the molecules spend within a nanoscopic compartment ($_{comp}$). EGFR (green), CD59 (blue), DPPE (purple).

The molecules that are characterized by compartmentalized diffusion move within compartments with a diffusion constant of D_{conf} = 0.3-0.6 μm^2/s on a short time scale ($t <$ $_{comp}$), while on a longer time scale, they diffuse freely with a slower diffusion constant of D_{free} = 0.04-0.08 μm^2/s. Visually and conceptually, these results show a strong resemblance to the hop diffusion that has been described by Kusumi and co-workers using the more invasive 40 nm gold particle tracking.[42] The data suggests that all types of molecules in the plasma membrane; lipids, GPI-anchored proteins, and transmembrane proteins experience similar restrictions to the long-term diffusion, indicating that the barriers restricting free diffusion is of a generic nature. The size of the nanoscopic compartments and the duration of the transient confinement within the nanoscopic compartments, are consistent with those reported in other cell lines by Kusumi and co-workers.[24] In addition, the duration of the detected confinements is only accessible at fast temporal sampling.

This kind of compartmentalized diffusion is in contrast to what has been reported in studies where single fluorescent dye labeled lipids and proteins were tracked at a comparable sampling frequency.[26, 27] It is also in contrast to studies of lipid and protein dynamics using STED-FCS, which access a similar millisecond temporal scale.[43, 44] In those studies, plasma membrane molecules are reported to diffuse freely, or to be transiently trapped in cholesterol-assisted membrane domains. The dye tracking studies are, however, limited by the photo-(in)stability of organic fluorophores, which in the case of Wieser *et al.* limits the median trajectory lengths to ~6 displacements, and as a consequence, trajectories were analyzed as an ensemble and not individually. In the case of Sahl *et al.*, a non-camera based three-point detector setup was used, and the observation area was limited to a diffraction limited spot. Those respective limitations most probably preclude the observation of a long-term compartmentalization of molecules. In the case of the STED-FCS measurements, it is possible that no compartmentalization was observed since the studies were carried out in PtK2 cells, which have been reported to have small membrane compartments of 43 nm.[24] This compartment size is close to the smallest focal spot size of the STED-FCS measurements, and resolving compartments in this regime is possibly without reach of the technique. Our tracking study benefits from fast and long trajectories over a large field of view. In this way, dynamics on a fast temporal scale is accessed, but long-term confinement over a larger area is also accessible

On the other hand, even though QDs have the advantage of being less than half the diameter of the gold particles (eight times smaller volume(!)), yet they share some of the same probe related issues. The 20 nm diameter might still hinder their free access to all parts of the plasma membrane[45], and in particular SAv-QDs are multivalent[46] following a Poisson distribution in the bio-conjugation. They therefore have an inherent risk of cross-linking target molecules. In our case we minimize cross-binding by adding excess free biotin shortly after QD labeling, but the risk of cross-linking is not entirely eliminated. Cross-binding of molecules might enhance or induce the observation of compartmentalized diffusion as clusters of molecules would be expected to experience a different membrane diffusion dynamics than single molecules would, e.g. complexes of a few molecules would likely have a harder time escaping a confinement, than a single molecule would. This could be the reason why compartmentalized diffusion is only observed when using larger probes as opposed to the smaller dyes. The exact influence of the probe on the observed compartmentalized diffusion will have to be investigated further to settle that the observed diffusion is not

a probe induced artifact. The biological reason for the compartmentalization will also have to be investigated further. A likely explanation for the observed compartmentalization is that the actin defines membrane compartments on the inside of the plasma membrane, and that the strong inter leaflet coupling convey the restrictions to the outer leaflet of the plasma membrane.

One important difference between our data and the hop-diffusion reported by Kusumi and co-workers is the absence of the very fast diffusion constant 5-8 $\mu m^2/s$ within the nanoscopic compartments. In agreement with the dye tracking studies, our short term diffusion is about a factor of 10 slower than this reported diffusion constants. Although the reason for this discrepancy is still to be determined there are several possibilities. For example, our sampling frequency (1.75 kHz) is more than a factor of 20 slower than that of Kusumi and co-workers, which could possibly preclude the detection of the fast component. Furthermore, our fast component comes from fitting the entire time window of $0.5<nt_{lag}<$ $_{barrier}$ ($n\approx$ -15) whilst the fast component identified by Kusumi and co-workers results from fitting a time window of $50<nt_{lag}<100$ µs (n=2-4) that is inaccessible at our sampling frequency. In contrast, as has been argued previously, in a case of very fast membrane diffusion, the frictional drag exerted by the gold particles and experienced by the membrane molecule has to be taken into account.[17] Normally (and in our case), this drag can be neglected because the diffusion of the probe in solution is much faster than the corresponding diffusion of the molecule in the membrane. However, the diffusion constant of a 50 nm antibody stabilized and functionalized 40 nm gold particle in water as calculated from the Stokes-Einstein equation is 8.7 $\mu m^2/s$ (and even lower if the viscosity close to the cell membrane is considered to be higher than that of pure water, μ_{water} = 1.002 cP at 20 °C). As this value is not much larger than the 5-8 $\mu m^2/s$ diffusion constant of the membrane molecules, it is expected that the probe will impact the collective diffusion of the probe-membrane-molecule complex. Another point of concern related to the apparent fast diffusion in cells is, that whereas lipid diffusion in a pure lipid bilayer is of the order of 5-10 $\mu m^2/s$[47], model studies of lipid diffusion in membranes containing proteins[48, 49] and simulations thereof[50] has shown that the diffusion in this case is considerably slower, the reasons being of hydrodynamic nature caused by crowding and lipid shell effects. Membrane topography studies of cells have also been suggested to interfere with observation of fast 2D diffusion[29]. We therefore think, that this fast diffusion constant is not a true reflection of the natural behavior of membrane molecules.

In conclusion, we here show that it is possible to access a sub-millisecond time regime with a standard wide-field fluorescence microscopy setup. This fast time regime is relevant for the study of many biological phenomena including the study of plasma membrane lateral dynamics and organization, but it has previously been inaccessible in fluorescent-based studies due to limited brightness and stability in the luminescence of standard organic fluorescent probes and proteins. The superior brightness of QDs allow for temporally fast and long trajectories that can be individually analyzed. The work shows details of compartmentalized diffusion of all types of membrane molecules studied, and mimicks in many ways the hop diffusion previously observed by Kusumi and co-workers using more invasive gold nano-particles. Further studies will have to be conducted in order to determine the nature of these confining barriers, and the influence of the probe in the studies. In particular further improvements in controlling the QD probe valency are desperately needed.

SUPPORTING INFORMATION

Supporting information available: SI1) Spatial precision of imaging, SI2) Experimental details. This material is available free of charge via the Internet at http://pubs.acs.org.

AUTHOR CONTRIBUTIONS

MPC and BCL conceived the experiments. MPC performed the experiments. BCL wrote the analysis program. MPC and BCL analyzed the experiments. MPC and BCL wrote the paper.

ACKNOWLEDGMENT

We thank A. Y. Ting for the pcDNA3-EGFR-BLAP construct. This work was supported by the Villum Kann Rasmussen Foundation (to BioNET), Leo Pharma Forskningsfond, the Lundbeck Foundation, the Novo Nordisk Foundation, and the Danish Natural Research Foundation (to MEMPHYS – Center for Biomembrane Physics) and DaMBIC (Danish Molecular Biomedical Imaging Center).

ABBREVIATIONS

BSA, Bovine Serum Albumin; EGFR, Epidermal Growth Factor Receptor; GPI-AP, glucosylphosphatidylinositol-anchored protein; PBS, Phosphate buffered saline; SPT, Single particle tracking; sAv, Streptavidin.

REFERENCES

1. Saxton, M. J.; Jacobson, K. *Annu Rev Biophys Biomol Struct* **1997,** 26, 373-99.
2. Pinaud, F.; Clarke, S.; Sittner, A.; Dahan, M. *Nat Methods* **2010,** 7, (4), 275-85.
3. Wieser, S.; Schutz, G. J. *Methods* **2008,** 46, (2), 131-40.
4. Brameshuber, M.; Schutz, G. J. *Nat Methods* **2008,** 5, (2), 133-4.
5. Alcor, D.; Gouzer, G.; Triller, A. *Eur J Neurosci* **2009,** 30, (6), 987-97.
6. Owen, D. M.; Williamson, D.; Rentero, C.; Gaus, K. *Traffic* **2009,** 10, (8), 962-71.
7. Andrews, N. L.; Lidke, K. A.; Pfeiffer, J. R.; Burns, A. R.; Wilson, B. S.; Oliver, J. M.; Lidke, D. S. *Nat Cell Biol* **2008,** 10, (8), 955-63.
8. Fujiwara, T.; Ritchie, K.; Murakoshi, H.; Jacobson, K.; Kusumi, A. *J Cell Biol* **2002,** 157, (6), 1071-81.
9. Itano, M. S.; Neumann, A. K.; Liu, P.; Zhang, F.; Gratton, E.; Parak, W. J.; Thompson, N. L.; Jacobson, K. *Biophys J* **2011,** 100, (11), 2662-70.
10. Jaqaman, K.; Kuwata, H.; Touret, N.; Collins, R.; Trimble, W. S.; Danuser, G.; Grinstein, S. *Cell* **2011,** 146, (4), 593-606.
11. Wieser, S.; Weghuber, J.; Sams, M.; Stockinger, H.; Schutz, G. J. *Soft Matter* **2009,** 5, (17), 3287-3294.
12. Jacobson, K.; Mouritsen, O. G.; Anderson, R. G. *Nat Cell Biol* **2007,** 9, (1), 7-14.
13. Lingwood, D.; Simons, K. *Science* **2010,** 327, (5961), 46-50.
14. Pinaud, F.; Michalet, X.; Iyer, G.; Margeat, E.; Moore, H. P.; Weiss, S. *Traffic* **2009,** 10, (6), 691-712.
15. Chen, Y.; Thelin, W. R.; Yang, B.; Milgram, S. L.; Jacobson, K. *J Cell Biol* **2006,** 175, (1), 169-78.

16. Kusumi, A.; Sako, Y.; Yamamoto, M. *Biophys J* **1993,** 65, (5), 2021-40.

17. Clausen, M. P.; Lagerholm, B. C. *Curr Protein Pept Sci* **2011**.

18. Chen, Y.; Yang, B.; Jacobson, K. *Lipids* **2004,** 39, (11), 1115-9.

19. Simson, R.; Sheets, E. D.; Jacobson, K. *Biophys J* **1995,** 69, (3), 989-93.

20. Sheets, E. D.; Lee, G. M.; Simson, R.; Jacobson, K. *Biochemistry* **1997,** 36, (41), 12449-58.

21. Dietrich, C.; Yang, B.; Fujiwara, T.; Kusumi, A.; Jacobson, K. *Biophys J* **2002,** 82, (1 Pt 1), 274-84.

22. Suzuki, K.; Ritchie, K.; Kajikawa, E.; Fujiwara, T.; Kusumi, A. *Biophys J* **2005,** 88, (5), 3659-80.

23. Umemura, Y. M.; Vrljic, M.; Nishimura, S. Y.; Fujiwara, T. K.; Suzuki, K. G.; Kusumi, A. *Biophys J* **2008,** 95, (1), 435-50.

24. Murase, K.; Fujiwara, T.; Umemura, Y.; Suzuki, K.; Iino, R.; Yamashita, H.; Saito, M.; Murakoshi, H.; Ritchie, K.; Kusumi, A. *Biophys J* **2004,** 86, (6), 4075-93.

25. Kusumi, A.; Nakada, C.; Ritchie, K.; Murase, K.; Suzuki, K.; Murakoshi, H.; Kasai, R. S.; Kondo, J.; Fujiwara, T. *Annu Rev Biophys Biomol Struct* **2005,** 34, 351-78.

26. Wieser, S.; Moertelmaier, M.; Fuertbauer, E.; Stockinger, H.; Schutz, G. J. *Biophys J* **2007,** 92, (10), 3719-28.

27. Sahl, S. J.; Leutenegger, M.; Hilbert, M.; Hell, S. W.; Eggeling, C. *Proc Natl Acad Sci U S A* **2010,** 107, (15), 6829-34.

28. Mascalchi, P.; Haanappel, E.; Carayon, K.; Mazeres, S.; Salome, L. *Soft Matter* **2012,** 8, (16), 4462-4470.

29. Adler, J.; Shevchuk, A. I.; Novak, P.; Korchev, Y. E.; Parmryd, I. *Nat Methods* **2010,** 7, (3), 170-1.

30. Dahan, M.; Levi, S.; Luccardini, C.; Rostaing, P.; Riveau, B.; Triller, A. *Science* **2003,** 302, (5644), 442-5.

31. Rosenthal, S. J.; Chang, J. C.; Kovtun, O.; McBride, J. R.; Tomlinson, I. D. *Chem Biol* **2011,** 18, (1), 10-24.

32. Arnspang Christensen, E.; Brewer, J. R.; Lagerholm, B. C. **2012**.

33. Wu, C.; Asokan, S. B.; Berginski, M. E.; Haynes, E. M.; Sharpless, N. E.; Griffith, J. D.; Gomez, S. M.; Bear, J. E. *Cell* **2012,** 148, (5), 973-87.

34. Kenworthy, A. K. *Methods Mol Biol* **2007,** 398, 179-92.

35. Howarth, M.; Ting, A. Y. *Nat Protoc* **2008,** 3, (3), 534-45.

36. Howarth, M.; Takao, K.; Hayashi, Y.; Ting, A. Y. *Proc Natl Acad Sci U S A* **2005,** 102, (21), 7583-8.

37. Sbalzarini, I. F.; Koumoutsakos, P. *J Struct Biol* **2005,** 151, (2), 182-95.

38. Lagerholm, B. C.; Averett, L.; Weinreb, G. E.; Jacobson, K.; Thompson, N. L. *Biophys J* **2006,** 91, (8), 3050-60.

39. Bannai, H.; Levi, S.; Schweizer, C.; Dahan, M.; Triller, A. *Nat Protoc* **2006,** 1, (6), 2628-34.

40. Saxton, M. J. *Biophys J* **1994,** 66, (2 Pt 1), 394-401.

41. Powles, J. G.; Mallett, M. J. D.; Rickayzen, G.; Evans, W. A. B. *P Roy Soc Lond a Mat* **1992,** 436, (1897), 391-403.

42. Kusumi, A.; Shirai, Y. M.; Koyama-Honda, I.; Suzuki, K. G.; Fujiwara, T. K. *FEBS Lett* **2010,** 584, (9), 1814-23.

43. Eggeling, C.; Ringemann, C.; Medda, R.; Schwarzmann, G.; Sandhoff, K.; Polyakova, S.; Belov, V. N.; Hein, B.; von Middendorff, C.; Schonle, A.; Hell, S. W. *Nature* **2009,** 457, (7233), 1159-62.

44. Mueller, V.; Ringemann, C.; Honigmann, A.; Schwarzmann, G.; Medda, R.; Leutenegger, M.; Polyakova, S.; Belov, V. N.; Hell, S. W.; Eggeling, C. *Biophys J* **2011,** 101, (7), 1651-60.

45. Howarth, M.; Liu, W.; Puthenveetil, S.; Zheng, Y.; Marshall, L. F.; Schmidt, M. M.; Wittrup, K. D.; Bawendi, M. G.; Ting, A. Y. *Nat Methods* **2008,** 5, (5), 397-9.

46. Mittal, R.; Bruchez, M. P. *Bioconjug Chem* **2011,** 22, (3), 362-8.

47. Machan, R.; Hof, M. *Biochim Biophys Acta* **2010,** 1798, (7), 1377-91.

48. Peters, R.; Cherry, R. J. *Proc Natl Acad Sci U S A* **1982,** 79, (14), 4317-21.

49. Ramadurai, S.; Holt, A.; Krasnikov, V.; van den Bogaart, G.; Killian, J. A.; Poolman, B. *J Am Chem Soc* **2009,** 131, (35), 12650-6.

50. Niemela, P. S.; Miettinen, M. S.; Monticelli, L.; Hammaren, H.; Bjelkmar, P.; Murtola, T.; Lindahl, E.; Vattulainen, I. *Journal of the American Chemical Society* **2010,** 132, (22), 7574-5.

TRANSIENT CONFINEMENT IN PLASMA MEMBRANES EXPLORED BY HIGH-SPEED TRACKING USING QUANTUM DOTS

SUPPLEMENTARY INFORMATION

Mathias P. Clausen and B. Christoffer Lagerholm

SI 1: SPATIAL PRECISION OF IMAGING

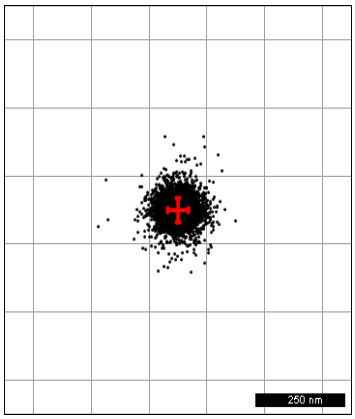

Supplementary Figure 1: Spatial precision. Superimposed centroid positions obtained from 18 trajectories for a total of N=6083 positions showed together with the geometric mean of the centroid positions (cross) of sAv-^{655}QD that were non-specifically adsorbed to a glass surface and imaged at 1750 Hz sampling and with acquisition time of 0.52 msec. The standard deviation, $\delta_{x,y}$, of the positions were δ_x=30 nm and δ_y=26 nm. This is the minimum precision by which we can determine the position of single QDs in the measurements.

This provides an estimate of the lower limit of the minimum uncertainty of high speed SPT in the case of completely stationary QDs. However, the uncertainty is always greater for non-stationary QDs as a result of mobility during the image integration in which case the uncertainty will also depend on the particle diffusion rate, D, the image acquisition time, t_{aq}, and the mode of diffusion, i.e. for normal diffusion the accuracy would be $\delta r = (\delta x^2 + \delta x^2 + 4\ D\ t_{aq})^{1/2}$. Note however that this uncertainty is less for non-stationary particles that undergo confined diffusion as is the case here.

SI 2: EXPERIMENTAL DETAILS

Cell culture

Mouse embryonic fibroblasts from an Ink4a/Arf null mouse (IA32) were used for microscopy studies[32]. Cells were grown in humidified atmosphere at 37 °C in 5 % CO_2. Cells were grown until 80-90 % of confluence and split every third day in 1:5-1:10 ratios using the endo-peptidase Trypsin. Cells were grown in Dulbecco's modified eagle's medium (DMEM) with high glucose, and with standard concentrations of glutamax and penicillin-streptomycin, and 10 % fetal bovine serum (FBS). Cells were seeded in appropriate density and number (30,000) on coverslips in 6-wells plates, and left for six-eight hours to attach to the glass. Cells were then transfected and left over night in media containing 10 μM biotin, and labeled and imaged the following two days.

Plasmids

The plasmids used for transfection were pcDNA3.1-EGFR-BLAP, encoding the EGFR with a BLAP-tag in an extracellular domain, pDISPLAY-BirA-KDEL encoding bacterial biotin ligase with an ER anchor[46]. A pcDNA3.1-CD59-BLAP was made by cloning the CD59 part of the plasmid pAEMTX-ACPwt-GPI (Covalys, now New England Biolabs) using a BLAP primer.

QD Labeling of Molecules of Interest

In the case of the studies of biotin-cap-DPPE (Avanti Polar Lipids), we first bulk loaded cells with the lipid by use of fatty-acid free BSA (Sigma, A-8806)[46]. For this labeling, we prepared a 100 μg/ml lipid stock solution in absolute ethanol (stored at 4 ^{o}C). Cells were then loaded by diluting the lipid stock to 1 μg/ml in 0.1 % fatty-acid free BSA in Dulbecco's phosphate buffered saline with 0.1 g/L $CaCl_2$ and 0.1 g/L $MgCl_2$ (D-PBS) and by incubation for 5 minutes at RT. In the case of BLAP-CD59 and BLAP-EGFR, we first co-transfected cells by use of JetPEI (Polyplus Transfection) with the respective plasmids and pDISPLAY-BirA-KDEL encoding bacterial biotin ligase with an ER anchor[47] and grew overnight in the presence of 10 μM biotin. All QD labeling was subsequently done by washing the cells 3X in D-PBS and by blocking for non-specific binding in D-PBS with 1% BSA for 1-2 minutes. Cells were then labeled with a 1 nM filtered solution (0.22 μm syringe filter) of sAv-^{655}QD in D-PBS with 1% BSA for 2 minutes at RT after which further binding was blocked by addition of 100 μl of 1 mM biotin and a further incubation at RT for 2 minutes. Labeled cells were finally washed 3X in D-PBS and imaged in D-PBS with 1% BSA.

Microscopy

All samples were imaged on an Olympus IX-81 inverted and with a 150X 1.45 NA UApo TIRFM Olympus oil immersion microscope objective and by use of a 100W Hg arc lamp for fluorescence excitation. The excitation power at the objective back aperture plane and with a filter cube consisting of a HQ470/40 nm fluorescence excitation filter, a Q495LP dichroic mirror (Chroma Technology) and a 510LP emission filter was measured to be 35 mW/cm^2. Data was acquired on an Andor DU860D-CS0-BW and using Andor IQ software. This camera has an active image area of (128 x 128) pixels^2 with a pixel dimension of (24 x 24) μm^2 and a full frame readout rate of 512 Hz. This camera further has a flexible readout format such that smaller areas of interest can be read out at much higher frame rates. In this work, we have limited our imaging to areas of interest to (20 x 128)

pixels^2 resulting in achievable readout rates of up to ~1750 Hz when the camera is operated in the frame transfer mode. This set-up results in a projected pixel size of (160 nm)^2.

10.4 Compartmentalized diffusion revealed by STED-FCS

COMPARTMENTALIZED DIFFUSION REVEALED BY STED-FCS

Debora M. Andrade[‡*], Mathias P. Clausen[†*], Christian Eggeling[‡], & B. Christoffer Lagerholm[†]

[†]MEMPHYS – Center for Biomembrane Physics, and Danish Molecular Biomedical Imaging Center (DaMBIC), University of Southern Denmark, Campusvej 55, DK-5230 Odense M, Denmark

[‡]Department of Nanobiophotonics, Max Planck Institute for Biophysical Chemistry, Am Fassberg 11, 37077 Göttingen, Germany

[*]Equal contibution

ABSTRACT

Studies of membrane dynamics on a (sub-)millisecond time-scale have led to conflicting conclusions about the reasons for observed hop-diffusion. Whereas single particle tracking (SPT) experiments using large quantum dots and gold nano-particles suggest that plasma membrane proteins and lipids are restricted in their motion due to confining barriers, studies using fluorescent dyes have failed to show this, and the role of the probe in these experiments is therefore questioned. Here, we cross-validate our previous QD tracking observation of compartmentalized diffusion in the mouse embryo fibroblasts cell line IA32 by using the complementary technique stimulated emission depletion - fluorescence correlation spectroscopy (STED-FCS) to follow the diffusion of dye-labeled lipids. We observe that the apparent diffusion constant of lipids in IA32 cells and NRK cells increase with smaller focal spot, which is an indication of diffusion in a meshwork of confining barriers. This compartmentalized diffusion is not observed in the isogenic cell line IA32-2xKD, which has a less dense actin cytoskeleton, and we further find the compartmentalized diffusion in IA32 and NRK cells to be strongly associated with the actin cytoskeleton.

INTRODUCTION

Our study using fluorescent quantum dots (QDs) for fast tracking suggests that plasma membrane lipids and proteins in the mouse embryo fibroblast cell line IA32 are subject to compartmentalized diffusion mimicking the previously reported hop-diffusion [1]. We used QDs that are approximately 20 nm in diameter, and therefore less bulky than the alternative 40 nm gold particles, which traditionally have been used to visualize hop-diffusion [2]. Yet, the size of QDs can possibly perturb the natural motion of their target molecules, as in particular the valence of QDs is not well defined [3]. Multivalent QDs induce cross-linking of target molecules, which might enhance the observation of compartmentalized hop-like diffusion, as complexes of a few molecules would likely have a harder time escaping a confinement, than a single molecule would. In this study, we therefore wanted to cross-validate our findings by using monovalent probes, but as monovalent QDs are not easily available [4], we decided to use fluorescent dyes, which are less invasive.

A high temporal acquisition rate is crucial for being able to resolve hop-diffusion, as it has been found to only happen on a fast time scale. This challenges its observation using SPT with fluorescent dyes, as the brightness of organic dyes limits the obtainable acquisitions rate. Further, their photo-(in)stability limits observations to relatively few displacements before irreversible photo-bleaching, which possibly also precludes the observation

of hop-diffusion [5]. In this study we therefore decided to use STED-FCS as the analyzing method [6]. STED-FCS features the same combination of high temporal and high spatial resolution as SPT at fast acquisition rates, but is because of the small observation window, less affected to the photo-limitations of the dyes. STED-FCS has previously been applied to study the dynamics of lipids and proteins in cell membranes, and the method has revealed important details of differences in diffusion dynamics between a glycerophospholipid (DPPE) and sphingomyelin [7, 8]. So far, most STED-FCS studies have been done in PtK2 cells, and no indication of hop-diffusion has been reported using STED-FCS.

The main goal of this study was to investigate if we would be able to confirm our observation of compartmentalized hop-like diffusion in IA32 cells in a setup with the same temporal resolution, and a minimal influence of the probe. As will be shown, this was in fact the case, so our next goal was to determine the molecular origin of the barriers compartmentalizing the diffusion, and restricting free diffusion of membrane molecules.

METHODS

Lipids

We investigated the diffusion of 1,2-dipalmitoyl-*sn*-glycero-3-phosphoethanolamine (DPPE), 1-palmitoyl-2-hydroxy-*sn*-glycero-3-phosphoethanolamine (lyso-PE), and sphingomyelin (SM) labeled in the head groups with the fluorescent marker ATTO-647N (ATTO-Tec). These fluorescent lipid analogs were bulk loaded into IA32, NRK, or IA32-2xKD cells via BSA delivery, and incubation on ice for 30 min.

STED-FCS measurements

The lipid dynamics was analyzed by placing the focused superimposed FCS and STED laser beams at random positions in the lamellipodia of the cells. A series of five 10 s recordings was carried out at each spot before focusing the laser beams on a different spot, and measuring a new series of recordings at a different STED laser intensity. The measurements were carried out at room temperature. The correlation data was recorded such that there were 20-100 fluorescent molecules in the focal spot in confocal measurements, and 1-5 fluorescent molecules in the focal spot at the highest STED power. The values and errors of the reported diffusion parameters were obtained from at least 20 measurements, and up to 150 measurements in a combination of the same, and different spots, as well as from at least five different cells. The reported parameters are the median values, and the error is the standard deviation of the mean.

Drug treatments

Latrunculin B (Lat B): Cells were incubated with a concentration of 0.1-1 μM Lat B (Sigma) for 30 min at 37 °C, and then washed, and imaged. Lat B is commonly used to disrupt the actin cytoskeleton, as it binds monomeric G-actin and prevents polymeric F-actin assembly.

CK-666: Cells were treated with 100 μM CK-666 (Sigma) for 3-6 hours at 37 °C, and imaged in the presence of CK-666. CK-666 is a selective inhibitor of Arp2/3 assisted actin branching, and it binds Arp2/3 and prevents the complex to switch to its active conformation.

Cholesterol Oxidase (COase): Cells were treated with 1 U/ml *Streptomyces Spec.* COase (Sigma) for 30 min at 37 °C, and then washed, and imaged. COase oxidizes cholesterol, into cholestenon and is commonly used to "remove" cholesterol from the plasma membrane.

STED-FCS SETUP

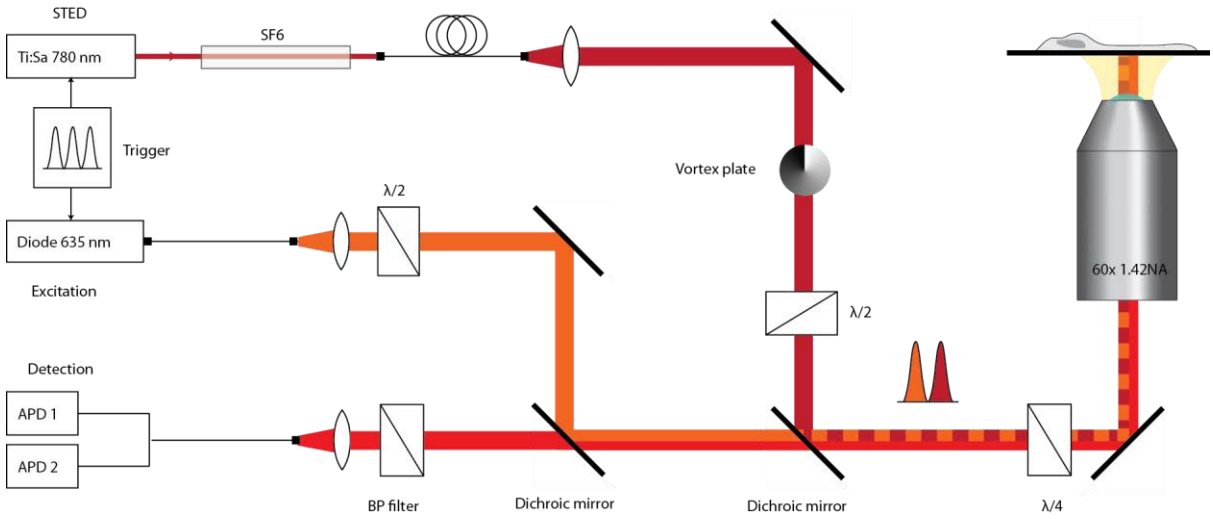

Figure 1: Schematic illustration of STED-FCS setup. The excitation (orange) and STED (dark red) laser beams are superimposed using two dichroic mirrors and focused unto the sample. The emitted fluorescence (red) from the sample is filtered using a band-pass (BP) filter and detected onto two avalanche photon detectors (APD). The vortex plate induces a clockwise 2π-phase shift across the STED beam, which generates the doughnut shaped focal intensity distribution in the focal plane. The circular polarization of both laser beams is maintained by a combination of λ/2, and λ/4 wave plates.

The STED nanoscope (Figure 1) was based on a home-built confocalized microscope setup equipped with a 635 nm laser (PicoQuant) with an 80 ps pulse width for excitation of ATTO-647N fluorescence. The STED beam was provided by a MaiTai Titanium:Sapphire laser system (Spectra-Physics) operating at 780 nm with a repetition rate of 76 MHz. The pulse timing of both lasers was adjusted using a home-built electronic delay unit, where the STED pulses served as the trigger master. The STED laser pulses were stretched to a pulse length of approximately 250-350 ps using a 30 cm optical SF6 glass rod, and a 120 m long polarization maintaining single-mode fiber (AMS Technologies). Fluorescence excitation and collection was realized using an oil immersion 60x, 1.42NA objective (Olympus). The laser beams were spatially superimposed, and the fluorescence light filtered by appropriate dichroic filters (AHF Analysentechnik). The doughnut-shaped focal spot of the STED beam featuring a central zero intensity was produced by introducing a phase-modifying plate (RPC Photonics) into the beam path, imprinting on the wave front a helical phase ramp $\exp(i\ )$ with 0 2π. A /4-wave plate and a /2-wave plate ensured circular polarization of the STED, and of the excitation beam. Precise positioning of the laser foci in the sample, and sample scanning was realized by a beam scanning device (mirror tilting system PSH 10/2, Piezosystem Jena) for lateral directions and an objective lens positioning system (MIPOS 250, Piezosystem Jena) for the axial direction. The fluorescence was descanned and coupled into a multi-mode fiber splitter (Fiber Optic Network Technology) with an aperture size corresponding to 1.4x the magnified excitation spot. The 50:50 split fluorescence signal was then detected by two single-photon counting avalanche photo diodes (SPCM-AQR-13-FC, Perkin Elmer Optoelectronics), and the recorded fluorescence counts were further processed by a hardware correlator card (Flex02-01D, Correlator.com). The

focal intensity distribution of the excitation and STED light was measured by scanning a scattering gold bead of 40 nm in diameter using a non-confocal detector (MP 963 Photon Counting Module, Perkin Elmer). The laser powers *P* were measured directly at the sample plane. Together with the full-width-at-half-maximum (FWHM) of the focal laser intensity distribution (~240 nm for 635 nm) they allow for the calculation of the time-averaged intensity $I = P / (\pi(\mathrm{FWHM}^2 / 2))$ (usually ~15-25 kW/cm^2 stemming from P = 5-8 µW for the excitation light) and a pulse peak intensity $I_{peak} = I/(\ f)$ with pulse width ~250-350 ps and repetition rate f = 76 MHz for the STED light. Calibration of the diameter $d(P_{STED})$ of the effective focal fluorescence spots formed by a certain STED power P_{STED} was performed either by imaging 80 nm large fluorescence beads, or by STED-FCS measurements of the fluorescent lipid analogs in supported lipid bilayers.

Data analysis

Fluorescence intensity fluctuations were auto-correlated taking anomalous diffusion dynamics, triplet state population, and other dye-related kinetics causing changes in the fluorescence brightness into account [9-11]

$$( ) \left(-\right) \quad ( ) \quad ( ) \quad ( )$$

With:

$\left(\ + \left(\frac{\tau}{\tau_D}\right)^{\alpha}\right)^{-}$ (anomalous diffusion dynamics)

$\frac{}{-}$ $\left(--\right)$ (triplet state formation)

$\left(--\right)$ (kinetic processes)

Here, N is the number of molecules in the focal spot, τ the characteristic diffusion time, T is the fraction of molecules in the triplet state, τ the triplet state lifetime, K the amplitude of the other kinetic processes, and τ the correlation time for the other kinetics. At the excitation intensities applied, T and τ of ATTO-647N labels were approximately 0.1 and 5 µs, respectively, and fixed throughout the analysis. For the cell measurement K and τ were fixed to 0.1 and 0.1 ms, respectively. This kinetic term might stem from the population of an additional dark state or conformational fluctuations of the dye-lipid system leading to changes in the fluorescence brightness [7].

The apparent diffusion constants were calculated assuming two-dimensional diffusion from D $\frac{^2}{(2)}$.

Calibration

For calibration of the focal spot area, the diffusion of fluorescently labeled lipids in a supported lipid bilayer (SLB) was used. The SLB was prepared by spin coating of a mixture of trace amounts of the fluorescently labeled lipid and unlabeled DOPE lipid [12]. The full-width-at-half-maximum (FWHM) of the focal spot in confocal recordings was 240 nm. Assuming free diffusion with constant diffusion constant D, the FWHM at a given STED power was calculated as $\mathrm{FWHM}_{\mathrm{STED}} = \mathrm{FWHM}_{\mathrm{confocal}}\sqrt{\quad / \quad}$.

RESULTS

Lipid dynamics measured by STED-FCS

In STED nanoscopy, a spatial resolution below the diffraction limit can be obtained [13, 14]. This is achieved by superimposing a doughnut-shaped STED laser spot on a normal Gaussian shaped excitation laser spot. The STED laser will reversibly switch off fluorescent dyes everywhere except for in the sub-diffraction-limited zero intensity center. By increasing the STED laser power the effective fluorescence focal spot with zero STED intensity can be controlled.

To obtain dynamic information of the diffusion of lipids in the plasma membrane we used STED combined with FCS [7]. We measured the transit times through the focal spots, and calculated the corresponding diffusion constants assuming two-dimensional diffusion as described in the methods. We further differentiated between different types of diffusion in the plasma membrane by applying the so-called FCS diffusion law [15]. This law states that a molecule undergoing free diffusion will have a linear dependence between the focal transit time $_D$ and the focal spot area w^2, and that an extrapolation of the $_D$-w^2-slope to zero focal area will have an intercept at the origin. Molecules that are transiently trapped in nano-domains or diffuse in a meshwork of barriers will also have a linear dependency between $_D$ and w^2, but the slope and intercept with the $_D$-axis will respectively be less steep and positive (trap-diffusion), and more steep negative (hop-diffusion). Alternatively, the apparent diffusion constants $D_{apparent}$ can be plotted as a function of w^2. In the $D_{apparent}$-w^2-plot, free diffusion will give the same diffusion constant independent of the focal area ($D^{STED}/D^{confocal} \approx$ trapped diffusion will show a decrease in the apparent diffusion constant with decreased focal areas ($D^{STED}/D^{confocal} < 1$), while the apparent diffusion constant for meshwork diffusion will increase with decreased focal areas ($D^{STED}/D^{confocal} > 1$).

As the area of the focal spot is of key importance in STED-FCS measurements, this was calibrated measuring lipid diffusion at different STED intensity in a supported lipid bilayer (SLB). Typical correlation curves obtained for an SLB is given in Figure 2A. The indicated diffusion times are = 2.6 ms, and = 0.07 ms at the highest STED power corresponding to a diffusion constant, D = 4 μm^2/s. The correlation curves obtained from measurements in cells are much noisier as shown in Figure 2B. The indicated diffusion times are = 26 ms, and = 0.4 ms.

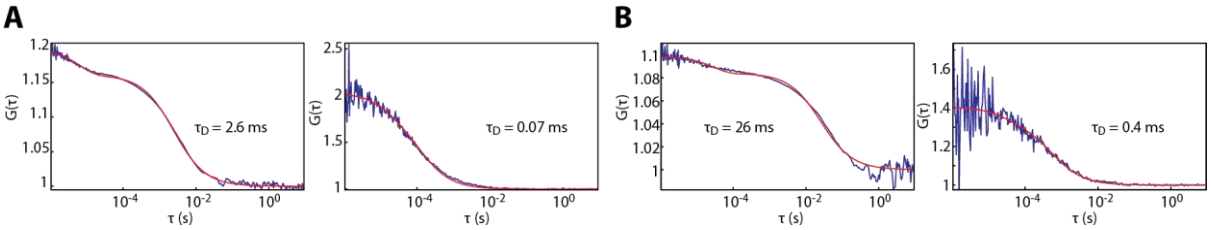

Figure 2: STED-FCS correlation curves. A) Typical correlation curves for an SLB at no (left) and high (right) STED intensity. The characteristic diffusion times are indicated in the figure. Note the different scales. B) Typical correlation curves for a cell at no (left) and high (right) STED intensity. The characteristic diffusion times are indicated in the figure.

Lipid diffusion in IA32 cells

We first investigated the diffusion of the fluorescent DPPE-lipid analog in the mouse embryo fibroblast cell line IA32 as our previous tracking experiments have indicated that DPPE undergo hop-like diffusion when labeled with QDs in these cells. The focal diffusion time $_D$ as a function of the focal area FWHM^2 is plotted in Figure

3A, with the data fitted by linear regression. As seen from the insert, the extrapolation of the linear regression has a negative intercept with the $_D$-axis, which is a sign of the molecules diffusing in a meshwork of confining barriers.

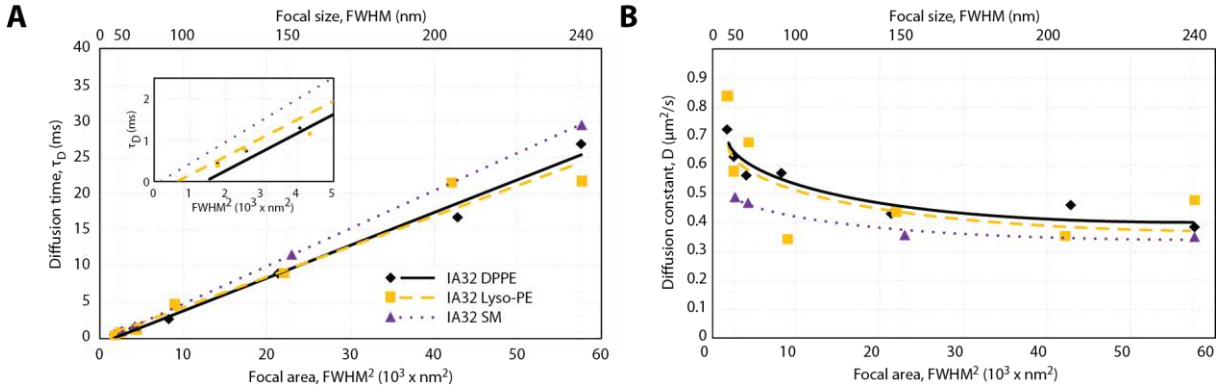

Figure 3: Lipid diffusion vs. focal area for different lipids. A) Diffusion time, $_D$, as a function of focal area (FWHM^2) for DPPE (black, rhombus, solid line), lyso-PE (yellow, squares, dashed line), and SM (purple, triangles, dotted line). Linear fits to the data are shown. The insert shows the extrapolation of the linear regression to highlight the intercept with the axis. B) Apparent diffusion constant *D* as a function of focal area. The shown trendline is a power regression and is just inserted for visualization.

Plotting the apparent diffusion constant as a function of the focal area clearly supports this trend (Figure 3B), as an increase in diffusion constant is seen for decreased focal areas. The confocal diffusion constant is $D^{confocal}$ = 0.4 ± 0.2 μm^2/s, while the diffusion constant at the smallest focal spot (highest STED intensity) is D^{STED} = 0.7 ± 0.4 μm^2/s. This corresponds to a relative increase by a factor of $D^{STED}/D^{confocal}$ = 1.8 ± 1.3, and is thus in agreement with what was previously indicated using fast QD tracking.

Measurements of the diffusion of a lyso-PE complemented the finding of compartmentalized diffusion measured by STED-FCS (Figure 3). The slope in the $_D$-FWHM^2-plot for lyso-PE also had a negative intercept with the $_D$-axis, and the relative diffusion constant changed by a factor of $D^{STED}/D^{confocal}$ = 1.8 ± 1.2.

The diffusion dynamics of sphingomyelin (SM) only showed a slight indication of hop-diffusion; the slope in the $_D$-FWHM^2-plot had a slightly negative intercept with the $_D$-axis, and the relative diffusion constant was changed by a factor of $D^{STED}/D^{confocal}$ = 1.4 ± 0.8.

The measurements in IA32 cells are in contrast to what have previously been reported for lipid diffusion in the rat kangaroo (Potorous tridactylis) kidney epithelial cell line PtK2. In these cells, the diffusion for DPPE and lyso-PE was reported to be free and independent of the focal spot area with a diffusion constant of *D* = 0.5 ± 0.2 μm^2/s [7, 8]. SM was in PtK2 cells reported to experience trapping events in cholesterol dependent domains resulting in a $D^{STED}/D^{confocal}$ = 0.2. The STED-FCS measurements in PtK2 cells, on the other hand, are in contrast to the lipid hop-diffusion reported for PtK2 cells using gold nano-particle tracking [16].

Cell type dependent lipid diffusion

The compartment sizes in IA32 cells were by QD tracking reported to be approximately 150 nm [1], whereas the compartment sizes in PtK2 cells were determined to be 43 nm [16]. It has been suggested that STED-FCS given the noisy measurements, cannot resolve the small compartments in PtK2 cells as these are right on the limit of the focal spot size [17]. We therefore decided to measure the DPPE dynamics in the normal rat kidney epithelial

cell line NRK, where lipid hop-diffusion was reported between large compartments of 210 nm (Figure 4) [16]. The extrapolation of the linear regression in the $_D$-FWHM^2-plot (insert in Figure 4A) has a negative intercept with the $_D$-axis, and therefore the STED-FCS data suggests hop-diffusion for DPPE in NRK cells.

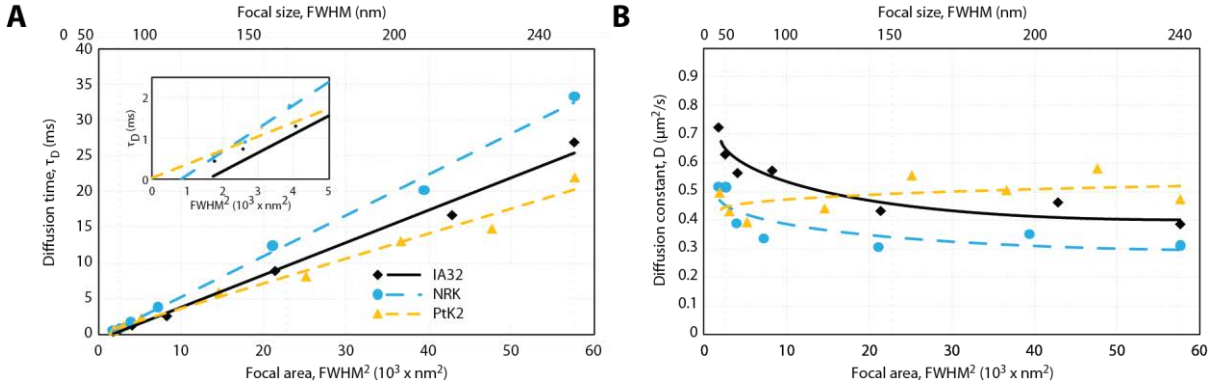

Figure 4: Lipid diffusion vs. focal area for different cells. A) Diffusion time, $_D$, as a function of focal area (FWHM^2) for DPPE in IA32 cell (black, rhombus, solid line), NRK cells (blue, circles, long dashed line), and PtK2 cells (yellow, triangles, dashed line). Linear fits to the data are shown. The insert shows the extrapolation of the linear regression to highlight the intercept with the axis. B) Apparent diffusion constant *D* as a function of focal area. The shown trendline is a power regression and is just inserted for visualization.

The apparent diffusion constant for confocal measurements was $D^{confocal}$ = 0.3 ± 0.2 µm^2/s. The diffusion constant increased with smaller focal spots to D^{STED} = 0.5 ± 0.2 µm^2/s corresponding to an increase by a factor of $D^{STED}/D^{confocal}$ = 1.7 ± 1.3.

For comparison, previous published results of DPPE diffusion in PtK2 are also inserted in Figure 4 [8]. The intercept of the curve with the $_D$-axis is as seen slightly positive indicating slight trapping, and the relative diffusion constant was $D^{STED}/D^{confocal}$ = 0.8.

Our STED-FCS recordings support the notion of lipid compartmentalized diffusion in cell lines that were previously reported to have compartment sizes significantly above the smallest STED focal spots, but not in cells that have compartment sizes close to the minimal STED focal spot size. It is therefore probable that the observation of compartmentalized diffusion by STED-FCS is prevented for small compartment sizes.

Actin dependent compartmentalized diffusion

The actin cytoskeleton has been suggested to be the key factor causing compartmentalized hop-diffusion. We therefore investigated the effect on the observed compartmentalized diffusion of manipulating the actin cytoskeleton in NRK and IA32 cells (Figure 5). For NRK cells, we treated the cells with different concentrations (0.1 µM and 1 µM) of Latrunculin B (Lat B) (Figure 5A). Lat B is a general actin toxin, which disrupts actin by binding G-actin and prevents polymerization of F-actin filaments throughout the cell including the cortical actin, and therefore results in a less dense actin network. In untreated NRK cells, the relative diffusion constant was as given above $D^{STED}/D^{confocal}$ = 1.7 ± 1.3. This ratio decreased gradually when treating the cells with increasing concentration of Lat B, and was for cells treated with 1 µM Lat B $D^{STED}/D^{confocal}$ = 1.4 ± 1.0. This result indicates that the hop-diffusion is gradually diminished when preventing actin polymerization, and that the diffusion approaches normal free diffusion. The apparent diffusion constant relative to that in untreated cells increased for all focal sizes suggesting that the diffusion is less hindered, and therefore faster.

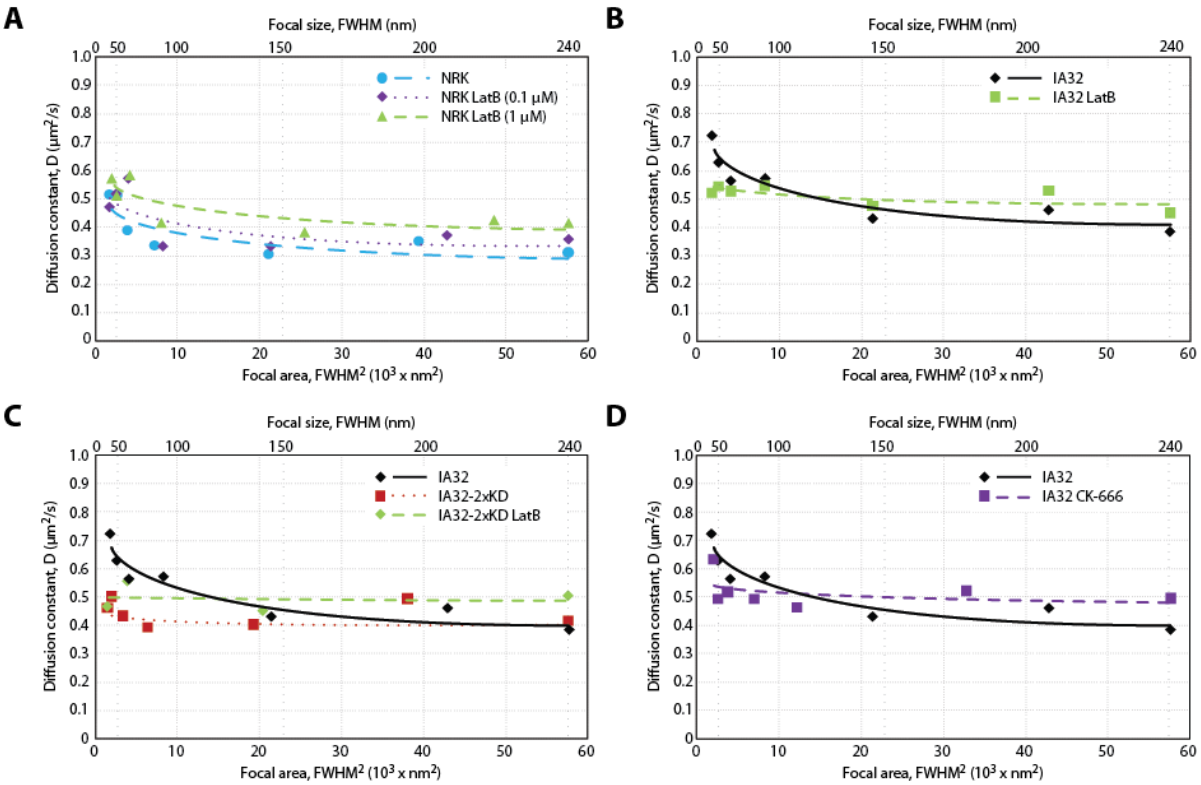

Figure 5: Actin dependent diffusion of DPPE. The plots show the diffusion constant for DPPE as a function of focal area for different treatments of the actin cytoskeleton in different cell lines. A) Latrunculin B (Lat B) treatment in NRK cells. B) Lat B treatment in IA32 cells. C) Lat B treatments in IA32-2xKD cells. D) CK-666 treatment in IA32 cells. The shown trendline is a power regression and is just inserted for visualization.

When we treated IA32 cells with 1 μM Lat B it also resulted in a change in diffusion dynamics (Figure 5B). There was no longer a significant increase in apparent diffusion constant for smaller focal spots, rather the diffusion constant was almost unchanged as we decreased the focal area indicating that the diffusion in this case was dominantly free, $D^{STED}/D^{confocal} = 1.0 \pm 0.7$. The apparent diffusion constant relative to that in untreated cells was for confocal measurements increased in agreement with the actin cytoskeleton being less dense, and the lipids being less restricted. However, for small focal spot sizes, the diffusion constant in Lat B treated cells was smaller than in untreated cells, which was unexpected and is unexplainable by the FCS diffusion law. This result suggests that actin filaments are responsible for causing hop-diffusion, but that, when F-actin formation is prevented, other mechanisms affect lipid diffusion, and hinders fast lipid diffusion.

To further investigate the role of the actin cytoskeleton, we were fortunate to have an IA32 isogenic cell line IA32-2xKD, which has a double knock-down in Arp2 and Arp3 [18]. The Arp2/3 complex is in normal cells responsible for F-actin branching by binding to existing filaments, and nucleating actin filament growth in a 70 degree angle. The IA32-2xKD cells therefore have a much less dense cortical actin network with only limited support to the plasma membrane as compared to IA32 cells (Figure 6).

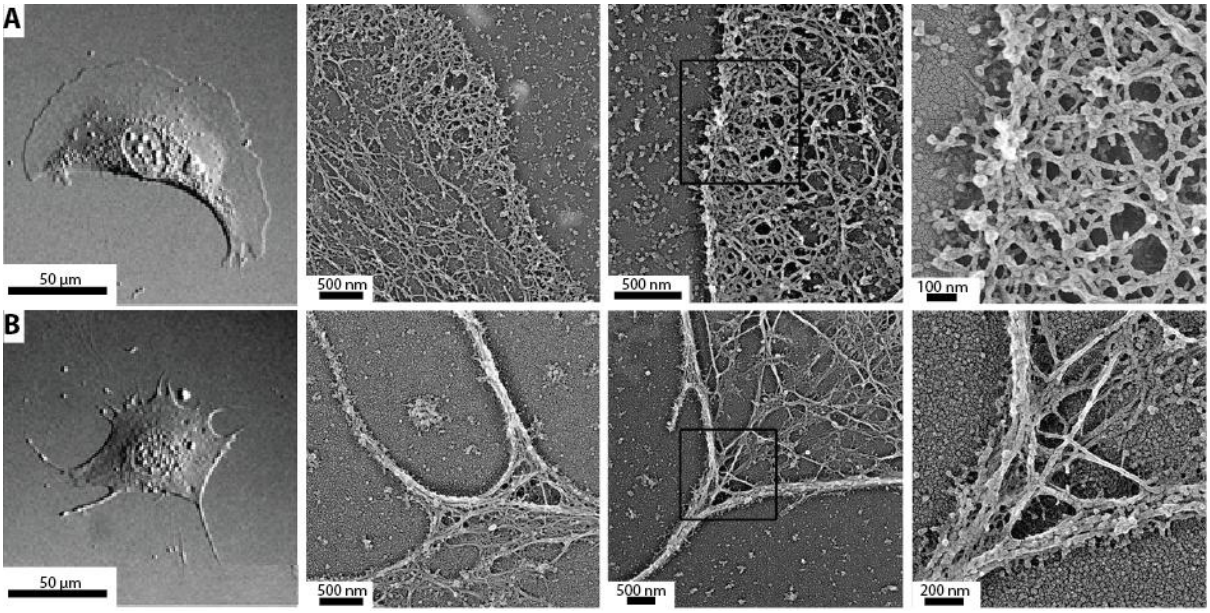

Figure 6: Cell morphology and cortical actin in IA32 and IA32-2xKD cells. DIC image (left), and cryo-shadowing EM images showing the leading edge actin networks A) IA32 cells, and B) IA32-2xKD cells. Center images are different cells, right panels are magnified portion of center panels indicated by black boxes. (Reprintet with permission from [18].)

The diffusion constant was in IA32-2xKD cells essentially independent of the area of the focal spot (Figure 5C), $D^{STED}/D^{confocal} = 1.1 \pm 0.8$. This would suggest free lipid diffusion in agreement with the F-actin meshwork compartments being larger than the focal spots, and therefore the lipids would not be subject to hop-diffusion on the spatial scale at which they were measured. Treating IA32-2xKD cells with 1 µM Lat B did not change the situation, as the diffusion was still dominated by free diffusion, $D^{STED}/D^{confocal} = 1.0 \pm 1.5$. The diffusion constant was slightly increases compared to IA32.

We next mimicked the IA32-2xKD knock down of Arp2/3 in IA32 cells. We treated the cells with CK-666, which prevents Arp 2/3 assisted F-actin branching by inhibition of Arp2/3 (Figure 5D). When treating IA32 cells with 100 µM CK-666 this gave similar results for the diffusion constant as in IA32-2xKD cells and in IA32 cells treated with Lat B. The apparent diffusion constant was essentially independent of the focal spot size, $D^{STED}/D^{confocal} = 1.0 \pm 0.6$, suggesting that the molecules diffuse freely. The diffusion constant was increased for confocal measurements, but did not reach the diffusion constant at high STED powers in untreated cells.

Altogether, our measurements strongly suggest that compartmentalized diffusion is closely associated with the actin cytoskeleton.

Cholesterol independent compartmentalized diffusion

Cholesterol is known to also be a key player for the organization in the plasma membrane. We therefore treated NRK and IA32 cells with COase that oxidizes cholesterol in the plasma membrane, and measured the effect on the lipid dynamics. For both cell lines, the apparent hop-diffusion was essentially unaffected (Figure 7). The apparent diffusion constant was gradually increased for decreased focal spots, and the relative diffusion constant was $D^{STED}/D^{confocal} = 1.7 \pm 0.9$, and $D^{STED}/D^{confocal} = 1.7 \pm 0.8$ for NRK cell and IA32 cells respectively. These results suggest that the plasma membrane cholesterol content is not responsible, or directly associated with the observed compartmentalized diffusion.

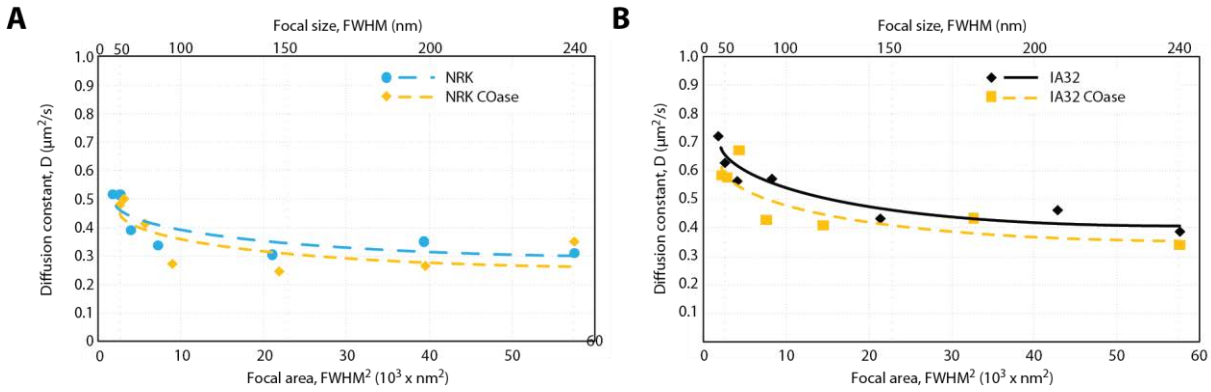

Figure 7: Cholesterol dependent diffusion of DPPE. The plots show the diffusion constant for DPPE as a function of focal area when treating cells with COase in A) NRK cell, and B) IA32 cells. The shown trendline is a power regression and is just inserted for visualization.

A summary of all reported diffusion constants is given in Table 1.

Cell (Molecule) – Treatment (conc.)	$D^{confocal}$ ± std.dev. (µm²/s)	D^{STED} ± std.dev. (µm²/s)	$D^{STED}/D^{confocal}$ ± std.dev.
IA32	0.4 ± 0.2	0.7 ± 0.4	1.8 ± 1.3
IA32 (Lyso-PE)	0.4 ± 0.2	0.7 ± 0.3	1.8 ± 1.2
IA32 (SM)	0.4 ± 0.2	0.5 ± 0.2	1.3 ± 0.8
PtK2	0.5 ± 0.2	0.4 ± 0.2	0.8 ± 0.5
NRK	0.3 ± 0.2	0.5 ± 0.2	1.7 ± 1.3
NRK – Lat B (0.1 µM)	0.4 ± 0.1	0.5 ± 0.2	1.4 ± 0.6
NRK – Lat B (1 µM)	0.4 ± 0.2	0.6 ± 0.2	1.4 ± 0.6
IA32 – Lat B (1 µM)	0.5 ± 0.2	0.5 ± 0.3	1.0 ± 0.7
IA32-2xKD	0.4 ± 0.2	0.5 ± 0.2	1.1 ± 0.8
IA32-2xKD – Lat B (1 µM)	0.5 ± 0.3	0.5 ± 0.7	1.0 ± 1.5
IA32 - CK666	0.5 ± 0.2	0.5 ± 0.2	1.0 ± 0.6
NRK COase	0.3 ± 0.2	0.5 ± 0.2	1.7 ± 0.9
IA32 - COase	0.3 ± 0.1	0.6 ± 0.2	1.7 ± 0.8

Table 1: Diffusion constant measured for confocal and STED.

DISCUSSION, OUTLOOK AND CONCLUSION

In this study, we have investigated the lateral dynamics of lipids in NRK and IA32 cells using STED-FCS. We recorded focal transit times as a function of the area of the focal spot and determined the corresponding apparent diffusion constants. The measurements consistently showed that the apparent diffusion constant for the lipid DPPE increased when the focal spot area was decreased. This result suggests that DPPE is subject to compartmentalized diffusion in a meshwork of confining barriers. The study firmly shows that compartmentalized diffusion dependent on the actin cytoskeleton.

Compartmentalized diffusion has previously been reported for lipids in NRK and IA32 cells, but only from SPT studies using gold nano-particles, or QDs [1, 19]. Gold nano-particles and QDs are limited by their size, and in particular the probes are typically multivalent, and therefore bind more than one target molecule in the plasma membrane. This can possibly induce hop-diffusion, or enhance the observation of hop-diffusion. In this study, the target molecule is directly labeled with the fluorescent dye ATTO-647N. Whereas this dye could possibly alter the natural partitioning of DPPE, we ensure that only single molecules are followed, and accordingly we can rule out that probe induced cross-linking is the cause of the observed diffusion. Control studies of previously reported lipid diffusion in PtK2 cells showed that the dynamics was independent on the position of the probe (head- or chain-labeled), still we would need to confirm in our studies that the compartmentalized

diffusion is independent of the probe, and e.g. study the DPPE dynamics when labeled with a different dye than ATTO-647N.

Our study is the first STED-FCS report suggesting compartmentalized diffusion. Previous studies have concluded that DPPE diffuses freely, and that SM is transiently trapped in small domains. These studies have primarily been carried out in PtK2 cells. PtK2 cells have been reported to have membrane compartments of 43 nm [16], and it has been suggested that the small size of the compartments on the same scale as the minimal focal spot size is what preclude their observation by STED-FCS [20]. Further, the substantial noise of FCS measurements could challenge the observation of small compartments. Given that compartmentalized diffusion in our case was observed in cell lines with larger compartments, this might in fact be the case.

In order to find the molecular explanation for the observed diffusion, we manipulated the actin cytoskeleton and the plasma membrane cholesterol content as these components are typically found to be main actors of the membrane organization. Lat B treatment in NRK cells showed a gradual decrease in the observed compartmentalized diffusion, and a faster diffusion. This would be in agreement with the actin cytoskeleton opening up to form larger compartments in which DPPE diffuse unrestricted. Lat B is a relatively harsh actin toxin, and the cell morphology changed significantly (but reversibly) upon treatment.

For IA32 cells, we had three different ways to investigate the influence of the actin cytoskeleton. Besides Lat B treatment, we could directly evaluate the dependence of Arp2/3 dependent actin branching as we had a IA32 cell line with an Arp2/3 knock down (IA32-2xKD). The knock-down was further mimicked in normal IA32 cells using the Arp2/3 inhibitor CK-666. CK-666 treatment changed the cell morphology less than Lat B treatment. Experiments in all three different scenarios showed that the apparent diffusion constant changed in such a way that it was independent on the focal spot area, indicating free diffusion. The diffusion constant was, however, not measured to be as fast as for small focal spot in untreated cells. This observation suggests that some other membrane phenomenon prevents (the observation of) fast unrestricted diffusion over larger areas, when actin filaments are less abundant. The actin cytoskeleton provides mechanical support for the plasma membrane, and one hypothesis that we have for not observing fast diffusion in cells with perturbed actin cytoskeleton is, that when this mechanical support is removed, the membrane is more likely to have a pronounced three-dimensional topography. If one imagines the plasma membrane as a canvas stretched over F-actin acting as tent poles, then when the F-actin is removed, the plasma membrane will collapse and have a higher tendency towards showing membrane curvature. In our analysis we assume two-dimensional diffusion, so if the molecules have a significant movement in the third dimension, the diffusion will effectively be observed as being slower.

Hop-diffusion, as described from gold nano-particle SPT observations, reports that lipids and proteins diffuse very fast with a diffusion constant of 5-8 $\mu m^2/s$ within membrane compartments [21]. This fast diffusion was not observed by SPT with QDs. STED-FCS has the temporal resolution to observe diffusion this fast, and indeed measurements on SLBs resulted in a diffusion constant of 4 $\mu m^2/s$ (the diffusion in supported bilayers is slower than in free standing membranes [22]). In cells, however, the fastest diffusion constant that we measured was 0.7 $\mu m^2/s$, or roughly a factor of 10 below what is reported for hop-diffusion. In order to measure the diffusion constant within compartments by STED-FCS, the focal spot should be significantly smaller than the compartment size to ensure that the molecules are unaffected by the barriers. In the measurements, we do not

have any control of where the focal spot is placed relative to the compartments and the reported diffusion is an average over all molecular transit times. This would be likely to effectively cause a diffusion constant that is smaller than the real free diffusion constant. We do, however, not believe that this effect would decrease the observed diffusion constant by a factor of 10, and we question whether a diffusion of 5-8 $\mu m^2/s$ is a true reflection of the lipid diffusion in the plasma membrane. Lipids and proteins diffusing in a crowded environment have a significantly decreased diffusion, and further, if the lipids were in fact diffusing this fast, the size of the gold particle would affect the collective diffusion of the probe and the lipid [23-27].

In conclusion, our STED-FCS study of lipid dynamics in the plasma membrane of cells support the idea that lipids experience compartmentalized diffusion in a cell type dependent manner. The actin cytoskeleton was determined to play a key role for the observation of compartmentalized diffusion, whereas cholesterol could be manipulated without significance for the observed diffusion. We suggest that when cortical actin network is removed from the cell, the plasma membrane loses its mechanical support and therefore shows more curved topology explaining why we do not always observe an increase in diffusion constant when disrupting actin. We further do not observe a very fast diffusion constant for the lipids when observed at the smallest focal spot sizes, and we think this fast component as reported from SPT with gold nano-particles is not a true reflection of the lipid dynamics.

REFERENCES

1. Clausen, M.P. and B.C. Lagerholm, Transient confinement in plasma membranes explored by high-speed tracking using quantum dots. 2012.

2. Fujiwara, T., K. Ritchie, H. Murakoshi, K. Jacobson, and A. Kusumi, Phospholipids undergo hop diffusion in compartmentalized cell membrane. J Cell Biol, 2002. 157(6): p. 1071-81.

3. Rosenthal, S.J., J.C. Chang, O. Kovtun, J.R. McBride, and I.D. Tomlinson, Biocompatible quantum dots for biological applications. Chem Biol, 2011. 18(1): p. 10-24.

4. Howarth, M., W. Liu, S. Puthenveetil, Y. Zheng, L.F. Marshall, M.M. Schmidt, . . . A.Y. Ting, Monovalent, reduced-size quantum dots for imaging receptors on living cells. Nat Methods, 2008. 5(5): p. 397-9.

5. Wieser, S., M. Moertelmaier, E. Fuertbauer, H. Stockinger, and G.J. Schutz, (Un)confined diffusion of CD59 in the plasma membrane determined by high-resolution single molecule microscopy. Biophys J, 2007. 92(10): p. 3719-28.

6. Kastrup, L., H. Blom, C. Eggeling, and S.W. Hell, Fluorescence fluctuation spectroscopy in subdiffraction focal volumes. Phys Rev Lett, 2005. 94(17): p. 178104.

7. Eggeling, C., C. Ringemann, R. Medda, G. Schwarzmann, K. Sandhoff, S. Polyakova, . . . S.W. Hell, Direct observation of the nanoscale dynamics of membrane lipids in a living cell. Nature, 2009. 457(7233): p. 1159-62.

8. Mueller, V., C. Ringemann, A. Honigmann, G. Schwarzmann, R. Medda, M. Leutenegger, . . . C. Eggeling, STED nanoscopy reveals molecular details of cholesterol- and cytoskeleton-modulated lipid interactions in living cells. Biophys J, 2011. 101(7): p. 1651-60.

9. Haustein, E. and P. Schwille, Fluorescence correlation spectroscopy: novel variations of an established technique. Annu Rev Biophys Biomol Struct, 2007. 36: p. 151-69.

10. Widengren, J., U. Mets, and R. Rigler, Fluorescence correlation spectroscopy of triplet states in solution: a theoretical and experimental study. The Journal of Physical Chemistry, 1995. 99(36): p. 13368-13379.

11. Rigler, R. and E. Elson, Fluorescence Correlation Spectroscopy - Theory and Applications. 2001.

12. Simonsen, A.C. and L.A. Bagatolli, Structure of spin-coated lipid films and domain formation in supported membranes formed by hydration. Langmuir, 2004. 20(22): p. 9720-8.

13. Hell, S.W., Wichmann, J., Breaking the diffraction resolution limit by stimulated emission: stimulated-emission-depletion fluorescence microscopy. Optics Letters, 1994. 19(11): p. 780-782.

14. Hell, S.W., Microscopy and its focal switch. Nat Methods, 2009. 6(1): p. 24-32.

15. He, H.T. and D. Marguet, Detecting nanodomains in living cell membrane by fluorescence correlation spectroscopy. Annu Rev Phys Chem, 2011. 62: p. 417-36.

16. Murase, K., T. Fujiwara, Y. Umemura, K. Suzuki, R. Iino, H. Yamashita, . . . A. Kusumi, Ultrafine membrane compartments for molecular diffusion as revealed by single molecule techniques. Biophys J, 2004. 86(6): p. 4075-93.

17. Kusumi, A., T.K. Fujiwara, R. Chadda, M. Xie, T.A. Tsunoyama, Z. Kalay, . . . K.G. Suzuki, Dynamic Organizing Principles of the Plasma Membrane that Regulate Signal Transduction: Commemorating the Fortieth Anniversary of Singer and Nicolson's Fluid-Mosaic Model. Annu Rev Cell Dev Biol, 2012. 28: p. 215-50.

18. Wu, C., Sreeja B. Asokan, Matthew E. Berginski, Elizabeth M. Haynes, Norman E. Sharpless, Jack D. Griffith, . . . James E. Bear, Arp2/3 Is Critical for Lamellipodia and Response to Extracellular Matrix Cues but Is Dispensable for Chemotaxis. Cell, 2012. 148(5): p. 973-987.

19. Suzuki, K., K. Ritchie, E. Kajikawa, T. Fujiwara, and A. Kusumi, Rapid hop diffusion of a G-protein-coupled receptor in the plasma membrane as revealed by single-molecule techniques. Biophys J, 2005. 88(5): p. 3659-80.

20. Kusumi, A., K.G. Suzuki, R.S. Kasai, K. Ritchie, and T.K. Fujiwara, Hierarchical mesoscale domain organization of the plasma membrane. Trends Biochem Sci, 2011. 36(11): p. 604-15.

21. Kusumi, A., C. Nakada, K. Ritchie, K. Murase, K. Suzuki, H. Murakoshi, . . . T. Fujiwara, Paradigm shift of the plasma membrane concept from the two-dimensional continuum fluid to the partitioned fluid: high-speed single-molecule tracking of membrane molecules. Annu Rev Biophys Biomol Struct, 2005. 34: p. 351-78.

22. Machan, R. and M. Hof, Lipid diffusion in planar membranes investigated by fluorescence correlation spectroscopy. Biochim Biophys Acta, 2010. 1798(7): p. 1377-91.

23. Clausen, M.P. and B.C. Lagerholm, The Probe Rules in Single Particle Tracking. Curr Protein Pept Sci, 2011.

24. Peters, R. and R.J. Cherry, Lateral and rotational diffusion of bacteriorhodopsin in lipid bilayers: experimental test of the Saffman-Delbruck equations. Proc Natl Acad Sci U S A, 1982. 79(14): p. 4317-21.

25. Ramadurai, S., A. Holt, V. Krasnikov, G. van den Bogaart, J.A. Killian, and B. Poolman, Lateral diffusion of membrane proteins. J Am Chem Soc, 2009. 131(35): p. 12650-6.

26. Adler, J., A.I. Shevchuk, P. Novak, Y.E. Korchev, and I. Parmryd, Plasma membrane topography and interpretation of single-particle tracks. Nat Methods, 2010. 7(3): p. 170-1.

27. Niemela, P.S., M.S. Miettinen, L. Monticelli, H. Hammaren, P. Bjelkmar, T. Murtola, . . . I. Vattulainen, Membrane proteins diffuse as dynamic complexes with lipids. Journal of the American Chemical Society, 2010. 132(22): p. 7574-5.

Curriculum vitae

Name:
Mathias Porsmose Clausen

Date and Place of Birth:
January 21st, 1984, Odense, Denmark

Nationality:
Danish

Work Address:
MEMPHYS – Center for Biomembrane Physics, Department of Physics, Chemistry and Pharmacy, University of Southern Denmark, Campusvej 55, DK-5230 Odense M, Denmark
Tel: (+45) 6550 3686. Fax: (+45) 6550 4048
E-mail: mpc@memphys.sdu.dk

Home Address:
Allégade 20B, st., DK-5000 Odense C, Denmark
Tel: (+45) 3025 4005
E-mail: mathiaspclausen@gmail.com

Educational Degrees:

- MSc in Biophysics, University of Southern Denmark, 2009, (grade point average 11.9)
- BSc in Biophysics, University of Southern Denmark, 2007, (grade point average 12)
- Gymnasium, Odense Katedralskole, 2003, (grade point average 10.5)

Current Employment:

- PhD student in Biophysics, University of Southern Denmark, November 2009 - October 2012 (Supervisors: Ass. Prof. Dr. B. Christoffer Lagerholm, Prof. Dr. Ole G. Mouritsen)

Future Employment:

- Postdoctoral fellow, Weatherall Institute of Molecular Medicine, Human Immunology Unit, John Radcliffe Hospital, University of Oxford, February 2013 - (Mentor: Prof. Dr. Christian Eggeling)

Selected Awards and Honors:

- EliteForsk PhD travel stipend, 2011
- Novo Scholarship, 2009
- Carlsberg Memorial Scholarship, 2008
- Graduate School of Molecular Biophysics Scholarship, 2008
- Oticon Scholarship for Physics Students, 2007, 2006, 2005

Prizes:

- 1st Prize, scientific communication, *Research Grand Prix 2010*, University of Southern Denmark, 2010
- 2nd Prize, poster presentation, *10th Internat. Summer School on Biophysics*, Ruđer Boŝković Institute, Rovinj, 2009

Publications:

- Yde, C.W.*, *Clausen, M.P.**, Bennetzen, M.V. *, Lykkesfeldt, A.E., Mouritsen, O.G. & Guerra, B. "The Antipsychotic Drug Chlorpromazine Enhances the Cytotoxic Effect of Tamoxifen in Tamoxifen-sensitive and Tamoxifen-resistant Human Breast Cancer Cells", Anticancer Drugs 20, 723-735 (2009).
- *Mathias P. Clausen* & B. Christoffer Lagerholm, "The Probe Rules in Single Particle Tracking", Current Protein and Peptide Science, 12 (8), 699-713 (2011) (Cover)
- *Mathias P. Clausen*, Eva C. Arnspang, Byron Ballou, James E. Bear & B. Christoffer Lagerholm, "Single Molecule Multi-species Tracking in Live Cells", *Submitted*
- *Mathias P. Clausen* & B. Christoffer Lagerholm, "High-speed Single Particle Tracking in Plasma Membranes Using Quantum Dots", *Submitted*
- Eva C. Arnspang, Jeremy Schwartzentruber, *Mathias P. Clausen*, Christina Lyngsø, Jakob L. Hansen, Paul W. Wiseman, B. Christoffer Lagerholm, "Bridging the Gap between Single Molecule and Ensemble Methods for Measuring Lateral Dynamics in the Plasma Membrane", *Submitted*
- Thomas E. Rasmussen, *Mathias P. Clausen*, Eva C. Arnspang, Liselotte Jauffred, Lene Oddershede & B. Christoffer Lagerholm, "Single Molecule Applications of Quantum Dots", *In preparation*
- Debora M. Andrade*, *Mathias P. Clausen**, Alf Honigman, Veronika Müller, Marc Bates, Stefan W. Hell, Christian Eggeling & B. Christoffer Lagerholm, "Compartmentalized Diffusion Revealed by STED-FCS", *In preparation*

International Research Experience:

- NanoBiophotonics, Max Planck Inst. for Biophysical Chemistry, Göttingen, visiting PhD student, January-April 2012 (Prof. Dr. Dr. Stefan W. Hell, Dr. Christian Eggeling)
- Spatio Temporal Modeling Center, University of New Mexico, visiting PhD student, July 2011 (Ass. Prof. Dr. Keith A. Lidke)

- Cancer and Immunobiology, University of Basel, visiting PhD student, January - February 2010 (Prof. Dr. Matthias P. Wymann)

Danish Research Group Associations:

- MEMPHYS (Center for Biomembrane Physics), University of Southern Denmark, Bachelor-, Master- and PhD student, 2005- (Prof. Dr. Ole G. Mouritsen, Ass. Prof. Dr. B. Christoffer Lagerholm)
- CEBI (Center for Experimental Bioinformatics), University of Southern Denmark, ITEC student, 2008 (Prof. Dr. Jens S. Andersen, Dr. J. Bunkenborg)
- BMR (Biomedical Research), University of Southern Denmark, Bachelor student, 2006-2007 (Ass. Prof. Dr. Barbara Guerra)

Recent Poster Presentations:

- Biophysical Society Meeting, San Diego, "High-Speed Quantum Dot Tracking in Plasma Membranes Reveals Short-Lived Small-Size Corralled Diffusion", February 2012
- Weber Symposium, Lihue, "Parallel and Fast Tracking of Quantum Dots in Plasma Membranes", June 2011
- Biophysical Society Meeting, Baltimore, "Influence of Quantum Dot Labels on Single Molecule Movement in the Plasma Membrane", February 2011

Selected Oral Presentations:

- 7th Annual Biophysics PhD Meeting, Holbæk, "Single Molecule Studies of the Lateral Organization of the Plasma Membrane", June 2012
- 10 years of MEMPHYS symposium, Odense, "Hitchhiking on Lipids and Protein", April 2011
- Research Grand Prix, Odense, "The Magic Bullet", April 2010
- 10th International Summer School on Biophysics, Ruđer Bošković Institute, Rovinj, "Single Particle Tracking in Live Cells Using Quantum Dots", September 2009

Published Abstracts:

- *Clausen, M.P.* & Lagerholm, C., High-Speed Quantum Dot Tracking in Plasma Membranes Reveals Short-Lived Small-Size Corralled Diffusion. Biophysical Journal 102, 298a-298a (2012).
- Lagerholm, C. & *Clausen, M.P.*, High-Speed Single Quantum Dot Imaging in Live Cells Reveals Hop Diffusion. Biophysical Journal 100, 252a-252a (2011).
- *Clausen, M.P.* & Lagerholm, C., Influence of Quantum Dot Labels on Single Molecule Movement in the Plasma Membrane. Biophysical Journal 100, 479a-479a (2011).
- Lagerholm, C., Christensen, E.A., *Clausen, M.L.* & Kulatunga, P., Multispecies Single Molecule Imaging With Quantum Dots. Biophysical Journal 96, 283a-283a (2009).
- Olsen, O.D., Ostenfeld, M.S., Bennetzen, M., *Clausen, M.L.*, Nylandsted, J. & Jaaettela, M., Anti-cancer agent siramesine induces selective cathepsin induced cell death. Apmis 116, 439-439 (2008).

Job Experience:

- Teaching assistant, University of Southern Denmark, 2005-10 (Courses taught: Advanced Molecular Biology, Physical Chemistry, Biology – from Molecule to Eco-System, Science Statistics, Introduction to Biophysics)
- DrugMode Aps (Odense, Denmark), Research assistant: 2D-gel image analysis and biostatistics, 2006-2008
- Liplasome Pharma Aps (Lyngby, Denmark), Research assistant: Liposomal drug delivery, 2006

Organizational Experience:

- Graduate School of Molecular Biophysics, Key coordinator, 2009-2012 (Organizer of: 4th, 5th, 6th, and 7th Annual Biophysics PhD Meeting 2009-12, and Cross Institutional Course on Molecular Biophysics 2009-12)
- Philos, Member of steering group, 2009-2012, PhD association at University of Southern Denmark (Organizer of seminars, workshops etc.)